Theory of Many-Particle Systems

Lecture notes for P654, Cornell University, spring 2005.

Chapter 1

Preliminaries

1.1 Thermal average

In the literature, two types of theories are constructed to describe a system of many particles: Theories of the many-particle ground state, and theories that address a thermal average at temperature T. In this course, we'll limit ourselves to finite-temperature thermal equilibria and to nonequilibrium situations that arise from a finite-temperature equilibrium by switching on a time-dependent perturbation in the Hamiltonian. In all cases of interest to us, results at zero temperature can be obtained as the zero temperature limit of the finite-temperature theory.

Below, we briefly recall the basic results of equilibrium statistical mechanics. The thermal average of an observable A is defined as

$$\langle A \rangle = \mathrm{tr}\, \hat{A}\hat{\rho}, \tag{1.1}$$

where $\hat{\rho}$ is the density matrix and $\hat{A}$ is the operator corresponding to the observable A. The density matrix $\hat{\rho}$ describes the thermal distribution over the different eigenstates of the system. The symbol tr denotes the "trace" of an operator, the summation over the expectation values of the operator over an orthonormal basis set,

$$\mathrm{tr}\, A\rho = \sum_n \langle n|A\rho|n\rangle. \tag{1.2}$$

The basis set $\{|n\rangle\}$ can be the collection of many-particle eigenstates of the Hamiltonian $\hat{H}$, or any other orthonormal basis set.

In the canonical ensemble of statistical mechanics, the trace is taken over all states with N particles and one has

$$\hat{\rho} = \frac{1}{Z} e^{-\hat{H}/T}, \quad Z = \mathrm{tr}\, e^{-\hat{H}/T}, \tag{1.3}$$

where $\hat{H}$ is the Hamiltonian. Using the basis of N-particle eigenstates $|n\rangle$ of the Hamiltonian $\hat{H}$, with eigenvalues E_n, the thermal average $\langle A\rangle$ can then be written as

$$\langle A\rangle = \frac{\sum_n e^{-E_n/T}\langle n|\hat{A}|n\rangle}{\sum_n e^{-E_n/T}}. \tag{1.4}$$

In the grand-canonical ensemble, the trace is taken over all states, irrespective of particle number, and one has

$$\rho = \frac{1}{Z}e^{-(\hat{H}-\mu\hat{N})/T}, \quad Z = \mathrm{tr}\, e^{-(\hat{H}-\mu\hat{N})/T}. \tag{1.5}$$

Here μ is the chemical potential and N is the particle number operator. Usually we will include the term $-\mu\hat{N}$ into the definition of the Hamiltonian $\hat{H}$, so that expressions for the thermal average in the canonical and grand canonical ensembles are formally identical.

1.2 Schrödinger, Heisenberg, and interaction picture

There exist formally different but mathematically equivalent ways to formulate the quantum mechanical dynamics. These different formulations are called "pictures". For an observable $\hat{A}$, the expectation value in the quantum state $|\psi\rangle$ is

$$\overline{A} = \langle\psi|\hat{A}|\psi\rangle. \tag{1.6}$$

The time-dependence of the expectation value of A can be encoded through the time-dependence of the quantum state ψ, or through the time-dependence of the operator $\hat{A}$, or through both. You can find a detailed discussion of the pictures in a textbook on quantum mechanics, e.g., chapter 8 of *Quantum Mechanics*, by A. Messiah, North-Holland (1961).

1.2.1 Schrödinger picture

In the *Schrödinger picture*, all time-dependence is encoded in the quantum state $|\psi(t)\rangle$; operators are time independent, except for a possible explicit time dependence.[1] The time-evolution of the quantum state $|\psi(t)\rangle$ is governed by a unitary evolution operator $\hat{U}(t,t_0)$ that relates the quantum state at time t to the quantum state at a reference time t_0,

$$|\psi(t)\rangle = \hat{U}(t,t_0)|\psi(t_0)\rangle. \tag{1.7}$$

[1] An example of an operator with an explicit time dependence is the velocity operator in the presence of a time-dependent vector potential,

$$\hat{\mathbf{v}} = \frac{1}{m}\left(-i\hbar\boldsymbol{\nabla} - \frac{e}{c}\mathbf{A}(\mathbf{r},t)\right).$$

Quantum states at two arbitrary times t and t' are related by the evolution operator $\hat{U}(t,t') = \hat{U}(t,t_0)\hat{U}^\dagger(t',t_0)$. The evolution operator $\hat{U}$ satisfies the group properties $\hat{U}(t,t) = \hat{1}$ and $\hat{U}(t,t') = \hat{U}(t,t'')\hat{U}(t'',t')$ for any three times t, t', and t'', and the unitarity condition

$$\hat{U}(t,t') = \hat{U}^\dagger(t',t). \tag{1.8}$$

The time-dependence of the evolution operator $\hat{U}(t,t_0)$ is given by the Schrödinger equation

$$i\hbar\frac{\partial\hat{U}(t,t_0)}{\partial t} = \hat{H}\hat{U}(t,t_0). \tag{1.9}$$

For a time-independent Hamiltonian $\hat{H}$, the evolution operator $\hat{U}(t,t_0)$ is an exponential function of $\hat{H}$,

$$\hat{U}(t,t') = \exp[-i\hat{H}(t-t')/\hbar]. \tag{1.10}$$

If the Hamiltonian $\hat{H}$ is time dependent, there is no such simple result as Eq. (1.10) above, and one has to solve the Schrödinger equation (1.9).

1.2.2 Heisenberg picture

In the *Heisenberg picture*, the time-dependence is encoded in operators $\hat{A}(t)$, whereas the quantum state $|\psi\rangle$ is time independent. The Heisenberg picture operator $\hat{A}(t)$ is related to the Schrödinger picture operator $\hat{A}$ as

$$\hat{A}(t) = \hat{U}(t_0,t)\hat{A}\hat{U}(t,t_0), \tag{1.11}$$

where t_0 is a reference time. The Heisenberg picture quantum state $|\psi\rangle$ has no dynamics and is equal to the Schrödinger picture quantum state $|\psi(t_0)\rangle$ at the reference time t_0. The time evolution of $\hat{A}(t)$ then follows from Eq. (1.9) above,

$$\frac{d\hat{A}(t)}{dt} = \frac{i}{\hbar}[\hat{H}(t),\hat{A}(t)]_- + \frac{\partial\hat{A}(t)}{\partial t}, \tag{1.12}$$

where $\hat{H}(t) = \hat{U}(t_0,t)\hat{H}(t_0)\hat{U}(t,t_0)$ is the Heisenberg representation of the Hamiltonian and the last term is the Heisenberg picture representation of an eventual explicit time dependence of the observable A. The square brackets $[\cdot,\cdot]_-$ denote a commutator. The Heisenberg picture Hamiltonian $\hat{H}(t)$ also satisfies the evolution equation (1.12),

$$\frac{d\hat{H}(t)}{dt} = \frac{i}{\hbar}[\hat{H}(t),\hat{H}(t)]_- + \frac{\partial\hat{H}}{\partial t} = \frac{\partial\hat{H}(t)}{\partial t}.$$

For a time-independent Hamiltonian, the solution of Eq. (1.12) takes the familiar form

$$\hat{A}(t) = e^{i\hat{H}(t-t_0)/\hbar}\hat{A}e^{-i\hat{H}(t-t_0)/\hbar}. \tag{1.13}$$

You can easily verify that the Heisenberg and Schrödinger pictures are equivalent. Indeed, in both pictures, the expectation values $(\overline{A})_t$ of the observable A at time t is related to the operators $\hat{A}(t_0)$ and quantum state $|\psi(t_0)\rangle$ at the reference time t_0 by the same equation,

$$\begin{aligned}(\overline{A})_t &= \langle\psi(t)|\hat{A}|\psi(t)\rangle \\ &= \langle\psi(t_0)|\hat{U}(t_0,t)\hat{A}\hat{U}(t,t_0)|\psi(t_0)\rangle \\ &= \langle\psi|\hat{A}(t)|\psi\rangle. \end{aligned} \tag{1.14}$$

1.2.3 Interaction picture

The *interaction picture* is a mixture of the Heisenberg and Schrödinger pictures: both the quantum state $|\psi(t)\rangle$ and the operator $\hat{A}(t)$ are time dependent. The interaction picture is usually used if the Hamiltonian is separated into a time-independent unperturbed part $\hat{H}_0$ and a possibly time-dependent perturbation $\hat{H}_1$,

$$\hat{H}(t) = \hat{H}_0 + \hat{H}_1. \tag{1.15}$$

In the interaction picture, the operators evolve according to the unperturbed Hamiltonian $\hat{H}_0$,

$$\hat{A}(t) = e^{i\hat{H}_0(t-t_0)/\hbar}\hat{A}(t_0)e^{-i\hat{H}_0(t-t_0)/\hbar}, \tag{1.16}$$

whereas the quantum state $|\psi\rangle$ evolves according to a modified evolution operator $\hat{U}_I(t,t_0)$,

$$\hat{U}_I(t,t_0) = e^{i\hat{H}_0(t-t_0)/\hbar}\hat{U}(t,t_0). \tag{1.17}$$

You easily verify that this assignment leads to the same time-dependent expectation value (1.14) as the Schrödinger and Heisenberg pictures.

The evolution operator that relates interaction picture quantum states at two arbitrary times t and t' is

$$\hat{U}_I(t,t') = e^{i\hat{H}_0(t-t_0)/\hbar}\hat{U}(t,t')e^{-i\hat{H}_0(t'-t_0)/\hbar}. \tag{1.18}$$

The interaction picture evolution operator also satisfies the group and unitarity properties.

A differential equation for the time dependence of the operator $\hat{A}(t)$ is readily obtained from the definition (1.16),

$$\frac{d\hat{A}(t)}{dt} = \frac{i}{\hbar}[\hat{H}_0, \hat{A}(t)]_- + \frac{\partial\hat{A}(t)}{\partial t}. \tag{1.19}$$

The time dependence of the interaction picture evolution operator is governed by the interaction-picture representation of the perturbation $\hat{H}_1$ only,

$$i\hbar\frac{\partial\hat{U}_I(t,t_0)}{\partial t} = \hat{H}_1(t)\hat{U}_I(t,t_0), \tag{1.20}$$

where

$$\hat{H}_1(t) = e^{i\hat{H}_0(t-t_0)/\hbar}\hat{H}_1 e^{-i\hat{H}_0(t-t_0)}. \tag{1.21}$$

The solution of Eq. (1.20) is not a simple exponential function of $\hat{H}_1$, as it was in the case of the Schrödinger picture. The reason is that the perturbation $\hat{H}_1$ is always time dependent in the interaction picture, see Eq. (1.21).[2] (An exception is when $\hat{H}_1$ and $\hat{H}_0$ commute, but in that case $\hat{H}_1$ is not a real perturbation.) However, we can write down a formal solution of Eq. (1.20) in the form of a "time-ordered" exponential. For $t > t_0$, this time-ordered exponential reads

$$\hat{U}_I(t,t_0) = T_t e^{-(i/\hbar)\int_{t_0}^{t} dt'\,\hat{H}_1(t')}. \tag{1.22}$$

In this formal solution, the exponent has to be interpreted as its power series, and in each term the "time-ordering operator" T_t arranges the factors $\hat{H}$ with descending time arguments. For example, for a product of two operators $\hat{H}_1$ taken at different times t and t' one has

$$T_t\hat{H}_1(t)\hat{H}_1(t') = \begin{cases} \hat{H}_1(t)\hat{H}_1(t') & \text{if } t > t', \\ \hat{H}_1(t')\hat{H}_1(t) & \text{if } t' > t. \end{cases} \tag{1.23}$$

Taking the derivative to t is straightforward now: since t is the largest time in the time integration in Eq. (1.22), the time-ordering operator ensures that upon differentiation to t the factor $\hat{H}_1(t)$ always appears on the left, so that one immediately recovers Eq. (1.20). Similarly, the conjugate evolution operator $\hat{U}(t_0,t)$ is given by an "anti-time-ordered" exponential,

$$\hat{U}_I(t_0,t) = \tilde{T}_t e^{(i/\hbar)\int_{t_0}^{t} dt'\,\hat{H}_1(t')}, \tag{1.24}$$

where the operator $\tilde{T}_t$ arranges the factors $\hat{H}_1$ with ascending time arguments.

Operators in the Heisenberg picture can be expressed in terms of the corresponding operators in the interaction picture using the evolution operator $\hat{U}_I$. Denoting the Heisenberg picture operators with a subscript "H", one has

$$\hat{A}_{\rm H}(t) = \hat{U}_I(t_0,t)\hat{A}(t)\hat{U}_I(t,t_0), \tag{1.25}$$

[2] Indeed, one would be tempted to write

$$\hat{U}_I(t,t_0) = e^{-(i/\hbar)\int_{t_0}^{t} dt'\,\hat{H}_1(t')}.$$

However, since $\hat{H}_1$ does not commute with itself if evaluated at different times, taking a derivative to t does not simply correspond to left-multiplication with $\hat{H}_1(t)$.

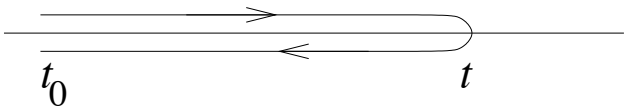

Figure 1.1: Contour used to the operator $\hat{A}_{\rm H}(t)$ in the Heisenberg picture from the corresponding operator $\hat{A}(t)$ in the interaction picture.

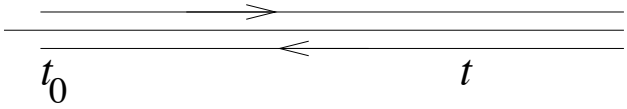

Figure 1.2: Keldysh contour. The arguments t and t' can be taken on each branch of the contour.

where $\hat{A}(t)$ is the interaction picture operator, see Eq. (1.16). Using the formal solution (1.22) for the evolution operator, this expression can be written as

$$\begin{aligned}\hat{A}_{\rm H}(t) &= \left[\tilde{T}_t e^{(i/\hbar)\int_{t_0}^{t} dt' \hat{H}_1(t')}\right] \hat{A}(t) \left[T_t e^{-(i/\hbar)\int_{t_0}^{t} dt' \hat{H}_1(t')}\right] \\ &= \left[\tilde{T}_t e^{-(i/\hbar)\int_{t}^{t_0} dt' \hat{H}_1(t')}\right] \hat{A}(t) \left[T_t e^{-(i/\hbar)\int_{t_0}^{t} dt' \hat{H}_1(t')}\right]. \end{aligned} \tag{1.26}$$

It is tempting to combine the two integrals in the exponent into a single integral starting out at time t_0, going to t, and then returning to t_0. In order to do so, one has to be careful that the order of the operators is preserved: the time-ordered integral from t_0 to t should be kept at the right of the operator $\hat{A}(t)$, whereas the anti-time-ordered integral from t back to t_0 should remain at the left of $\hat{A}(t)$. The correct order is preserved if we shift to an integration over a "contour" c that starts at time t_0, goes to time t, and returns to time t_0, and order all products according to their position along the contour: operators that have time arguments that appear "late" in the contour appear on the left of operators with time arguments that appear "early" in the contour. The contour c is shown in Fig. 1.1. Note that "early" and "late" according to the contour-ordering does not have to be earlier or later according to the true physical time. Writing such a "contour-ordering" operator as $T_{\rm c}$, we then find the formal expression

$$\hat{A}_{\rm H}(t) = T_{\rm c} e^{-(i/\hbar)\int_{\rm c} dt' \hat{H}_1(t')} A(t). \tag{1.27}$$

In fact, instead of the contour shown in Fig. 1.1, one can use the "Keldysh contour", which is shown in Fig. 1.2. The Keldysh contour starts from t_0, extends past time t up to infinite time, and then returns to t_0. The integration for times larger than t is redundant and cancels from the exponent.

In these notes we'll use all three pictures. Mostly, the context provides sufficient information to find out which picture is used. As a general rule, operators without time argument

are operators in the Schrödinger picture, whereas operators with time argument are in the Heisenberg and interaction pictures. We'll use this convention even if the Schrödinger picture operators have an explicit time dependence, cf. Eq. (1.15) above.

1.3 imaginary time

When performing a calculation that involves a thermal average, it is often convenient to introduce operators that are a function of the *imaginary time* τ.

Unlike real time arguments, imaginary times have no direct physical meaning. Imaginary time is used for the theorist's convenience, because Green functions, the mathematical machinery used to approach the many-particle problem, have very useful mathematical properties if regarded as a function of a complex time and frequency, instead of just real times and frequencies. The imaginary time formalism is usually not used for time-dependent Hamiltonians: it would be awkward to specify how a certain time dependence $\hat{H}(t)$ translates into imaginary time!

You can see why imaginary times can be useful from the following observation: A thermal average brings about a negative exponents $e^{-\hat{H}/T}$, whereas the real time dependence brings about imaginary exponents $e^{i\hat{H}t}$. For calculations, it would have been much easier if all exponents were either real or imaginary. To treat both real and imaginary exponents at the same time is rather awkward. Therefore, we'll opt to consider operators that depend on an imaginary time argument, so that the imaginary exponent $e^{i\hat{H}t}$ is replaced by $e^{\hat{H}\tau}$. If only imaginary times are used, only real exponents occur. This leads to much simpler calculations, as we'll see soon. The drawback of the change from real times to imaginary times is that, at the end of the calculation, one has to perform an analytical continuation from imaginary times to real times, which requires considerable mathematical care.

In the Schrödinger picture, the imaginary time variable appears in the evolution operator $\hat{U}(\tau,\tau')$, which now reads

$$\hat{U}(\tau,\tau') = e^{-\hat{H}(\tau-\tau')/\hbar}, \quad -\hbar\frac{\partial}{\partial\tau}\hat{U}(\tau,\tau') = \hat{H}\hat{U}(\tau,\tau'). \tag{1.28}$$

Since a thermal average necessarily involves a time-independent Hamiltonian, we could give an explicit expression for the evolution operator. Note that the evolution operator (1.28) satisfies the group properties $\hat{U}(\tau,\tau) = 1$ and $\hat{U}(\tau,\tau')\hat{U}(\tau',\tau'') = \hat{U}(\tau,\tau'')$, but that it is no longer unitary.

In the Heisenberg picture, the imaginary time variable appears through the relation

$$\hat{A}(\tau) = e^{\hat{H}\tau/\hbar}\hat{A}e^{-\hat{H}\tau/\hbar}, \quad \frac{\partial\hat{A}(\tau)}{\partial\tau} = \frac{1}{\hbar}[\hat{H},\hat{A}]_-, \tag{1.29}$$

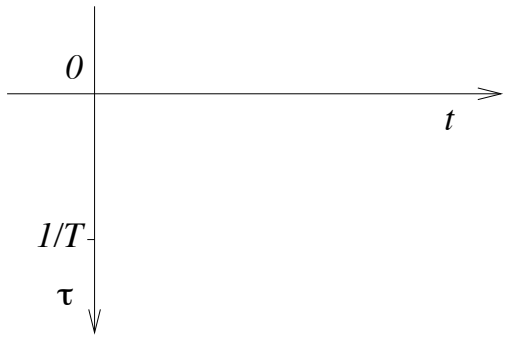

Figure 1.3: Relation between real time t and imaginary time τ.

where $\hat{A}$ is the corresponding real-time operator. Again, $\hat{H}$ is assumed to be time independent.

In the interaction picture, the time dependence of the operators is given by

$$\hat{A}(\tau) = e^{\hat{H}_0\tau/\hbar}\hat{A}e^{-\hat{H}_0\tau/\hbar}, \quad \frac{\partial\hat{A}(\tau)}{\partial\tau} = \frac{1}{\hbar}[\hat{H}_0, \hat{A}]_-, \tag{1.30}$$

whereas the time dependence of the quantum state $|\psi(\tau)\rangle$ is given by the interaction picture evolution operator

$$\hat{U}_I(\tau,\tau') = e^{\hat{H}_0\tau/\hbar}e^{-\hat{H}(\tau-\tau')/\hbar}e^{-\hat{H}_0\tau'/\hbar}, \quad -\hbar\frac{\partial}{\partial\tau}\hat{U}_I(\tau,\tau') = \hat{H}_1(\tau)\hat{U}(\tau,\tau'). \tag{1.31}$$

Here $\hat{H}_1(\tau) = e^{\hat{H}_0\tau/\hbar}\hat{H}_1e^{-\hat{H}_0\tau/\hbar}$ is the perturbation in the interaction picture.

The relation between the real time t and the imaginary time τ is illustrated in Fig. 1.3.

Since the interaction Hamiltonian $\hat{H}_1(\tau)$ depends on the imaginary time τ, the solution of Eq. (1.31) is not a simple exponential. However, as in the previous section, we can write down a formal solution using the concept of a time-ordering operator acting on imaginary times,

$$\hat{U}_I(\tau,\tau') = T_\tau e^{-(1/\hbar)\int_{\tau'}^{\tau} d\tau''\hat{H}_1(\tau'')}. \tag{1.32}$$

The imaginary-time-ordering operator T_τ arranges factors $\hat{H}_1(\tau'')$ from left to right with descending time arguments (ascending time arguments if $\tau' > \tau$). Similarly, the Heisenberg picture operator $\hat{A}_{\rm H}(\tau)$ can be expressed in terms of a contour-ordered exponential,

$$\hat{A}_{\rm H}(\tau) = T_{\rm c}e^{\int_{\rm c} d\tau'\hat{H}_1(\tau')}\hat{A}(\tau), \tag{1.33}$$

where the contour c goes from $\tau' = 0$ to $\tau' = \tau$ and back, see Fig. 1.4.

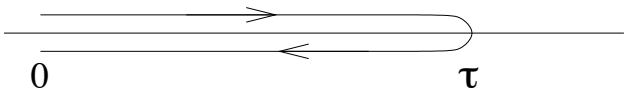

Figure 1.4: Contour used to the operator $\hat{A}_{\rm H}(\tau)$ in the Heisenberg picture from the corresponding operator $\hat{A}(\tau)$ in the interaction picture. The horizontal axis denotes imaginary time, not real time.

1.4 Exercises

Exercise 1.1: Evolution equation for expectation value (Ehrenfest Theorem)

Show that the time dependence of the expectation value of an observable A satisfies the differential equation

$$\frac{d}{dt}\left(\overline{A}\right)_t = \frac{i}{\hbar}\left(\overline{[\hat{H},\hat{A}]_-}\right)_t,$$

if the operator $\hat{A}$ has no explicit time dependence.

Exercise 1.2: Free particle, Schrödinger picture.

For a free particle with mass m, express the expectation values $(\overline{x_\alpha})_t$ and $(\overline{p_\alpha})_t$ of the components of the position and momentum at time t in terms of the corresponding expectation values at time 0 ($\alpha = x, y, z$). Use the Schrödinger picture.

Exercise 1.3: Free particle, Heisenberg picture

Derive the Heisenberg picture evolution equations for the position and momentum operators of a free particle. Use your answer to express the expectation values $(\overline{x_\alpha})_t$ and $(\overline{p_\alpha})_t$ of the components of the position and momentum at time t in terms of the corresponding expectation values at time 0 ($\alpha = x, y, z$).

Exercise 1.4: Harmonic oscillator

Derive and solve the Heisenberg picture evolution equations for the position and momentum operators x and p of a one-dimensional harmonic oscillator with mass m and frequency ω_0.

Do the same for the corresponding creation and annihilation operators

$$\begin{aligned} a^\dagger &= (\omega_0 m/2\hbar)^{1/2} x - i(2\hbar\omega_0 m)^{-1/2} p \\ a &= (\omega_0 m/2\hbar)^{1/2} x + i(2\hbar\omega_0 m)^{-1/2} p. \end{aligned} \tag{1.34}$$

Verify that the energy is time-independent.

Exercise 1.5: Imaginary time

Derive and solve the imaginary-time Heisenberg picture evolution equations for the position and momentum operators of a one-dimensional harmonic oscillator with mass m and frequency ω_0. Do the same for the corresponding creation and annihilation operators, see Eq. (1.34).

Chapter 2

Green functions

Throughout this course we'll make use of "Green functions". These are nothing but the expectation value of a product of operators evaluated at different times. There is a number of important ways in which Green functions are defined and there are important relations between the different definitions. Quite often, a certain application calls for one Green function, whereas it is easier to calculate a different Green function for the same system.

We now present the various definitions of Green functions in the general case and the general relations between the Green functions. In the later chapters we discuss various physical applications that call for the use of Green functions.

For now, we'll restrict our attention to Green functions (or "correlation functions") defined for two operators $\hat{A}$ and $\hat{B}$, which do not need to be hermitian. Green functions defined for more than two operators can be defined in a similar way. In the applications, we'll encounter cases where the operators $\hat{A}$ and $\hat{B}$ are fermion or boson creation or annihilation operators, or displacements of atoms in a lattice, or current or charge densities.

We say that the operators $\hat{A}$ and $\hat{B}$ satisfy commutation relations if they describe bosons or if they describe fermions and they are even functions of fermion creation and annihilation operators. We'll refer to this case as the "boson" case, and use a $-$ sign in the formulas below. We say that the operators $\hat{A}$ and $\hat{B}$ satisfy anticommutation relations if they describe fermions and they are odd functions of in fermion creation and annihilation operators. We'll call this case the "fermion case", and use a $+$ sign in the formulas of the next sections.

2.1 Green functions with real time arguments

The so-called "greater" and "lesser" Green functions are defined as

$$G^{>}_{A;B}(t,t') \equiv -i\langle \hat{A}(t)\hat{B}(t')\rangle, \tag{2.1}$$

$$G^<_{A;B}(t,t') \equiv \pm i\langle \hat{B}(t')\hat{A}(t)\rangle, \tag{2.2}$$

where the + sign is for fermions and the − sign for bosons. Here the brackets $\langle \ldots \rangle$ denote an appropriately defined equilibrium or non-equilibrium average — more on that below. One further defines "retarded" and "advanced" Green functions, which are expectation values of the commutator of $\hat{A}(t)$ and $\hat{B}(t')$,

$$\begin{aligned} G^{\rm R}_{A;B}(t,t') &\equiv -i\theta(t-t')\langle [\hat{A}(t),\hat{B}(t')]_\pm\rangle, \\ &= \theta(t-t')[G^>_{A;B}(t,t') - G^<_{A;B}(t,t')] \qquad (2.3) \\ G^{\rm A}_{A;B}(t,t') &\equiv i\theta(t'-t)\langle [\hat{A}(t),\hat{B}(t')]_\pm\rangle \\ &= \theta(t'-t)[G^<_{A;B}(t,t') - G^>_{A;B}(t,t')]. \qquad (2.4) \end{aligned}$$

respectively, where $\theta(x) = 1$ if $x > 0$, $\theta(x) = 0$ if $x < 0$ and $\theta(0) = 1/2$. Here, $[\cdot,\cdot]_+$ is the anticommutator, $[\hat{A},\hat{B}]_+ = \hat{A}\hat{B} + \hat{B}\hat{A}$. Note that, by definition, $G^{\rm R}$ is zero for $t - t' < 0$ and $G^{\rm A}$ is zero for $t - t' > 0$.

One verifies that greater and lesser Green functions satisfy the relation

$$G^>_{A;B}(t,t') = -(G^>_{B^\dagger,A^\dagger}(t',t))^*, \quad G^<_{A;B}(t,t') = -(G^<_{B^\dagger,A^\dagger}(t',t))^*, \tag{2.5}$$

from which it follows that

$$G^{\rm A}_{B^\dagger;A^\dagger}(t';t) = G^{\rm R}_{A;B}(t;t')^*. \tag{2.6}$$

Also, note that by virtue of their definitions, one has the relation

$$G^>_{A;B}(t,t') = -(\pm 1)G^<_{B;A}(t',t), \tag{2.7}$$

from which it follows that

$$G^{\rm R}_{A;B}(t;t') = -(\pm 1)G^{\rm A}_{B;A}(t';t), \tag{2.8}$$

where the + sign applies to fermions and the − sign to bosons.

In the previous chapter we have seen that formal expressions for Heisenberg picture operators can be obtained using time-ordered and contour-ordered expressions. For that reason it is useful to define time-ordered and contour-ordered Green functions. Another reason why it is useful to consider time-ordered and contour-ordered Green functions is that there exists more mathematical machinery to calculate them than to calculate the Green functions defined sofar. A typical calculation thus starts at calculating time-ordered or contour-ordered Green functions and then uses these results to find physical quantities of interest.

Time ordered Green functions are defined as

$$\begin{aligned} G_{A;B}(t,t') &\equiv -i\langle T_t \hat{A}(t)\hat{B}(t')\rangle \\ &= -i\theta(t-t')\langle \hat{A}(t)\hat{B}(t')\rangle \pm i\theta(t'-t)\langle \hat{B}(t')\hat{A}(t)\rangle \\ &= \theta(t-t')G^{>}_{A;B}(t,t') + \theta(t'-t)G^{<}_{A;B}(t,t'). \end{aligned} \tag{2.9}$$

As before, the symbol "T_t" represents the "time-ordering operator". For fermions, time ordering is defined with an additional factor -1 for every exchange of operators, hence

$$T_t\hat{A}(t)\hat{B}(t') \equiv \begin{cases} \hat{A}(t)\hat{B}(t') & \text{if } t > t', \\ -(\pm)\hat{B}(t')\hat{A}(t) & \text{if } t < t'. \end{cases} \tag{2.10}$$

The "anti time-ordered" Green function and contour-ordered Green functions are defined similarly. Recall that for contour-ordered Green functions it is not the physical time argument, but the location on a contour along the time axis that determines the order of the operators.

If the averages $\langle \ldots \rangle$ are taken in thermal equilibrium (or, more generally, if they are taken in a stationary state), the Green functions depend on the time difference $t - t'$ only. Then, Fourier transforms of these Green functions are defined as

$$G^{>}_{A;B}(\omega) = \int_{-\infty}^{\infty} dt e^{i\omega t} G^{>}_{A;B}(t), \tag{2.11}$$

$$G^{<}_{A;B}(\omega) = \int_{-\infty}^{\infty} dt e^{i\omega t} G^{<}_{A;B}(t), \tag{2.12}$$

with similar definitions for the retarded, advanced, and time-ordered Green functions. Since $G^{\mathrm{R}}(t-t')$ is zero for $t < t'$, its Fourier transform $G^{\mathrm{R}}(\omega)$ is analytic for $\mathrm{Im}\,\omega > 0$. Similarly, the Fourier transform of the advanced Green function, $G^{\mathrm{A}}(\omega)$, is analytic for $\mathrm{Im}\,\omega < 0$. The inverse Fourier transforms are

$$G^{>}_{A;B}(t) = \frac{1}{2\pi}\int_{-\infty}^{\infty} d\omega e^{-i\omega t} G^{>}_{A;B}(\omega), \tag{2.13}$$

$$G^{<}_{A;B}(t) = \frac{1}{2\pi}\int_{-\infty}^{\infty} d\omega e^{-i\omega t} G^{<}_{A;B}(\omega). \tag{2.14}$$

Note that the fact that $G^{\mathrm{R}}(\omega)$ is analytic for $\mathrm{Im}\,\omega > 0$ implies that $G^{\mathrm{R}}(t-t') = 0$ for $t < t'$, and, similarly, that the fact that $G^{\mathrm{A}}(\omega)$ is analytic for $\mathrm{Im}\,\omega < 0$ implies that $G^{\mathrm{R}}(t-t') = 0$ for $t > t'$.

2.2 Green functions with imaginary time arguments

Green functions for operators with imaginary time arguments are referred to as "temperature Green functions". The temperature Green function $\mathcal{G}_{A;B}(\tau_1;\tau_2)$ for the operators $\hat{A}$ and $\hat{B}$ is defined as

$$\mathcal{G}_{A;B}(\tau_1;\tau_2) \equiv -\langle T_\tau \hat{A}(\tau_1)\hat{B}(\tau_2)\rangle. \tag{2.15}$$

Here, the brackets denote a thermal average and the symbol T_τ denotes time-ordering,

$$T_\tau \hat{A}(\tau_1)\hat{B}(\tau_2) = \theta(\tau_1-\tau_2)\hat{A}(\tau_1)\hat{B}(\tau_2) - (\pm 1)\theta(\tau_2-\tau_1)\hat{B}(\tau_2)\hat{A}(\tau_1). \tag{2.16}$$

As discussed previously, the + sign applies if the operators $\hat{A}$ and $\hat{B}$ satisfy fermion anticommutation relations, i.e., if they are of odd degree in fermion creation/annihilation operators. The $-$ sign applies if $\hat{A}$ and $\hat{B}$ are boson operators or if they are of even degree in fermion creation/annihilation operators. Note that, again, a factor -1 is added for every exchange of fermion operators. The definition (2.15) of the temperature Green function is used for the interval $-\hbar/T < \tau_1 - \tau_2 < \hbar/T$ only.

Temperature Green functions are used only for calculations that involve a thermal equilibrium at temperature T. Hence, making use of the cyclic property of the trace, we find

$$\begin{aligned}
\mathcal{G}_{A;B}(\tau_1,\tau_2) &= -\theta(\tau_1-\tau_2)\frac{1}{Z}\mathrm{tr}\, e^{\tau_1\hat{H}/\hbar}\hat{A}e^{-\tau_1\hat{H}/\hbar}e^{\tau_2\hat{H}/\hbar}\hat{B}e^{-\tau_2\hat{H}/\hbar}e^{-\hat{H}/T} \\
&\quad \pm \theta(\tau_2-\tau_1)\frac{1}{Z}\mathrm{tr}\, e^{\tau_2\hat{H}/\hbar}\hat{B}e^{-\tau_2\hat{H}/\hbar}e^{\tau_1\hat{H}/\hbar}\hat{A}e^{-\tau_1\hat{H}/\hbar}e^{-\hat{H}/T} \\
&= -\theta(\tau_1-\tau_2)\frac{1}{Z}\mathrm{tr}\, e^{(\tau_1-\tau_2)\hat{H}/\hbar}\hat{A}e^{-(\tau_1-\tau_2)\hat{H}/\hbar}\hat{B}e^{-\hat{H}/T} \\
&\quad \pm \theta(\tau_2-\tau_1)\frac{1}{Z}\mathrm{tr}\, \hat{B}e^{(\tau_1-\tau_2)\hat{H}/\hbar}\hat{A}e^{-(\tau_1-\tau_2)\hat{H}/\hbar}e^{-\hat{H}/T} \\
&= \mathcal{G}_{A;B}(\tau_1-\tau_2,0),
\end{aligned} \tag{2.17}$$

so that $\mathcal{G}(\tau_1,\tau_2)$ depends on the imaginary time difference $\tau_1-\tau_2$ only. Hence, we can write $\mathcal{G}(\tau_1-\tau_2)$ instead of $\mathcal{G}(\tau_1,\tau_2)$. For $\mathcal{G}_{A;B}(\tau)$ with $0 \le \tau < \hbar/T$ we further have

$$\begin{aligned}
\mathcal{G}_{A;B}(\tau) &= -\frac{1}{Z}\mathrm{tr}\, e^{\tau\hat{H}/\hbar}\hat{A}e^{-\tau\hat{H}/\hbar}\hat{B}e^{-\hat{H}/T} \\
&= -\frac{1}{Z}\mathrm{tr}\, e^{-\hat{H}/T}e^{\tau\hat{H}/\hbar}\hat{A}e^{-\tau\hat{H}/\hbar}\hat{B} \\
&= -\frac{1}{Z}\mathrm{tr}\, e^{(\tau-\hbar/T)\hat{H}/\hbar}\hat{A}e^{-(\tau-\hbar/T)\hat{H}/\hbar}e^{-\hat{H}/T}\hat{B} \\
&= -(\pm 1)\mathcal{G}_{A;B}(\tau-\hbar/T).
\end{aligned} \tag{2.18}$$

Hence, on the interval $-\hbar/T < \tau < \hbar/T$, $\mathcal{G}(\tau)$ is periodic with period $\hbar/T$ and antiperiodic with the same period for fermions. This property is used to extend the definition of the temperature Green function $\mathcal{G}(\tau)$ to the entire imaginary time axis

If the operators $\hat{A}$ and $\hat{B}$ and the Hamiltonian $\hat{H}$ are all symmetric, the temperature Green function is symmetric or antisymmetric in the time argument, for the boson and fermion cases, respectively,

$$\mathcal{G}_{A;B}(\tau) = -(\pm 1)\mathcal{G}_{A;B}(-\tau) \text{ if } \hat{A},\ \hat{B},\ \hat{H} \text{ symmetric.} \tag{2.19}$$

Using the periodicity of $\mathcal{G}$, one may write $\mathcal{G}$ as a Fourier series,

$$\mathcal{G}_{A;B}(\tau) = \frac{T}{\hbar}\sum_n e^{-i\omega_n\tau}\mathcal{G}_{A;B}(i\omega_n), \tag{2.20}$$

with frequencies $\omega_n = 2\pi nT/\hbar$, n integer, for bosons and $\omega_n = (2n+1)\pi T/\hbar$ for fermions. The inverse relation is

$$\mathcal{G}_{A,B}(i\omega_n) = \int_0^{\hbar/T} d\tau e^{i\omega_n\tau}\mathcal{G}_{A,B}(\tau). \tag{2.21}$$

The frequencies ω_n are referred to as "Matsubara frequencies".

There exists a very useful expression for the temperature Green function in the interaction picture. Let us recall the definition of the temperature Green function $\mathcal{G}_{A;B}(\tau_1,\tau_2)$ for the case $0 < \tau_2 < \tau_1 < \hbar/T$,

$$\begin{aligned}\mathcal{G}_{A;B}(\tau_1,\tau_2) &= -\langle \hat{A}_{\rm H}(\tau_1)\hat{B}_{\rm H}(\tau_2)\rangle \\ &= -\frac{\operatorname{tr} e^{-\hat{H}/T}\hat{A}_{\rm H}(\tau_1)\hat{B}_{\rm H}(\tau_2)}{\operatorname{tr} e^{-\hat{H}/T}}.\end{aligned} \tag{2.22}$$

We wrote the index "H" denoting Heisenberg picture operators explicitly, to avoid confusion with the interaction picture operators to be used shortly.

In the previous chapter, we have seen that the imaginary-time Heisenberg picture operators $\hat{A}_{\rm H}(\tau_1)$ and $\hat{B}_{\rm H}(\tau_2)$ can be written in terms of the contour-ordered product of the corresponding interaction picture operators and an exponential of the perturbation to the Hamiltonian, see Eq. (1.27). Similarly, nothing that the exponential $e^{-\hat{H}/T}$ is nothing but the imaginary time evolution operator, Eq. (1.22) implies that it can be written as

$$e^{-\hat{H}/T} = e^{-\hat{H}_0/T}T_\tau e^{-\int_0^{\hbar/T} d\tau' \hat{H}_1(\tau')/T}. \tag{2.23}$$

Substituting these results into Eq. (2.22), we find

$$\mathcal{G}_{A;B}(\tau_1,\tau_2) = -\frac{\operatorname{tr} T_{\rm c} e^{-\hat{H}_0/T}e^{-\int_{\rm c} d\tau' \hat{H}_1(\tau')/T}\hat{A}(\tau_1)\hat{B}(\tau_2)}{\operatorname{tr} T_\tau e^{-\hat{H}_0/T}e^{-\int_0^{\hbar/T} d\tau' \hat{H}_1(\tau')/T}}, \tag{2.24}$$

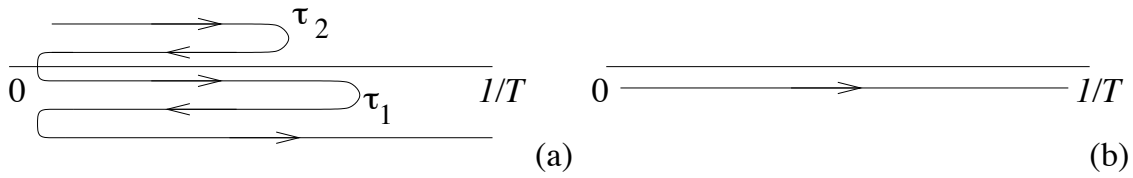

Figure 2.1: Integration contour for the evaluation of the imaginary time Green function $\mathcal{G}_{A;B}(\tau_1, \tau_2)$ using the interaction picture. The contour shown in (a) can be deformed to a simple line connecting the points $\tau = 0$ and $\tau = \hbar/T$ (b).

where the contour c is shown in Fig. 2.1. The contour can be deformed into a straight integration from 0 to $\hbar/T$, see Fig. 2.1, so that we obtain the remarkably simple result

$$\begin{aligned} \mathcal{G}_{A;B}(\tau_1, \tau_2) &= -\frac{\mathrm{tr}\, T_\tau e^{-\hat{H}_0/T} e^{-\int_0^{\hbar/T} d\tau' \hat{H}_1(\tau')/T} \hat{A}(\tau_1)\hat{B}(\tau_2)}{\mathrm{tr}\, T_\tau e^{-\hat{H}_0/T} e^{-\int_0^{\hbar/T} d\tau' \hat{H}_1(\tau')/T}} \\ &= -\frac{\langle T_\tau e^{-\int_0^{\hbar/T} d\tau' \hat{H}_1(\tau')/T} \hat{A}(\tau_1)\hat{B}(\tau_2)\rangle_0}{\langle T_\tau e^{-\int_0^{\hbar/T} d\tau' \hat{H}_1(\tau')/T}\rangle_0}, \end{aligned} \tag{2.25}$$

where the brackets $\langle \ldots \rangle_0$ denote an average with respect to the unperturbed Hamiltonian $\hat{H}_0$. One easily verifies that this final result does not depend on the assumption $\tau_2 > \tau_1$.

2.3 Green functions in thermal equilibrium

In thermal equilibrium, all Green functions defined in the previous two sections are related. This is an enormous help in actual calculations.

In many applications is it difficult, if not impossible, to calculate Green functions exactly. Instead, we have to rely on perturbation theory or other approximation methods. Whereas physical observables are often expressed in terms of greater and lesser Green functions (for correlation functions) or advandced and retarded Green functions (for response functions), the theoretical machinery is optimized for the calculation of the time-ordered, contour-ordered, and imaginary time Green functions. The relations we explored in this chapter allow one to relate retarded, advanced, and temperature Green functions to the temperature, time-ordered, and contour-ordered Green functions. Hence, these relations are a crucial link between what can be calculated easily and what is desired to be calculated.

Before we explain those relations, it is helpful to define a "real part" and "imaginary part" of a Green function. In the time representation, we define the "real part" $\Re G$ of the

retarded, advanced, and time-ordered Green functions as

$$\Re G^{\rm R}_{A;B}(t;t') = \frac{1}{2}\left(G^{\rm R}_{A;B}(t;t') + G^{\rm R}_{B^\dagger;A^\dagger}(t';t)^*\right), \tag{2.26}$$

$$\Re G^{\rm A}_{A;B}(t;t') = \frac{1}{2}\left(G^{\rm A}_{A;B}(t;t') + G^{\rm A}_{B^\dagger;A^\dagger}(t';t)^*\right), \tag{2.27}$$

$$\Re G_{A;B}(t;t') = \frac{1}{2}\left(G_{A;B}(t;t') + G_{B^\dagger;A^\dagger}(t';t)^*\right). \tag{2.28}$$

Similarly, we define the "imaginary part" $\Im G$ as

$$\Im G^{\rm R}_{A;B}(t;t') = \frac{1}{2i}\left(G^{\rm R}_{A;B}(t;t') - G^{\rm R}_{B^\dagger;A^\dagger}(t';t)^*\right), \tag{2.29}$$

$$\Im G^{\rm A}_{A;B}(t;t') = \frac{1}{2i}\left(G^{\rm A}_{A;B}(t;t') - G^{\rm A}_{B^\dagger;A^\dagger}(t';t)^*\right), \tag{2.30}$$

$$\Im G_{A;B}(t;t') = \frac{1}{2i}\left(G_{A;B}(t;t') - G_{B^\dagger;A^\dagger}(t';t)^*\right). \tag{2.31}$$

These "real" and "imaginary" parts of Green functions are different from the standard real and imaginary parts $\mathrm{Re}\, G$ and $\mathrm{Im}\, G$. In particular, $\Re G$ and $\Im G$ are not necessarily real numbers. The quantities $\Re G$ and $\Im G$ are defined with respect to a "hermitian conjugation" that consists of ordinary complex conjugation, interchange and hermitian conjugation of the operators $\hat{A}$ and $\hat{B}$, and of the time arguments. The assignments $\Re$ and $\Im$ are invariant under this hermitian conjugation and are preserved under Fourier transform of the time variable t,

$$\Re G_{A;B}(\omega) = \frac{1}{2}\left(G_{A;B}(\omega) + G_{B^\dagger;A^\dagger}(\omega)^*\right), \tag{2.32}$$

$$\Im G_{A;B}(\omega) = \frac{1}{2i}\left(G_{A;B}(\omega) - G_{B^\dagger;A^\dagger}(\omega)^*\right). \tag{2.33}$$

with similar expressions for the retarded and advanced Green functions.

By virtue of Eq. (2.6), the retarded and advanced Green functions are hermitian conjugates, hence

$$\Re G^{\rm R}(\omega) = \Re G^{\rm A}(\omega), \tag{2.34}$$

$$\Im G^{\rm R}(\omega) = -\Im G^{\rm A}(\omega). \tag{2.35}$$

Similarly, by employing their definitions and with repeated use of the relation

$$\langle \hat{A}(t)\hat{B}(t')\rangle^* = \langle \hat{B}^\dagger(t')\hat{A}^\dagger(t)\rangle, \tag{2.36}$$

one finds a relation between the real parts of the time-ordered and the retarded or advanced Green functions,

$$\Re G^{\rm R}(\omega) = \Re G(\omega), \tag{2.37}$$
$$\Re G^{\rm A}(\omega) = \Re G(\omega). \tag{2.38}$$

Shifting the t-integration from the real axis to the line $t - i\hbar/T$, one derives the general relation

$$\int dt e^{i\omega t}\langle \hat{A}(t)\hat{B}(0)\rangle = e^{\hbar\omega/T}\int dt e^{i\omega t}\langle \hat{B}(0)\hat{A}(t)\rangle, \tag{2.39}$$

valid in thermal equilibrium. Using Eq. (2.39), together with Eq. (2.36), one finds a relation for the imaginary parts of the time-ordered and retarded or advanced Green functions. This relation follows from the fact that the imaginary parts of the retarded, advanced, and time-ordered Green functions do not involve theta functions. Indeed, for the imaginary part of the retarded and advanced functions one finds

$$\begin{aligned}
\Im G^{\rm R}_{A;B}(\omega) &= -\Im G^{\rm A}_{A;B}(\omega) \\
&= -\frac{1}{2}\int_{-\infty}^{\infty} dt e^{i\omega t}\langle \hat{A}(t)\hat{B}(0) \pm \hat{B}(0)\hat{A}(t)\rangle \\
&= -\frac{1}{2}\left(1 \pm e^{-\hbar\omega/T}\right)\int_{-\infty}^{\infty} dt e^{i\omega t}\langle \hat{A}(t)\hat{B}(0)\rangle \\
&= -\frac{i}{2}\left(1 \pm e^{-\hbar\omega/T}\right) G^{>}_{A;B}(\omega),
\end{aligned} \tag{2.40}$$

whereas for the time-ordered Green function one has

$$\begin{aligned}
\Im G_{A;B}(\omega) &= -\frac{1}{2}\int_{-\infty}^{\infty} dt e^{i\omega t}\langle \hat{A}(t)\hat{B}(0) - (\pm 1)\hat{B}(0)\hat{A}(t)\rangle \\
&= -\frac{1}{2}\left(1 - (\pm 1)e^{-\hbar\omega/T}\right)\int_{-\infty}^{\infty} dt e^{i\omega t}\langle \hat{A}(t)\hat{B}(0)\rangle \\
&= -\frac{i}{2}\left(1 - (\pm)e^{-\hbar\omega/T}\right) G^{>}_{A;B}(\omega).
\end{aligned} \tag{2.41}$$

Hence, we find

$$\Im G^{\rm R}(\omega) = \frac{1 + (\pm 1)e^{-\hbar\omega/T}}{1 - (\pm 1)e^{-\hbar\omega/T}}\Im G(\omega), \tag{2.42}$$
$$\Im G^{\rm A}(\omega) = -\frac{1 + (\pm 1)e^{-\hbar\omega/T}}{1 - (\pm 1)e^{-\hbar\omega/T}}\Im G(\omega), \tag{2.43}$$

where the + sign is for fermion operators and the − sign for boson operators.

With the help of the Fourier representation of the step function,

$$\theta(t) = \frac{1}{2\pi i}\int_{-\infty}^{\infty} d\omega' \frac{e^{i\omega' t}}{\omega' - i\eta}, \tag{2.44}$$

where η is a positive infinitesimal, and of the second line of Eq. (2.40), one shows that knowledge of the imaginary part of the retarded Green function (or of the advanced Green function) is sufficient to calculate the full retarded Green function,

$$\begin{aligned} G^{\mathrm{R}}_{AB}(\omega) &= -\frac{1}{2\pi}\int d\omega' \frac{1}{\omega' - \omega - i\eta}\int_{-\infty}^{\infty} dt e^{i\omega' t}\langle \hat{A}(t)\hat{B}(0) \pm \hat{B}(0)\hat{A}(t)\rangle \\ &= \frac{1}{\pi}\int_{-\infty}^{\infty} d\omega' \frac{\Im G^{\mathrm{R}}_{A;B}(\omega')}{\omega' - \omega - i\eta}. \end{aligned} \tag{2.45}$$

Similarly, one finds

$$G^{\mathrm{A}}_{A;B}(\omega) = -\frac{1}{\pi}\int_{-\infty}^{\infty} d\omega' \frac{\Im G^{\mathrm{A}}_{A;B}(\omega')}{\omega' - \omega + i\eta}. \tag{2.46}$$

The numerator of the fractions in Eqs. (2.45) and (2.46) is known as the "spectral density",

$$A_{A;B}(\omega) = -2\Im G^{\mathrm{R}}(\omega) = 2\Im G^{\mathrm{A}}(\omega). \tag{2.47}$$

The spectral density satisfies the normalization condition

$$\frac{1}{2\pi}\int_{-\infty}^{\infty} d\omega A_{A;B}(\omega) = \langle [\hat{A}, \hat{B}]_{\pm}\rangle. \tag{2.48}$$

Similarly, we can express the Fourier transforms $G^{>}(\omega)$ and $G^{<}(\omega)$ of the greater and lesser Green functions in terms of the spectral density,

$$G^{>}_{A;B}(\omega) = -\frac{iA_{A;B}(\omega)}{1 \pm e^{-\hbar\omega/T}}, \tag{2.49}$$

$$G^{<}_{A;B}(\omega) = \frac{iA_{A;B}(\omega)}{1 \pm e^{\hbar\omega/T}}. \tag{2.50}$$

Since the spectral density is real (in the sense that $A = \Re A$), we conclude that the greater and lesser Green functions are purely imaginary ($G^{>} = i\Im G^{>}$, $G^{<} = i\Im G^{<}$).

The greater and lesser Green functions describe time-dependent correlations of the observables A and B. In the next section, we'll see that the retarded and advanced Green

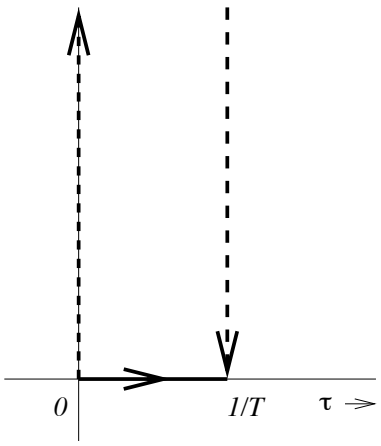

Figure 2.2: Integration contours for derivation of Eq. (2.51).

functions describe the response of the observable A to a perturbation B. The imaginary part of the response represents the dissipation. For that reason, Eqs. (2.49) and (2.50) are referred to as the "fluctuation-dissipation theorem".

Finally, by shifting integration contours as shown in Fig. 2.2, one can write the Fourier transform of the temperature Green function for $\omega_n > 0$ as

$$\begin{aligned}
\mathcal{G}_{A;B}(i\omega_n) &= -\int_0^{\hbar/T} d\tau e^{i\omega_n\tau}\langle\hat{A}(\tau)\hat{B}(0)\rangle \\
&= -i\int_0^{\infty} dt\langle\hat{A}(t)\hat{B}(0)\rangle e^{-\omega_n t} \\
&\quad + i\int_0^{\infty} dt\langle\hat{A}(t-i\hbar/T)\hat{B}(0)\rangle e^{-\omega_n t+i\hbar\omega_n/T} \\
&= -i\int_0^{\infty} dt\langle\hat{A}(t)\hat{B}(0)\rangle e^{-\omega_n t} \\
&\quad + i\int_0^{\infty} dt\langle\hat{B}(0)\hat{A}(t)\rangle e^{-\omega_n t+i\hbar\omega_n/T} \\
&= G^{\mathrm{R}}_{A;B}(i\omega_n). \qquad (2.51)
\end{aligned}$$

Here, we made use of the fact that $\exp(i\omega_n/T) = -(\pm 1)$ and of the fact that the Fourier transform of the retarded Green function is analytic in the upper half of the complex plane. In order to find the temperature Green function for negative Matsubara frequencies, one can make use of the relation

$$\mathcal{G}_{A;B}(i\omega_n) = \mathcal{G}_{B^\dagger;A^\dagger}(-i\omega_n)^*. \qquad (2.52)$$

Writing the retarded Green function in terms of the spectral density using Eqs. (2.45) and (2.47), one thus obtains the general expression

$$\mathcal{G}_{A;B}(i\omega_n) = -\frac{1}{2\pi}\int d\omega' \frac{A_{A;B}(\omega')}{\omega' - i\omega_n}, \tag{2.53}$$

which is valid for positive and for negative Matsubara frequencies.

2.4 Green functions outside thermal equilibrium

While there exists an elaborate and well-established framework to deal with systems in thermal equilibrium, a description of systems out of equilibrium seems to be a rather hopeless task. Here we describe a method to deal with systems out of equilibrium if it is known that the system was in equilibrium at some reference time t_0. After time t_0, a known perturbation was added to the Hamiltonian that drove the system out of equilibrium.

In order to describe the effect of the perturbation, we write the Hamiltonian as

$$\hat{H} = \hat{H}_0 + \hat{H}_1, \tag{2.54}$$

where the time dependence of the perturbation $\hat{H}_1$ is such that it is switched on slowly after a time t_0 long before the times we are interested in. Since we know the Hamiltonian for all times, we can we can express any operators at times t in terms of the corresponding operators at time t_0. In the interaction picture, this relation is given by Eq. (1.27), which we repeat here

$$\hat{A}_{\rm H}(t) = T_{\rm c} e^{-(i/\hbar)\int_{\rm c} dt' \hat{H}_1(t')} \hat{A}(t).$$

Here we choose c to be the Keldysh contour, see Fig. 1.2, which starts at the reference time t_0 runs to infinite time, and then returns to time t_0.

What does this imply for Green functions? Expressing both $\hat{A}(t)$ and $\hat{B}(t')$ in terms of the corresponding operators without the perturbation, one has for, *e.g.,* the greater Green function

$$G^{>}_{A;B}(t,t') = -i\langle T_c e^{-i\int_c dt_1 H_1(t_1)} \hat{A}(t)\hat{B}(t')\rangle_0, \tag{2.55}$$

where the brackets $\langle \ldots \rangle_0$ indicate a thermal average at time t_0. The contour c now consists of two trips from t_0 to infinity and back: one from the time evolution of $\hat{A}$ and one from the time evolution of $\hat{B}$, see Fig. 2.3. The time t corresponding to $\hat{A}$ will be assigned to the second part of the contour, whereas the time t' corresponding to $\hat{B}$ will be assigned to the first part of the contour. However, matters simplify considerably if we look at the contour-ordered Green function. In that case, the times t and t' represent positions on the

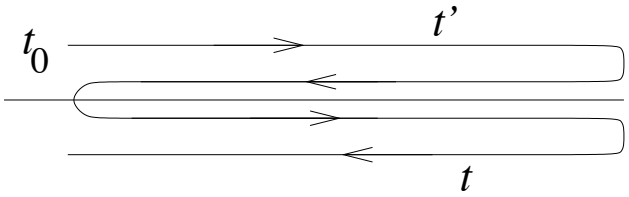

Figure 2.3: Contours used to calculate the greater Green functions $G^>$.

Keldysh contour. For a contour-ordered Green function, the contour time that appears on the left in the Green function is always later (in the contour sense). One can deform the contour of Fig. 2.3 such that the contour goes directly from t' to t, without the intermediate excursion to the reference time t_0 without one of the excursions to infinity. What remains is the standard Keldysh contour of Fig. 1.2, so that one has the simple result

$$G_{A;B}(t,t') = -i\langle T_c e^{-(i/\hbar)\int_c dt_1 H_1(t_1)} \hat{A}(t)\hat{B}(t')\rangle_0, \tag{2.56}$$

where c is the Keldysh contour.

Notice that if both both arguments are on the upper branch of the Keldysh contour, the contour-ordered Green function is nothing but the time-ordered Green function,

$$G(t,t') = -i\langle T_t \hat{A}_{\rm H}(t)\hat{B}_{\rm H}(t')\rangle, \quad t,\, t' \text{ upper branch.} \tag{2.57}$$

(We dropped the index "$A;B$" of the Green functions as no confusion is possible here.) Similarly, if both arguments are on the lower branch, $G(t,t')$ is equal to the "anti-time-ordered" Green function,

$$\begin{aligned} G(t,t') &= -i\theta(t'-t)\langle \hat{A}_{\rm H}(t)\hat{B}_{\rm H}(t')\rangle \pm i\theta(t-t')\langle \hat{B}_{\rm H}(t')\hat{A}_{\rm H}(t)\rangle \\ &\equiv -i\langle \tilde{T}_t \hat{A}_{\rm H}(t)\hat{B}_{\rm H}(t')\rangle, \quad t,\, t' \text{ lower branch,} \end{aligned} \tag{2.58}$$

whereas, if t is on the upper branch and t' is on the lower branch, or vice versa, one has

$$\begin{aligned} G(t,t') &= G^<(t,t') \qquad \text{if } t \text{ upper branch, } t' \text{ lower branch,} \\ G(t,t') &= G^>(t,t') \qquad \text{if } t \text{ lower branch, } t' \text{ upper branch.} \end{aligned} \tag{2.59}$$

We use this property to represent the Green function $G(t,t')$ as a 2×2 matrix, where the matrix index indicates what branch of the Keldysh contour is referred to (1 for upper branch and 2 for lower branch)

$$\begin{pmatrix} G_{11}(t,t') & G_{12}(t,t') \\ G_{21}(t,t') & G_{22}(t,t') \end{pmatrix} = \begin{pmatrix} -i\langle T_t \hat{A}_{\rm H}(t)\hat{B}_{\rm H}(t')\rangle & G^<(t,t') \\ G^>(t,t') & -i\langle \tilde{T}_t \hat{A}_{\rm H}(t)\hat{B}_{\rm H}(t')\rangle \end{pmatrix}. \tag{2.60}$$

In the matrix notation, the arguments t and t' refer to physical times, not contour positions.

In the literature, one usually uses a different representation of the matrix Green function (2.60),

$$\underline{G}(t,t') = \frac{1}{2}\begin{pmatrix} 1 & 1 \\ 1 & -1 \end{pmatrix}\begin{pmatrix} G_{11}(t,t') & G_{12}(t,t') \\ G_{21}(t,t') & G_{22}(t,t') \end{pmatrix}\begin{pmatrix} 1 & 1 \\ -1 & 1 \end{pmatrix}. \tag{2.61}$$

Note that the transformation in Eq. (2.61) is invertible, although it is not merely a shift of basis. Using Eq. (2.60) you quickly verify that

$$\underline{G}(t,t') = \begin{pmatrix} G^{\mathrm{R}}(t,t') & G^{\mathrm{K}}(t,t') \\ 0 & G^{\mathrm{A}}(t,t') \end{pmatrix}, \tag{2.62}$$

where $G^{\mathrm{R}}(t,t')$ and $G^{\mathrm{A}}(t,t')$ are the standard retarded and advanced Green functions (but now calculated outside equilibrium) and

$$G^{\mathrm{K}}(t,t') = G^{>}(t,t') + G^{<}(t,t') \tag{2.63}$$

is the so-called Keldysh Green function. Note that the special structure of the matrix (2.62) is preserved under matrix multiplication.

In equilibrium, or in a steady state situation, the matrix Green function $\underline{G}(t,t')$ depends on the time difference $t-t'$ only. In that case, one can look at the Fourier transform $\underline{G}(\omega)$. The Fourier transforms of the retarded and advanced Green functions were discussed previously. In thermal equilibrium, the Fourier transform of the Keldysh Green function satisfies the relation

$$G^{\mathrm{K}}_{A;B}(\omega) = (G^{\mathrm{R}}_{A;B}(\omega) - G^{\mathrm{A}}_{A;B}(\omega))\frac{e^{\hbar\omega/T} - (\pm 1)}{e^{\hbar\omega/T} + (\pm 1)} = -iA_{A;B}(\omega)\frac{e^{\hbar\omega/T} - (\pm 1)}{e^{\hbar\omega/T} + (\pm 1)}. \tag{2.64}$$

2.5 Linear Response

A special application of a non-equilibrium calculation is if we are interested in the response to first order in the perturbation $\hat{H}_1$ only. This situation is called *linear response*. Expanding Eq. (1.27) to first order in the perturbation $\hat{H}_1$, one has

$$\hat{A}_{\mathrm{H}}(t) = -\frac{i}{\hbar}\int_{t_0}^{t} dt'(\hat{A}(t)\hat{H}_1(t') - \hat{H}_1(t')\hat{A}(t)), \tag{2.65}$$

where $\hat{A}(t)$ and $\hat{H}_1(t)$ are the operators in the interaction picture: their time dependence is given by the *unperturbed* Hamiltonian $\hat{H}_0$.

The thermal average is performed for the observables at time t_0. Since the Hamiltonian for all earlier times is given by $\hat{H}_0$, this simply corresponds to a thermal average with respect to the Hamiltonian $\hat{H}_0$,

$$\langle \hat{A}(t) \rangle - \langle \hat{A} \rangle_0 = -\frac{i}{\hbar} \int_{t_0}^{t} \langle [\hat{A}(t), \hat{H}_1(t')]_- \rangle_0. \tag{2.66}$$

Since $\hat{H}_1(t) = 0$ for $t < t_0$, this can be rewritten as

$$\begin{aligned} \langle \hat{A}(t) \rangle - \langle \hat{A} \rangle_0 &= -\frac{i}{\hbar} \int_{-\infty}^{t} \langle [\hat{A}(t), \hat{H}_1(t')]_- \rangle_0 \\ &= \frac{1}{\hbar} \int_{-\infty}^{\infty} dt' G^{\mathrm{R}}_{A;\hat{H}_1}(t, t'), \end{aligned} \tag{2.67}$$

Here G^{R} is the retarded Green function, and we used the fact that $G^{\mathrm{R}}(t, t') = 0$ for $t' > t$.

Quite often, we are interested in the response to a perturbation that is known in the frequency domain,

$$\hat{H}_1 = \frac{1}{2\pi} \int d\omega e^{-i(\omega + i\eta)t} \hat{H}_1(\omega). \tag{2.68}$$

Here η is a positive infinitesimal and the factor $\exp(\eta t)$ has been added to ensure that $\hat{H}_1 \to 0$ if $t \to -\infty$. (In practice one does not need to require that $\hat{H}_1 = 0$ for times smaller than a reference time t_0; in most cases it is sufficient if $\hat{H}_1 \to 0$ fast enough if $t \to -\infty$.) Then Eq. (2.67) gives, after Fourier transform,

$$\begin{aligned} \langle \hat{A}(\omega) \rangle - \langle \hat{A}(\omega) \rangle_0 &= \int dt e^{i\omega t} (\langle \hat{A} \rangle - \langle \hat{A} \rangle_0) \\ &= G^{\mathrm{R}}_{A;H_1}(\omega + i\eta). \end{aligned} \tag{2.69}$$

Equation (2.69) is known as the "Kubo formula". It shows that the linear response to a perturbation $\hat{H}_1$, which is a nonequilibrium quantity, can be calculated from a retarded equilibrium Green function. For this reason, retarded Green functions (and advanced Green functions) are often referred to as "response functions".

Although the Kubo formula involves an integration over the real time t', for actual calculations, we can still use the imaginary time formalism and calculate the temperature Green function $\mathcal{G}_{A;H_1}(\tau)$. The response $\langle \hat{A}(\omega) \rangle$ is then found by Fourier transform of $\mathcal{G}$ to the Matsubara frequency domain, followed by analytical continuation $i\omega_n \to \omega$.

2.6 Harmonic oscillator

We'll now illustrate the various definitions and the relations between the Green functions by calculating all Green functions for the one-dimensional harmonic oscillator.

The Hamiltonian for a one-dimensional quantum-mechanical harmonic oscillator with mass m and frequency ω_0 is

$$\hat{H} = \frac{1}{2m}\hat{p}^2 + \frac{1}{2}m\omega_0^2\hat{x}^2. \tag{2.70}$$

The momentum and position operators satisfy canonical commutation relations,

$$[\hat{p},\hat{p}]_- = [\hat{x},\hat{x}]_- = 0, \quad [\hat{p},\hat{x}]_- = -i\hbar. \tag{2.71}$$

We now demonstrate two methods to calculate various harmonic oscillator Green functions if the harmonic oscillator is in thermal equilibrium at temperature T. First, we calculate all Green functions explicitly using the fact that we can diagonalize the harmonic oscillator Hamiltonian. Of course, our explicit solution will be found to obey the general relations between the different Green functions derived in the previous chapter. Then we use a different method, the so-called "equation of motion method" to find the temperature Green function $\mathcal{G}_{x;x}$.

The harmonic oscillator can be diagonalized by switching to creation and annihilation operators,

$$\hat{a} = x\sqrt{\frac{m\omega_0}{2\hbar}} + i\hat{p}\sqrt{\frac{1}{2m\omega_0\hbar}}, \quad \hat{a}^\dagger = x\sqrt{\frac{m\omega_0}{2\hbar}} - i\hat{p}\sqrt{\frac{1}{2m\omega_0\hbar}}, \tag{2.72}$$

so that

$$\hat{H} = \hbar\omega_0\left(\hat{a}^\dagger\hat{a} + \frac{1}{2}\right). \tag{2.73}$$

The creation and annihilation operators satisfy the commutation relation

$$[\hat{a},\hat{a}]_- = [\hat{a}^\dagger,\hat{a}^\dagger]_- = 0, \quad [\hat{a},\hat{a}^\dagger]_- = 1. \tag{2.74}$$

The explicit calculation of the Green functions uses the known Heisenberg time-evolution of the creation and annihilation operators,

$$\hat{a}(t) = e^{-i\omega_0 t}\hat{a}(0), \quad \hat{a}^\dagger(t) = e^{i\omega_0 t}\hat{a}^\dagger(0), \tag{2.75}$$

the commutation relations (2.74), and the equal-time averages

$$\langle\hat{a}(0)\hat{a}(0)\rangle \;=\; \langle\hat{a}^\dagger(0)\hat{a}^\dagger(0)\rangle = 0, \quad \langle\hat{a}^\dagger(0)\hat{a}(0)\rangle = \frac{1}{e^{\hbar\omega_0/T}-1}. \tag{2.76}$$

With the help of these results, one easily constructs averages involving the creation and annihilation operators at unequal times,

$$\begin{aligned}
\langle \hat{a}(t)\hat{a}(0)\rangle &= 0 \\
\langle \hat{a}(t)\hat{a}^\dagger(0)\rangle &= \frac{e^{-i\omega_0 t}}{1-e^{-\hbar\omega_0/T}}, \\
\langle \hat{a}^\dagger(t)\hat{a}(0)\rangle &= \frac{e^{i\omega_0 t}}{e^{\hbar\omega_0/T}-1}, \\
\langle \hat{a}^\dagger(t)\hat{a}^\dagger(0)\rangle &= 0.
\end{aligned} \tag{2.77}$$

Knowing these expectation values, it is straightforward to calculate all different Green functions involving the creation and annihilation operators,

$$\begin{aligned}
G^{>}_{a,a^\dagger}(t) &= \frac{-ie^{-i\omega_0 t}}{1-e^{-\hbar\omega_0/T}}, \\
G^{<}_{a,a^\dagger}(t) &= \frac{-ie^{-i\omega_0 t}}{e^{\hbar\omega_0/T}-1} \\
G^{\mathrm{R}}_{a,a^\dagger}(t) &= -i\theta(t)e^{-i\omega_0 t}, \\
G^{\mathrm{A}}_{a,a^\dagger}(t) &= i\theta(-t)e^{-i\omega_0 t}, \\
G_{a,a^\dagger}(t) &= \frac{-ie^{-i\omega_0 t}\,\mathrm{sign}\,(t)}{1-e^{-\hbar\omega_0\,\mathrm{sign}(t)/T}}.
\end{aligned} \tag{2.78}$$

Their Fourier transforms are

$$\begin{aligned}
G^{>}_{a,a^\dagger}(\omega) &= -2\pi i\delta(\omega-\omega_0)\frac{e^{\hbar\omega_0/T}}{e^{\hbar\omega_0/T}-1}, \\
G^{<}_{a,a^\dagger}(\omega) &= -2\pi i\delta(\omega-\omega_0)\frac{1}{e^{\hbar\omega_0/T}-1}, \\
G^{\mathrm{R}}_{a,a^\dagger}(\omega) &= -\frac{1}{\omega_0-\omega-i\eta}, \\
G^{\mathrm{A}}_{a,a^\dagger}(\omega) &= -\frac{1}{\omega_0-\omega+i\eta}, \\
G_{a,a^\dagger}(\omega) &= \frac{-1}{(\omega_0-\omega-i\eta)(1-e^{-\hbar\omega_0/T})} - \frac{1}{(\omega_0-\omega+i\eta)(1-e^{\hbar\omega_0/T})},
\end{aligned} \tag{2.79}$$

where η is a positive infinitesimal. From this we conclude that the spectral density is

$$A_{a,a^\dagger} = 2\pi\delta(\omega-\omega_0). \tag{2.80}$$

For the calculation of the imaginary time Green functions we need the Heisenberg time evolution for imaginary time, which is found from Eq. (2.75) by substituting $t \to -i\tau$,

$$\hat{a}(\tau) = e^{-\omega_0\tau}\hat{a}(0), \quad \hat{a}^\dagger(\tau) = e^{\omega_0\tau}\hat{a}^\dagger(0). \tag{2.81}$$

From this, one finds

$$\langle \hat{a}(\tau)\hat{a}^\dagger(0)\rangle = \frac{e^{-\omega_0\tau}}{1-e^{-\omega_0\hbar/T}}, \quad \langle \hat{a}^\dagger(\tau)\hat{a}(0)\rangle = \frac{e^{\omega_0\tau}}{e^{\omega_0\hbar/T}-1}, \tag{2.82}$$

hence, for $-\hbar/T < \tau < \hbar/T$,

$$\mathcal{G}_{a;a^\dagger}(\tau) = -\theta(\tau)\frac{e^{-\omega_0\tau}}{1-e^{-\omega_0\hbar/T}} - \theta(-\tau)\frac{e^{-\omega_0\tau-\omega_0\hbar/T}}{1-e^{-\omega_0\hbar/T}}. \tag{2.83}$$

You verify that the temperature Green function is periodic in τ, $\mathcal{G}(\tau+\hbar/T) = \mathcal{G}(\tau)$. The Fourier transform is

$$\mathcal{G}_{a;a^\dagger}(i\omega_n) = -\frac{1}{\omega_0 - i\omega_n}, \tag{2.84}$$

where $\omega_n = 2\pi T n/\hbar$, n integer, is a bosonic Matsubara frequency.

We can also calculate Green functions involving the position x at different times. Upon inverting Eq. (2.72) one finds

$$\begin{aligned} G^>_{x;x}(t) &= -i\langle \hat{x}(t)\hat{x}(0)\rangle \\ &= \frac{-i\hbar}{2m\omega_0}\langle \hat{a}(t)\hat{a}^\dagger(0) + \hat{a}^\dagger(t)\hat{a}(0)\rangle, \end{aligned} \tag{2.85}$$

plus terms that give zero after thermal averaging. Expressions for the other Green functions are similar. Using the averages calculated above, we then find

$$\begin{aligned} G^>_{x;x}(t) &= \frac{-i\hbar}{2m\omega_0}\left(\frac{e^{i\omega_0 t}}{e^{\omega_0\hbar/T}-1} + \frac{e^{-i\omega_0 t}}{1-e^{-\omega_0\hbar/T}}\right), \\ G^<_{x;x}(t) &= \frac{-i\hbar}{2m\omega_0}\left(\frac{e^{-i\omega_0 t}}{e^{\omega_0\hbar/T}-1} + \frac{e^{i\omega_0 t}}{1-e^{-\omega_0\hbar/T}}\right), \\ G^R_{x;x}(t) &= -\theta(t)\frac{\hbar}{m\omega_0}\sin(\omega_0 t), \\ G^A_{x;x}(t) &= \theta(-t)\frac{\hbar}{m\omega_0}\sin(\omega_0 t), \\ G_{x;x}(t) &= \frac{-i\hbar}{2m\omega_0}\left(\frac{e^{i\omega_0|t|}}{e^{\omega_0\hbar/T}-1} + \frac{e^{-i\omega_0|t|}}{1-e^{-\omega_0\hbar/T}}\right), \\ \mathcal{G}_{x;x}(\tau) &= -\frac{\hbar}{m\omega_0}\left(\frac{e^{\omega_0\tau}}{e^{\omega_0\hbar/T}-1} + \frac{e^{-\omega_0\tau}}{1-e^{-\omega_0\hbar/T}}\right). \end{aligned} \tag{2.86}$$

The Fourier transforms are

$$\begin{aligned}
G^{>}_{x;x}(\omega) &= \frac{-i\pi\hbar}{m\omega_0}\left(\frac{\delta(\omega+\omega_0)}{e^{\omega_0\hbar/T}-1}+\frac{\delta(\omega-\omega_0)}{1-e^{-\omega_0\hbar/T}}\right)\\
G^{<}_{x;x}(\omega) &= \frac{-i\pi\hbar}{m\omega_0}\left(\frac{\delta(\omega-\omega_0)}{e^{\omega_0\hbar/T}-1}+\frac{\delta(\omega+\omega_0)}{1-e^{-\omega_0\hbar/T}}\right)\\
G^{R}_{x;x}(\omega) &= -\frac{\hbar}{2m\omega_0}\left(\frac{1}{\omega_0-\omega-i\eta}+\frac{1}{\omega_0+\omega+i\eta}\right),\\
G^{A}_{x;x}(\omega) &= -\frac{\hbar}{2m\omega_0}\left(\frac{1}{\omega_0-\omega+i\eta}+\frac{1}{\omega_0+\omega-i\eta}\right),\\
G_{x;x}(\omega) &= \frac{\hbar}{m}\left[\frac{1}{(\omega^2-(\omega_0-i\eta)^2)(1-e^{-\omega_0\hbar/T})}-\frac{1}{(\omega^2-(\omega_0+i\eta)^2)(e^{\omega_0\hbar/T}-1)}\right]\\
\mathcal{G}_{x;x}(i\omega_n) &= -\frac{\hbar}{m(\omega_0^2+\omega_n^2)}
\end{aligned} \tag{2.87}$$

In this case, the spectral density is

$$A_{x;x}(\omega)=\frac{\pi\hbar}{m\omega_0}(\delta(\omega-\omega_0)-\delta(\omega+\omega-0)). \tag{2.88}$$

Note that both the Green functions $G_{a;a^\dagger}$ and the Green functions $G_{x;x}$ we just calculated satisfy all the relations derived in the previous chapter.

We now illustrate a different method to calculate the Green functions. We'll look at the example of the temperature Green function $\mathcal{G}_{x;x}(\tau)$, although the same method can also be applied to time-ordered real-time Green functions and Green functions involving other operators. The starting point in this method are the equations of motion for the Heisenberg operators $\hat{x}$ and $\hat{p}$,

$$\partial_\tau\hat{x}(\tau) = \frac{1}{\hbar}[\hat{H},\hat{x}(\tau)]_- = -\frac{i}{m}\hat{p}(\tau), \tag{2.89}$$

$$\partial_\tau\hat{p}(\tau) = \frac{1}{\hbar}[\hat{H},\hat{p}(\tau)]_- = mi\omega_0^2\hat{x}(\tau). \tag{2.90}$$

Then, using the definition of the temperature Green function, we find

$$\partial_\tau\mathcal{G}_{x;x}(\tau) = -\delta(\tau)\langle\hat{x}(\tau)\hat{x}(0)-\hat{x}(0)\hat{x}(\tau)\rangle+\frac{i}{m}\left[\theta(\tau)\langle\hat{p}(\tau)\hat{x}(0)\rangle+\theta(-\tau)\langle\hat{x}(0)\hat{p}(\tau)\rangle\right] \tag{2.91}$$

The first term arises from the derivative of the theta-function and is zero upon setting $\tau=0$ in the thermal average. In the second term we recognize the temperature Green function $\mathcal{G}_{p;x}(\tau)$, hence

$$\partial_\tau\mathcal{G}_{x;x}(\tau)=-\frac{i}{m}\mathcal{G}_{p;x}(\tau). \tag{2.92}$$

Taking one more derivative to τ, we find

$$\begin{aligned}\partial_\tau^2 \mathcal{G}_{x;x}(\tau) &= \frac{i}{m}\delta(\tau)\langle \hat{p}(\tau)\hat{x}(0) - \hat{x}(0)\hat{p}(\tau)\rangle - \omega_0^2\left[\theta(\tau)\langle \hat{x}(\tau)\hat{x}(0)\rangle + \theta(-\tau)\langle \hat{x}(0)\hat{x}(\tau)\rangle\right] \\ &= \frac{\hbar}{m}\delta(\tau) + \omega_0^2 \mathcal{G}_{x;x}(\tau). \end{aligned} \tag{2.93}$$

This equation is best solved by Fourier transform,

$$-\omega_n^2 \mathcal{G}_{x;x}(i\omega_n) = \frac{\hbar}{m} + \omega_0^2 \mathcal{G}_{x;x}(i\omega_n), \tag{2.94}$$

which reproduces Eq. (2.87) above. The advantage of the equation of motion approach is that one does not have to diagonalize the Hamiltonian in order to use it. However, more often than not the set of equations generated by this approach does not close, and one has to use a truncation scheme of some sort.

2.7 Exercises

Exercise 2.1: Lehmann representation

Explicit representations for Green functions can be obtained using the set of many-particle eigenstates $\{|n\rangle\}$ of the Hamiltonian H, as a basis set. For example, the greater Green function in the canonical ensemble can be written as

$$\begin{aligned} G^{>}_{A;B}(t,t') &= -\frac{i}{Z}\mathrm{tr}\,\hat{A}(t)\hat{B}(t')e^{-H/T} \\ &= -\frac{i}{Z}\sum_n e^{-E_n/T}\langle n|\hat{A}(t)\hat{B}(t')|n\rangle, \end{aligned} \tag{2.95}$$

where $Z=\sum_n e^{-E_n/T}$ is the canonical partition function. (In the grand canonical ensemble, similar expressions are obtained.) Inserting a complete basis set and using

$$\sum_{n'}|n'\rangle\langle n'| = 1,$$

we write Eq. (2.95) as

$$G^{>}_{A;B}(t,t') = -\frac{i}{Z}\sum_{n,n'} e^{-E_n/T+i(t-t')(E_n-E_{n'})}\langle n|\hat{A}|n'\rangle\langle n'|\hat{B}|n\rangle. \tag{2.96}$$

Performing the Fourier transform to time, one finds

$$G^{>}_{A;B}(\omega) = -\frac{2\pi i}{Z}\sum_{n,n'} e^{-E_n/T}\delta(E_n-E_{n'}+\omega)\langle n|\hat{A}|n'\rangle\langle n'|\hat{B}|n\rangle. \tag{2.97}$$

With the Lehmann representation, the general relations we derived in Sec. 2.3 can be verified explicitly.

(a) Verify that $G^{>}_{A;B}$ is purely imaginary (with respect to hermitian conjugation, as defined in Sec. 2.3).

(b) Derive Lehmann representations of the retarded, advanced, lesser, time-ordered, and temperature Green functions. Use the frequency representation.

(c) Derive the Lehmann representation of the spectral density $A_{A;B}(\omega)$.

(d) Verify the relations between the different types of Green functions that were derived in Sec. 2.3 using the Lehmann representations derived in (b) and (c).

Exercise 2.2: Spectral density

In this exercise we consider the spectral density $A_{A;B}(\omega)$ for the case $\hat{A} = c$, $\hat{B} = c^\dagger$ that the operators $\hat{A}$ and $\hat{B}$ are fermion or boson annihilation and creation operators, respectively. In this case, the spectral density $A_{c;c^\dagger}(\omega)$ can be viewed as the energy resolution of a particle created by the creation operator $c^\dagger$. To show that this is a plausible idea, you are asked to prove some general relations for the spectral density $A_{c;c^\dagger}(\omega)$. Consider the cases of fermions and bosons separately.

(a) The spectral density $A_{c;c^\dagger}(\omega)$ is normalized,

$$\frac{1}{2\pi}\int_{-\infty}^{\infty} d\omega A_{c;c^\dagger}(\omega) = 1. \tag{2.98}$$

(b) For fermions, the spectral density $A_{c;c^\dagger}(\omega) \geq 0$. For bosons, $A_{c;c^\dagger}(\omega) \geq 0$ if $\omega > 0$ and $A_{c;c^\dagger}(\omega) \leq 0$ if $\omega < 0$. (Hint: use the Lehmann representation of the spectral density.)

(c) The average occupation $\bar{n} = \langle c^\dagger c \rangle$ is

$$\bar{n} = \frac{1}{2\pi}\int_{-\infty}^{\infty} d\omega A_{c;c^\dagger}(\omega)\frac{1}{e^{\hbar\omega/T} \pm 1}. \tag{2.99}$$

(d) Now consider a Hamiltonian that is quadratic in creation and annihilation operators,

$$H = \sum_n \varepsilon_n c_n^\dagger c_n.$$

For this Hamiltonian, calculate the spectral density $A(n,\omega) \equiv A_{c_n;c_n^\dagger}(\omega)$.

Exercise 2.3: Harmonic oscillator

For the one-dimensional harmonic oscillator with mass m and frequency ω_0, calculate the retarded, advanced, greater, lesser, time-ordered, and temperature Green functions $G_{x;p}$ and $G_{p;p}$. List your results both in frequency and time representations.

Chapter 3

The Fermi Gas

3.1 Fermi Gas

Let us now consider a gas of non-interacting fermions. Since we deal with a system of many fermions, we use second quantization language. In second quantization notation, the Hamiltonian is written in terms of creation and annihilation operators $\hat{\psi}^\dagger_\sigma(\mathbf{r})$ and $\hat{\psi}_\sigma(\mathbf{r})$ of an electron at position $\mathbf{r}$ and with spin σ,

$$\hat{H} = \int d\mathbf{r} \sum_{\sigma,\sigma'} \hat{\psi}^\dagger_{\sigma'}(\mathbf{r}) \mathcal{H}_{\sigma'\sigma} \hat{\psi}_\sigma(\mathbf{r}), \tag{3.1}$$

where $\mathcal{H}$ is the first-quantization Hamiltonian. For free fermions, one has $\mathcal{H} = \hat{p}^2/2m$ with $\hat{p} = -i\hbar\partial_{\mathbf{r}}$, but many of the results we derive below also apply in the more general case when $\mathcal{H}$ contains a scalar potential, a magnetic field, or spin-orbit coupling. The operators $\hat{\psi}^\dagger_\sigma(\mathbf{r})$ and $\hat{\psi}_\sigma(\mathbf{r})$ satisfy anticommutation relations,

$$[\hat{\psi}_\sigma(\mathbf{r}), \hat{\psi}_{\sigma'}(\mathbf{r}')]_+ = [\hat{\psi}^\dagger_\sigma(\mathbf{r}), \hat{\psi}^\dagger_{\sigma'}(\mathbf{r}')]_+ = 0, \quad [\hat{\psi}_\sigma(\mathbf{r}), \hat{\psi}^\dagger_{\sigma'}(\mathbf{r}')]_+ = \delta_{\sigma\sigma'}\delta(\mathbf{r}-\mathbf{r}'). \tag{3.2}$$

In the Heisenberg picture, the operators $\hat{\psi}^\dagger$ and $\hat{\psi}$ are time dependent, and their time-dependence is given by

$$\partial_t \hat{\psi}_\sigma(\mathbf{r},t) \;=\; \frac{i}{\hbar}[\hat{H}, \hat{\psi}_\sigma(\mathbf{r},t)]_- = -\frac{i}{\hbar}\sum_{\sigma'} \mathcal{H}_{\sigma\sigma'} \hat{\psi}_{\sigma'}(\mathbf{r},t). \tag{3.3}$$

Note that the time-evolution of the Heisenberg picture annihilation operator $\hat{\psi}$ is formally identical to that of a single-particle wavefunction ψ in the Schrödinger picture.

Below we calculate the Green functions for the pair of operators $\hat{\psi}_\sigma(\mathbf{r})$ and $\hat{\psi}^\dagger_{\sigma'}(\mathbf{r}')$. We will denote these Green functions as $G_{\sigma,\sigma'}(\mathbf{r},\mathbf{r}';t)$. Using the equation of motion for the operator $\hat{\psi}(\mathbf{r},t)$, one can derive an equation of motion for the retarded Green function,

$$\begin{aligned}\partial_t G^{\rm R}_{\sigma,\sigma'}(\mathbf{r},\mathbf{r}';t) &= -i\delta(t)\langle\hat{\psi}_\sigma(\mathbf{r},t)\hat{\psi}^\dagger_{\sigma'}(\mathbf{r}',0)+\hat{\psi}^\dagger_{\sigma'}(\mathbf{r}',0)\hat{\psi}_\sigma(\mathbf{r},t)\rangle \\ &\quad - i\theta(t)\partial_t\langle\hat{\psi}_\sigma(\mathbf{r},t)\hat{\psi}^\dagger_{\sigma'}(\mathbf{r}',0)+\hat{\psi}^\dagger_{\sigma'}(\mathbf{r}',0)\hat{\psi}_\sigma(\mathbf{r},t)\rangle \\ &= -i\delta(t)\delta(\mathbf{r}-\mathbf{r}')\delta_{\sigma'\sigma}-\frac{i}{\hbar}\sum_{\sigma''}\mathcal{H}_{\sigma\sigma''}G^{\rm R}_{\sigma'',\sigma'}(\mathbf{r},\mathbf{r}';t). \qquad (3.4)\end{aligned}$$

where $\mathcal{H}_{\sigma\sigma'}$ is the first-quantization form of the single-particle Hamiltonian operating on the first argument of the Green function, see Eq. (3.3) above. The differential equation (3.6) is solved with the boundary condition $G^{\rm R}(t)=0$ for $t<0$. A similar calculation shows that the advanced Green function $G^{\rm A}$ satisfies the same equation, but with the boundary condition $G^{\rm A}(t)=0$ for $t>0$. The Keldysh Green function $G^{\rm K}$ satisfies the equation

$$\partial_t G^{\rm K}_{\sigma,\sigma'}(\mathbf{r},\mathbf{r}';t) = -\frac{i}{\hbar}\sum_{\sigma''}\mathcal{H}_{\sigma\sigma''}G^{\rm K}_{\sigma'',\sigma'}(\mathbf{r},\mathbf{r}';t) \qquad (3.5)$$

There are no boundary conditions for this equation. However, in equilibrium, $G^{\rm K}$ can be expressed in terms of $G^{\rm R}$ and $G^{\rm A}$, see Eq. (2.64). This information is sufficient to make the solution of Eq. (3.5) unique, even in non-equilibrium situtations.

Performing a Fourier transform, one finds

$$\frac{1}{\hbar}\sum_{\sigma''}(\hbar\omega\delta_{\sigma\sigma''}-\mathcal{H}_{\sigma\sigma''})G^{\rm R}_{\sigma'',\sigma'}(\mathbf{r},\mathbf{r}';\omega)=\delta_{\sigma\sigma'}\delta(\mathbf{r}-\mathbf{r}'), \qquad (3.6)$$

with similar equations for $G^{\rm A}$ and $G^{\rm K}$.

A formal solution of Eq. (3.6) can be obtained in in terms of the eigenvalues ε_μ and eigenfunctions $\phi_{\mu,\sigma}(\mathbf{r})$ of $\mathcal{H}$,

$$G^{\rm R}_{\sigma,\sigma'}(\mathbf{r},\mathbf{r}';\omega) = \hbar\sum_\mu\frac{\phi_{\mu,\sigma}(\mathbf{r})\phi^*_{\mu,\sigma'}(\mathbf{r}')}{\hbar\omega-\varepsilon_\mu+i\eta}, \qquad (3.7)$$

$$G^{\rm A}_{\sigma,\sigma'}(\mathbf{r},\mathbf{r}';\omega) = \hbar\sum_\mu\frac{\phi_{\mu,\sigma}(\mathbf{r})\phi^*_{\mu,\sigma'}(\mathbf{r}')}{\hbar\omega-\varepsilon_\mu-i\eta}, \qquad (3.8)$$

where η is a positive infinitesimal. One verifies that both the retarded and the advanced Green functions are analytical in the upper and lower half planes of the complex plane,

respectively. The spectral density $A_{\sigma\sigma'}(\mathbf{r},\mathbf{r}';\omega)$ is easily calculated from Eqs. (3.7) or (3.8),

$$A_{\sigma\sigma'}(\mathbf{r},\mathbf{r}';\omega) = 2\pi \sum_{\mu} \phi_{\mu,\sigma}(\mathbf{r})\phi^*_{\mu,\sigma'}(\mathbf{r}')\delta(\omega - \varepsilon_\mu/\hbar). \tag{3.9}$$

Notice that our calculation of the retarded and advanced Green functions did not use the requirement of thermal equilibrium. In thermal equilibrium, the other Green functions (greater, lesser, temperature, time-ordered) follow directly from the spectral density calculated here. Outside thermal equilibrium, calculation of the other Green functions requires knowledge of how the non-equilibrium state has been obtained.

3.2 Ideal Fermi Gas

In the absence of an impurity potential, the Hamiltonian is

$$\mathcal{H}_{\sigma\sigma'} = -\frac{\hbar^2}{2m}\partial^2_{\mathbf{r}}\delta_{\sigma\sigma'} \tag{3.10}$$

For fermions confined to a volume V with periodic boundary conditions, the eigenfunctions of the Hamiltonian (3.10) are plane waves,

$$\phi_{\mathbf{k}}(\mathbf{r}) = \frac{1}{\sqrt{V}} e^{i\mathbf{k}\cdot\mathbf{r}}. \tag{3.11}$$

(We dropped the spin index here.) Hence the free fermion Green function reads

$$G^{\mathrm{R}}(\mathbf{r},\mathbf{r}';\omega) = \frac{1}{V}\sum_{\mathbf{k}} \frac{e^{i\mathbf{k}\cdot(\mathbf{r}-\mathbf{r}')}}{\omega + i\eta - \varepsilon_{\mathbf{k}}/\hbar}, \quad G^{\mathrm{A}}(\mathbf{r},\mathbf{r}';\omega) = \frac{1}{V}\sum_{\mathbf{k}} \frac{e^{i\mathbf{k}\cdot(\mathbf{r}-\mathbf{r}')}}{\omega - i\eta - \varepsilon_{\mathbf{k}}/\hbar}, \tag{3.12}$$

with $\varepsilon_{\mathbf{k}} = \hbar^2 k^2/2m$. Replacing the $\mathbf{k}$-summation by an integration, one finds

$$G^{\mathrm{R}}(\mathbf{r},\mathbf{r}';\omega) = -\frac{m}{2\pi\hbar}\frac{e^{ik|\mathbf{r}-\mathbf{r}'|}}{|\mathbf{r}-\mathbf{r}'|}, \tag{3.13}$$

$$G^{\mathrm{A}}(\mathbf{r},\mathbf{r}';\omega) = -\frac{m}{2\pi\hbar}\frac{e^{-ik|\mathbf{r}-\mathbf{r}'|}}{|\mathbf{r}-\mathbf{r}'|}. \tag{3.14}$$

For the retarded Green function, k is the solution of $\omega + i\eta - \varepsilon_k = 0$ such that $\mathrm{Im}\, k > 0$, whereas for the advanced Green function, k is the solution of $\omega - i\eta - \varepsilon_k = 0$ with $\mathrm{Im}\, k < 0$.

It is interesting to note that the same result can be obtained without using the quadratic dispersion relation $\varepsilon_k = \hbar^2 k^2/2m$. Hereto one defines k as above and linearizes the spectrum around $\hbar\omega$

$$\varepsilon_{\mathbf{k}'} = \hbar\omega + \hbar v(|\mathbf{k}'| - k), \tag{3.15}$$

where v is the velocity. Then, performing the Fourier transform, one finds

$$\begin{aligned} G^{\mathrm{R}}(\mathbf{r},\mathbf{r}';\omega) &= \frac{1}{(2\pi)^3}\int_0^{2\pi} d\phi \int_{-1}^{1} d\cos\theta \int_0^{\infty} k'^2 dk' \frac{e^{ik'|\mathbf{r}-\mathbf{r}'|\cos\theta}}{i\eta - v(k'-k)} \\ &= \frac{1}{(2\pi)^2 i|\mathbf{r}-\mathbf{r}'|}\int_0^{\infty} k' dk' \frac{e^{ik'|\mathbf{r}-\mathbf{r}'|} - e^{-ik'|\mathbf{r}-\mathbf{r}'|}}{i\eta - v(k'-k)} \\ &\approx \frac{k}{4\pi^2 i|\mathbf{r}-\mathbf{r}'|v}\int_{-\infty}^{\infty} dx \frac{e^{i(k+x/v)|\mathbf{r}-\mathbf{r}'|} - e^{-i(k+x/v)|\mathbf{r}-\mathbf{r}'|}}{i\eta - x} \\ &= -\frac{m}{2\pi\hbar}\frac{e^{ik|\mathbf{r}-\mathbf{r}'|}}{|\mathbf{r}-\mathbf{r}'|}, \end{aligned} \tag{3.16}$$

and a similar result for the advanced Green function. For non-infinitesimal η, the final result needs to be multiplied by $e^{-\eta|\mathbf{r}-\mathbf{r}'|/v}$.

Because the ideal Fermi gas is translationally invariant, the Green functions depend on the position difference $\mathbf{r}-\mathbf{r}'$ only. Fourier transforming with respect to $\mathbf{r}-\mathbf{r}'$, one has

$$\begin{aligned} G^{\mathrm{R}}_{\mathbf{k}}(\omega) &= \int d\mathbf{r} G^{\mathrm{R}}(\mathbf{r}-\mathbf{r}';\omega) e^{-i\mathbf{k}\cdot(\mathbf{r}-\mathbf{r}')} \\ &= \frac{1}{\omega + i\eta - \varepsilon_{\mathbf{k}}/\hbar}, \end{aligned} \tag{3.17}$$

$$G^{\mathrm{A}}_{\mathbf{k}}(\omega) = \frac{1}{\omega - i\eta - \varepsilon_{\mathbf{k}}/\hbar}. \tag{3.18}$$

Alternatively, one may consider the Green function corresponding to the operators $\hat{\psi}_{\mathbf{k}}$ and $\hat{\psi}^{\dagger}_{\mathbf{k}'}$ that annihilate and create a fermion in an eigenstate with wavevector $\mathbf{k}$ and $\mathbf{k}'$, respectively. In terms of the operators $\hat{\psi}(\mathbf{r})$ and $\hat{\psi}^{\dagger}(\mathbf{r})$, one has

$$\hat{\psi}_{\mathbf{k}} = \frac{1}{\sqrt{V}}\int d\mathbf{r}\hat{\psi}(\mathbf{r})e^{-i\mathbf{k}\cdot\mathbf{r}}, \quad \hat{\psi}^{\dagger}_{\mathbf{k}} = \frac{1}{\sqrt{V}}\int d\mathbf{r}\hat{\psi}^{\dagger}(\mathbf{r})e^{i\mathbf{k}\cdot\mathbf{r}}.$$

Denoting this Green function with $G_{\mathbf{k},\mathbf{k}'}$, one has

$$G^{\mathrm{R}}_{\mathbf{k},\mathbf{k}'}(\omega) = \frac{1}{V}\int d\mathbf{r}d\mathbf{r}' G^{\mathrm{R}}(\mathbf{r},\mathbf{r}';\omega)e^{-i\mathbf{k}\cdot\mathbf{r}+i\mathbf{k}'\cdot\mathbf{r}'}$$

$$= \frac{\delta_{\mathbf{k},\mathbf{k}'}}{\omega + i\eta - \varepsilon_{\mathbf{k}}/\hbar}, \tag{3.19}$$

$$G^{\mathrm{A}}_{\mathbf{k},\mathbf{k}'}(\omega) = \frac{\delta_{\mathbf{k},\mathbf{k}'}}{\omega - i\eta - \varepsilon_{\mathbf{k}}/\hbar}. \tag{3.20}$$

3.3 Boltzmann equation

If the potential $U(\mathbf{r})$ varies slowly on the scale of the Fermi wavelength, one expects that the electrons will follow trajectories that are described by classical mechanics. In such a situation, one would expect that the Boltzmann equation will be a valid description of the many-electron system.

The Boltzmann equation describes the time-evolution of the distribution function $f_{\mathbf{k}}(\mathbf{r},t)$ that is the occupation of electronic states with wavevector $\mathbf{k}$ and position $\mathbf{r}$. Without collisions between electrons and without scattering from quantum impurities or phonons, the Boltzmann equation reads

$$\left(\partial_t + \mathbf{v}_{\mathbf{k}} \cdot \partial_{\mathbf{r}} - \hbar^{-1}\partial_{\mathbf{R}} U \cdot \partial_{\mathbf{k}}\right) f_{\mathbf{k}}(\mathbf{r},t) = 0, \tag{3.21}$$

where $\mathbf{v}_{\mathbf{k}} = \hbar^{-1}\partial_{\mathbf{k}}\varepsilon_{\mathbf{k}}$ is the electron's velocity. The use of a distribution that depends on an electron's position as well as its momentum is allowed only if the spatial variation of f is slow on the inverse of the scale for the $\mathbf{k}$-dependence of f. A faster spatial variation would violate the Heisenberg uncertainty relations. Hence, we expect that the Boltzmann equation works for slowly varying potentials.

We'll now show how the distribution function f and the Boltzmann equation can be obtained in the Green function language. For this, we'll use the real-time Keldysh formulation.

So far we have dealt with Green functions that depend on two spatial coordinates $\mathbf{r}$ and $\mathbf{r}'$ or on two wavenumbers $\mathbf{k}$ and $\mathbf{k}'$. For a semiclassical description, it is useful to use a "mixed" representation in which the Green function $\underline{G}$ is chosen to depend on sum and difference coordinates, followed by a Fourier transform to the difference coordinate,

$$\underline{G}(\mathbf{R},T;\mathbf{k},\omega) = \int d\mathbf{r} \int dt e^{-i\mathbf{k}\cdot\mathbf{r}+i\omega t} \underline{G}(\mathbf{R}+\mathbf{r}/2, T+t/2; \mathbf{R}-\mathbf{r}/2, T-t/2). \tag{3.22}$$

We'll refer to $\mathbf{R}$ and T as "center coordinate" and "center time", and to $\mathbf{k}$ and ω as momentum and frequency. The reason why one chooses to Fourier transform to the differences of spatial and temporal coordinates is the $\underline{G}(\mathbf{r},t;\mathbf{r}',t')$ is a fast oscillating function of $\mathbf{r}-\mathbf{r}'$ and $t-t'$, whereas it is a slowly varying function of the center coordinates $\mathbf{R} = (\mathbf{r}+\mathbf{r}')/2$ and $T = (t+t')/2$. In fact, for the ideal Fermi gas, $\underline{G}(\mathbf{r},t;\mathbf{r}',t')$ does not depend on $\mathbf{R}$ and

T at all. After Fourier transform, the oscillating dependence on the differences $\mathbf{r}-\mathbf{r}'$ and $t-t'$ results in a much less singular dependence on $\mathbf{k}$ and ω.

In order to write the first-quantization operators $\mathcal{H}$ and ∂t in the mixed representation, we first these operators in a form in which they depend on two spatial coordinates $\mathbf{r}$ and $\mathbf{r}'$ and two time coordinates,

$$\mathcal{H}(\mathbf{r},t;\mathbf{r}',t') \equiv \left(-\frac{\hbar^2}{2m}\partial_{\mathbf{r}}^2 - \mu + U(\mathbf{r})\right)\delta(\mathbf{r}-\mathbf{r}')\delta(t-t'), \quad (\partial_t)(\mathbf{r},t;\mathbf{r}',t') \equiv \partial_t\delta(\mathbf{r}-\mathbf{r}')\delta(t-t'). \tag{3.23}$$

Here U is the potential and we included the chemical potential μ in the definition of the Hamiltonian. In this notation, the operator action corresponds to a convolution with respect to the primed variables. Transforming to the mixed representation, we then find that the first-quantization Hamiltonian $\mathcal{H}$ and the time derivative ∂t take a particularly simple form,

$$\mathcal{H} = \varepsilon_{\mathbf{k}} - \mu + U(\mathbf{R},T), \quad \partial_t = -i\omega. \tag{3.24}$$

The matrix Green function $\underline{G}$ satisfies the differential equation

$$\left(\partial_t + \frac{i}{\hbar}\mathcal{H}\right)\underline{G}(\mathbf{r},t;\mathbf{r}',t') = -i\delta(t-t')\delta(\mathbf{r}-\mathbf{r}')\underline{1}, \tag{3.25}$$

where $\underline{1}$ is the 2×2 unit matrix, cf. Sec. 2.4. The equation has to be solved with the boundary condition $G^{\mathrm{R}} = 0$ for $t < t'$, $G^{\mathrm{A}} = 0$ for $t > t'$. In equilibrium, G^{K} is given by Eq. (2.64). In Eq. (3.25), the Green function $\underline{G}$ can be viewed a first-quantization operators. In operator language, Eq. (3.25) reads

$$\left(\partial_t + \frac{i}{\hbar}\mathcal{H}\right)\underline{G} = -i\underline{\mathcal{I}}, \tag{3.26}$$

where $\mathcal{I}$ is the identity operator and $\underline{\mathcal{I}} = \mathcal{I}\underline{1}$. Implicitly, we already used the operator picture in Sec. 3.1, when we calculated the Green functions of the Fermi gas using the equation of motion method and in Sec. 4.1. Considering the derivative to t', we find the related operator identity

$$\underline{G}\left(\partial_t + \frac{i}{\hbar}\mathcal{H}\right) = -i\underline{\mathcal{I}}. \tag{3.27}$$

Instead of working with Eqs. (3.26) and (3.27), one prefers to work with the sum and difference equations,

$$\left[\left(\partial_t + \frac{i}{\hbar}\mathcal{H}\right), \underline{G}\right]_- = 0 \tag{3.28}$$

$$\left[\left(\partial_t + \frac{i}{\hbar}\mathcal{H}\right), \underline{G}\right]_+ = -2i\mathcal{I}, \tag{3.29}$$

where $[\cdot,\cdot]_-$ and $[\cdot,\cdot]_+$ denote commutator and anticommutator, respectively.

Mathematically, the way Green functions act as first-quantization operators, as well as the way first-quantization operators act on single-particle Green functions, is a "convolution". The main disadvantage of the mixed representation (3.22) is that convolutions become rather awkward. Using Eq. (3.22) and its inverse to express the Wigner representation of the convolution (or operator product) $A_1 A_2$ in terms of the Wigner representations of the two factors A_1 and A_2, one finds

$$\begin{aligned} [A_1 A_2](\mathbf{R}, T; \mathbf{k}, \omega) &= e^{\frac{i}{2}\mathcal{D}} A_1(\mathbf{R}, T; \mathbf{k}, \omega) A_2(\mathbf{R}, T; \mathbf{k}, \omega), \\ \mathcal{D} &= \frac{\partial_1}{\partial_1 \mathbf{R}} \frac{\partial_2}{\partial_2 \mathbf{k}} - \frac{\partial_1}{\partial_1 T} \frac{\partial_2}{\partial_2 \omega} - \frac{\partial_2}{\partial_2 \mathbf{R}} \frac{\partial_1}{\partial_1 \mathbf{k}} + \frac{\partial_2}{\partial_2 T} \frac{\partial_1}{\partial_1 \omega}, \end{aligned} \tag{3.30}$$

where ∂_1 refers to a derivative with respect to an argument of A_1 and ∂_2 refers to a derivative

with respect to an argument of A_2.[1]

We now make use of the fact that the potential U is a slowly varying function of its arguments $\mathbf{R}$ and T. Then we expect that the Green function $G^{\rm K}$ will also be a slowly varying function of $\mathbf{R}$ and T. Calculating the operator products according to the rule (3.30) we can expand the exponential and truncate the expansion after first order. One then finds that a commutator becomes equal to a Poisson bracket,

$$\begin{aligned} -i[A_1,A_2]_- &= [A_1,A_2]_{\rm Poisson} \\ &= \left(\frac{\partial_1}{\partial_1\mathbf{R}}\frac{\partial_2}{\partial_2\mathbf{k}} - \frac{\partial_1}{\partial_1 T}\frac{\partial_2}{\partial_2\omega} - \frac{\partial_2}{\partial_2\mathbf{R}}\frac{\partial_1}{\partial_1\mathbf{k}} + \frac{\partial_2}{\partial_2 T}\frac{\partial_1}{\partial_1\omega}\right) A_1A_2. \end{aligned} \tag{3.31}$$

Similarly, truncating the expansion of the exponential after the first order, one finds that

[1] One may prove Eq. (3.30) as follows. Writing $A = A_1A_2$, we have

$$A(\mathbf{R},T;\mathbf{k},\omega) = \int d\mathbf{r}\int dt e^{-i\mathbf{k}\cdot\mathbf{r}+i\omega t}\int d\mathbf{r}'\int dt' A_1(\mathbf{R}+\mathbf{r}/2,T+t/2;\mathbf{r}',t')A_2(\mathbf{r}',t';\mathbf{R}-\mathbf{r}/2,T-t/2).$$

Now shift variables to $\mathbf{r}=\mathbf{r}_1+\mathbf{r}_2$, $\mathbf{r}'=\mathbf{R}+(\mathbf{r}_2-\mathbf{r}_1)/2$, $t=t_1+t_2$, $t'=T+(t_2-t_1)/2$. This variable transformation has unit jacobian, hence

$$\begin{aligned} A(\mathbf{R},T;\mathbf{k},\omega) &= \int d\mathbf{r}_1 d\mathbf{r}_2\int dt_1dt_2 e^{-i\mathbf{k}\cdot\mathbf{r}_1+i\omega t_1-i\mathbf{k}\cdot\mathbf{r}_2+i\omega t_2} \\ &\quad\times A_1(\mathbf{R}+(\mathbf{r}_1+\mathbf{r}_2)/2,T+(t_1+t_2)/2;\mathbf{R}+(\mathbf{r}_2-\mathbf{r}_1)/2,T+(t_2-t_1)/2) \\ &\quad\times A_2(\mathbf{R}+(\mathbf{r}_2-\mathbf{r}_1)/2,T+(t_2-t_1)/2;\mathbf{R}-(\mathbf{r}_1+\mathbf{r}_2)/2,T-(t_1+t_2)/2). \end{aligned}$$

If it weren't for the fact that the argument of A_2 contained $\mathbf{r}_1$ and t_1, the integrations over $\mathbf{r}_1$ and t_1 could be done and would give us the mixed representation Green function $A_1(\mathbf{R}+\mathbf{r}_2/2,T+t_2/2;\mathbf{k},\omega)$. Similarly, without the appearance of $\mathbf{r}_2$ and t_2 in the arguments of A_1, the integrations over $\mathbf{r}_2$ and t_2 would simply give $A_2(\mathbf{R}-\mathbf{r}_1/2,T-t_1/2;\mathbf{k},\omega)$. We can formally remedy this situation by writing

$$\begin{aligned} &A_1(\mathbf{R}+(\mathbf{r}_1+\mathbf{r}_2)/2,T+(t_1+t_2)/2;\mathbf{R}+(\mathbf{r}_2-\mathbf{r}_1)/2,T+(t_2-t_1)/2) \\ &\quad= e^{(1/2)\mathbf{r}_2\cdot\partial_{\mathbf{R}}+(1/2)t_2\partial_T}A_1(\mathbf{R}+\mathbf{r}_1/2,T+t_1/2;\mathbf{R}-\mathbf{r}_1/2,T-t_1/2), \\ &A_2(\mathbf{R}+(\mathbf{r}_2-\mathbf{r}_1)/2,T+(t_2-t_1)/2;\mathbf{R}-(\mathbf{r}_1+\mathbf{r}_2)/2,T-(t_1+t_2)/2) \\ &\quad= e^{-(1/2)\mathbf{r}_1\cdot\partial_{\mathbf{R}}-(1/2)t_1\partial_T}A_2(\mathbf{R}+\mathbf{r}_2/2,T+t_2/2;\mathbf{R}-\mathbf{r}_2/2,T-t_2/2). \end{aligned}$$

Now the integrations can be done, with the formal result

$$\begin{aligned} A(\mathbf{R},T;\mathbf{k},\omega) &= A_1(\mathbf{R},T;\mathbf{k}-(i/2)\partial_{2,\mathbf{R}},\omega+(i/2)\partial_{2,T})A_2(\mathbf{R},T;\mathbf{k}+(i/2)\partial_{1,\mathbf{R}},\omega-(i/2)\partial_{1,T}) \\ &= e^{(i/2)\mathcal{D}}A_1(\mathbf{R},T;\mathbf{k},\omega)A_2(\mathbf{R},T;\mathbf{k},\omega). \end{aligned}$$

Here the derivatives $\partial_{2,\mathbf{R}}$ and $\partial_{2,T}$ act on the factor A_2, whereas the derivatives $\partial_{1,\mathbf{R}}$ and $\partial_{1,T}$ act on the factor A_1.

the derivatives cancel when calculating an anticommutator,

$$[A_1, A_2]_+ = 2A_1A_2. \tag{3.32}$$

This approximation is known as the "gradient expansion".

In the gradient approximation, one quickly finds the retarded and advanced Green functions,

$$G^{\mathrm{R}}(\mathbf{R}, T; \mathbf{k}, \omega) = \frac{\hbar}{\hbar\omega + i\eta - \varepsilon_{\mathbf{k}} + \mu - U(\mathbf{R}, T)}, \tag{3.33}$$

$$G^{\mathrm{A}}(\mathbf{R}, T; \mathbf{k}, \omega) = \frac{\hbar}{\hbar\omega - i\eta - \varepsilon_{\mathbf{k}} + \mu - U(\mathbf{R}, T)}, \tag{3.34}$$

where η is a positive infinitesimal. (Addition of η is necessary to enforce the appropriate boundary conditions for advanced and retarded Green functions.) From this result, we conclude that the spectral density A is a delta function,

$$A(\mathbf{R}, T; \mathbf{k}, \omega) = 2\pi\hbar\delta(\hbar\omega - \varepsilon_{\mathbf{k}} + \mu - U(\mathbf{R}, T)). \tag{3.35}$$

Calculation of the Keldysh Green function from Eq. (3.29) shows that $G^{\mathrm{K}}(\mathbf{R}, T; \mathbf{k}, \omega)$ is proportional to $2\pi\hbar\delta(\hbar\omega - \varepsilon_{\mathbf{k}} + \mu - U(\mathbf{R}, T))$, but fails to determine the prefactor. In order to determine the prefactor, which determines the distribution function, we consider the Keldysh component of Eq. (3.28. In the gradient approximation, the differential equation (3.28) for the Keldysh component reads

$$\frac{\partial G^{\mathrm{K}}}{\partial T} + \mathbf{v}_{\mathbf{k}} \cdot \frac{\partial G^{\mathrm{K}}}{\partial \mathbf{R}} - \frac{\partial \mathcal{H}}{\partial \mathbf{R}} \cdot \frac{\partial G^{\mathrm{K}}}{\partial \mathbf{k}} + \frac{\partial \mathcal{H}}{\partial T}\frac{\partial G^{\mathrm{K}}}{\partial \omega} = 0, \tag{3.36}$$

where $\mathbf{v}_{\mathbf{k}} = \partial_{\mathbf{k}}\mathcal{H}$. Integrating this equation over ω, and using Eq. (3.24) for $\mathcal{H}$, we find

$$\left(\partial_T + \mathbf{v}_{\mathbf{k}} \cdot \partial_{\mathbf{R}} - \partial_{\mathbf{R}} U_{\mathrm{ext}} \cdot \partial_{\mathbf{k}}\right) f_{\mathbf{k}}(\mathbf{R}, T) = 0 \tag{3.37}$$

where

$$f_{\mathbf{k}}(\mathbf{R}, T) = \frac{1}{2} - \frac{1}{4\pi i}\int d\omega G^{\mathrm{K}}(\mathbf{R}, T; \omega, \mathbf{k}). \tag{3.38}$$

Equation (3.37) is nothing but the Boltzmann equation (3.21). The function f is the "distribution function": it specifies the density of electrons with wavevector $\mathbf{k}$. Indeed, since the definition of f contains an integration over frequency ω, $f_{\mathbf{k}}$ is related to an equal-time Green function.

Using the relationship $G^< = (G^{\rm K} + iA)/2$, together with Eq. (3.35), one quickly finds expressions for the charge density and current density in terms of the distribution function f. For the charge density, one has

$$\begin{aligned}
\rho_e(\mathbf{r},t) &= e\sum_\sigma \langle \hat\psi_\sigma(\mathbf{r},t)\hat\psi^\dagger_\sigma(\mathbf{r},t)\rangle \\
&= -ie\sum_\sigma G^<_{\sigma,\sigma}(\mathbf{r},t;\mathbf{r},t) \\
&= -\frac{ie}{2\pi V}\sum_{\mathbf{k},\sigma}\int d\omega G^<_{\sigma,\sigma}(\mathbf{r},t;\mathbf{k},\omega) \\
&= \frac{e}{V}\sum_{\mathbf{k},\sigma} f_{\mathbf{k},\sigma}(\mathbf{r},t), \qquad (3.39)
\end{aligned}$$

where we reinserted the summation over spin. Similarly, for the current density, one finds

$$\mathbf{j}_e(\mathbf{r},t) = \frac{e}{V}\sum_{\mathbf{k},\sigma}\mathbf{v}_\mathbf{k} f_{\mathbf{k},\sigma}(\mathbf{r},t). \qquad (3.40)$$

Also note that, by Eqs. (2.64) and (3.35), one has $f_\mathbf{k} = [1+\exp((\varepsilon_\mathbf{k}-\mu)/T)]^{-1}$ in equilibrium, independent of $\mathbf{R}$ and T.

Our derivation of the Boltzmann equation was for a particle moving in a smooth potential. It does not hold for impurities with a short-range potential. Such impurities scatter particles into different quantum states. Such quantum scattering events give rise to a "collision term" in the Boltzmann equation. We return to this issue in the next chapters, when we consider the effect of impurities in more detail.

3.4 Exercises

Exercise 3.1: Fermi gas in one or two dimensions

Calculate the retarded Green function for the ideal Fermi gas in one and in two dimensions in the coordinate representation.

Exercise 3.2: Non-interacting bosons

Repeat the analysis of Sec. 3.1 for a gas of non-interacting bosons. In particular, show that the retarded and advanced Green functions for the Bose gas are identical to the retarded and

advanced Green functions of the Fermi gas. (Of course, Bosons will have integer spin, whereas Fermions will have half-odd-integer spin.) Will the other Green functions be identical as well?

Exercise 3.3: Vector potential and Gauge invariance

In Sec. 3.3 we derived the Boltzmann equation in the presence of a scalar potential. In this exercise you are asked to see what happens if one has both a scalar potential and a vector potential that both vary slowly in time and space.

The first-quantization Hamiltonian now has the form

$$\mathcal{H} = \frac{1}{2m}\left(-i\hbar\partial_{\mathbf{r}} - \frac{e}{c}\mathbf{A}(\mathbf{r},t)\right)^2 + e\phi(\mathbf{r},t), \tag{3.41}$$

where we wrote the scalar electromagnetic potential ϕ instead of the potential U. The vector potential $\mathbf{A}$ and the scalar potential ϕ are related to the magnetic and electric fields as

$$\mathbf{E} = -\frac{1}{c}\partial_t\mathbf{A} - \partial_{\mathbf{r}}\phi, \quad \mathbf{B} = \partial_{\mathbf{r}} \times \mathbf{A}. \tag{3.42}$$

The vector potential $\mathbf{A}$ and the scalar potential ϕ are not uniquely determined by the electric and magnetic fields. Gauge invariance requires that all physical observables be invariant under the transformation

$$\mathbf{A}(\mathbf{r},t) \to \mathbf{A}(\mathbf{r},t) + \partial_{\mathbf{r}}\chi(\mathbf{r},t), \quad \phi(\mathbf{r},t) \to \phi(\mathbf{r},t) - \partial_t\chi(\mathbf{r},t), \tag{3.43}$$

where χ is an arbitrary function of $\mathbf{r}$ and t.

(a) Show that in the mixed representation and in the gradient approximation, one has

$$\mathcal{H} = \frac{1}{2m}\left(\hbar\mathbf{k} - \frac{e}{c}\mathbf{A}(\mathbf{R},T)\right)^2 + e\phi(\mathbf{R},T). \tag{3.44}$$

(b) Argue that the wavevector $\mathbf{k}$ has to change according to the rule

$$\mathbf{k} \to \mathbf{k} + \frac{e}{\hbar c}\partial_{\mathbf{R}}\chi(\mathbf{R},T) \tag{3.45}$$

if the gauge transformation (3.43) is applied.

The canonical momentum $\hbar\mathbf{k}$ is an argument of the distribution function f in the Boltzmann Equation (3.21). However, as you have just showed, $\hbar\mathbf{k}$ is not a gauge invariant quantity.

One may make the momentum argument of f gauge invariant by switching to the kinetic momentum $\hbar\mathbf{k}_{\rm kin}$,

$$\mathbf{k} = \mathbf{k}_{\rm kin} + (e/\hbar c)\mathbf{A}(\mathbf{R}, T)). \tag{3.46}$$

A differential equation for the Keldysh Green function $G^{\rm K}(\mathbf{R}, T; \mathbf{k}_{\rm kin}, \omega)$ in the gradient approximation can be obtained from Eq. (3.36). However, one must take care in dealing with the partial derivatives in that equation: The partial derivatives to $\mathbf{R}$ and T are meant to be taken at constant canonical momentum $\hbar\mathbf{k}$, not at constant kinetic momentum $\hbar\mathbf{k}_{\rm kin}$.

(c) Show that $G^{\rm K}(\mathbf{R}, T; \mathbf{k}_{\rm kin}, \omega)$ satisfies the differential equation

$$\begin{aligned} \hbar\frac{\partial G^{\rm K}}{\partial T} + \mathbf{v}\cdot\frac{\partial G^{\rm K}}{\partial \mathbf{R}} - \frac{e}{c}\mathbf{v}\cdot\left(\frac{\partial G^{\rm K}}{\partial \mathbf{k}_{\rm kin}}\cdot\frac{\partial \mathbf{A}}{\partial \mathbf{R}}\right) + \frac{e}{c}\left(\mathbf{v}\cdot\frac{\partial \mathbf{A}}{\partial \mathbf{R}}\right)\cdot\frac{\partial G^{\rm K}}{\partial \mathbf{k}_{\rm kin}} \\ - \left(\frac{\partial \mathcal{H}}{\partial \mathbf{R}} + \frac{e}{c}\frac{\partial \mathbf{A}}{\partial T}\right)\cdot\frac{\partial G^{\rm K}}{\partial \mathbf{k}_{\rm kin}} + \left(\frac{\partial \mathcal{H}}{\partial T} - \frac{e}{c}\mathbf{v}\cdot\frac{\partial \mathbf{A}}{\partial T}\right)\frac{\partial G^{\rm K}}{\partial \omega} &= 0, \end{aligned} \tag{3.47}$$

where now the partial derivatives to $\mathbf{R}$, T, and $\mathbf{k}_{\rm kin}$ have their standard meaning.

(d) Integrate over frequency to find a kinetic equation for the distribution function $f_{\mathbf{k}_{\rm kin}}(\mathbf{R}, T)$. Express your final answer in terms of the electric field $\mathbf{E}$ and the magnetic field $\mathbf{B}$.

(e) One may want to further adapt Eq. (3.47) by replacing the frequency $\hbar\omega$ by $\hbar\omega - e\phi(\mathbf{R}, T)$. Show that this substitution gives a manifestly gauge invariant evolution equation for the Green function.

Exercise 3.4: Quasiclassical approximation

If the Green function $\underline{G}$ has an important ω-dependence, as is, *e.g.,* the case for electron-phonon scattering, one does not want to define a distribution function by integrating the Green function over the frequency ω. In such circumstances, $\underline{G}$ may still be a sharply peaked function of momentum. When that is the case, an equation can be derived for the so-called "quasiclassical Green function"

$$\underline{g}(\mathbf{R}, \mathbf{n}, t, t') = \frac{i}{\pi}\int d\xi \underline{G}(\mathbf{R}, \mathbf{k}, t, t'), \tag{3.48}$$

where $\xi = \varepsilon_{\mathbf{k}}$ and $\mathbf{n}$ indicates the direction of $\mathbf{k}$.

We now derive an equation for the quasiclassical Green function using the gradient expansion for the spatial coordinates, but not for the temporal coordinates. As in Ex. 3.3 we want to use the kinetic momentum, not the canonical momentum, as the argument of the Green function in the mixed representation. If we use the kinetic momentum, $\mathbf{n}$ represents the direction of the electron's kinetic momentum, not its canonical momentum. Thus, instead of Eq. (3.22), we define

$$\underline{G}(\mathbf{R},\mathbf{k}_{\rm kin};t,t') = \int d\mathbf{r} e^{-i[\mathbf{k}_{\rm kin}+(e/2\hbar c)(\mathbf{A}(t,\mathbf{R})+\mathbf{A}(t',\mathbf{R}))]\cdot\mathbf{r}}\underline{G}(\mathbf{R}+\mathbf{r}/2,t;\mathbf{R}-\mathbf{r}/2,t'). \tag{3.49}$$

(a) Show that the Green function $\underline{G}$ of Eq. (3.49) satisfies the differential equation

$$\begin{aligned} 0 = {} & (\hbar\partial_{t_1} + ei\phi(\mathbf{R},t_1) + \hbar\partial_{t_2} - ei\phi(\mathbf{R},t_2))\,\underline{G} \\ & + \mathbf{v}\cdot\left[\partial_{\mathbf{R}} - \frac{ei}{c}\left(\mathbf{A}(\mathbf{R},t_1)-\mathbf{A}(\mathbf{R},t_2)\right)\right]\underline{G} \\ & + \frac{e}{2c}(\mathbf{v}\times(\mathbf{B}(\mathbf{R},t_1)+\mathbf{B}(\mathbf{R},t_2)))\cdot\frac{\partial\underline{G}}{\partial\mathbf{k}_{\rm kin}} - \frac{1}{2}\left(\mathbf{E}(\mathbf{R},t_1)+\mathbf{E}(\mathbf{R},t_2)\right)\cdot\frac{\partial\underline{G}}{\partial\mathbf{k}_{\rm kin}}. \end{aligned} \tag{3.50}$$

(b) Integrate this equation over $\xi = \varepsilon_{\mathbf{k}_{\rm kin}}$ to find an equation for the quasiclassical Green function $\underline{g}$.

(c) Argue that the advanced and retarded components of the quasiclassical Green function are particularly simple:

$$g^{\rm R} = 1, \quad g^{\rm A} = -1. \tag{3.51}$$

(d) If the potentials ϕ and $\mathbf{A}$ are a slow function of time, one may Fourier transform to $t_1 - t_2$ and use the gradient expansion for the temporal coordinates. What is the corresponding kinetic equation? Comment on the subtle differences between the equation you just obtained and the Boltzmann equation.

Chapter 4

Scattering from a single impurity

In this chapter, we consider non-interacting electrons in the presence of a external potential. This is another problem for which an exact solution is possible. In the first section of this chapter, we recall the standard quantum-mechanical solution of the problem. In the second section, we show how the same results can be obtained using the many-electron Green function formalism and diagrammatic perturbation theory.

In first quantization notation, the Hamiltonian we consider is

$$\mathcal{H} = -\frac{\hbar^2}{2m}\partial_{\mathbf{r}}^2 + U(\mathbf{r}), \tag{4.1}$$

where $U(\mathbf{r})$ is the impurity potential. Here and in the remainder of this chapter we drop reference to the spin index σ. In second quantization notation, the Hamiltonian is written in terms of creation and annihilation operators $\hat{\psi}^\dagger(\mathbf{r})$ and $\hat{\psi}(\mathbf{r})$ of an electron at position $\mathbf{r}$

$$\hat{H} = -\frac{\hbar^2}{2m}\int d\mathbf{r}\hat{\psi}^\dagger(\mathbf{r})\partial_{\mathbf{r}}^2\hat{\psi}(\mathbf{r}) + \int d\mathbf{r}\hat{\psi}^\dagger(\mathbf{r})U(\mathbf{r})\hat{\psi}(\mathbf{r}). \tag{4.2}$$

4.1 Scattering theory and Friedel Sum Rule

In the presence of an impurity, which is described by the potential $U(\mathbf{r})$, eigenfunctions of the Hamiltonian (4.1) are no longer plane waves. In this chapter, we consider the case of a single impurity, and assume that the potential U has a finite range. Then we can try to find an eigenfunction $|\psi_{\mathbf{k}}\rangle$ of $\mathcal{H}$ with *incoming* wave boundary condition corresponding to

the unperturbed state $|\mathbf{k}\rangle$ far away from the impurity. This solution can be written as[1]

$$|\psi_{\mathbf{k}}\rangle = |\mathbf{k}\rangle + \frac{1}{\hbar}G^{0\mathrm{R}}(\varepsilon_{\mathbf{k}}/\hbar)\mathcal{U}|\psi_{\mathbf{k}}\rangle \tag{4.3}$$

$$= |\mathbf{k}\rangle + \frac{1}{\hbar}G^{0\mathrm{R}}(\varepsilon_{\mathbf{k}}/\hbar)\mathcal{U}|\mathbf{k}\rangle + \frac{1}{\hbar^2}G^{0\mathrm{R}}(\varepsilon_{\mathbf{k}}/\hbar)\mathcal{U}G^{0\mathrm{R}}(\varepsilon_{\mathbf{k}}/\hbar)\mathcal{U}|\mathbf{k}\rangle + \ldots, \tag{4.4}$$

where $\mathcal{U}$ is the first-quantization operator corresponding to the potential $U(\mathbf{r})$ and G^0 is the free particle Green function, seen as an operator on the wavefunction $|\psi_{\mathrm{k}}\rangle$. The easiest way to see that Eq. (4.4) provides the correct wavefunction is to verify that $|\psi_{\mathbf{k}}\rangle$ solves the Schrödinger equation and has the correct boundary conditions. The series (4.4) is known as the Born series. Truncating the series after the nth order in U yields the nth Born approximation. Defining the T-matrix as

$$\begin{aligned}\mathcal{T}(\omega^+) &= \frac{1}{\hbar}\mathcal{U} + \frac{1}{\hbar^2}\mathcal{U}G^{0\mathrm{R}}(\omega)\mathcal{U} + \ldots \\ &= \mathcal{U}[\hbar - G^{0\mathrm{R}}(\omega)\mathcal{U}]^{-1} \\ &= \frac{1}{\hbar}\mathcal{U} + \frac{1}{\hbar}\mathcal{U}G^{0\mathrm{R}}(\omega)\mathcal{T}(\omega^+),\end{aligned} \tag{4.5}$$

where $\omega^+ = \omega + i\eta$, η being a positive infinitesimal, we can rewrite this as

$$|\psi_{\mathbf{k}}\rangle = |k\rangle + \sum_{\mathbf{k}'} \frac{T_{\mathbf{k}'\mathbf{k}}(\varepsilon_{\mathbf{k}} + i\eta)}{(\varepsilon_{\mathbf{k}} - \varepsilon_{\mathbf{k}'})/\hbar + i\eta}|k'\rangle, \tag{4.6}$$

with $T_{\mathbf{k}'\mathbf{k}}(\omega) = \langle\mathbf{k}'|\mathcal{T}(\omega)|\mathbf{k}\rangle$. The T-matrix is related to the retarded Green function G^{R} of the total Hamiltonian $\mathcal{H}$ as

$$G^{\mathrm{R}}(\omega) = G^{0\mathrm{R}}(\omega) + G^{0\mathrm{R}}(\omega)\mathcal{T}(\omega^+)G^{0\mathrm{R}}(\omega). \tag{4.7}$$

Note that in this notation, where we have a summation over discrete set of wavevectors, the T-matrix is of order $1/V$. Using Eq. (3.13) one then finds that the asymptotic form of the wavefunction of the scattered wave (4.6) is

$$\psi_{\mathbf{k}}(\mathbf{r}) = e^{i\mathbf{k}\mathbf{r}} + f(\mathbf{k}', \mathbf{k})\frac{e^{i\mathbf{k}'\cdot\mathbf{r}}}{r} + \mathcal{O}(1/r^2), \quad f(\mathbf{k}, \mathbf{k}') = -\frac{mV}{2\pi\hbar}T_{\mathbf{k}\mathbf{k}'}(\varepsilon_{\mathbf{k}}/\hbar + i\eta), \tag{4.8}$$

where the wavevector $\mathbf{k}'$ is defined as $k\hat{r}$, $\hat{r}$ being the unit vector in the direction of $\mathbf{r}$.

[1]You can find a good discussion of stationary scattering theory in section 37 of *Quantum Mechanics*, by L. I. Schiff, McGraw-Hill (1968).

With this result we can now write expressions for two useful quantities from collision theory: the differential cross section $d\sigma/d\Omega$, where $d\Omega$ denotes an element of solid angle, which is

$$\frac{d\sigma}{d\Omega} = |f(\mathbf{k}', \mathbf{k})|^2 = \frac{m^2 V^2}{4\pi^2\hbar^2}|T_{\mathbf{k}',\mathbf{k}}(\varepsilon_{\mathbf{k}}/\hbar + i\eta)|^2, \tag{4.9}$$

and the transition rate

$$W_{\mathbf{k}'\mathbf{k}} = 2\pi\hbar|T_{\mathbf{k}'\mathbf{k}}(\varepsilon_{\mathbf{k}} + i\eta)|^2\delta(\varepsilon_{\mathbf{k}'} - \varepsilon_{\mathbf{k}}). \tag{4.10}$$

The transition rate gives the probability per unit time that a particle is scattered out of plane wave state $\mathbf{k}$ into plane wave state $\mathbf{k}'$. To lowest order in the impurity potential U, Eq. (4.10) is nothing but the Fermi golden rule. The total rate for scattering out of the state $|\mathbf{k}\rangle$ is found by summation of Eq. (4.10) over all outgoing momenta,

$$\frac{1}{\tau_{\mathbf{k}}} = 2\pi\hbar\sum_{\mathbf{k}'}|T_{\mathbf{k}'\mathbf{k}}(\varepsilon_{\mathbf{k}} + i\eta)|^2\delta(\varepsilon_{\mathbf{k}'} - \varepsilon_{\mathbf{k}}). \tag{4.11}$$

Taking the hermitian conjugate of Eq. (4.5) and substituting $\mathcal{U} = \mathcal{U}^\dagger = \hbar\mathcal{T}^\dagger - \mathcal{T}^\dagger G^{0\mathrm{A}}\mathcal{U}$ in the second term of Eq. (4.5), one finds

$$\mathcal{T} = \frac{1}{\hbar}\mathcal{U} + \mathcal{T}^\dagger G^{0\mathrm{R}}\mathcal{T} - \frac{1}{\hbar}\mathcal{T}^\dagger G^{0\mathrm{A}}\mathcal{U}G^{0\mathrm{R}}\mathcal{T}. \tag{4.12}$$

The first and third term on the right hand side are hermitian, so that

$$\Im\mathcal{T} \;=\; \mathcal{T}^\dagger\Im G^{0\mathrm{R}}\mathcal{T}. \tag{4.13}$$

Using Eq. (3.20), this result can be written as

$$\frac{1}{2i}\left(T_{\mathbf{k}\mathbf{k}'}(\omega^+) - T_{\mathbf{k}'\mathbf{k}}(\omega^+)^*\right) = -\pi\sum_{\mathbf{k}_1}T^*_{\mathbf{k}_1\mathbf{k}}(\omega^+)T_{\mathbf{k}_1\mathbf{k}'}(\omega^+)\delta(\omega - \varepsilon_{\mathbf{k}_1}/\hbar). \tag{4.14}$$

This result is known as the "generalized optical theorem". The "standard" optical theorem is obtained setting $\mathbf{k}' = \mathbf{k}$,

$$\mathrm{Im}\, T_{\mathbf{k}\mathbf{k}}(\omega^+) = -\pi\sum_{\mathbf{k}_1}|T_{\mathbf{k}_1\mathbf{k}}(\omega^+)|^2\delta(\omega - \varepsilon_{\mathbf{k}_1}/\hbar). \tag{4.15}$$

The optical theorem relates the forward scattering amplitude to the intensity of the total scattered wave.

The density of levels $dN(\omega)/d\hbar\omega$ is expressed in terms of the Green function as

$$\frac{dN(\omega)}{d\hbar\omega} = \sum_{\mu} \delta(\hbar\omega - \varepsilon_\mu) = -\frac{1}{\pi\hbar}\mathrm{Im}\,\mathrm{tr}\,G^{\mathrm{R}}(\omega). \tag{4.16}$$

The *impurity density of states* $(dN/d\hbar\omega)_{\mathrm{imp}}$ is defined as the difference between the density of states with and without impurity. Using the general relation

$$\mathrm{tr}\,G(\omega) = -\frac{\partial}{\partial\omega}\ln\det G(\omega), \tag{4.17}$$

one can show that

$$\left(\frac{dN}{d\hbar\omega}\right)_{\mathrm{imp}} = \frac{1}{\pi\hbar}\frac{\partial\delta(\omega)}{\partial\omega}, \tag{4.18}$$

where $\delta(\omega) = \arg\det\mathcal{T}(\omega)$ is the so-called "total scattering phase shift". Zero eigenvalues of $\mathcal{T}$, which correspond to states that do not scatter at all, should be left out from the calculation of the total scattering phase shift. Equation (4.18) is known as the "Friedel sum rule". At zero temperature, as a result of the introduction of the impurity, the number of electrons in a many-electron system is changed by the amount[2]

$$N_{\mathrm{imp}} = \hbar\int_{-\infty}^{\varepsilon_F}\left(\frac{dN}{d\hbar\omega}\right)_{\mathrm{imp}} d\omega = \frac{\delta(\varepsilon_F)}{\pi}, \tag{4.19}$$

where we took $\delta(-\infty) = 0$ and ε_F is the Fermi energy.

In order to make things more explicit, let us now study the case $U(\mathbf{r}) = u\delta(\mathbf{r})$ of a delta-function potential at the origin in detail. Fourier transforming to the basis of plane-wave states and using second-quantization notation, the potential U is written as

$$U = \frac{u}{V}\sum_{\mathbf{k},\mathbf{q}}\hat{\psi}^\dagger_{\mathbf{k}+\mathbf{q}}\hat{\psi}_{\mathbf{k}}. \tag{4.20}$$

Then the equation for the T-matrix becomes

$$T_{\mathbf{k},\mathbf{k}'}(\omega + i\eta) = \frac{u}{\hbar V}\frac{1}{1 - (u/\hbar)\overline{G^{0\mathrm{R}}(\omega)}}, \tag{4.21}$$

[2]Strictly speaking, the derivation of Eq. (4.19) applies to potential scattering only. One may, however, extend the Friedel sum rule to the case of scattering from a dynamical impurity. See, e.g., chapter 5 of *The Kondo problem to heavy fermions*, by A. C. Hewson.

where we abbreviated

$$\overline{G^{0\mathrm{R}}(\omega)} = \frac{1}{V}\sum_{\mathbf{k}} G^{0\mathrm{R}}_{\mathbf{kk}}(\omega) = \frac{1}{V}\sum_{\mathbf{k}} \frac{1}{\omega + i\eta - \varepsilon_{\mathbf{k}'}/\hbar}. \tag{4.22}$$

(A similar definition can be made for $\overline{G^{0\mathrm{A}}(\omega)}$.) Note that the T-matrix is isotropic: For a delta-function scatterer, scattering is equally probable in all directions. Since T is isotropic, only one of the eigenvalues of T is nonzero. The simplest way to calculate the corresponding phase shift δ is to note that $T(\omega + i\eta) = T(\omega - i\eta)^*$, so that

$$e^{2i\delta(\omega)} = \frac{T(\omega + i\eta)}{T(\omega - i\eta)} = \frac{1 - (u/\hbar)\overline{G^0(\omega - i\eta)}}{1 - (u/\hbar)\overline{G^0(\omega + i\eta)}}. \tag{4.23}$$

The real part of $\overline{G^0(\omega + i\eta)}$ depends weakly on ω. Formally, for a quadratic dispersion relation $\varepsilon_{\mathbf{k}} = \hbar^2 k^2/2m$ and a delta-function scatterer, $\mathrm{Re}\,\overline{G^0(\omega + i\eta)}$ is ultraviolet divergent. The high-energy part of the energy integration can be cut off by introducing a finite width of the conduction band, or by noting that for high energies the approximation of a delta function scatterer breaks down: high energies correspond to small length scales, and on sufficiently short length scales the spatial structure of the potential must be resolved. The imaginary part of $\overline{G^0(\omega + i\eta)}$ is related to the density of states ν_0 (per unit volume) at the energy $\hbar\omega$ in the absence of the impurity,

$$\mathrm{Im}\,\overline{G^0(\omega + i\eta)} = -\pi\hbar\nu_0(\omega) = -\frac{k^2}{2\pi v}, \tag{4.24}$$

Here $v = \hbar^{-1}\partial\varepsilon/\partial k$ is the velocity at wavevector $\mathbf{k}$.

With the help of Eq. (4.24), we can express T in terms of δ and ν_0,

$$\begin{aligned} T_{\mathbf{kk}'}(\omega \pm i\eta) &= -\frac{1}{\pi\hbar\nu_0 V} e^{\pm i\delta(\omega)} \sin\delta(\omega) \\ &= -\frac{2\pi v}{k^2 V} e^{\pm i\delta(\omega)} \sin\delta(\omega). \end{aligned} \tag{4.25}$$

Hence, in this case we find for the differential cross section

$$\frac{d\sigma}{d\Omega} = \frac{m^2 v^2}{k^4\hbar^2} \sin^2\delta(\omega), \tag{4.26}$$

and for the total scattering cross section (the integral of $d\sigma/d\Omega$ over the full solid angle)

$$\sigma = \frac{4\pi m^2 v^2}{k^4\hbar^2} \sin^2\delta(\omega). \tag{4.27}$$

4.2 Diagrammatic perturbation theory

In this section, we'll use the Green function formalism to describe the electron gas in the presence of an impurity. The main goal of this section is to introduce the formal machinery of diagrammatic perturbation theory. We first describe the calculation using the imaginary-time formalism. Then the same calculation is described using the real-time formalism.

4.2.1 imaginary time formalism

We are interested in the electron density $n(\mathbf{r})$ of a gas of noninteracting electrons in the presence of a potential $U(\mathbf{r})$. The electron density can be expressed in terms of the many-electron temperature Green function, using

$$n(\mathbf{r}) = \langle\hat{\psi}^\dagger(\mathbf{r})\hat{\psi}(\mathbf{r})\rangle = \lim_{\tau\uparrow 0}\mathcal{G}(\mathbf{r},\mathbf{r};\tau). \tag{4.28}$$

Here $\mathcal{G}$ is the temperature Green function in the presence of the impurity potential. We now calculate $\mathcal{G}$ using diagrammatic perturbation theory. It is advantageous to change to the momentum representation,

$$\hat{\psi}_{\mathbf{k}} = \frac{1}{V^{1/2}}\int d\mathbf{r}\hat{\psi}(\mathbf{r})e^{-i\mathbf{k}\cdot\mathbf{r}}, \quad \hat{\psi}(\mathbf{r}) = \frac{1}{V^{1/2}}\sum_{\mathbf{k}}\hat{\psi}_{\mathbf{k}}e^{i\mathbf{k}\cdot\mathbf{r}},$$

so that the temperature Green function in momentum representation reads

$$\begin{aligned}\mathcal{G}_{\mathbf{k};\mathbf{k}'}(\tau) &= -\langle T_\tau[\hat{\psi}_{\mathbf{k}}(\tau)\hat{\psi}^\dagger_{\mathbf{k}'}(0)]\rangle \\ &= \frac{1}{V}\int d\mathbf{r}d\mathbf{r}'\mathcal{G}(\mathbf{r},\mathbf{r}';\tau)e^{-i(\mathbf{k}\cdot\mathbf{r}-\mathbf{k}'\cdot\mathbf{r}')}.\end{aligned} \tag{4.29}$$

The Hamiltonian is separated into an "unperturbed" part H_0 and the "perturbation" H_1,

$$H = H_0 + H_1, \tag{4.30}$$

with

$$H_0 = \sum_{\mathbf{k}}(\varepsilon_{\mathbf{k}}-\mu)\hat{\psi}^\dagger_{\mathbf{k}}\hat{\psi}_{\mathbf{k}}, \tag{4.31}$$

$$H_1 = \sum_{\mathbf{k}}\sum_{\mathbf{q}}U_{\mathbf{q}}\hat{\psi}^\dagger_{\mathbf{k}+\mathbf{q}}\hat{\psi}_{\mathbf{k}}, \tag{4.32}$$

where $U_{\mathbf{q}}$ is the Fourier transform of the scattering potential,

$$U_{\mathbf{q}} = \frac{1}{V}\int d\mathbf{r}U(\mathbf{r})e^{-i\mathbf{q}\cdot\mathbf{r}}. \tag{4.33}$$

Here, we have included the chemical potential into the unperturbed Hamiltonian H_0.

It is not clear a priori that the perturbation H_1 is small. Still, in the method of diagrammatic perturbation theory, it is assumed that an expansion in H_1 is possible, and that resummation of that expansion gives the correct results. Since we are going to expand in H_1, we need the temperature Green function for the "unperturbed" Hamiltonian H_0,

$$\mathcal{G}^0_{\mathbf{k};\mathbf{k}'}(\tau) = -\delta_{\mathbf{k},\mathbf{k}'}\theta(\tau)\frac{e^{-(\varepsilon_{\mathbf{k}}-\mu)\tau/\hbar}}{1+e^{-(\varepsilon_{\mathbf{k}}-\mu)/T}} + \delta_{\mathbf{k};\mathbf{k}'}\theta(-\tau)\frac{e^{-(\varepsilon_{\mathbf{k}}-\mu)\tau/\hbar}}{1+e^{(\varepsilon_{\mathbf{k}}-\mu)/T}}. \tag{4.34}$$

The Fourier transform of the temperature Green function is

$$\mathcal{G}^0_{\mathbf{k};\mathbf{k}'}(i\omega_n) = \frac{\delta_{\mathbf{k},\mathbf{k}'}}{i\omega_n - (\varepsilon_{\mathbf{k}}-\mu)/\hbar}. \tag{4.35}$$

Since $\mathcal{G}^0_{\mathbf{k};\mathbf{k}'}$ is nonzero only if $\mathbf{k}=\mathbf{k}'$, we drop the second index if no confusion is possible.

In order to prepare ourselves for a perturbative calculation in $\hat{H}_1$, we switch to the interaction picture. Using Eq. (2.25), we then write the temperature Green function as

$$\mathcal{G}_{\mathbf{k};\mathbf{k}'}(\tau) \;=\; \frac{-\langle T_\tau e^{-\int_0^{\hbar/T} d\tau' \hat{H}_1(\tau')/\hbar}\hat{\psi}_{\mathbf{k}}(\tau)\hat{\psi}^\dagger_{\mathbf{k}'}(0)\rangle_0}{\langle T_\tau e^{-\int_0^{\hbar/T} d\tau' \hat{H}_1(\tau')/\hbar}\rangle_0}, \tag{4.36}$$

where the brackets $\langle\ldots\rangle_0$ indicate an thermal average with respect to the unperturbed Hamiltonian H_0 only. In order to avoid misunderstandings about the order of the creation and annihilation operators in the perturbation $\hat{H}_1$, we increase the imaginary time argument of the creation operators by a positive infinitesimal η,

$$\hat{H}_1(\tau) = \sum_{\mathbf{k}}\sum_{\mathbf{q}} U_{\mathbf{q}}\hat{\psi}^\dagger_{\mathbf{k}+\mathbf{q}}(\tau+\eta)\hat{\psi}_{\mathbf{k}}(\tau). \tag{4.37}$$

The next step is to expand the evolution operator in powers of H_1 and calculate the thermal average with respect to the Hamiltonian $\hat{H}_0$. The calculation of the thermal average is done with the help of Wick's theorem. In the language of the general formulation of Sec. 2, Wick's theorem allows one to calculate the thermal average of an imaginary time-ordered product of the form $\langle T_\tau A_1(\tau_1)\ldots A_{2n}(\tau_{2n})\rangle_0$, where all operators A_i, $i=1,\ldots,2n$ are linear in fermion creation and annihilation operators and the average is taken with respect to a Hamiltonian H_0 that is quadratic in fermion creation and annihilation operators. Clearly, every order in the perturbation expansion of Eq. (4.36) satisfies these criteria. Wick's theorem states that

$$\begin{aligned}\langle T_\tau \hat{A}_1(\tau_1)\ldots\hat{A}_{2n}(\tau_{2n})\rangle_0 \;&=\; \left(-\frac{1}{2}\right)^n \sum_P (-1)^P \mathcal{G}^0_{A_{P(1)},A_{P(2)}}(\tau_{P(1)},\tau_{P(2)})\times\ldots \\ &\quad\times \mathcal{G}^0_{A_{P(2n-1)},A_{P(2n)}}(\tau_{P(2n-1)},\tau_{P(2n)}),\end{aligned} \tag{4.38}$$

where the sum is over all permutations P of the numbers $1, 2, \ldots, 2n$ and $(-1)^P$ is the sign of the permutation. In our case, only Green functions with one creation operator and one annihilation operator are nonzero. That simplifies the set of allowed permutations, and we can write Wick's theorem as

$$\begin{aligned}\langle T_\tau \hat{\psi}_{\mathbf{k}_1}(\tau_1)\ldots\hat{\psi}_{\mathbf{k}_n}(\tau_n)\hat{\psi}^\dagger_{\mathbf{k}'_n}(\tau'_n)\ldots\hat{\psi}^\dagger_{\mathbf{k}'_1}(\tau'_1)\rangle_0 \\ = \quad (-1)^n\sum_P (-1)^P \mathcal{G}^0_{\mathbf{k}_1,\mathbf{k}'_{P(1)}}(\tau_1,\tau'_{P(1)})\ldots\mathcal{G}^0_{\mathbf{k}_n,\mathbf{k}'_{P(n)}}(\tau_n,\tau'_{P(n)}),\end{aligned} \tag{4.39}$$

where now P is a permutation of the numbers 1, 2, ..., n only. For a proof of Wick's theorem, see, *e.g.,* the book *Methods of quantum field theory in statistical physics*, by A. A. Abrikosov, L. P. Gorkov, and I. E. Dzyaloshinski, Dover (1963). Wick's theorem applies to time-ordered products only.

We have to average numerator and denominator in Eq. (4.36) separately. To zeroth order in the perturbation $\hat{H}_1$, the numerator gives $\mathcal{G}^0_{\mathbf{k},\mathbf{k}'}(\tau)$, whereas the denominator gives 1, hence we find

$$\mathcal{G}_{\mathbf{k},\mathbf{k}'}(\tau) = \mathcal{G}^0_{\mathbf{k}}(\tau)\delta_{\mathbf{k},\mathbf{k}'} + \text{higher order terms} \tag{4.40}$$

Let us now calculate the first order corrections. The first-order correction to the numerator of Eq. (4.36) is

$$\begin{aligned}&\frac{1}{\hbar}\int_0^{\hbar/T} d\tau' \sum_{\mathbf{q},\mathbf{k}''} U_{\mathbf{q}}\left[\mathcal{G}^0_{\mathbf{k},\mathbf{k}''+\mathbf{q}}(\tau-\tau')\mathcal{G}^0_{\mathbf{k}'',\mathbf{k}'}(\tau'-0) - \mathcal{G}^0_{\mathbf{k}'',\mathbf{k}''+\mathbf{q}}(-\eta)\mathcal{G}^0_{\mathbf{k},\mathbf{k}'}(\tau)\right] \\ &= \frac{1}{\hbar}\int_0^{\hbar/T} d\tau' U_{\mathbf{k}-\mathbf{k}'}\mathcal{G}^0_{\mathbf{k}}(\tau-\tau')\mathcal{G}^0_{\mathbf{k}'}(\tau') - \frac{1}{\hbar}\mathcal{G}^0_{\mathbf{k}}(\tau)\delta_{\mathbf{k},\mathbf{k}'}\int_0^{\hbar/T} d\tau' U_0 \sum_{\mathbf{k}''}\mathcal{G}^0_{\mathbf{k}''}(-\eta),\end{aligned}$$

whereas the first-order correction to the denominator is

$$-\frac{1}{\hbar}\int_0^{\hbar/T} d\tau' \sum_{\mathbf{q},\mathbf{k}''} U_{\mathbf{q}}\mathcal{G}^0_{\mathbf{k}'',\mathbf{k}''+\mathbf{q}}(-\eta) = -\frac{1}{\hbar}\int_0^{\hbar/T} d\tau' U_0 \sum_{\mathbf{k}''}\mathcal{G}^0_{\mathbf{k}''}(-\eta)$$

Dividing numerator and denominator and keeping terms to first order in U only, we find that the first-order correction to the numerator cancels against the second term of the first-order correction to the denominator. Using this, together with the fact that $\mathcal{G}^0_{\mathbf{k},\mathbf{k}'}$ is nonzero only if $\mathbf{k} = \mathbf{k}'$, we find the simple result

$$\mathcal{G}_{\mathbf{k};\mathbf{k}'}(\tau) \quad = \quad \mathcal{G}^0_{\mathbf{k}}(\tau)\delta_{\mathbf{k},\mathbf{k}} + \frac{1}{\hbar}\int_0^{\hbar/T} d\tau_1 U_{\mathbf{k}-\mathbf{k}'}\mathcal{G}^0_{\mathbf{k}}(\tau-\tau_1)\mathcal{G}^0_{\mathbf{k}'}(\tau_1) + \ldots, \tag{4.41}$$

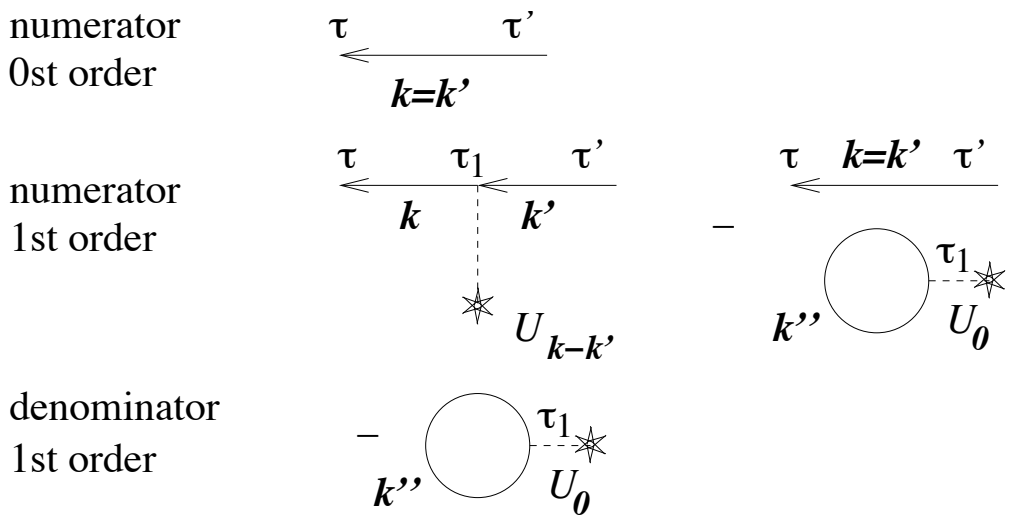

Figure 4.1: Diagrammatic representation of the numerator and denominator of Eq. (4.36) up to first order in U. Single arrows correspond to the unperturbed Green function $\mathcal{G}^0_{\mathbf{k},\mathbf{k}'}(\tau,\tau')$, whereas the dashed lines with the stars correspond to the impurity potential $U_{\mathbf{q}}$.

where the dots indicate terms of order two and higher.

The number of terms contributing to the Green function in higher orders in $\hat{H}_1$ increases very rapidly. In order to handle the higher-order contributions it is useful to use diagrams to represent the terms. The diagrams that represent the first order calculation are shown in Fig. 4.1. The solid arrows represent the Green functions $\mathcal{G}^0$ of the unperturbed Hamiltonian $\hat{H}_0$, whereas the dashed lines with the star represent the impurity potential U.

For the terms contributing to the numerator in Eq. (4.36), we discriminate two types of contributions: disconnected diagrams (the right diagram) and connected diagrams (the left diagram in Fig. 4.1). It was the disconnected diagram that canceled against the first-order correction to the denominator in Eq. (4.36). In fact, one can easily convince oneself all disconnected diagrams in the perturbative expansion of the numerator cancel against the diagrammatic expansion of the numerator. Thus, for the calculation of $\mathcal{G}$ we can ignore the denominator if we keep connected diagrams only.

Now we can write down the higher-order contributions to the Green function,

$$\begin{aligned}\mathcal{G}_{\mathbf{k};\mathbf{k}'}(\tau) &= \mathcal{G}^0_{\mathbf{k}}(\tau)\delta_{\mathbf{k},\mathbf{k}} + \frac{1}{\hbar}\int_0^{\hbar/T} d\tau_1 \mathcal{G}^0_{\mathbf{k}}(\tau-\tau_1)U_{\mathbf{k}-\mathbf{k}'}\mathcal{G}^0_{\mathbf{k}'}(\tau_1) \\ &\quad + \frac{1}{\hbar^2}\int_0^{\hbar/T} d\tau_1 \int_0^{\hbar/T} d\tau_2 \sum_{\mathbf{k}_1} \mathcal{G}^0_{\mathbf{k}}(\tau-\tau_1)U_{\mathbf{k}-\mathbf{k}_1}\mathcal{G}^0_{\mathbf{k}_1}(\tau_1-\tau_2)U_{\mathbf{k}_1-\mathbf{k}'}\mathcal{G}^0_{\mathbf{k}'}(\tau_2) + \ldots .\end{aligned} \tag{4.42}$$

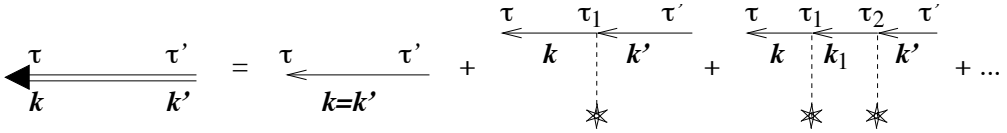

Figure 4.2: Diagrammatic representation of Eq. (4.42). The double arrow corresponds to the full Green function $\mathcal{G}_{\mathbf{k},\mathbf{k}'}(\tau,\tau')$. The momentum argument of the impurity potential is the difference in electron momenta at the scattering vertex.

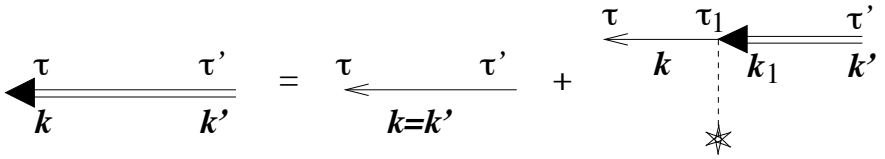

Figure 4.3: Diagrammatic representation of the Dyson equation for impurity scattering, Eq. (4.43).

Diagrammatically this result may be represented as in Fig. 4.2. The double arrow represents the full Green function, while the single arrows correspond to the Green functions of the free electron Hamiltonian H_0. As before, the dashed lines with the stars correspond to scattering from the impurity potential U. The series can be written as a self-consistent equation for $\mathcal{G}_{\mathbf{k},\mathbf{k}'}(\tau)$,

$$\mathcal{G}_{\mathbf{k};\mathbf{k}'}(\tau) = \mathcal{G}^0_{\mathbf{k}}(\tau)\delta_{\mathbf{k},\mathbf{k}'} + \frac{1}{\hbar}\sum_{\mathbf{k}_1}\int_0^{1/T} d\tau_1 \mathcal{G}^0_{\mathbf{k}}(\tau-\tau_1)U_{\mathbf{k}-\mathbf{k}_1}\mathcal{G}_{\mathbf{k}_1;\mathbf{k}'}(\tau_1). \tag{4.43}$$

This equation is called the "Dyson" equation. It is represented diagrammatically in Fig. 4.3.

Equation (4.43) is an integral equation for the Green function $\mathcal{G}_{\mathbf{k};\mathbf{k}'}(\tau)$: it contains both a convolution with respect to the imaginary time variable τ_1 and a summation over the intermediate momentum $\mathbf{k}_1$. The convolution can be handled by Fourier transformation,

$$\mathcal{G}_{\mathbf{k};\mathbf{k}'}(i\omega_n) = \mathcal{G}^0_{\mathbf{k}}(i\omega_n)\delta_{\mathbf{k},\mathbf{k}'} + \frac{1}{\hbar}\sum_{\mathbf{k}_1}\mathcal{G}^0_{\mathbf{k}}(i\omega_n)U_{\mathbf{k}-\mathbf{k}_1}\mathcal{G}_{\mathbf{k}_1;\mathbf{k}'}(i\omega_n), \tag{4.44}$$

but the summation over the momentum $\mathbf{k}_1$ is more complicated. It can not be carried out exactly for an arbitrary impurity potential. As a simple example, we return to the case of a point scatterer, $U(\mathbf{r}) = u\delta(\mathbf{r})$. In this case, $U_{\mathbf{k}-\mathbf{k}_1} = u/V$ does not depend on $\mathbf{k}$ and $\mathbf{k}_1$, see Eq. (4.20). Summing Eq. (4.44) over $\mathbf{k}$, we find

$$\sum_{\mathbf{k}}\mathcal{G}_{\mathbf{k};\mathbf{k}'}(i\omega_n) = \mathcal{G}^0_{\mathbf{k}';\mathbf{k}'}(i\omega_n) + \frac{u}{\hbar V}\left(\sum_{\mathbf{k}}\mathcal{G}^0_{\mathbf{k}}(i\omega_n)\right)\left(\sum_{\mathbf{k}}\mathcal{G}_{\mathbf{k};\mathbf{k}'}(i\omega_n)\right), \tag{4.45}$$

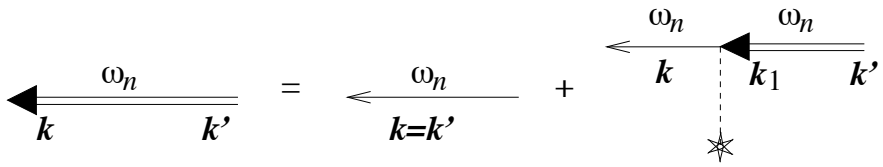

Figure 4.4: Diagrammatic representation of the Matsubara frequency representation of the Dyson equation for impurity scattering, Eq. (4.44). Notice that the Matsubara frequency ω_n is conserved at every scattering event.

from which we derive

$$\sum_{\mathbf{k}} \mathcal{G}_{\mathbf{k};\mathbf{k}'}(i\omega_n) = \frac{\mathcal{G}^0_{\mathbf{k}'}(i\omega_n)}{1-(u/\hbar V)\sum_{\mathbf{k}} \mathcal{G}^0_{\mathbf{k}}(i\omega_n)}, \tag{4.46}$$

and, hence,

$$\mathcal{G}_{\mathbf{k};\mathbf{k}'}(i\omega_n) = \mathcal{G}^0_{\mathbf{k}}(i\omega_n)\delta_{\mathbf{k},\mathbf{k}'} + \frac{u}{\hbar V}\mathcal{G}^0_{\mathbf{k}}(i\omega_n)\frac{1}{1-(u/\hbar)\,\overline{\mathcal{G}^0(i\omega_n)}}\mathcal{G}^0_{\mathbf{k}'}(i\omega_n), \tag{4.47}$$

where we abbreviated

$$\overline{\mathcal{G}^0(i\omega_n)} = \frac{1}{V}\sum_{\mathbf{k}} \mathcal{G}^0_{\mathbf{k};\mathbf{k}}(i\omega_n). \tag{4.48}$$

What remains is to perform the inverse Fourier transform,

$$\mathcal{G}_{\mathbf{k};\mathbf{k}'}(\tau) = \frac{T}{\hbar}\sum_n e^{-i\omega_n\tau}\mathcal{G}_{\mathbf{k};\mathbf{k}'}(i\omega_n). \tag{4.49}$$

This is done with the help of the following trick. The summation in Eq. (4.49) is written as an integration over the contour C_1, see Fig. 4.5,

$$\mathcal{G}_{\mathbf{k};\mathbf{k}'}(\tau) = \frac{1}{4\pi i}\int_{C_1} dz e^{-z\tau}\left[\tanh(\hbar z/2T)-1\right]\mathcal{G}_{\mathbf{k};\mathbf{k}'}(i\omega_n\to z). \tag{4.50}$$

We are interested in the case of negative τ.[3] Then we make use of the fact that $\mathcal{G}$ is analytic for all frequencies away from the real and imaginary axes, so that we may deform the contour C_1 into the contour C_2, see Fig. 4.5. Note that there is no contribution from the segments

[3]If we would have wanted to calculate the temperature Green function for positive τ, we would have used Eq. (4.50) with a factor $[\tanh(\hbar z/2T)+1]$ instead of $[\tanh(\hbar z/2T)-1]$.

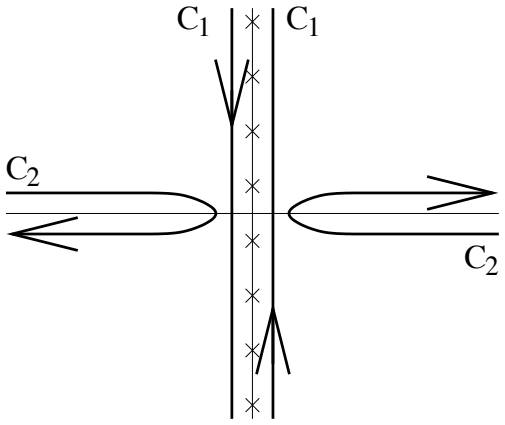

Figure 4.5: Integration contours for the derivation of Eq. (4.50) and (4.51).

near infinity by virtue of the factor $[\tanh(\hbar z/2T)-1]$ for $\mathrm{Re}\, z > 0$ and by virtue of the factor $e^{-z\tau}$ for $\mathrm{Re}\, z < 0$. We thus obtain

$$\begin{aligned}
\mathcal{G}_{\mathbf{k};\mathbf{k}'}(\tau) &= \frac{1}{4\pi i}\sum_{\pm}(\pm)\int_{-\infty}^{\infty} d\omega e^{-\omega\tau}[\tanh(\hbar\omega/2T)-1]\mathcal{G}_{\mathbf{k};\mathbf{k}'}(i\omega_n \to \omega \pm i\eta), \\
&= \frac{e^{-(\varepsilon_{\mathbf{k}}-\mu)\tau/\hbar}}{1+e^{(\varepsilon_{\mathbf{k}}-\mu)/T}} - \frac{u}{\hbar V}\sum_{\pm}\left(\frac{\pm 1}{2\pi i}\right)\int_{-\infty}^{\infty} d\omega \frac{e^{-\omega\tau}}{1+e^{\hbar\omega/T}}\,\frac{1}{\omega^{\pm}-(\varepsilon_{\mathbf{k}}-\mu)/\hbar} \\
&\quad \times \frac{1}{1-(u/\hbar)\,\overline{\mathcal{G}^0(\omega^{\pm})}}\,\frac{1}{\hbar\omega^{\pm}-(\varepsilon_{\mathbf{k}'}-\mu)/\hbar},
\end{aligned} \tag{4.51}$$

where $\omega^{\pm} = \omega \pm i\eta$ and η is a positive infinitesimal. The first term in Eq. (4.51) is the temperature Green function in the absence of the potential, cf. Eq. (4.34). The second term is the correction that arises as a result of scattering from the impurity at $\mathbf{r} = 0$.

We first use this result to calculate the change in the total number of electrons due to the presence of the impurity,

$$\begin{aligned}
N_{\mathrm{imp}} &= \lim_{\tau\uparrow 0}\sum_{\mathbf{k}}\left(\mathcal{G}_{\mathbf{k};\mathbf{k}}(\tau) - \mathcal{G}^0_{\mathbf{k};\mathbf{k}}(\tau)\right) \\
&= -\frac{u}{\hbar V}\sum_{\pm}\left(\frac{\pm 1}{2\pi i}\right)\sum_{\mathbf{k}}\int_{-\infty}^{\infty} d\omega \frac{1}{1+e^{\hbar\omega/T}}\,\frac{1}{(\omega^{\pm}-(\varepsilon_{\mathbf{k}}-\mu)/\hbar)^2}\,\frac{1}{1-(u/\hbar)\overline{\mathcal{G}^0(\omega^{\pm})}} \\
&= -\sum_{\pm}\left(\frac{\pm 1}{2\pi i}\right)\int_{-\infty}^{\infty} d\omega \frac{1}{1+e^{\hbar\omega/T}}\frac{\partial}{\partial\omega}\log\left[1-(u/\hbar)\overline{\mathcal{G}^0(\omega^{\pm})}\right].
\end{aligned} \tag{4.52}$$

This result can be rewritten in terms of the T matrix and the scattering phase shifts. Using the relation (4.23) between $\bar{\mathcal{G}}$, the T-matrix, and the scattering phase shift, we recover the Friedel sum rule,

$$N_{\rm imp} = \frac{1}{\pi}\int d\omega \left(-\frac{\partial}{\partial\omega}\frac{1}{1+e^{\hbar\omega/T}}\right)\delta_0(\hbar\omega+\mu). \tag{4.53}$$

At zero temperature, Eq. (4.53) simplifies to Eq. (4.19) above.

In order to find how the density change depends on the distance r to the impurity site, we have to change variables from the momenta $\mathbf{k}$ and $\mathbf{k}'$ to the positions $\mathbf{r}$ and $\mathbf{r}'$. Hereto, we start again from the second term in Eq. (4.51) and note that the $\mathbf{k}$-dependence is through the factors $1/(\omega^+ - (\varepsilon_{\mathbf{k}}-\mu)/\hbar)$ only. The corresponding Fourier transform has been considered in Sec. 4.1 and the result for the asymptotic behavior as $r\to\infty$ is

$$n_{\rm imp}(\mathbf{r}) \;=\; \lim_{\tau\uparrow 0}\sum_{\pm}\left(\frac{\pm 1}{2\pi i}\right)\int_{-\infty}^{\infty} d\omega \frac{m^2 v}{2\pi r^2 k^2\hbar^2}\frac{\sin\delta_0(\hbar\omega+\mu)e^{-\omega\tau}}{1+e^{\hbar\omega/T}}e^{\pm i[\delta_0(\hbar\omega+\mu)+2(k_F+\omega/v_F)r]}.$$

In order to perform the ω-integration, we expand the phase shift $\delta_0(\hbar\omega+\mu)$ around $\omega=0$ and keep terms that contribute to leading order in $1/r$ only. The result is

$$n_{\rm imp}(\mathbf{r}) \;=\; -\frac{\sin\delta_0(\mu)}{4\pi^2 r^3}\int d\omega\left(-\frac{\partial}{\partial\omega}\frac{1}{1+e^{\hbar\omega/T}}\right)\cos[\delta_0(\mu)+2(k_F+\omega/v_F)r]. \tag{4.54}$$

At zero temperature, this simplifies to Eq. (4.79). These density oscillations are known as "Friedel oscillations". At zero temperature, Friedel oscillations fall off algebraically, proportional to $1/r^3$. At finite temperatures, the main cause of decay are the thermal fluctuations of the phase shift $2\omega r/v_F$, which are important for $T \gtrsim \hbar v_F/r$.

The final results (4.53) and (4.54) are to be multiplied by two if spin degeneracy is taken into account.

4.2.2 real-time formalism

We now present the same calculation using Green functions with real time arguments. The real-time formalism makes use of contour-ordered Green functions, where the integration contour is the Keldysh contour. The electron density can be calculated as

$$n(\mathbf{r},t) = \langle\hat{\psi}^\dagger(\mathbf{r})\hat{\psi}(\mathbf{r})\rangle = -iG^<(\mathbf{r},t;\mathbf{r},t). \tag{4.55}$$

Alternatively, we can use the anticommutation relations of the fermion creation and annihilation operators, to write $G^<(\mathbf{r},t;\mathbf{r}',t) = G^>(\mathbf{r},t;\mathbf{r}',t)+i\delta(\mathbf{r}-\mathbf{r}')$. Hence, using $G^K = G^> + G^<$, we find

$$n(\mathbf{r},t) = -\frac{i}{2}G^K(\mathbf{r},t;\mathbf{r},t) + \frac{1}{2}\lim_{\mathbf{r}'\to\mathbf{r}}\delta(\mathbf{r}-\mathbf{r}'). \tag{4.56}$$

If we are interested in the change of the density due to the presence of the impurity, we don't care about the delta function contribution. Hence, it will be our goal to calculate the Keldysh Green function $G^K(\mathbf{r},t;\mathbf{r},t)$.

As before, we like to calculate $n(\mathbf{r})$ in perturbation theory using Wick's theorem. However, Wick's theorem applies to time-ordered or contour-ordered Green functions only. Hence, although we are interested in the Keldysh Green function only, we'll have to calculate the full contour-ordered Green function $G(\mathbf{r},t;\mathbf{r}',t')$ where t and t' are located on the Keldysh contour.

We now arrange the perturbation theory in such a way that the Hamiltonian $\hat{H}_1$ corresponding to the impurity potential is switched on slowly after the reference time t_0. For a time t on the Keldysh contour, we write

$$\hat{H}_1(t) = \int d\mathbf{r}\hat{\psi}^\dagger(\mathbf{r},t+\eta)U(\mathbf{r},t)\hat{\psi}(\mathbf{r},t), \tag{4.57}$$

where the time dependence of U ensures the switching on of the impurity potential. The infinitesimal η is added to the argument of the creation operator to guarantee that the creation operator appears left of the annihilation operator in a contour ordered product: the contour time $t_1+\eta$ is an infinitesimal amount "later" (in the contour sense) than t_1. With this convention, the thermal average at time t_0 will be done with respect to the unperturbed Hamiltonian $\hat{H}_0$ only. Of course, at the end of the calculation we will take the limit $t_0 \to -\infty$.

Note that in writing Eq. (4.57) we have kept the coordinate representation. The calculation outlined below can be done using the momentum representation as well.

We start from Eq. (2.56),

$$G(\mathbf{r},t;\mathbf{r}',t') = -i\langle T_{\rm c} e^{-i\int_{\rm c} dt_1 \hat{H}_1(t_1)/\hbar}\hat{\psi}(\mathbf{r},t)\hat{\psi}^\dagger(\mathbf{r}',t')\rangle_0, \tag{4.58}$$

and expand the exponential. For real-time Green functions, Wick's theorem reads

$$\begin{aligned}&\langle T_{\rm c}\hat{\psi}(\mathbf{r}_1,t_1)\ldots\hat{\psi}(\mathbf{r}_n,t_n)\hat{\psi}^\dagger(\mathbf{r}'_n,t'_n)\ldots\hat{\psi}^\dagger(\mathbf{r}'_1,t'_1)\rangle_0 \\ &\quad = \; i^n\sum_P(-1)^P G^0(\mathbf{r}_1,t_1;\mathbf{r}'_{P(1)},t'_{P(1)})\ldots G^0(\mathbf{r}_n,t_n;\mathbf{r}'_{P(n)},t'_{P(n)}).\end{aligned} \tag{4.59}$$

Up to first order in $\hat{H}_1$ one finds

$$\begin{aligned}G(\mathbf{r},t;\mathbf{r}',t') \;&=\; G^0(\mathbf{r},t;\mathbf{r}',t') + \frac{1}{\hbar}\int_{\rm c} dt_1 \int d\mathbf{r}_1 U(\mathbf{r}_1,t_1)[G^0(\mathbf{r},t;\mathbf{r}_1,t_1)G^0(\mathbf{r}_1,t_1;\mathbf{r}',t') \\ &\quad - G^0(\mathbf{r},t;\mathbf{r}',t')G^0(\mathbf{r}_1,t_1;\mathbf{r}_1,t_1+\eta)] + \ldots,\end{aligned} \tag{4.60}$$

where the dots represent terms of order two and higher. Neither the potential $U(\mathbf{r}_1,t_1)$ nor the Green function $G^0(\mathbf{r}_1,t_1;\mathbf{r}_1,t_1+\eta)$ depends depend on whether t_1 is on the upper or lower

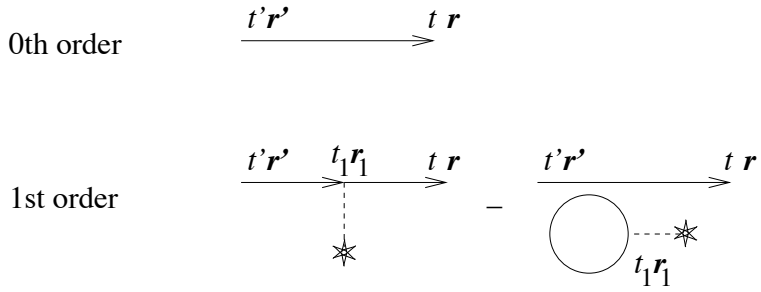

Figure 4.6: Diagrammatic representation of Eq. (4.61). The solid arrows represent the unperturbed contour-ordered Green function G^0. The dashed lines and the stars represent the impurity potential U.

branch of the Keldysh contour. Hence, upon integration over t_1 the second term between brackets vanishes and one finds

$$G(\mathbf{r},t;\mathbf{r}',t') = G^0(\mathbf{r},t;\mathbf{r}',t') + \frac{1}{\hbar}\int_c dt_1 \int d\mathbf{r}_1 U(\mathbf{r}_1,t_1) G^0(\mathbf{r},t;\mathbf{r}_1,t_1) G^0(\mathbf{r}_1,t_1;\mathbf{r}',t') + \ldots \tag{4.61}$$

Diagrammatically, the two first order terms can be represented as in Fig. 4.6. Upon integration over t_1, the disconnected rightmost diagram vanishes. This property is preserved in higher orders of perturbation theory: all disconnected diagrams vanish upon performing the intermediate integration over the Keldysh contour. Hence, only connected diagrams contribute to the perturbation expansion of G, see Fig. 4.7. Recognizing G in the perturbative series, one arrives at a self-consistent equation for G,

$$G(\mathbf{r},t;\mathbf{r}',t') = G^0(\mathbf{r},t;\mathbf{r}',t') + \frac{1}{\hbar}\int_c dt_1 \int d\mathbf{r}_1 U(\mathbf{r}_1,t_1) G^0(\mathbf{r},t;\mathbf{r}_1,t_1) G(\mathbf{r}_1,t_1;\mathbf{r}',t') \tag{4.62}$$

The self-consistent equation is shown in the second line of Fig. 4.7.

Solving the integral equation (4.62) is not entirely straightforward because the intermediate integration over t_1 is over the Keldysh contour, not over the real time axis. We write the contour integration as

$$\int_c dt \ldots \rightarrow \int_{t_0}^{\infty} dt[\text{ upper branch }] - \int_{t_0}^{\infty} dt[\text{ lower branch}].$$

If we write the contour-ordered Green function $G(t,t')$ as $G_{ij}(t,t')$, with $i = 1$ or 2 ($j = 1$ or 2), if t (t') is on the upper or lower branch of the Keldysh contour, respectively, the contour

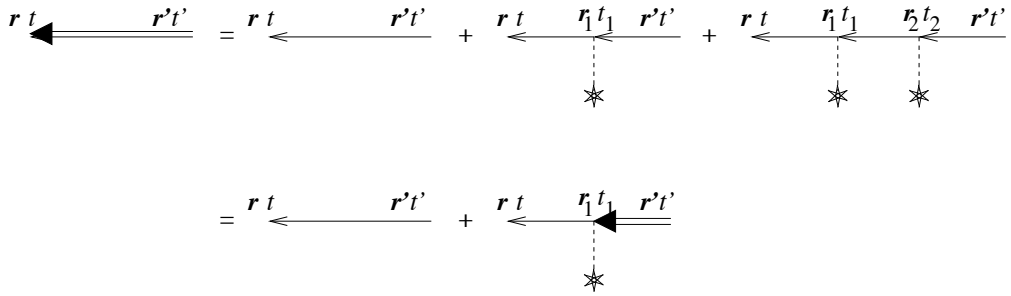

Figure 4.7: Diagrammatic representation of the contour-ordered Green function G. The double arrow represents the contour-ordered Green function. The single arrows represent the unperturbed contour-ordered Green function G^0.

integration in Eq. (4.62) amounts to matrix multiplication at each impurity vertex, combined with insertion of a minus sign at the lower branch argument. Hence, we have

$$\begin{aligned} G_{ij}(\mathbf{r},t;\mathbf{r}',t') &= G^0_{ij}(\mathbf{r},t;\mathbf{r}',t') \\ &\quad + \frac{1}{\hbar}\int d\mathbf{r}_1 \int dt_1 \sum_k G^0_{ik}(\mathbf{r},t;\mathbf{r}_1,t_1)U(\mathbf{r}_1,t_1)\sigma_{z,k}G_{kj}(\mathbf{r}_1,t_1,\mathbf{r}',t'), \end{aligned} \tag{4.63}$$

where $\sigma_{z,1}=1$ and $\sigma_{z,2}=-1$. Hence, in this matrix notation, every impurity vertex carries a Pauli matrix σ_z. Upon transformation to the matrix representation of Eq. (2.61), σ_z maps to the unit matrix, so that one has the simple result

$$\underline{G}(\mathbf{r},t;\mathbf{r}',t') = \underline{G}^0(\mathbf{r},t;\mathbf{r}',t') + \frac{1}{\hbar}\int d\mathbf{r}_1 \int dt_1 \underline{G}^0(\mathbf{r},t;\mathbf{r}_1,t_1)U(\mathbf{r}_1,t_1)\underline{G}(\mathbf{r}_1,t_1,\mathbf{r}',t'). \tag{4.64}$$

The solution of this equation is found by Fourier transform. As before, we choose the impurity potential to be of delta-function form. We switch on the potential by setting

$$U(\mathbf{r},t) = u\delta(\mathbf{r})e^{\eta t}, \tag{4.65}$$

where η is a positive infinitesimal. Then, upon Fourier transforming Eq. (4.64) to time and space coordinates, one finds

$$\underline{G}_{\mathbf{k},\mathbf{k}'}(\omega) = \underline{G}^0_{\mathbf{k},\mathbf{k}}(\omega)\delta_{\mathbf{k},\mathbf{k}'} + \frac{u}{\hbar V}\underline{G}^0_{\mathbf{k},\mathbf{k}}(\omega)\left(\sum_{\mathbf{k}_1}\underline{G}_{\mathbf{k}_1,\mathbf{k}'}(\omega)\right). \tag{4.66}$$

Summing over $\mathbf{k}$, we find

$$\sum_{\mathbf{k}}\underline{G}_{\mathbf{k},\mathbf{k}'}(\omega) = \left[1 - \frac{u}{\hbar V}\sum_{\mathbf{k}}\underline{G}^0_{\mathbf{k},\mathbf{k}}(\omega)\right]^{-1}\underline{G}^0_{\mathbf{k}'}(\omega), \tag{4.67}$$

where the inverse means matrix inversion. Hence, upon resubstitution into Eq. (4.66),

$$\underline{G}_{\mathbf{k},\mathbf{k}'}(\omega) = \underline{G}^0_{\mathbf{k}}(\omega)\delta_{\mathbf{k},\mathbf{k}'} + \frac{u}{\hbar V}\underline{G}^0_{\mathbf{k}}(\omega)\left[1 - \frac{u}{\hbar V}\sum_{\mathbf{k}}\underline{G}^0_{\mathbf{k}}(\omega)\right]^{-1}\underline{G}^0_{\mathbf{k}'}(\omega), \tag{4.68}$$

The matrix Green function $\underline{G}$ has a special matrix structure: the lower left element of the matrix is zero, see Eq. (2.61). This special matrix structure is preserved under multiplication and matrix inversion, which makes the matrix inversion in Eq. (4.68) rather straightforward. Abbreviating

$$\overline{\underline{G}^0(\omega)} = \frac{1}{V}\sum_{\mathbf{k}}\underline{G}^0_{\mathbf{k}}(\omega), \tag{4.69}$$

we then find that the Keldysh component of $\underline{G}$ reads

$$\begin{aligned} G^{\rm K}_{\mathbf{k},\mathbf{k}'}(\omega) &= G^{0\rm K}_{\mathbf{k}'}(\omega) + \frac{u}{V}\frac{G^{0\rm K}_{\mathbf{k}}(\omega)G^{0\rm A}_{\mathbf{k}'}(\omega)}{\hbar - u\overline{G^{0\rm A}(\omega)}} + \frac{u^2}{V}\frac{G^{0\rm R}_{\mathbf{k}}(\omega)\overline{G^{0\rm K}(\omega)}G^{0\rm A}_{\mathbf{k}'}(\omega)}{(\hbar - u\overline{G^{0\rm R}(\omega)})(\hbar - u\overline{G^{0\rm A}(\omega)})} \\ &\quad + \frac{u}{V}\frac{G^{0\rm R}_{\mathbf{k}}(\omega)G^{0\rm K}_{\mathbf{k}'}(\omega)}{(\hbar - u\overline{G^{0\rm R}(\omega)})} \\ &= G^{0\rm K}_{\mathbf{k}'}(\omega) + \frac{u}{V}\tanh(\hbar\omega/2T)\left[\frac{G^{0\rm R}_{\mathbf{k}}(\omega)G^{0\rm R}_{\mathbf{k}'}(\omega)}{\hbar - u\overline{G^{0\rm R}(\omega)})} - \frac{G^{0\rm A}_{\mathbf{k}}(\omega)G^{0\rm A}_{\mathbf{k}'}(\omega)}{\hbar - u\overline{G^{0\rm A}(\omega)})}\right], \end{aligned} \tag{4.70}$$

where, in the last equality, we used Eq. (2.64) for the Keldysh Green function $G^{0\rm K}$.[4] Using Eqs. (3.17) and (3.18) for $G^{0\rm R}$ and $G^{0\rm A}$ it is easy to verify that one recovers the same result as in the imaginary time formalism upon Fourier transform to time and space.

Both the imaginary-time and Keldysh formalism can be used for equilibrium calculations. In spite of their simplicity, the calculations in this section have shown the advantages and disadvantages of the imaginary-time and Keldysh formalisms: The imaginary-time formalism requires a tedious analytical continuation in order to find physically meaningful results, whereas the Keldysh formalism needs matrix operations. What formalism you prefer to use is a matter of taste. For nonequilibrium calculations, the situation is different, however. Nonequilibrium calculations can be done using the Keldysh formalism only.

[4]The same result can be obtained in a simpler way if one solves Eq. (4.68) for the retarded and advanced components of $\underline{G}$ and then applies Eq. (2.64) to the Keldysh Green function $G^{\rm K}$.

4.3 Exercises

Exercise 4.1: Friedel oscillations

For an impurity with a general potential $U(\mathbf{r})$, calculate the shift in the electronic density to first order in U. Compare your result to Eq. (4.54).

Exercise 4.2: Scattering from a single impurity in one dimension

In this exercise, we consider scattering from a delta-function impurity in one dimension. The impurity has potential $U(x) = u\delta(x)$ and is located at the origin.

It is our aim to calculate the full Green function $\mathcal{G}(x, x'; i\omega_n)$ in coordinate representation. In order to calculate $\mathcal{G}(x, x'; i\omega_n)$, one may either use the Green function in momentum space and Fourier transform back to coordinate space, as we did in Sec. 4.2, or derive the Dyson equation in coordinate representation. Following the latter method, you can verify that one finds

$$\mathcal{G}(x, x'; i\omega_n) = \mathcal{G}^0(x, x'; i\omega_n) + \mathcal{G}^0(x, 0; i\omega_n)\frac{u}{\hbar - \mathcal{G}^0(0, 0; i\omega_n)u}\mathcal{G}^0(0, x'; i\omega_n).$$

(a) Calculate the temperature Green function in coordinate representation.

(b) Use your answer to (a) to calculate the retarded Green function. If $x' < 0$, show that it can be written as

$$G^{\mathrm{R}}(x, x'; \omega) = tG^{0\mathrm{R}}(x, x'; \omega)\theta(x) + [1 + re^{i\phi(x,x')}]G^{0\mathrm{R}}(x, x', \omega)\theta(-x). \quad (4.71)$$

The complex numbers t and r are called "transmission" and "reflection" amplitude.

(c) Explain the origin of the phase shift $\phi(x, x')$ in Eq. (4.71).

Exercise 4.3: Alternative derivation of the Friedel Sum rule

The Friedel sum rule(4.19) relates the change ΔN in the total number of particles as the result of the presence of an impurity to the phase shifts that particles experience while scattering off the impurity. You have seen a formal derivation of the Friedel sum rule in Sec. 4.1. Here, we will consider a more elementary derivation of the Friedel sum rule for the case of a spherically symmetric scatterer.

If a flux of noninteracting particles is elastically scattered on a spherically symmetric potential at $\mathbf{r} = 0$, the wave function at large values of r will be of the form

$$\psi(\mathbf{r}) \approx e^{ikz} + f(\theta)\frac{e^{ikr}}{r}, \tag{4.72}$$

where z is the direction of the incoming flux, see Eq. (4.8) above. Since the scattered wave in Eq. (4.72) has axial symmetry about the z-axis, it may be expanded in Legendre polynomials,

$$\psi(\mathbf{r}) = \sum_{\ell=0}^{\infty} a_\ell P_\ell(\cos\theta) R_{k\ell}(r) \tag{4.73}$$

The constants a_ℓ are expansion coefficients.

(a) Show that the radial functions $R_{k\ell}$ satisfy the "radial Schrödinger equation"

$$r^{-2}\frac{\partial}{\partial r} r^2 \frac{\partial R_{k\ell}}{\partial r} + \left(k^2 - \frac{\ell(\ell+1)}{r^2} - \frac{2m}{\hbar^2} U(r) \right) R_{k\ell} = 0, \tag{4.74}$$

where the energy eigenvalues are written as $\hbar^2 k^2/2m$, the energy of a free particle, and $U(r)$ is the scattering potential.

(b) Show that, at distances sufficiently large that $U(r) \approx 0$, the radial functions $R_{k\ell}$ will approach the asymptotic expansion

$$R_{k\ell} \approx \frac{2}{r}\sin(kr - \ell\pi/2 + \delta_\ell) \tag{4.75}$$

Both the factor of 2 and the factor $\ell\pi/2$ are introduced for convenience, so that the asymptotic behavior of $R_{k\ell}$ reduces to the solutions for $R_{k\ell}$ when $U(r)$ vanishes identically, by putting $\delta_\ell = 0$. The δ_ℓ are the so-called scattering phases. They depend on the scattering potential $U(r)$ and approach zero when $U(r)$ vanishes.

(c) The change in the number of states near the Fermi surface as a result of the scattering potential generally depends on the δ_ℓ's. To see this, we first have to connect the general δ_ℓ's in the expression (4.75) for the radial functions in the expansion of the *total* wavefunction (4.73) to the function $f(\theta)$ defined in (4.72). Apart from an overall normalization, the coefficients a_ℓ in (4.73) are fixed by the requirement that the function $\Psi - e^{ikz}$ is of the form $f(\theta)e^{ikr}/r$, i.e. has only terms of the form of an outgoing wave, e^{ikr}/r. Argue that this requirement leads to the identification

$$f(\theta) = \frac{1}{2ik}\sum_{\ell=0}^{\infty}(2\ell+1)\left[e^{2i\delta_\ell} - 1\right] P_\ell(\cos\theta). \tag{4.76}$$

Hint: use the fact that for large r the plane wave e^{ikz} can be expanded in terms of Legendre polynomials as

$$e^{ikz} = e^{ikr\cos\theta} = \frac{1}{2ikr}\sum_{\ell=0}^{\infty}(2\ell+1)P_\ell(\cos\theta)\left[(-1)^{\ell+1}e^{-ikr} + e^{ikr}\right].$$

Let us now consider the change in the number of states in the presence of the impurity. Hereto we imagine a large sphere of radius L about the origin, and impose that the wavefunction vanishes on this sphere. In the absence of the potential ($\delta_\ell = 0$), Eq. (4.75) then yields

$$kL - \frac{\ell\pi}{2} = n\pi \implies k_{n\ell} = \frac{\ell\pi}{2L} + \frac{n\pi}{L} \tag{4.77}$$

In the presence of the scattering potential, the wavenumbers $k'_{n\ell}$ satisfy $k'_{n\ell} = \ell\pi/(2L) + n\pi/L - \delta_\ell/L$, so we get for the change in wavenumber

$$k'_{n\ell} - k_{n\ell} = -\frac{\delta_\ell}{L} \tag{4.78}$$

Let us first consider the special case in which only δ_0 is nonzero. The spacing of successive values of k_{n0} is π/L [see Eq. (4.77)]; if we now consider a given value of k, say $k = k_F$, and imagine turning on the potential, then each allowed k value shifts, according to Eq. (4.78), by an amount $-\delta_0(k_F)/L$. Then the number of states k with $k < k_F$ increases by an amount

$$N_{\rm imp} = \frac{\delta_0}{L}\cdot\frac{L}{\pi} = \frac{\delta_0}{\pi}.$$

(d) Extend these arguments to prove the general Friedel sum rule (4.19), which reads, in terms of the phase shifts δ_ℓ,

$$N_{\rm imp} = \pi^{-1}\sum_\ell (2\ell+1)\delta_\ell(k_F).$$

(e) Using similar arguments, argue that, at zero temperature, the density of electrons far from a small spherically symmetric impurity shows oscillations

$$n_{\rm imp}(r) \approx -\frac{1}{4\pi^2 r^3}\cos[2k_F r + \delta_0(k_F)]\sin[\delta_0(k_F)], \tag{4.79}$$

where δ_0 is a scattering phase shift evaluated at the Fermi energy.

Exercise 4.4: Anderson model for impurity scattering

In some applications, a simple scattering potential is not a good description for an impurity. This is the case, for example, if the impurity introduces an extra localized state for electrons in an otherwise perfect lattice. In this case, one can use the following Hamiltonian to describe the impurity,

$$\mathcal{H} = \sum_{\mathbf{k},\sigma} \varepsilon_{\mathbf{k}\sigma} \hat{\psi}^\dagger_{\mathbf{k}\sigma} \hat{\psi}_{\mathbf{k}\sigma} + \varepsilon_{\rm imp} \sum_\sigma \hat{\psi}^\dagger_{\rm i\sigma} \hat{\psi}_{\rm i\sigma} + \sum_{\mathbf{k}\sigma} (V_{\mathbf{k}} \hat{\psi}^\dagger_{\mathbf{k}\sigma} \hat{\psi}_{\rm i\sigma} + V^*_{\mathbf{k}} \hat{\psi}^\dagger_{\rm i\sigma} \hat{\psi}_{\mathbf{k}\sigma}). \tag{4.80}$$

Here $\varepsilon_{\rm imp}$ is the energy of the extra localized state. The second line of Eq. (4.80) represents "hybridization" of the impurity state with the Bloch states $|\mathbf{k}\rangle$ of the lattice. The matrix element $V_{\mathbf{k}}$ describes the overlap of the impurity state with the state $|\mathbf{k}\rangle$. For a strongly localized impurity orbital at the origin, one can neglect the $\mathbf{k}$-dependence of the matrix elements $V_{\mathbf{k}}$.

For this system, we define Green functions with respect to the wavevectors of the Bloch states and with respect to the impurity site. Hence, the temperature Green function is denoted as $\mathcal{G}_{\mathbf{k}',\mathbf{k}}(i\omega_n)$, $\mathcal{G}_{\rm i,\mathbf{k}}(i\omega_n)$, $\mathcal{G}_{\mathbf{k}',\rm i}(i\omega_n)$, and $\mathcal{G}_{\rm i,i}(i\omega_n)$, etc.

(a) Show that the temperature Green function satisfies the equations

$$\begin{aligned} 1 &= (i\omega_n - \varepsilon_{\rm imp})\mathcal{G}_{\rm i,i}(i\omega_n) - \sum_{\mathbf{k}'} V^*_{\mathbf{k}'} \mathcal{G}_{\mathbf{k}',\rm i}(i\omega_n), \\ 0 &= (i\omega_n - \varepsilon_{\mathbf{k}'})\mathcal{G}_{\mathbf{k}',\rm i}(i\omega_n) - V_{\mathbf{k}'} \mathcal{G}_{\rm i,i}(i\omega_n), \\ 0 &= (i\omega_n - \varepsilon_{\rm imp})\mathcal{G}_{\rm i,\mathbf{k}}(i\omega_n) - \sum_{\mathbf{k}'} V^*_{\mathbf{k}'} \mathcal{G}_{\mathbf{k}',\mathbf{k}}(i\omega_n), \\ \delta_{\mathbf{k}'\mathbf{k}} &= (i\omega_n - \varepsilon_{\mathbf{k}'})\mathcal{G}_{\mathbf{k}',\mathbf{k}}(i\omega_n) - V_{\mathbf{k}'} \mathcal{G}_{\rm i,\mathbf{k}}(i\omega_n). \end{aligned}$$

Solve these equations and analytically continue your answer to find the retarded Green function $G^{\rm R}$.

(b) Show that the T-matrix is given by

$$T_{\mathbf{k}'\mathbf{k}}(\varepsilon) = V_{\mathbf{k}'} G_{\rm i,i}(\varepsilon) V^*_{\mathbf{k}}.$$

Calculate the total scattering phase shift $\delta(\varepsilon)$, and the impurity density of states $\nu_{\rm imp}(\varepsilon)$.

(c) Evaluate your expressions for the special case of a "flat conduction band": the conduction electron states have a constant density of states ν_0 for energies $-D < \varepsilon < D$, where D is the bandwidth. For the hybridization matrix elements, you may set $|V_{\mathbf{k}}|^2 = V^2/N_{\rm s}$, where $N_{\rm s}$ is the total number of lattice sites in the sample. (For a lattice, the number of available wavevectors also equals $N_{\rm s}$.) The conduction electron density of states ν_0 is defined as density of states per site.

Exercise 4.5: Resonant tunneling

In this exercise we consider a "quantum well", which is formed between two tunnel barriers in a three-dimensional metal or semiconductor structure. The tunnel barriers have a potential $U(\mathbf{r}) = u(\delta(x-a) + \delta(x+a))$.

Since the system is translation invariant in the y and z directions, but not in the x direction, we use a mixed notation, in which Green functions are Fourier transformed with respect to y and z, but not with respect to x. The Green function is diagonal in the momenta k_y and k_z.

(a) Following the same method as in exercise 4.2, calculate the retarded Green function $G^{\rm R}_{k_y,k_z;k_y,k_z}(x,x';\omega)$. Express your answer in the same form as Eq. (4.71) and calculate the transmission and reflection amplitudes t_{k_y,k_z} and r_{k_y,k_z}.

(b) When is the transmission is unity? Find a simple physical argument for this relation. (Hint: use your answer to Ex. 4.2.)

Chapter 5

Many impurities

We have seen that it was a difficult (but still doable!) task to calculate the Green function for a single impurity. In the presence of many impurities, the calculation of the Green function is as good as impossible.

One might ask whether that is a big problem. Do we really want to calculate the Green function in the presence of many impurities? The answer is no, and the reason is very simple: Nobody knows the exact locations and potentials of all impurities in a realistic sample! Of course, if we don't know the exact potential $U(\mathbf{r})$, it does not make sense to try to calculate the exact Green function in the presence of that potential.

The information one usually does have is the concentration of impurities, *i.e.*, the number of impurities per unit volume and, if the chemical species of the impurity atoms and their preferred location inside the lattice unit cell are known, the form of the potential of a single impurity. Because that is all information one has, one considers an *ensemble* of different samples, all with the same impurity concentration, but with different locations of the impurities. Such samples are called "macroscopically equivalent but microscopically different". We then calculate quantities that are averaged over this ensemble. Such an average is called a *disorder average*, to distinguish it from the *thermal average* we have been considering so far.

There is an important difference between disorder averages and thermal averages. In a thermal average, one averages over time-dependent fluctuations. According to the ergodic hypothesis, if one waits long enough, a sample will access all accessible states. Hence, the thermal average equals the time average. In a disorder average, one averages over impurity configurations. For a given sample, the impurities typically do not move. Hence, in order to obtain a disorder average experimentally one has to, somehow, involve many samples that

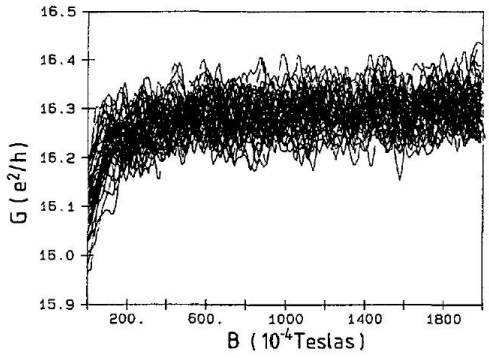

Figure 5.1: Reproducible magnetoconductance curves measured at $T = 45$ mK. Different curves are measured for different cool downs of the same GaAs wire. Figure is taken from D. Mailly and M. Sanquer, J. Phys. (France) I **2**, 357 (1992).

have the same impurity concentration but different impurity locations.[1]

One way of obtaining a disorder average experimentally is "thermal cycling": to repeatedly heat up and cool the same sample. The reason why this works is that, at sufficiently high temperatures, impurities are somewhat mobile. Hence, after heating up and cooling down the sample once, a different static impurity configuration is obtained. An example of this procedure is shown in Fig. 5.1. Here, the conductance of a metal wire is measured as a function of the magnetic field. The different curves correspond to different cool downs of the same wire. Within one cool down, the conductance curves are fully reproducible, as one would expect for a static impurity configuration. There are small differences between cool downs. Indeed, different cool downs should correspond to slightly different impurity configurations, for which one expect slightly different Green functions, and, hence, a slightly different conductance. From the experimental data of Fig. 5.1, one can calculate the average conductance for this "ensemble" of wires, the variance, and so on. The average and variance can then be compared to a theory. You can see plots of the average conductance and of the variance in Fig. 5.2.

In this chapter we discuss how a disorder average is taken in the Green function formalism.

[1]Some observables may be "self-averaging": all samples in the ensemble will behave in the same way, irrespective of the microscopic details of impurity configuration. In the case of a self-averaging observable, it is sufficient to measure one sample only.

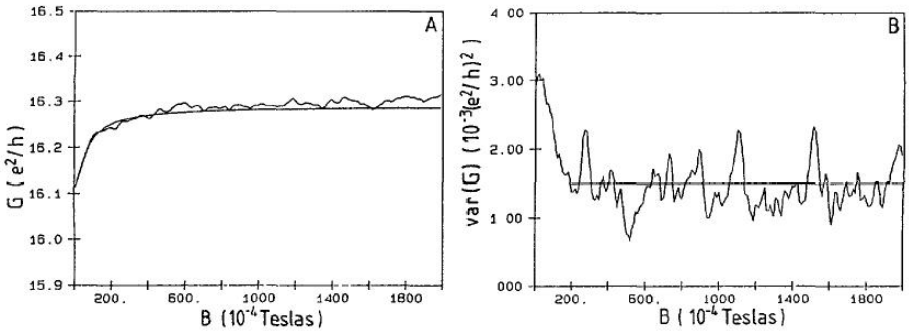

Figure 5.2: Average (a) and variance (b) of the magnetoconductance curves of Fig. 5.1, together with theoretical predictions. The average and variance were taken over 50 different disorder configurations. The figure is taken from D. Mailly and M. Sanquer, J. Phys. (France) I **2**, 357 (1992).

5.1 Disorder average

The joint effect of all impurities is described by the potential

$$U(\mathbf{r}) = \sum_{j=1}^{N_{\rm imp}} u(\mathbf{r} - \mathbf{r}_j), \tag{5.1}$$

where $\mathbf{r}_j$ is the location of the jth impurity. The Fourier transform of the impurity potential is

$$\begin{aligned} U_{\mathbf{q}} &= \frac{1}{V}\int d\mathbf{r} U(\mathbf{r}) e^{-i\mathbf{q}\cdot\mathbf{r}} \\ &= u_{\mathbf{q}} \sum_{j=1}^{N_{\rm imp}} e^{-i\mathbf{q}\cdot\mathbf{r}_j}, \end{aligned} \tag{5.2}$$

where $u_{\mathbf{q}}$ is the Fourier transform of the scattering potential for a single impurity. For delta-function impurities with $u(\mathbf{r}) = u\delta(\mathbf{r})$ one has $u_{\mathbf{q}} = u/V$, see Eq. (4.20).

In performing the disorder average for a Green function, we have to average products of the disorder potential $U_{\mathbf{q}}$ over the positions of the impurities. The corresponding averages are

$$\begin{aligned} \langle U_{\mathbf{q}} \rangle &= u_{\mathbf{q}} N_{\rm imp} \delta_{\mathbf{q},0}, \\ \langle U_{\mathbf{q}_1} U_{\mathbf{q}_2} \rangle &= u_{\mathbf{q}_1} u_{\mathbf{q}_2} [N_{\rm imp}(N_{\rm imp}-1)\delta_{\mathbf{q}_1,0}\delta_{\mathbf{q}_2,0} + N_{\rm imp}\delta_{\mathbf{q}_1+\mathbf{q}_2,0}], \\ \langle U_{\mathbf{q}_1} U_{\mathbf{q}_2} U_{\mathbf{q}_3} \rangle &= u_{\mathbf{q}_1} u_{\mathbf{q}_2} u_{\mathbf{q}_3} [N_{\rm imp}(N_{\rm imp}-1)(N_{\rm imp}-2)\delta_{\mathbf{q}_1,0}\delta_{\mathbf{q}_2,0}\delta_{\mathbf{q}_3,0} \end{aligned}$$

$$+ N_{\rm imp}(N_{\rm imp}-1)(\delta_{\mathbf{q}_1,0}\delta_{\mathbf{q}_2+\mathbf{q}_3,0} + \delta_{\mathbf{q}_2,0}\delta_{\mathbf{q}_1+\mathbf{q}_3,0} + \delta_{\mathbf{q}_3,0}\delta_{\mathbf{q}_1+\mathbf{q}_2,0})$$
$$+ N_{\rm imp}\delta_{\mathbf{q}_1+\mathbf{q}_2+\mathbf{q}_3,0}], \tag{5.3}$$

and so on. We'll consider the case when the sample is large and there are many impurities. In that case, we can neglect the difference between $N_{\rm imp}-1$ or $N_{\rm imp}-2$ and $N_{\rm imp}$ in the above formulas. Studying the case of many impurities does not mean that one can neglect, e.g., the term $N_{\rm imp}\delta_{\mathbf{q}_1+\mathbf{q}_2,0}$ in the second line of Eq. (5.3) with respect to the term $N_{\rm imp}^2\delta_{\mathbf{q}_1,0}\delta_{\mathbf{q}_2,0}$. The reason is that the former term has one more summation over the momenta, which may bring in extra factors volume. (Note that, for a fixed concentration of impurities, $N_{\rm imp}$ is proportional to the sample volume V.)

The disorder average is taken *after* the thermal average. Based on Eq. (5.3), one can formulate a set of diagrammatic rules for the impurity average that should be implemented on top of the diagrammatic rules for the thermal average. These rules are

- Momentum has to be conserved at an impurity vertex (a star in the diagram),
- Every impurity vertex (represented by a star in the diagram) contributed a factor $N_{\rm imp}$.
- An arbitrary number of dashed lines can meet at a single impurity vertex. Every dashed impurity line carrying a momentum $\mathbf{q}$ contributes a factor $u_{\mathbf{q}}$.

5.2 Disorder average of single-particle Green function

We now use the diagrammatic rules derived in the previous section to calculate the disorder average of the single-particle Green function. In this section, we'll use the imaginary-time formalism. The derivation in the real-time Keldysh formalism proceeds along the same lines.

Our first observation is that the disorder average restores translation invariance. Hence, $\langle \mathcal{G}_{\mathbf{k},\mathbf{k}'}(\tau)\rangle$ is nonzero only if $\mathbf{k}=\mathbf{k}'$,

$$\langle \mathcal{G}_{\mathbf{k},\mathbf{k}'}(\tau)\rangle = -\langle T_\tau \hat{\psi}_{\mathbf{k}}(\tau)\hat{\psi}^\dagger_{\mathbf{k}'}(0)\rangle \equiv \langle \mathcal{G}_{\mathbf{k}}(\tau)\rangle \delta_{\mathbf{k},\mathbf{k}'}. \tag{5.4}$$

A diagrammatic expansion for $\langle \mathcal{G}_{\mathbf{k}}(i\omega_n)\rangle$ is shown in Fig. 5.3. In this figure, all labels for the imaginary frequency and wavevector have been suppressed. You can include them in accordance with the diagrammatic rules of the previous section.

The diagrammatic expansion of Fig. 5.3 looks rather wild. One can introduce some order in this expansion with the concept of "irreducible diagrams". A diagram is called "irreducible" if it cannot be cut into two pieces by cutting a single internal fermion line. For example, the first, second, third, fifth, and eighth diagram in the expansion of Fig. 5.3 are

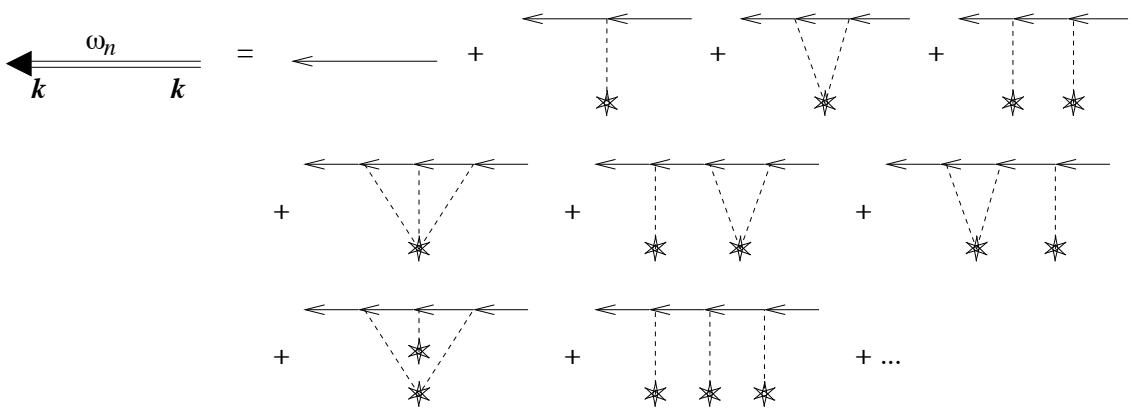

Figure 5.3: Diagrammatic expansion of the disorder averaged single-particle Green function $\langle \mathcal{G}_{\mathbf{k},\mathbf{k}'}(i\omega_n)\rangle$.

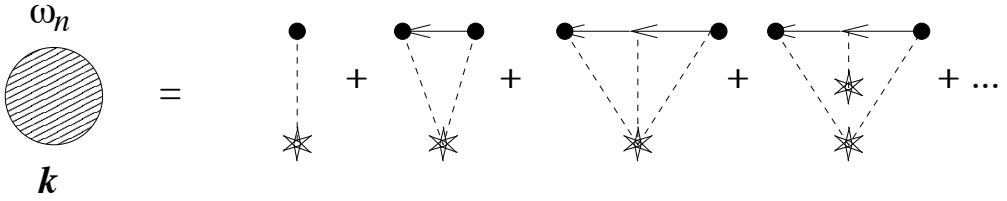

Figure 5.4: Diagrammatic expansion of the self energy $\Sigma_{\mathbf{k}}$ for the disorder averaged single-particle Green function $\langle \mathcal{G}_{\mathbf{k},\mathbf{k}'}(i\omega_n)\rangle$. The self energy is denoted by the shadded bubble at the left hand side of the figure.

irreducible. The other diagrams in Fig. 5.3 are "reducible". The sum of all irreducible diagrams, without the external fermion lines, is called the "self energy" $\Sigma_{\mathbf{k}}$. Diagrammatically, the self energy is given by the expansion of Fig. 5.4. In terms of the self energy, the disorder averaged Green function is seen to obey a Dyson equation, see Fig. 5.5,

$$\langle \mathcal{G}_{\mathbf{k},\mathbf{k}}(i\omega_n)\rangle = \mathcal{G}^0_{\mathbf{k},\mathbf{k}}(i\omega_n) + \mathcal{G}^0_{\mathbf{k},\mathbf{k}}(i\omega_n)\Sigma_{\mathbf{k}}(i\omega_n)\langle \mathcal{G}_{\mathbf{k},\mathbf{k}}(i\omega_n)\rangle. \tag{5.5}$$

The solution of the Dyson equation is

$$\langle \mathcal{G}_{\mathbf{k},\mathbf{k}}(i\omega_n)\rangle = \frac{\mathcal{G}^0_{\mathbf{k},\mathbf{k}}(i\omega_n)}{1-\mathcal{G}^0_{\mathbf{k},\mathbf{k}}(i\omega_n)\Sigma_{\mathbf{k}}(i\omega_n)} = \frac{1}{i\omega_n - \varepsilon_{\mathbf{k}} + \mu - \Sigma_{\mathbf{k}}(i\omega_n)}. \tag{5.6}$$

With this result, we have reduced the calculation of the disorder averaged single-particle Green function to that of the self energy $\Sigma_{\mathbf{k}}(i\omega_n)$.

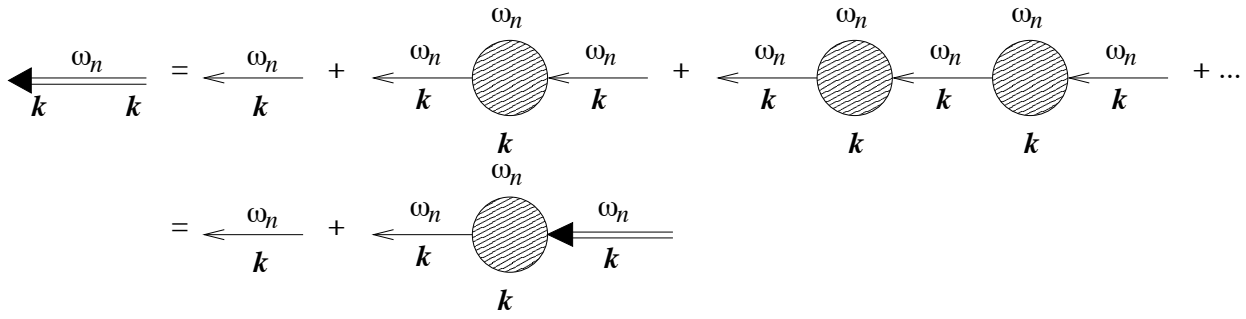

Figure 5.5: Diagrammatic representation of the Dyson equation for the disorder averaged Green function $\langle \mathcal{G}_{\mathbf{k},\mathbf{k}'}(i\omega_n)\rangle$.

The reason why the quantity $\Sigma_{\mathbf{k}}$ is called "self energy" is clear from Eq. (5.6): the self energy provides a shift of the energy $\varepsilon_{\mathbf{k}}$ that appears in the denominator of the single-particle Green function. The shift is caused by the average effect of scattering from all impurities.

Still, the diagrammatic expansion for the self energy is too complicated to be solved exactly. In the limit of a low impurity concentration, one can restrict the diagrammatic expansion to those diagrams that have one impurity vertex. Indeed, according to the diagrammatic rules of the previous section, every impurity vertex contributes a factor $N_{\rm imp}$, so that diagrams with two or more impurity vertices contribute to higher order in the impurity concentration. (See also exercise 5.1).) The approximation in which one considers diagrams with one impurity vertex is referred to as the "Born approximation". One refers to the "nth order Born approximation" as the Born approximation where only self energy diagrams with $n+1$ or less impurity lines are kept.

Diagrammatically, the Born approximation corresponds to the expansion shown in Fig. 5.6. For the self energy this implies

$$\begin{aligned}\Sigma_{\mathbf{k}}(i\omega_n) &= N_{\rm imp}\Bigg[u_0 + \sum_{\mathbf{q}} u_{-\mathbf{q}}\mathcal{G}^0_{\mathbf{k}+\mathbf{q}}(i\omega_n)u_{\mathbf{q}} \\ &\qquad + \sum_{\mathbf{q}_1,\mathbf{q}_2} u_{-\mathbf{q}_1}\mathcal{G}^0_{\mathbf{k}+\mathbf{q}_1}(i\omega_n)u_{\mathbf{q}_1-\mathbf{q}_2}\mathcal{G}^0_{\mathbf{k}+\mathbf{q}_2}(i\omega_n)u_{\mathbf{q}_2} + \ldots\Bigg]. \end{aligned} \tag{5.7}$$

If we compare this with the expression for the T-matrix of a single impurity, Eq. (4.5), we arrive at the important conclusion

$$\Sigma_{\mathbf{k}}(i\omega_n) = N_{\rm imp}T_{\mathbf{k},\mathbf{k}}(i\omega_n). \tag{5.8}$$

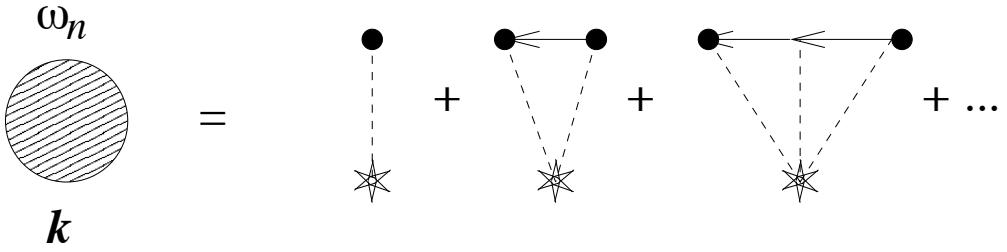

Figure 5.6: Diagrammatic expansion of the Born approximation for the self energy $\Sigma_{\mathbf{k}}$ for the disorder averaged single-particle Green function $\langle \mathcal{G}_{\mathbf{k},\mathbf{k}'}(i\omega_n)\rangle$.

In calculations, we'll be interested in the analytical continuation of the self energy to real frequencies $\omega \pm i\eta$. After analytical continuation, the real part of the self energy is nothing but a shift of the pole of the single-particle Green function. It will usually be neglected since it is a slow function of $\mathbf{k}$ and ω that can be absorbed in a redefinition of the chemical potential or in a redefinition of the energy $\varepsilon_{\mathbf{k}}$. The imaginary part of the self energy is more important. It can be expressed in terms of the scattering time $\tau_{\mathbf{k}}$ using the optical theorem, Eq. (4.15),

$$\begin{aligned} \mathrm{Im}\,\Sigma_{\mathbf{k}}(\omega + i\eta) &= -\mathrm{Im}\,\Sigma_{\mathbf{k}}(\omega - i\eta) \\ &= -N_{\mathrm{imp}}\pi \sum_{\mathbf{k}'} |T_{\mathbf{k}'\mathbf{k}}(\omega)|^2 \delta(\omega - \varepsilon_{\mathbf{k}'}) \\ &\equiv -\frac{1}{2\tau_{\mathbf{k}}}, \end{aligned} \tag{5.9}$$

where $1/\tau_{\mathbf{k}}$ is the rate for scattering out of the momentum eigenstate $|\mathbf{k}\rangle$. The scattering rate is N_{imp} times the scattering rate due to a single impurity only, see Eq. (4.11). (It is only in the limit of a low impurity concentration that the scattering rate is proportional to the number of impurities.)

One can also understand the first equality in Eq. (4.11) without making use of the optical theorem. To see this, we start from the second line in Eq. (4.11), write the T-matrix in terms of the retarded and advanced Green functions for the unperturbed Hamiltonian, cf. Eq. (4.5), and use the equality $2\pi\delta(\omega - \varepsilon_{\mathbf{k}}) = iG^{0\mathrm{R}}_{\mathbf{k}}(\omega) - iG^{0\mathrm{A}}_{\mathbf{k}}(\omega)$,

$$\begin{aligned} 2\pi \sum_{\mathbf{k}'} |T_{\mathbf{k}'\mathbf{k}}(\omega)|^2 \delta(\omega - \varepsilon_{\mathbf{k}'}) &= i \sum_{\mathbf{k}'} (G^{0\mathrm{R}}_{\mathbf{k}'}(\omega) - G^{0\mathrm{A}}_{\mathbf{k}'}(\omega)) \\ &\quad \times \left[u_{\mathbf{k}-\mathbf{k}'} + \sum_{\mathbf{k}_1} u_{\mathbf{k}-\mathbf{k}_1} G^{0\mathrm{R}}_{\mathbf{k}_1}(\omega) u_{\mathbf{k}_1-\mathbf{k}'} + \ldots \right] \end{aligned}$$

$$\times \left[u_{\mathbf{k}'-\mathbf{k}} + \sum_{\mathbf{k}_1} u_{\mathbf{k}'-\mathbf{k}_1} G^{0\mathrm{A}}_{\mathbf{k}_1}(\omega) u_{\mathbf{k}_1-\mathbf{k}} + \ldots \right]. \quad (5.10)$$

In this expansion, all terms that contain at least one retarded and one advanced Green function cancel. What remains is a difference of two terms, one involving retarded Green functions only and one involving advanced Green functions only,

$$\begin{aligned} \pi \sum_{\mathbf{k}'} |T_{\mathbf{k}'\mathbf{k}}(\omega)|^2 \delta(\omega - \varepsilon_{\mathbf{k}'}) &= \frac{i}{2} \sum_{\mathbf{k}'} \left[u_{\mathbf{k}-\mathbf{k}'} + \sum_{\mathbf{k}_1} u_{\mathbf{k}-\mathbf{k}_1} G^{0\mathrm{R}}_{\mathbf{k}_1}(\omega) u_{\mathbf{k}_1-\mathbf{k}'} + \ldots \right] G^{0\mathrm{R}}_{\mathbf{k}'}(\omega) u_{\mathbf{k}'-\mathbf{k}} \\ &\quad - \frac{i}{2} \sum_{\mathbf{k}'} u_{\mathbf{k}-\mathbf{k}'} G^{0\mathrm{A}}_{\mathbf{k}'} \left[u_{\mathbf{k}'-\mathbf{k}} + \sum_{\mathbf{k}_1} u_{\mathbf{k}'-\mathbf{k}_1} G^{0\mathrm{A}}_{\mathbf{k}_1}(\omega) u_{\mathbf{k}_1-\mathbf{k}} + \ldots \right] \\ &= -2\mathrm{Im}\, T_{\mathbf{k}'\mathbf{k}}(\omega). \end{aligned} \quad (5.11)$$

This is precisely the content of the optical theorem.

In the so-called "self-consistent Born approximation" one replaces the unperturbed Green function G^0 by the disorder averaged Green function $\langle G \rangle$ in the calculation of the T-matrix. In this way, one captures some effects of higher impurity concentrations. See exercise 5.3 for more details on the self-consistent Born approximation.

The imaginary part of the self energy gives the particle in a momentum eigenstate $|\mathbf{k}\rangle$ a finite lifetime, as you would expect for impurity scattering. You can see this explicitly if you use the result (5.6) for the disorder averaged temperature Green function to calculate the retarded Green function,

$$\langle G^{\mathrm{R}}_{\mathbf{k},\mathbf{k}}(t) \rangle = G^{0\mathrm{R}}_{\mathbf{k}\mathbf{k}}(t) e^{-t/2\tau_{\mathbf{k}}}. \quad (5.12)$$

In frequency representation, the finite lifetime shows up as a finite width of the delta-function peak of the spectral density,

$$\langle A_{\mathbf{k}}(\omega) \rangle = \frac{1/\tau_{\mathbf{k}}}{(\omega - \varepsilon_{\mathbf{k}})^2 + (1/2\tau_{\mathbf{k}})^2}. \quad (5.13)$$

We call the disorder "weak" if the broadening of the peak in the spectral density is much smaller than the energy $\varepsilon_{\mathbf{k}}$ or, equivalently, if the scattering life time is much larger than the period $1/\varepsilon_{\mathbf{k}}$.

5.3 Boltzmann Equation with impurity scattering

Short-range impurities scatter electrons into states with a different momentum. In this section we discuss how impurity scattering can be incorporated into the Boltzmann equation.

Our derivation of the Boltzmann equation from the Green function formalism uses the real-time Keldysh formalism. In the real-time formalism, the disorder average is done in the same way as in the imaginary-time formalism. In the Born approximation, one derives the Dyson equation, for the disorder averaged Green function,

$$\langle \underline{G} \rangle = \left[(i\partial_t - \mathcal{H}_0)^{-1} \underline{1} - \underline{\Sigma} \right]^{-1}, \tag{5.14}$$

where we have used operator language to write down the action of the single-particle Green functions. Here $\mathcal{H}_0$ is the Hamiltonian without the short-range impurity potential (but $\mathcal{H}_0$ may include a slowly varying external potential) and $\underline{\Sigma}$ is the self energy, the sum of all "irreducible" diagrams (excluding external fermion lines). The self energy has same matrix structure as the Green function,

$$\underline{\Sigma} = \begin{pmatrix} \Sigma^{\mathrm{R}}(\mathbf{r}, t; \mathbf{r}', t') & \Sigma^{\mathrm{K}}(\mathbf{r}, t; \mathbf{r}', t') \\ 0 & \Sigma^{\mathrm{A}}(\mathbf{r}, t; \mathbf{r}', t') \end{pmatrix}. \tag{5.15}$$

Repeating the calculation of the previous section for the self-energy Σ, we find, in momentum representation,

$$\begin{aligned} \Sigma^{\mathrm{R}}_{\mathbf{k}} &= N_{\mathrm{imp}} T_{\mathbf{kk}}(\omega + i\eta) \\ \Sigma^{\mathrm{A}}_{\mathbf{k}} &= N_{\mathrm{imp}} T_{\mathbf{kk}}(\omega - i\eta) \\ \Sigma^{\mathrm{K}}_{\mathbf{k}} &= N_{\mathrm{imp}} \sum_{\mathbf{k}'} T_{\mathbf{k},\mathbf{k}'}(\omega + i\eta) G^{0\mathrm{K}}_{\mathbf{k}'} T_{\mathbf{k}',\mathbf{k}}(\omega - i\eta) \\ &= N_{\mathrm{imp}} \sum_{\mathbf{k}'} |T_{\mathbf{k},\mathbf{k}'}(\omega)|^2 G^{0\mathrm{K}}_{\mathbf{k}'}. \end{aligned} \tag{5.16}$$

In the self-consistent Born approximation, $G^{0\mathrm{K}}$ is replaced by $\langle G^{\mathrm{K}} \rangle$.

The derivation of the Boltzmann equation in the presence of impurity scattering closely follows the derivation for the Boltzmann equation without impurities. We start by rewriting the Dyson equation as

$$(i\partial_t - \mathcal{H}_0 - \underline{\Sigma}) \langle \underline{G} \rangle = \underline{1} = \langle \underline{G} \rangle (i\partial_t - \mathcal{H}_0 - \underline{\Sigma}) \tag{5.17}$$

and subtract the far left and right hand sides. Taking the Keldysh component of the remaining equation, we find

$$[(i\partial_t - \mathcal{H})\underline{1} - \Re\Sigma, \langle G^{\mathrm{K}} \rangle]_- - [\Sigma^{\mathrm{K}}, \langle \Re G \rangle]_- = \frac{i}{2}[\Sigma^{\mathrm{K}}, \langle A \rangle]_+ - \frac{i}{2}[\Gamma, \langle G^{\mathrm{K}} \rangle]_+, \tag{5.18}$$

where $A = i(G^{\mathrm{R}} - G^{\mathrm{A}})$ is the spectral weight of the full Green function and

$$\begin{aligned} \Gamma &= i(\Sigma^{\mathrm{R}} - \Sigma^{\mathrm{A}}), \\ \Re\Sigma &= \frac{1}{2}(\Sigma^{\mathrm{R}} + \Sigma^{\mathrm{A}}), \\ \Re G &= \frac{1}{2}(G^{\mathrm{R}} + G^{\mathrm{A}}). \end{aligned} \tag{5.19}$$

The definition of "real" and "imaginary" parts is the same one as used in Chapter 2. Note that in equilibrium one has $G^{\mathrm{K}} = -i\tanh(\omega/2T)A$ and $\Sigma^{\mathrm{K}} = -i\tanh(\omega/2T)\Gamma$, so that the right hand side of Eq. (5.18) vanishes.

The self energy represents the effect of impurity scattering. We neglect spatial and temporal derivates of the self energy, as well as its dependence on momentum and energy. (This is consistent with the calculation of the self energy in the previous section.) This allows us to disregard the self energy in the left hand side of Eq. (5.18). For the right-hand side, we use the fact that the spectral density A is close to a delta function if $\tau\varepsilon_{\mathbf{k}} \gg 1$, cf. Eq. (5.13)

$$\langle A \rangle = 2\pi\delta[\omega - (\varepsilon_{\mathbf{k}} - \mu) - U]. \tag{5.20}$$

Similarly, the disorder-averaged Keldysh Green function $\langle G^{\mathrm{K}} \rangle$ is also strongly peaked as a function of ω,

$$\langle G^{\mathrm{K}} \rangle = -2\pi i\delta[\omega - (\varepsilon_{\mathbf{k}} - \mu) - U](1 - 2f_{\mathbf{k}}), \tag{5.21}$$

where the distribution function f is defined as in Eq. (3.38). Then, using the gradient expansion in Eq. (5.18), integrating over ω, and performing one partial integration, we find

$$(\partial_T + \mathbf{v}_{\mathbf{k}} \cdot \partial_{\mathbf{R}} - \partial_{\mathbf{R}} U \cdot \partial_{\mathbf{k}})\, f_{\mathbf{k}}(\mathbf{R}, T) = -2\pi \frac{N_{\mathrm{imp}}}{V} \sum_{\mathbf{k}'} |T_{\mathbf{k},\mathbf{k}'}|^2 \delta(\varepsilon_{\mathbf{k}} - \varepsilon_{\mathbf{k}'})(f_{\mathbf{k}} - f_{\mathbf{k}'}), \tag{5.22}$$

where $\mathbf{v}_{\mathbf{k}} = \partial_{\mathbf{k}}\varepsilon_{\mathbf{k}}$ is the velocity. The right-hand side of the Boltzmann equation is the "collision integral": it contains the effect of the collisions between electrons and impurities with a short-range potential.

5.4 Electrical conductivity

Impurities in a conductor form an obstacle for the flow of electrical current. In normal metals, application of an external electric field $\mathbf{E}$ gives a finite electrical current density $\mathbf{j} = \sigma\mathbf{E}$. The Boltzmann equation can be used to find a microscopic expression for the conductivity σ.

In equilibrium, the distribution function $f_{\mathbf{k}}$ is the Fermi function f^0,

$$f^0_{\mathbf{k}} = \frac{1}{1 + e^{(\varepsilon_{\mathbf{k}} - \mu)/T}}. \tag{5.23}$$

The presence of an electric field changes the distribution f. In this section, we are interested in the response to small electric fields. Hence, we only consider deviations from f^0 to linear order in the electric field,

$$f_{\mathbf{k}} = f^0_{\mathbf{k}} + f^1_{\mathbf{k}}. \tag{5.24}$$

After some algebra, one can rewrite Eq. (5.18) into a simple form,

$$\frac{e}{\hbar}\mathbf{E} \cdot \partial_{\mathbf{k}} f_{\mathbf{k}} = -\frac{f^1_{\mathbf{k}}}{\hbar \tau_{\mathbf{k},\mathrm{tr}}}, \tag{5.25}$$

In general, this simple form is known as the "relaxation time approximation", although it is exact for the problem we consider here. The time $\tau_{\mathbf{k},\mathrm{tr}}$ is known as the "transport mean free time". It is expressed in terms of the T-matrix of a single impurity as

$$\frac{1}{\tau_{\mathbf{k},\mathrm{tr}}} = \frac{2\pi N_{\mathrm{imp}}}{\hbar} \sum_{\mathbf{k}'} |T_{\mathbf{k}\mathbf{k}'}(\varepsilon_{\mathbf{k}})|^2 (1 - \cos\theta') \delta(\varepsilon_{\mathbf{k}} - \varepsilon_{\mathbf{k}'}), \tag{5.26}$$

where θ' is the angle between $\mathbf{k}$ and $\mathbf{k}'$.

Linearizing in the electric field $\mathbf{E}$, we find

$$f^1_{\mathbf{k}} \;=\; -e\tau_{\mathbf{k},\mathrm{tr}} \mathbf{E} \cdot \partial_{\mathbf{k}} f^0(\mathbf{k}). \tag{5.27}$$

Using Eq. (3.40) for the current density $\mathbf{j}$, we have

$$\mathbf{j} \;=\; \frac{2e^2}{V} \sum_{\mathbf{k}} \mathbf{v}_{\mathbf{k}} \left(\mathbf{E} \cdot \mathbf{v}_{\mathbf{k}}\right) \left(-\frac{\partial f^0_{\mathbf{k}}}{\partial \varepsilon_{\mathbf{k}}}\right) \tau_{\mathbf{k},\mathrm{tr}}, \tag{5.28}$$

where we inserted a factor two to account for spin degeneracy. We then perform the integration over $\mathbf{k}$ by first averaging over the angles and find

$$\sigma = -\frac{2e^2}{3V} \sum_{\mathbf{k}} v^2_{\mathbf{k}} \tau_{\mathbf{k},\mathrm{tr}} \frac{\partial f}{\partial \varepsilon_{\mathbf{k}}},$$

which we can rewrite in terms of the density n of electrons and for low temperatures T as

$$\sigma = \frac{n e^2 \tau_{\mathrm{tr}}(k_F)}{m}. \tag{5.29}$$

This is nothing but the well-known Drude formula for the conductivity.

5.5 Gaussian white noise

Dealing with the precise impurity potential is often cumbersome: whereas calculations start from the impurity potential, final results will have to be formulated in terms of the T-matrices and, subsequently, in an appropriate mean free time.

In the remainder of this course, we'll use a simpler model for the impurity potential than Eq. (5.1) above. In this model, which has been chosen to minimize calculational difficulties, both the positions and the potentials of the impurities are random: the entire impurity potential $U(\mathbf{r})$ is considered a random function, with a Gaussian distribution of zero average,

$$\langle U(\mathbf{r})\rangle = 0, \tag{5.30}$$

and with a delta-function correlated second moment,

$$\langle U(\mathbf{r})U(\mathbf{r}')\rangle = \frac{1}{2\pi\nu\tau}\delta(\mathbf{r}-\mathbf{r}'), \tag{5.31}$$

where τ is the mean free scattering time (see Sec. 5.2) and ν is the density of states at the Fermi level per unit volume,

$$\nu = \frac{k^2}{2\pi^2\hbar v_F}. \tag{5.32}$$

Higher moments of the impurity potential can be constructed using the rules for Gaussian averages. This random potential $U(\mathbf{r})$ is called "white noise" because it is delta-function correlated in space.

The model (5.31) is not faithful to the microscopic potentials. Yet, as many observables depend in essence only on a suitably defined mean free time (such as the "transport mean free time" for the conductivity), one can imagine doing a calculation in two steps: use a correct microscopic theory to calculate the relevant scattering times, and use the model (5.31) to find physical observables that are hard to get at using the full microscopic theory.

Performing the Fourier transform,

$$U_{\mathbf{q}} = \frac{1}{V}\int d\mathbf{r}U(\mathbf{r})e^{-i\mathbf{q}\cdot\mathbf{r}},$$

we find that the potential $U_{\mathbf{q}}$ is also random and Gaussian. Its first two moments are given by

$$\begin{aligned}\langle U_{\mathbf{q}}\rangle &= 0\\ \langle U_{\mathbf{q}}U_{\mathbf{q}'}\rangle &= \frac{1}{2\pi\nu\tau V}\delta_{\mathbf{q}+\mathbf{q}',0}.\end{aligned} \tag{5.33}$$

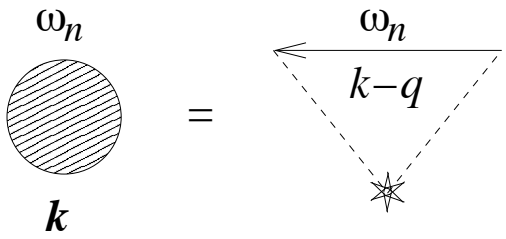

Figure 5.7: Self energy diagram for Gaussian white noise potential.

All higher moments can be factorized into the first and second moments. For the diagrammatic rules for impurity average this means that only those impurity vertices with two dashed lines contribute to the average.

To leading order in the impurity concentration, we then find only one diagram for the self energy, see Fig. 5.7. Hence, the self energy is given by

$$\begin{aligned}\Sigma_{\mathbf{k}} &= \sum_{\mathbf{q}} \mathcal{G}_{\mathbf{k}-\mathbf{q},\mathbf{k}-\mathbf{q}}(i\omega_n)\frac{1}{2\pi\nu\tau V} \\ &= \frac{1}{2\pi\nu\tau}\int \frac{d\mathbf{q}}{(2\pi)^3}\frac{1}{i\omega_n - \varepsilon_{\mathbf{k}-\mathbf{q}} + \mu} \\ &= -\frac{i}{2\tau}\,\mathrm{sign}\,(\omega_n). \end{aligned} \tag{5.34}$$

This is the same answer as we obtained previously in Sec. 5.2. In fact, the normalization (5.31) was chosen precisely to get this answer.[2]

5.6 Electrical conductivity from Kubo formula

We now re-calculate the electrical conductivity of a disordered metal in the Green function formalism. The calculation is considerably more cumbersome than the Boltzmann equation calculation of Sec. 5.4 (which, of course, is fully rigorous given our microscopic derivation of the Boltzmann equation). In order to keep the calculation simple, we will consider use Gaussian white noise as our model for the disorder potential.

[2]The most important difference between the Gaussian white noise potential and realistic impurity potentials is that, for Gaussian white noise, the impurity scattering lifetime and the transport mean free time are equal, whereas they are not for generic impurity scattering.

For a normal metal, the general response to an electrical field $\mathbf{E}$ takes the form

$$j_{e\alpha}(\mathbf{r},t) = \int dt' \int d\mathbf{r}' \sum_\beta \sigma_{\alpha\beta}(\mathbf{r},t;\mathbf{r}',t') E_\beta(\mathbf{r}',t'), \tag{5.35}$$

where $\sigma_{\alpha\beta}$ is the (nonlocal) conductivity tensor. The electric field is related to the electric potential ϕ and the vector potential $\mathbf{A}$,

$$\mathbf{E} = -\partial_{\mathbf{r}}\phi - \frac{1}{c}\partial_t \mathbf{A}. \tag{5.36}$$

This relation holds both for the external electric field and for the total electric field. If the current is carried by electrons, the electrical current operator is a sum of a "paramagnetic" contribution $\mathbf{j}^p$ and a "diamagnetic" contribution $\mathbf{j}^d$,

$$\mathbf{j}_e(\mathbf{r}) \;=\; \mathbf{j}_e^p(\mathbf{r}) + \mathbf{j}_e^d(\mathbf{r}), \tag{5.37}$$

where

$$\mathbf{j}_e^p(\mathbf{r}) \;=\; \frac{\hbar e}{2mi}\sum_\sigma \left[\hat\psi_\sigma^\dagger(\mathbf{r})(\partial_{\mathbf{r}}\hat\psi_\sigma(\mathbf{r})) - (\partial_{\mathbf{r}}\hat\psi_\sigma^\dagger(\mathbf{r}))\hat\psi_\sigma(\mathbf{r})\right], \tag{5.38}$$

$$\mathbf{j}_e^d(\mathbf{r}) \;=\; -\frac{e^2}{mc}\mathbf{A}(\mathbf{r})\sum_\sigma \hat\psi_\sigma^\dagger(\mathbf{r})\hat\psi_\sigma(\mathbf{r}). \tag{5.39}$$

In Sec. 2.5 we derived a general formalism to calculate the linear response to a perturbation $\hat H_1$. In our case, we want to find the current density as a response to an applied electric field. To linear order in the electric field, the electron's Hamiltonian is $\hat H_0 + \hat H_1$, where $\hat H_0$ is the Hamiltonian in the absence of the electric field and

$$\hat H_1 = \int d\mathbf{r}\rho_e(\mathbf{r})\phi(\mathbf{r},t) - \int d\mathbf{r}\mathbf{j}_e(\mathbf{r})A_{\rm ext}(\mathbf{r},t), \tag{5.40}$$

where

$$\rho_e(\mathbf{r}) = e\sum_\sigma \hat\psi_\sigma^\dagger(\mathbf{r})\hat\psi_\sigma(\mathbf{r}) \tag{5.41}$$

is the operator for the electronic charge density. Since we are interested in linear response, we only need to know $\hat H_1$ to linear order in $\mathbf{A}$, so that we can replace the electrical current density $\mathbf{j}_e$ in Eq. (5.40) by the paramagnetic current density $\mathbf{j}_e^p$.[3] We choose a gauge in which $\phi = 0$. This would be the natural choice if, e.g., the sample is a cylinder and the electric field is generated by a time-dependent flux through the sample, see Fig. 5.8.

[3] If the Hamiltonian $\hat H_0$ contains a vector potential $\mathbf{A}_0$ due to a magnetic field, we should replace $\mathbf{j}_e^p$ by $\mathbf{j}_e^p + (e/m)\mathbf{A}_0\rho_e$.

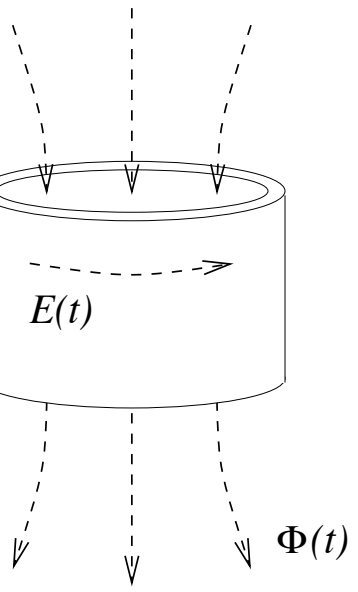

Figure 5.8: The gauge with zero scalar potential ϕ and a time-dependent vector potential $\mathbf{A}$ is the natural choice if the electric field is generated by a time-dependent flux through the sample.

Fourier transforming Eq. (5.35), we find

$$j_{e\alpha}(\mathbf{r},\omega) = \int d\mathbf{r}' \sum_{\beta} \sigma_{\alpha\beta}(\mathbf{r},\mathbf{r}';\omega) E_{\beta}(\mathbf{r}',\omega), \quad \alpha = 1,2,3, \tag{5.42}$$

where, in frequency representation, the electric field is related to the vector potential as

$$\mathbf{A}_{\rm ext}(\mathbf{r},\omega) = \frac{1}{i\omega}\mathbf{E}_{\rm ext}(\mathbf{r},\omega) = \int dt e^{i\omega t} A_{\rm ext}(\mathbf{r},t) \tag{5.43}$$

and

$$\sigma_{\alpha\beta}(\mathbf{r},\mathbf{r}';\omega) = \int dt e^{i\omega t} \sigma_{\alpha\beta}(\mathbf{r},t;\mathbf{r}',0). \tag{5.44}$$

According to the Kubo formula (2.69), the paramagnetic contribution to the conductivity is expressed in terms of the retarded current-density autocorrelation function, $\Pi^{\rm R}(\mathbf{r},\mathbf{r}';t)$,

$$\sigma_{\alpha\beta}(\mathbf{r},\mathbf{r}';\omega) \;\; = \;\; \frac{i}{\omega}\Pi^{\rm R}_{\alpha\beta}(\mathbf{r},\mathbf{r}';\omega) - \frac{e\rho_e(\mathbf{r})}{i\omega m}\delta(\mathbf{r}-\mathbf{r}')\delta_{\alpha\beta}. \tag{5.45}$$

where

$$\Pi^{\rm R}_{\alpha\beta}(\mathbf{r},\mathbf{r}';t) \equiv G^{\rm R}_{j_{e\alpha},j_{e\beta}}(\mathbf{r},\mathbf{r}';t) = -i\theta(t)\langle[j_{e\alpha}(\mathbf{r},t);j_{e\beta}(\mathbf{r}',0)]_{-}\rangle. \tag{5.46}$$

The second term in Eq. (5.45) represents the diamagnetic contribution to the current density.

For a translationally invariant system, the conductivity depends on the difference $\mathbf{r}-\mathbf{r}'$ only. Performing Fourier transforms for the conductivity and for the current density,

$$\sigma_{\alpha\beta}(\mathbf{q},\omega) = \frac{1}{V}\int d\mathbf{r}d\mathbf{r}' e^{-\mathbf{q}\cdot(\mathbf{r}-\mathbf{r}')}\sigma_{\alpha\beta}(\mathbf{r},\mathbf{r}';\omega), \tag{5.47}$$

$$\mathbf{j}_{e,\mathbf{q}} = \int d\mathbf{r} e^{-i\mathbf{q}\cdot\mathbf{r}}\mathbf{j}_e(\mathbf{r}), \tag{5.48}$$

we can write the Kubo formula for the conductivity as

$$\sigma_{\alpha\beta}(\mathbf{q},\omega) = \frac{i}{\omega}\Pi^{\mathrm{R}}_{\alpha\beta}(\mathbf{q},\omega) - \frac{e\rho_e}{i\omega m}\delta_{\alpha\beta}. \tag{5.49}$$

Here ρ_e is the electron charge density averaged over the entire sample (i.e., the $\mathbf{q}=0$ component of the charge density divided by the volume), and

$$\Pi^{\mathrm{R}}_{\alpha\beta}(\mathbf{q},t) = -i\theta(t)\frac{1}{V}\langle[j_{e\alpha,\mathbf{q}}(t), j_{e\beta,-\mathbf{q}}(0)]_-\rangle. \tag{5.50}$$

In general, the conductivity is defined as the response to the actual electric field in the sample, not as the response to the external field. If the electric fields are time dependent, the currents are time dependent and, thus, generate their own magnetic and electric fields. In addition an applied electric field may lead to a build-up of charge, which can screen the field. What we calculated above is the response to the external electric field. This procedure gives the correct result only if we can neglect the induced electric field. This is the case if, on the one hand, the frequency of the signal is sufficiently low that no magnetic fields are induced, whereas, on the other hand, the frequency is large enough compared to the size of the sample or the wavelength of the electric field that no screening charges are built up. In practice, both conditions are met if the electric field is perpendicular to the wavevector $\mathbf{q}$ or if the wavevector $\mathbf{q}$ is taken to zero *before* the frequency ω is made small.

Let us now calculate the conductivity of an electron gas. If there are no impurities, the conductivity is infinite (see exercise 5.6). So, in order to do a meaningful calculation, we consider the conductivity of an electron gas with impurities.

The conductivity follows from the current-current correlation function (5.50). For our calculation, we consider the imaginary-time version of that correlation function,

$$\Pi_{\alpha,\beta}(\mathbf{q},\tau-\tau') = -\frac{1}{V}\langle T_\tau j_{\mathbf{q},\alpha}(\tau) j_{-\mathbf{q},\beta}(\tau')\rangle, \tag{5.51}$$

and perform an analytical continuation to real frequencies at the end of the calculation. The current density operator $\mathbf{j}_\mathbf{q}$ is expressed in terms of the creation and annihilation operators

for electrons in momentum eigenstates $|\mathbf{k}\rangle$ as

$$\mathbf{j}_\mathbf{q} = \frac{e}{2m}\sum_{\mathbf{k}\sigma}(2\mathbf{k}+\mathbf{q})\hat{\psi}^\dagger_{\mathbf{k},\sigma}\hat{\psi}_{\mathbf{k}+\mathbf{q},\sigma}. \tag{5.52}$$

Since we are dealing with a non-interacting electron gas, we can perform the thermal average in Eq. (5.51) using Wick's theorem, with the result

$$\begin{aligned}\Pi_{\alpha;\beta}(\tau,\tau') &= \frac{e^2}{4m^2V}\sum_{\mathbf{k}\sigma}\sum_{\mathbf{k}'\sigma'}\mathcal{G}_{\mathbf{k}+\mathbf{q},\sigma;\mathbf{k}',\sigma'}(\tau'-\tau)\mathcal{G}_{\mathbf{k}'-\mathbf{q},\sigma';\mathbf{k},\sigma}(\tau-\tau') \\ &\quad\times(2k_\alpha+q_\alpha)(2k'_\beta-q_\beta),\end{aligned} \tag{5.53}$$

plus a term that does not depend on $\tau-\tau'$ and can be discarded because it vanishes after Fourier transform to the Matsubara frequency $i\Omega_n$ and subsequent analytical continuation $i\Omega_n \to \omega + i\eta$. It is important to note that the Green function in Eq. (5.53) is the full temperature Green function, calculated in the presence of the exact impurity potential. Fourier transforming Eq. (5.53) and changing variables $\mathbf{k}' \to \mathbf{k}'+\mathbf{q}$, we find

$$\begin{aligned}\Pi_{\alpha;\beta}(i\Omega_n) &= \frac{e^2T}{2m^2V}\sum_{\mathbf{k},\mathbf{k}',m}\mathcal{G}_{\mathbf{k}+\mathbf{q},\mathbf{k}'+\mathbf{q}}(i\omega_m+i\Omega_n)\mathcal{G}_{\mathbf{k}';\mathbf{k}}(i\omega_m) \\ &\quad\times(2k_\alpha+q_\alpha)(2k'_\beta+q_\beta),\end{aligned} \tag{5.54}$$

where we summed over the spin index. The Matsubara frequency $i\Omega_n$ is a *bosonic* Matsubara frequency, because the current-current correlation function involves operators that are even in the fermion creation and annihilation operators. The arguments of the single-particle Green functions, however, are fermionic Matsubara frequencies.

In order to calculate the full temperature Green function, we use the perturbative expansion of $\mathcal{G}$ in powers of the impurity potential, which is shown in Fig. 4.2, and then perform the disorder average. It is important to realize that, here, we calculate the impurity average of the product of two Green functions. That need not be the same as the product of the averages!

In order to keep the calculations simple, we'll restrict our attention to the case of a Gaussian white noise random potential. Then, diagrammatically, the impurity average means that we connect all pairs of impurity lines, as in Fig. 5.7. Still, it is an impossible task to sum all diagrams. We can further simplify the calculation by limiting ourselves to those diagrams in which no impurity lines cross. In exercise 5.1 you'll verify that this is a sensible approximation: diagrams in which impurity lines cross are a factor $\varepsilon_F\tau$ smaller than diagrams without crossed impurity lines.

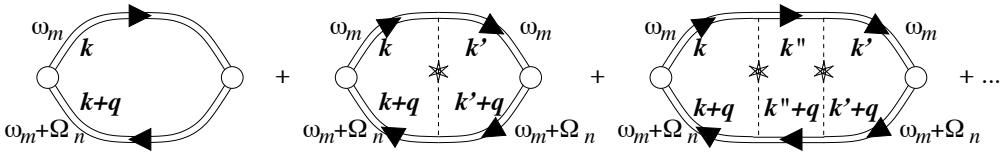

Figure 5.9: Diagrammatic representation of all diagrams without crossed lines that contribute to the conductivity. The double lines represent the disorder averaged Green function.

The diagrams without crossed lines can be summed up as in Fig. 5.9. The building blocks are the impurity averaged Green functions, which are represented by double arrows. The open circles at the two ends are called "current" vertices. They represent the factors $e(2\mathbf{k}+\mathbf{q})/2m$ and $e(2\mathbf{k}'+\mathbf{q})/2m$ that appear in the calculation of the current-current correlation function. These factors are referred to as the "bare current vertex", and they are denoted by the "bare vertex function" $\Gamma^0_\alpha(\mathbf{k}, i\omega_m; \mathbf{k}+\mathbf{q}, i\omega_m + i\Omega_n)$,

$$\Gamma^0_\alpha(\mathbf{k}, i\omega_m; \mathbf{k}+\mathbf{q}, i\omega_m + i\Omega_n) = \frac{e(2k_\alpha + q_\alpha)}{2m}. \tag{5.55}$$

The middle part of the diagram is a "ladder" which has the impurity averaged Green functions and impurity lines as building blocks.

All but the rightmost part of the ladder diagram can be written as a solid dot, see Fig. 5.10. This part of the diagram is known as a vertex correction. It is described by the vertex function $\Gamma_\alpha(\mathbf{k}, i\omega_m; \mathbf{k}+\mathbf{q}, i\omega_m + i\Omega_n)$. A self-consistent equation for the vertex function can be found from the second line of Fig. 5.10,

$$\begin{aligned}\Gamma_\alpha(\mathbf{k}, i\omega_m; \mathbf{k}+\mathbf{q}, i\omega_m + i\Omega_n) &= \Gamma^0_\alpha(\mathbf{k}, i\omega_m; \mathbf{k}+\mathbf{q}, i\omega_m + i\Omega_n) \\ &+ \frac{1}{2\pi\nu\tau V}\sum_{\mathbf{k}'}\langle\mathcal{G}_{\mathbf{k}'}(i\omega_m)\rangle\langle\mathcal{G}_{\mathbf{k}'+\mathbf{q}}(i\omega_m + i\Omega_n)\rangle\Gamma_\alpha(\mathbf{k}', i\omega_m; \mathbf{k}'+\mathbf{q}, i\omega_m + i\Omega_n),\end{aligned} \tag{5.56}$$

where Γ^0_α is the bare vertex function, see Eq. (5.55) above. Recall that the impurity averaged Green functions have only one momentum index because translation invariance is restored upon taking the disorder average. A self-consistent equation for the vertex function is found upon multiplication of Eq. (5.56) with $\langle\mathcal{G}_{\mathbf{k}}(i\omega_m)\rangle\langle\mathcal{G}_{\mathbf{k}+\mathbf{q}}(i\omega_m + i\Omega_n)\rangle$ and summation over $\mathbf{k}$. Solving for Γ, we find

$$\begin{aligned}&\Gamma_\alpha(\mathbf{k}, i\omega_m; \mathbf{k}+\mathbf{q}, i\omega_m + i\Omega_n) \\ &= \frac{e}{2m}\left[2k_\alpha + q_\alpha + \frac{\sum_{\mathbf{k}'}(2k'_\alpha + q_\alpha)\langle\mathcal{G}_{\mathbf{k}'}(i\omega_m)\rangle\langle\mathcal{G}_{\mathbf{k}'+\mathbf{q}}(i\omega_m + i\Omega_n)\rangle}{2\pi\nu\tau V - \sum_{\mathbf{k}'}\langle\mathcal{G}_{\mathbf{k}'}(i\omega_m)\rangle\langle\mathcal{G}_{\mathbf{k}'+\mathbf{q}}(i\omega_m + i\Omega_n)\rangle}\right].\end{aligned} \tag{5.57}$$

We are interested in the current-current correlator in the limit $\mathbf{q} \to 0$. The numerator of the last term of Eq. (5.57) goes to zero if $\mathbf{q} \to 0$. Hence, we conclude that, for our choice of

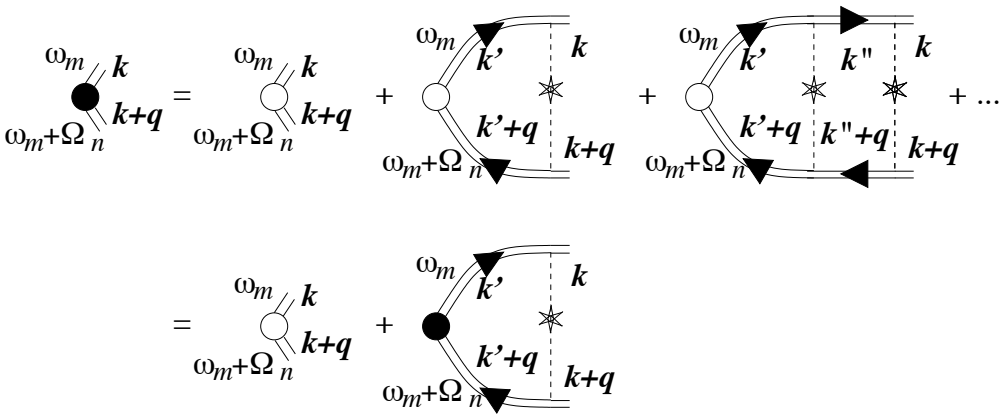

Figure 5.10: Diagrammatic representation of vertex correction Γ necessary for the calculation of the current-current correlator. The double lines represent the disorder averaged Green function.

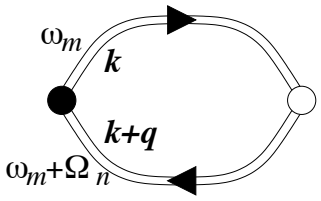

Figure 5.11: Diagrammatic representation of the current-current correlator in terms of the vertex function Γ (solid dot), the bare vertex function Γ^0 (open dot) and the disorder averaged Green function (double lines).

the random potential, there is no vertex correction.[4] This simplification one of the reasons why we have chosen the Gaussian white noise model for the random potential.

The current-current correlation function is easily expressed in terms of the vertex function Γ and the bare vertex function Γ^0, see Fig. 5.11,

$$\begin{aligned}\Pi_{\alpha,\beta}(i\Omega_n) &= \frac{2T}{V}\sum_{\mathbf{k},m}\Gamma_\alpha(\mathbf{k},i\omega_m;\mathbf{k}+\mathbf{q},i\omega_m+i\Omega_n)\Gamma^0_\beta(\mathbf{k}+\mathbf{q},i\omega_m+i\Omega_n;\mathbf{k},i\omega_m)\\ &\quad\times\mathcal{G}_{\mathbf{k}}(i\omega_m)\mathcal{G}_{\mathbf{k}+\mathbf{q}}(i\omega_m+i\Omega_n). \qquad (5.58)\end{aligned}$$

[4]Unlike for the Gaussian white noise used here, Γ and Γ^0 are different for a realistic impurity potential. This "vertex correction" amounts to the replacement of the impurity scattering lifetime τ with the "transport mean free time" $\tau_{\rm tr}$, see Sec. 5.3.

It remains to perform the summations over $\mathbf{k}$ and m and do the analytical continuation $i\Omega_n \to \omega + i\eta$. We first do the summation over m. As before, this is done by representing the Matsubara summation as an integral in the complex plane,

$$\begin{aligned}\Pi_{\alpha,\beta}(i\Omega_n) &= \frac{1}{2\pi i V}\int_{C_1} dz \sum_{\mathbf{k}} \Gamma_\alpha(\mathbf{k}, z; \mathbf{k}+\mathbf{q}, z+i\Omega_n)\Gamma^0_\beta(\mathbf{k}+\mathbf{q}, z+i\Omega_n; \mathbf{k}, z) \\ &\quad \times \mathcal{G}_{\mathbf{k},\mathbf{k}}(z)\mathcal{G}_{\mathbf{k}+\mathbf{q},\mathbf{k}+\mathbf{q}}(z+i\Omega_n)\tanh(z/2T). \qquad (5.59)\end{aligned}$$

The integrand has singularities at the real axis and at the axis $z = x - i\Omega_n$, x real. Hence, we deform the contour as shown in Fig. 5.12.

$$\begin{aligned}\Pi_{\alpha,\beta}(i\Omega_n) &= \frac{1}{2\pi i V}\int d\xi \tanh(\xi/2T) \sum_{\mathbf{k}}\sum_{\pm}(\pm 1) \\ &\quad \times \big[\Gamma_\alpha(\mathbf{k}, \xi^\pm; \mathbf{k}+\mathbf{q}, \xi+i\Omega_n)\Gamma^0_\beta(\mathbf{k}+\mathbf{q}, \xi+i\Omega_n, \mathbf{k}, \xi^\pm)\, \mathcal{G}_{\mathbf{k}}(\xi^\pm)\mathcal{G}_{\mathbf{k}+\mathbf{q}}(\xi+i\Omega_n) \\ &\quad + \Gamma_\alpha(\mathbf{k}, \xi-i\Omega_n; \mathbf{k}+\mathbf{q}, \xi^\pm)\Gamma^0_\beta(\mathbf{k}+\mathbf{q}, \xi^\pm, \mathbf{k}, \xi-i\Omega_n)\, \mathcal{G}_{\mathbf{k}}(\xi-i\Omega_n)\mathcal{G}_{\mathbf{k}+\mathbf{q}}(\xi^\pm)\big],\end{aligned}$$

where we used $\tanh(z/2T) = \tanh[(z+i\Omega_n)/2T]$ and $\xi^\pm = \xi \pm i\eta$. It is not necessary to add an infinitesimal $\pm i\eta$ to $\xi \pm i\Omega_n$, since $i\Omega_n$ is imaginary itself. Now we can perform the analytical continuation $i\Omega_n \to \omega + i\eta$,

$$\begin{aligned}\Pi_{\alpha,\beta}(\omega+i\eta) &= \frac{1}{2\pi i V}\int d\xi \tanh(\xi/2T) \sum_{\mathbf{k}} \\ &\quad \times \big[\Gamma^{\mathrm{RR}}_\alpha(\mathbf{k}, \xi; \mathbf{k}+\mathbf{q}, \xi+\omega)\Gamma^{0\,\mathrm{RR}}_\beta(\mathbf{k}+\mathbf{q}, \xi+\omega; \mathbf{k}, \xi)G^{\mathrm{R}}_{\mathbf{k}}(\xi)G^{\mathrm{R}}_{\mathbf{k}+\mathbf{q}}(\xi+\omega) \\ &\quad - \Gamma^{\mathrm{AR}}_\alpha(\mathbf{k}, \xi; \mathbf{k}+\mathbf{q}, \xi+\omega)\Gamma^{0\,\mathrm{RA}}_\beta(\mathbf{k}+\mathbf{q}, \xi+\omega; \mathbf{k}, \xi)G^{\mathrm{A}}_{\mathbf{k}}(\xi)G^{\mathrm{R}}_{\mathbf{k}+\mathbf{q}}(\xi+\omega) \\ &\quad + \Gamma^{\mathrm{AR}}_\alpha(\mathbf{k}, \xi-\omega; \mathbf{k}+\mathbf{q}, \xi)\Gamma^{0\,\mathrm{RA}}_\beta(\mathbf{k}+\mathbf{q}, \xi; \mathbf{k}, \xi-\omega)G^{\mathrm{A}}_{\mathbf{k}}(\xi-\omega)G^{\mathrm{R}}_{\mathbf{k}+\mathbf{q}}(\xi) \\ &\quad - \Gamma^{\mathrm{AA}}_\alpha(\mathbf{k}, \xi-\omega; \mathbf{k}+\mathbf{q}, \xi)\Gamma^{0\,\mathrm{AA}}_\beta(\mathbf{k}+\mathbf{q}, \xi; \mathbf{k}, \xi-\omega)G^{\mathrm{A}}_{\mathbf{k}}(\xi-\omega)G^{\mathrm{A}}_{\mathbf{k}+\mathbf{q}}(\xi)\big]. \qquad (5.60)\end{aligned}$$

Sofar our result has been quite general. Equation (5.60) is valid for any form of the vertex correction and even holds in the presence of electron-electron interactions (which will be discussed in a later chapter). We now specialize to the limit $\mathbf{q} \to 0$, which is needed to find the dc conductivity. As explained above, we should take the limit $\mathbf{q} \to 0$ before we take the limit $\omega \to 0$. For zero wavevector $\mathbf{q}$ there is no vertex renormalization, and hence

$$\begin{aligned}\Pi_{\alpha,\beta}(\omega+i\eta) &= \frac{e^2}{2\pi i V}\sum_{\mathbf{k}} \frac{k_\alpha k_\beta}{m^2}\int d\xi \tanh[(\xi-\mu)/2T] \qquad (5.61) \\ &\quad \times \left[\frac{1}{(\xi-\varepsilon_{\mathbf{k}}+i/2\tau)(\xi+\omega-\varepsilon_{\mathbf{k}}+i/2\tau)} - \frac{1}{(\xi-\varepsilon_{\mathbf{k}}-i/2\tau)(\xi+\omega-\varepsilon_{\mathbf{k}}+i/2\tau)}\right.\end{aligned}$$

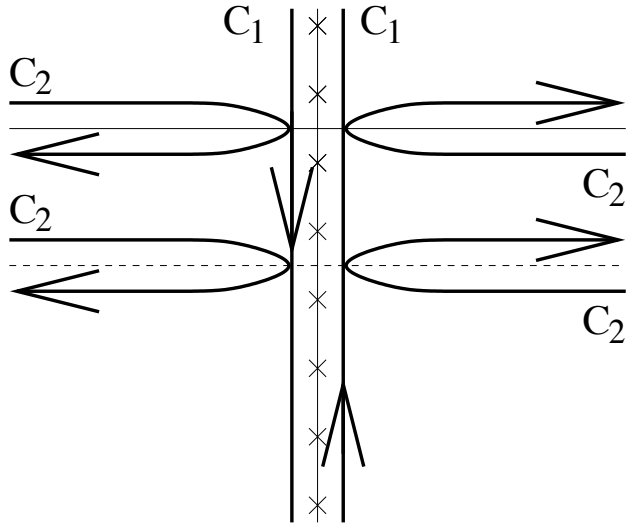

Figure 5.12: Integration contours for the calculation of the current-current correlator.

$$+\frac{1}{(\xi-\omega-\varepsilon_{\mathbf{k}}-i/2\tau)(\xi-\varepsilon_{\mathbf{k}}+i/2\tau)}-\frac{1}{(\xi-\omega-\varepsilon_{\mathbf{k}}-i/2\tau)(\xi-\varepsilon_{\mathbf{k}}-i/2\tau)}\Bigg],$$

where we shifted the ξ-integration by the chemical potential μ. We first perform a partial integration to ξ,

$$\begin{aligned}\Pi_{\alpha,\beta}(\omega+i\eta) &= \frac{e^2}{4\pi iVT}\int d\xi\frac{1}{\cosh^2[(\xi-\mu)/2T]}\\ &\quad\times\sum_{\mathbf{k}}\frac{k_\alpha k_\beta}{m^2}\left(\frac{1}{\omega}-\frac{1}{\omega+i/\tau}\right)\ln\frac{(\xi-\varepsilon_{\mathbf{k}})^2-(\omega+i/2\tau)^2}{(\xi-\varepsilon_{\mathbf{k}})^2+1/4\tau^2}.\end{aligned}$$

With this manipulation the summation over the wavevector $\mathbf{k}$ is convergent. The summation over $\mathbf{k}$ is separated into an angular average over the direction of $\mathbf{k}$ and an integration over the magnitude. The latter integration can be rewritten as an integral over the energy $\varepsilon_{\mathbf{k}}$ and yields

$$\Pi_{\alpha,\beta}(\omega+i\eta) = -\frac{2e^2\nu k_F^2\delta_{\alpha,\beta}}{3(1-i\omega\tau)m^2}. \tag{5.62}$$

We use the relation $\nu = mk_F/2\pi^2\hbar^2$ for the density of states per spin direction and per unit

volume, and the relation $n = k_F^3/3\pi^2 = \rho_e/e$ for the total particle density to rewrite this as[5]

$$\Pi^{\rm R}_{\alpha,\beta}(\omega) = -\frac{\rho_e e\delta_{\alpha,\beta}}{m(1-i\omega\tau)}. \tag{5.64}$$

Substituting this in Eq. (5.49), we find that the conductivity at wavevector $\mathbf{q} = 0$ and frequency ω is given by

$$\sigma_{\alpha\beta}(0,\omega) = \frac{e\rho_e\tau}{m(1-i\omega\tau)}. \tag{5.65}$$

In this limit $\omega \to 0$ this reproduces the well-known Drude formula.

It may be somewhat disappointing to recover the Drude formula after so much work. However, this whole calculation was not in vain. First of all, we have found a firm microscopic derivation of the Drude formula. But more importantly, with this formalism we are ready to study corrections to the Drude formula. One of these corrections, the weak localization correction, will be studied at length in a later chapter.

[5]You can verify this result in the limit $\omega \to 0$ without expanding around the Fermi surface. Starting point is Eq. (5.61), which we rewrite as

$$\Pi^{\rm R}_{\alpha,\beta}(0) = \frac{e^2}{\pi V}\sum_{\mathbf{k}} \frac{k_\alpha k_\beta}{m^2}\int d\xi \tanh[(\xi-\mu)/2T]{\rm Im}\,\langle G^{\rm R}_{\mathbf{k},\mathbf{k}}(\xi)\rangle^2.$$

We make use of the fact that the integral of $\langle G^{\rm R}(\xi)\rangle^2$ vanishes and perform the angular average over the wavevector $\mathbf{k}$,

$$\Pi^{\rm R}_{\alpha,\beta}(0) = -\frac{4e^2}{3\pi V m}\sum_{\mathbf{k}} \frac{k^2}{2m}\int d\xi \frac{1}{1+e^{(\xi-\mu)/T}}{\rm Im}\,\langle G^{\rm R}_{\mathbf{k},\mathbf{k}}(\xi)\rangle^2\delta_{\alpha\beta}.$$

Using the explicit form of ${\rm Im}\,\langle G^{\rm R}_{\mathbf{k},\mathbf{k}}(\xi)\rangle$ one verifies that

$${\rm Im}\,\langle G^{\rm R}_{\mathbf{k},\mathbf{k}}(\xi)\rangle^2 = -\frac{1}{2}\frac{\partial}{\partial\varepsilon_{\mathbf{k}}}\langle A_{\mathbf{k},\mathbf{k}}(\xi)\rangle. \tag{5.63}$$

Performing a partial integration with respect to $\varepsilon_{\mathbf{k}}$ one thus finds

$$\begin{aligned}\Pi^{\rm R}_{\alpha,\beta}(0) &= \frac{2e^2}{3\pi V m}\sum_{\mathbf{k}}\varepsilon_{\mathbf{k}}\int d\xi \frac{1}{1+e^{(\xi-\mu)/T}}\frac{\partial}{\partial\varepsilon_{\mathbf{k}}}\langle A_{\mathbf{k},\mathbf{k}}(\xi)\rangle\delta_{\alpha\beta}\\ &= -\frac{2e^2}{Vm}\sum_{\mathbf{k}}\int\frac{d\xi}{2\pi}\frac{1}{1+e^{(\xi-\mu)/T}}\langle A_{\mathbf{k},\mathbf{k}}(\xi)\rangle\delta_{\alpha\beta}\\ &= \frac{\rho_e e}{m}\delta_{\alpha\beta}.\end{aligned}$$

Note that the partial integration gives a factor 3/2 since the density of states is proportional to $\varepsilon_{\mathbf{k}}^{1/2}$. This is the desired result.

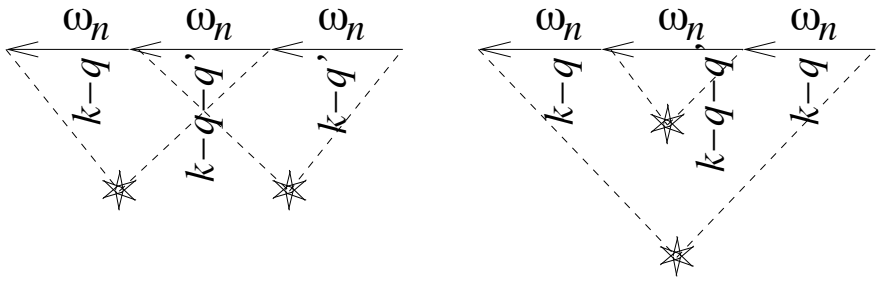

Figure 5.13: Diagrams that were omitted in the calculation of the self energy.

5.7 Exercises

Exercise 5.1: Corrections to the self energy

For the Gaussian white noise potential, we neglected some self-energy diagrams. The simplest diagrams we left out are shown in Fig. 5.13. Calculate these contributions to the self energy and show that they can be omitted if disorder if the impurity concentration is small.

Exercise 5.2: Boltzmann Equation

Derive Eq. (5.25).

Exercise 5.3: Self-consistent Born approximation

In the self-consistent Born approximation, one substitutes the unperturbed Green function $\mathcal{G}^0$ with the disorder averaged full Green function $\mathcal{G}$ in the calculation of the self energy. Since $\mathcal{G}$ depends on Σ, the result of this substitution is a self-consistent equation for the self energy Σ.

(a) Draw diagrams representing the equation for the disorder averaged Green function $\mathcal{G}$ and the self energy Σ in the self-consistent Born approximation.

(b) Write down a self-consistency equation for the self energy in terms of the T-matrix. *Hint: since the real part of Σ can be absorbed into the chemical potential, it is the imaginary part only that plays a role.*

(c) Discuss the solution if the T-matrix has only a weak energy dependence for energies within a distance $\ll \varepsilon_F$ from the Fermi level.

(d) Discuss the self-consistent Born approximation for the Gaussian white noise potential.

Exercise 5.4: One-dimensional conductor

It is possible to fabricate samples that behave as defect-free one-dimensional conductors. Examples are "quantum wires" in semiconductor heterostructures, or carbon nanotubes. At very low temperatures, interactions lead to a strongly correlated electronic ground state (the so-called "Luttinger Liquid"). However, at not too low temperatures, a description in terms of the Boltzmann equation may still be appropriate.

In a one-dimensional conductor, the relevant momenta p are in the vicinity of either p_F or $-p_F$, see figure 5.14. One usually refers to the two types of excitations as "right movers" and "left movers". As a result, in one dimension the distribution function f can be represented by two functions f_R and f_L that each depend on the kinetic energy $\varepsilon_{\rm kin}$ of the electrons only. In the absence of collisions, the Boltzmann equation then reads

$$\frac{\partial f_R}{\partial t} + v_F \frac{\partial f_R}{\partial x} + eEv_F \frac{\partial f_R}{\partial \varepsilon} = 0, \tag{5.66}$$

$$\frac{\partial f_L}{\partial t} - v_F \frac{\partial f_L}{\partial x} - eEv_F \frac{\partial f_L}{\partial \varepsilon} = 0, \tag{5.67}$$

where v_F is the Fermi velocity.

(a) Show that in one dimension, the Fermi velocity is related to the density of states at the Fermi level $\nu(\varepsilon_F)$.

Consider a one dimensional conductor in which the electric field exists only within a segment of length L. Assume that all electrons entering that segment are in thermal equilibrium, *i.e.,* their distribution function f is the Fermi function. Also assume that the one dimensional conductor is perfect, *i.e.,* that there are no collisions between the electrons or between electrons and impurities or defects.

(b) Solve the Boltzmann equation to find the electrical current in the conductor.

(c) What does your answer to (b) imply if expressed in terms of a "conductivity"? Does your answer make sense?

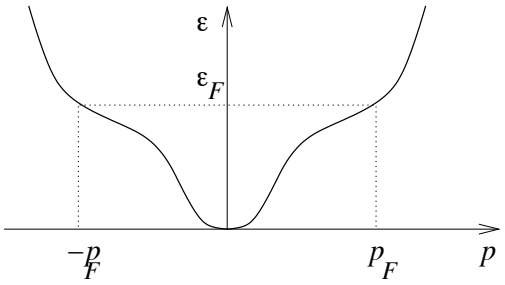

Figure 5.14: Dispersion relation of a one dimensional metal. All relevant momenta are close to p_F and $-p_F$.

(d) One can also express the answer to (b) in terms of the "conductance" G, defined as the quotient of the current I and the voltage $V = EL$ over the conductor. What conductance do you find? What physical properties does it depend on?

Exercise 5.5: Electrical conduction

In this exercise we return to the problem of electrical resistance of a perfect one-dimensional conductor. A possible measurement setup is shown in Fig. 5.15: The wire is connected to source and drain reservoirs. There exists a voltage difference V between the electrostatic potentials in the two reservoirs, and the current through the wire is measured. Technically, such a measurement of the resistance is referred to as a "two-terminal measurement", because the voltages and currents are measured with respect to the same reservoirs. The Boltzmann equation you solved in Ex. 5.4 is for this measurement setup.

In Ex. 5.4 you saw that, in a one-dimensional conductor, one can use the kinetic energy ε_F to label an electronic state, instead of the momentum p, together with a label that specifies whether the electron moves to the right or to the left. The Boltzmann equation [Eqs. (5.66 and (5.67) of Ex. 5.4] expresses the fact that the kinetic energy of a moving electron changes because of the presence of the electric field. However, the electron's *total* energy $\varepsilon_{\rm tot} = \varepsilon + e\phi$, which is the sum of potential energy $e\phi$ and kinetic energy ε, does not. We can use the fact that the total energy is conserved to write down a simpler version of the Boltzmann equation.[6]

(a) Argue that, if we describe the state of an electron in a one-dimensional conductor by

[6]This version is nothing but the quasiclassical kinetic equation you derived in Ex. 3.4.

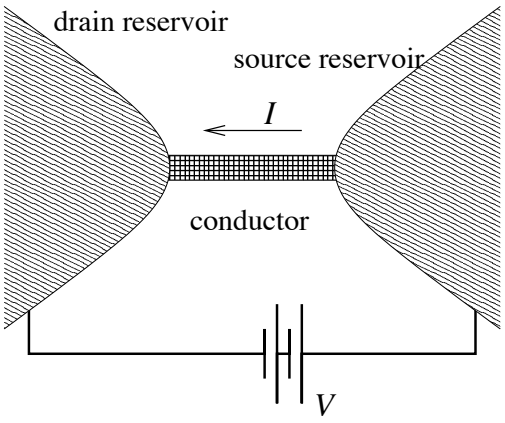

Figure 5.15: Setup for the two-terminal measurement of the electrical resistance of a metal.

specifying its total energy ε instead of its kinetic energy $\varepsilon_{\rm kin}$, the Boltzmann equation reads simply

$$\frac{\partial f_R}{\partial t} + v_F \frac{\partial f_R}{\partial x} = 0, \tag{5.68}$$

$$\frac{\partial f_L}{\partial t} - v_F \frac{\partial f_L}{\partial x} = 0. \tag{5.69}$$

Here $0 < x < L$ is the coordinate along the conductor.

(b) What are the appropriate boundary conditions for the distribution functions f_L and f_R at $x = 0$ and $x = L$?
Hint: both source and drain reservoirs have the same electron density.

(c) Solve the Boltzmann equation, calculate the current I as a function of the applied voltage V, and compare your answer with Ex. 5.4.

Exercise 5.6: Conductivity without impurities

Calculate the retarded current density correlation function $\Pi^{\rm R}_{\alpha;\beta}(\omega)$ for a non-interacting electron gas without impurities. Is the result the same as the limit $\tau \to \infty$ of Eq. (5.64)? What does your result imply for the relation between current density and electric field?

Chapter 6

Diffusion modes

Consider changing the potential ϕ at a certain time t. The electron density will adjust to the change in the potential. In this chapter we'll investigate how this adjustment takes place and how it depends on the presence of impurities.

6.1 Dielectric function

Consider a metal or other dielectric with an added charge. One example of such a charge is an ion with a different valence in a metal. We'll call this charge the "external charge" and denote the corresponding charge density by ρ_{ext}.

The external charge determines the "electrical displacement" $\mathbf{D}$, which is the solution of the Maxwell equation

$$\epsilon_0 \partial_{\mathbf{r}} \cdot \mathbf{D} = 4\pi \rho_{\text{ext}}. \tag{6.1}$$

Here, ϵ_0 is the permittivity of vacuum. In a dielectric, the external charge will induce a screening charge ρ_{ind}. The total charge, screening charge plus external charge, determines the electric field $\mathbf{E}$,

$$\epsilon_0 \partial_{\mathbf{r}} \cdot \mathbf{E} = 4\pi (\rho_{\text{ext}} + \rho_{\text{ind}}). \tag{6.2}$$

In the language of "external" and "induced" quantities, you may consider $\mathbf{E}$ as the "total electric field", and $\mathbf{D}$ as the "external electric field". The difference $\mathbf{E} - \mathbf{D}$ then corresponds to the "induced electric field".

In general, the electric field, the electric displacement, and their difference (or, more precisely, the longitudinal parts of these fields) can be written as gradients of electric potentials ϕ_{tot}, ϕ_{ext}, and ϕ_{ind}, respectively. These potentials are expressed in terms of the corresponding

charges as

$$\phi(\mathbf{r}) = \int d\mathbf{r}' V_{\rm C}(\mathbf{r}-\mathbf{r}')\rho(\mathbf{r}'), \tag{6.3}$$

where $V_{\rm C}(\mathbf{r}-\mathbf{r}') = 1/\epsilon_0|\mathbf{r}-\mathbf{r}'|$ is the Coulomb interaction.

For a sufficiently small external charge, the induced and total potentials are proportional to the external potential. This is the regime of "linear screening". The proportionality constant, which may be a non-local function in space and time, is called the inverse "relative permittivity" of the dielectric, or the dielectric response function,

$$\phi_{\rm tot}(\mathbf{r},t) = \int d\mathbf{r}' \int dt' \epsilon^{-1}(\mathbf{r},t;\mathbf{r}',t')\phi_{\rm ext}(\mathbf{r}',t'). \tag{6.4}$$

Instead of the dielectric response function, one often uses the so-called "polarizability function $\chi_e(\mathbf{r},t;\mathbf{r}',t')$", which gives the induced charge as a function of the external potential,

$$\rho_{\rm ind}(\mathbf{r},t) = \int d\mathbf{r}' \int dt' \chi_e^{\rm R}(\mathbf{r},t;\mathbf{r}',t')\phi_{\rm ext}(\mathbf{r}',t'). \tag{6.5}$$

From Eq. (6.5) we then conclude that

$$\epsilon^{-1}(\mathbf{r},t;\mathbf{r}',t') \;=\; \delta(\mathbf{r}-\mathbf{r}')\,\delta(t-t') + \int d\mathbf{r}'' V_{\rm C}(\mathbf{r}-\mathbf{r}'')\chi_e^{\rm R}(\mathbf{r}'',t;\mathbf{r}',t'). \tag{6.6}$$

In a translationally invariant medium, the dielectric response function $\epsilon^{-1}(\mathbf{r},t;\mathbf{r}',t')$ and the polarizability function $\chi_e(\mathbf{r},t;\mathbf{r}',t')$ depend on the differences $\mathbf{r}-\mathbf{r}'$ and $t-t'$ only. Then it is advantageous to perform a Fourier transform to position and time. Defining the Fourier transforms according to

$$\epsilon^{-1}(\mathbf{q},\omega) \;=\; \frac{1}{V}\int d\mathbf{r} d\mathbf{r}' \int dt e^{-i\mathbf{q}\cdot(\mathbf{r}-\mathbf{r}')+i\omega t}\epsilon^{-1}(\mathbf{r},t;\mathbf{r}',0), \tag{6.7}$$

$$\phi(\mathbf{q},\omega) \;=\; \int d\mathbf{r} \int dt e^{i\omega t - i\mathbf{q}\cdot\mathbf{r}}\phi(\mathbf{r},t), \tag{6.8}$$

with similar definitions for $\chi_e(\mathbf{q},\omega)$ and $\rho(\mathbf{q},\omega)$, we find

$$\phi_{\rm tot}(\mathbf{q},\omega) \;=\; \epsilon^{-1}(\mathbf{q},\omega)\phi_{\rm ext}(\mathbf{q},\omega), \tag{6.9}$$

$$\rho_{\rm ind}(\mathbf{q},\omega) \;=\; \chi_e(\mathbf{q},\omega)\phi_{\rm ext}(\mathbf{q},\omega). \tag{6.10}$$

Fourier transforming Eq. (6.6), we have

$$\epsilon^{-1}(\mathbf{q},\omega) = 1 + V_{\rm C}(\mathbf{q})\chi_e^{\rm R}(\mathbf{q},\omega), \tag{6.11}$$

where $V_{\rm C}(\mathbf{q}) = 4\pi/\epsilon_0 q^2$ is the Fourier transform of the Coulomb potential.

Let us now calculate the polarizability function χ_e for an electron gas without impurities. The simplest approach is to use the Boltzmann equation. We write $f = f^0 + f^1$, where f^0 is the equilibrium distribution function and f^1 is the first-order response to the external potential $\phi_{\rm ext}$. Linearizing and Fourier transforming the Boltzmann equation (3.21), we find

$$(-i\omega + i\mathbf{v_k}\cdot\mathbf{q})f^1_{\mathbf{k}}(\mathbf{q},\omega) - i(e/\hbar)\phi_{\rm ext}(\mathbf{q},\omega)\mathbf{q}\cdot\partial_{\mathbf{k}} f^0_{\mathbf{k}}(\mathbf{q},\omega) = 0. \tag{6.12}$$

Solving for f^1, we find

$$\chi_e^{\rm R}(\mathbf{q},\omega) = -2\frac{e^2}{V}\sum_{\mathbf{k}} \frac{\mathbf{q}\cdot\mathbf{v_k}}{\mathbf{q}\cdot\mathbf{v_k} - \omega - i\eta}\left(-\partial_\varepsilon f^0(\varepsilon_{\mathbf{k}})\right), \tag{6.13}$$

where a factor two has been inserted to account for spin degeneracy.

A calculation of χ_e that is totally inside the Green function formalism makes use of the Kubo formula, see Sec. 2.5. We make use of the fact that the external charge causes a change of the Hamiltonian given by

$$\hat{H}_1 = \int d\mathbf{r}\rho_e(\mathbf{r})\phi_{\rm ext}(\mathbf{r},t). \tag{6.14}$$

Then, according to the Kubo formula (2.69), we find that the induced charge density is given by Eq. (6.5), with

$$\chi_e(\mathbf{r},t;\mathbf{r}',t') = G^{\rm R}_{\rho_e,\rho_e}(\mathbf{r},t;\mathbf{r}',t'). \tag{6.15}$$

Using the Fourier transform of the charge density,

$$\rho_e(\mathbf{q}) \;=\; e\sum_\sigma \int d\mathbf{r} e^{-i\mathbf{q}\cdot\mathbf{r}}\hat{\psi}^\dagger_\sigma(\mathbf{r})\hat{\psi}_\sigma(\mathbf{r}) = e\sum_{\mathbf{k},\sigma}\hat{\psi}^\dagger_{\mathbf{k},\sigma}\hat{\psi}_{\mathbf{k}+\mathbf{q},\sigma}, \tag{6.16}$$

tother with the proper time dependence of the operators $\hat{\psi}_{\mathbf{k}+\mathbf{q},\sigma}$ and $\hat{\psi}^\dagger_{\mathbf{k},\sigma}$ in the ideal electron gas, we find

$$\chi_e(\mathbf{q};t) \;=\; -ie^2\theta(t)\frac{1}{V}\sum_{\mathbf{k}\sigma}\sum_{\mathbf{k}'\sigma'}\langle[\hat{\psi}^\dagger_{\mathbf{k},\sigma}\hat{\psi}_{\mathbf{k}+\mathbf{q},\sigma}, \hat{\psi}^\dagger_{\mathbf{k}',\sigma'}\hat{\psi}_{\mathbf{k}'-\mathbf{q},\sigma'}]_-\rangle e^{i(\varepsilon_{\mathbf{k}}-\varepsilon_{\mathbf{k}+\mathbf{q}})t/\hbar}. \tag{6.17}$$

The thermal average of the commutator is easily found to give $[f^0(\varepsilon_{\mathbf{k}}) - f^0(\varepsilon_{\mathbf{k}+\mathbf{q}})]\delta_{\mathbf{k},\mathbf{k}'-\mathbf{q}}\delta_{\sigma\sigma'}$, where f^0 is the Fermi distribution function. Finally, performing a Fourier transform to time, we find

$$\chi_e(\mathbf{q},\omega) \;=\; \frac{2e^2}{V}\sum_{\mathbf{k}}\frac{f^0(\varepsilon_{\mathbf{k}}-\mu) - f^0(\varepsilon_{\mathbf{k}+\mathbf{q}}-\mu)}{\varepsilon_{\mathbf{k}} - \varepsilon_{\mathbf{k}+\mathbf{q}} + \omega + i\eta}, \tag{6.18}$$

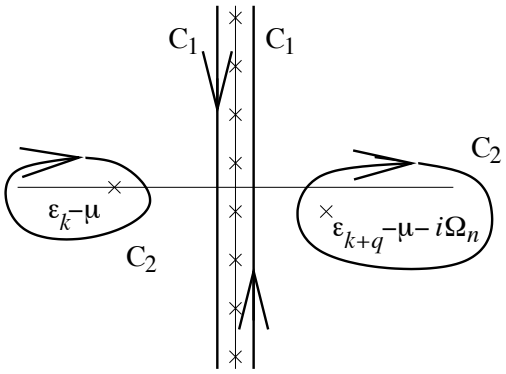

Figure 6.1: Integration contours for the calculation of the polarizability of the noninteracting electron gas.

where η is a positive infinitesimal. Note that χ_e, being a retarded correlation function, satisfies the general integral relation (2.45) that expresses the full retarded correlation function in terms of its imaginary part only.

An alternative method to calculate χ_e is to use the imaginary time formalism. One first calculates

$$\begin{aligned}\chi_e(\mathbf{q},\tau) &= -\frac{e^2}{V}\sum_{\mathbf{k}\sigma}\sum_{\mathbf{k}'\sigma'} T_\tau\langle\hat{\psi}^\dagger_{\mathbf{k},\sigma}(\tau+\eta)\hat{\psi}_{\mathbf{k}+\mathbf{q},\sigma}(\tau)\hat{\psi}^\dagger_{\mathbf{k}',\sigma'}(\eta)\hat{\psi}_{\mathbf{k}'-\mathbf{q},\sigma'}(0)\rangle \qquad (6.19)\\ &= \frac{e^2}{V}\sum_{\mathbf{k}\sigma}\sum_{\mathbf{k}'\sigma'}\left[\mathcal{G}_{\mathbf{k}+\mathbf{q},\sigma;\mathbf{k}',\sigma'}(\tau)\mathcal{G}_{\mathbf{k}'-\mathbf{q},\sigma';\mathbf{k},\sigma}(-\tau) - \mathcal{G}_{\mathbf{k}+\mathbf{q},\sigma;\mathbf{k},\sigma}(-\eta)\mathcal{G}_{\mathbf{k}'-\mathbf{q},\sigma';\mathbf{k}',\sigma'}(-\eta)\right].\end{aligned}$$

The positive infinitesimal η has been added to ensure the placement of creation operators in front of the annihilation operators at the same imaginary time in the time-ordered product. The second term does not depend on τ. After Fourier transform with respect to τ it will give a contribution proportional to $\delta_{\Omega_n,0}$, which can be discarded for the analytical continuation $i\Omega_n \to \omega + i\eta$ we need to do at the end of the calculation. Fourier transform of the first term and substitution of the exact results for the electron Green functions gives

$$\chi_e(\mathbf{q},i\Omega_n) = \frac{2Te^2}{V}\sum_{\mathbf{k},m}\frac{1}{[i\omega_m-(\varepsilon_{\mathbf{k}}-\mu)][i(\omega_m+\Omega_n)-(\varepsilon_{\mathbf{k}+\mathbf{q}}-\mu)]}. \qquad (6.20)$$

Here Ω_n is a bosonic Matsubara frequency (recall that $\rho_{\mathbf{q}}$ is quadratic in fermion creation and annihilation operators) and ω_m is a fermionic Matsubara frequency. In order to perform the

summation over ω_m, the summation is written as an integral over a suitably chosen contour in the complex plane, see Fig. 6.1. The integrand is a function of the complex variable z and has poles at the fermionic Matsubara frequencies $z = i\omega_m$, at $z = \varepsilon_{\mathbf{k}} - \mu$, and at $z = \varepsilon_{\mathbf{k+q}} - \mu - i\Omega_n$, hence

$$\begin{aligned}\chi_e(\mathbf{q}, i\Omega_n) &= \frac{e^2}{2\pi i V}\sum_{\mathbf{k}}\int_{C_1} dz \frac{\tanh(z/2T)}{[z-(\varepsilon_{\mathbf{k}}-\mu)][z+i\Omega_n-(\varepsilon_{\mathbf{k+q}}-\mu)]} \\ &= \frac{e^2}{V}\sum_{\mathbf{k}}\frac{\tanh[(\varepsilon_{\mathbf{k+q}}-\mu)/2T]-\tanh[(\varepsilon_{\mathbf{k}}-\mu)/2T]}{\varepsilon_{\mathbf{k}}-\varepsilon_{\mathbf{k+q}}+i\Omega_n}. \end{aligned} \tag{6.21}$$

Now the analytical continuation $\Omega_n \to \omega + i\eta$ is easily done and one recovers the result (6.18) upon substituting $\tanh((\varepsilon-\mu)/2T) = 1 - 2f^0(\varepsilon)$.

The Boltzmann equation result (6.13) agrees with what is found from the microscopic calculation in the limit $\mathbf{q} \to 0$. This is no surprise, once we recall that the Boltzmann equation was derived in the gradient approximation, *i.e.*, under the assumption that all external potential are slowly varying functions of spatial and temporal coordinates.

Let us now consider the dielectric response at finite frequency in more detail. The polarizability describes how the induced charge varies with the time-dependent external charge. A time-dependent induced charge requires a time-dependent current density $\mathbf{j}$, which, by the continuity relation, is proportional to the time derivative of the induced charge. The real part of the polarizability describes that part of the induced current that is out of phase with respect to the external electric field. For such currents, the time-average of $\mathbf{j}\cdot\mathbf{E}$ is zero, so that no energy is dissipated in one cycle. Hence, $\mathrm{Re}\,\chi_e$ describes the dissipationless response to an external potential. Similarly, the imaginary part of the polarizability describes dissipation: current and field are in phase, so that the time average of $\mathbf{j}\cdot\mathbf{E}$ is nonzero. Hence, the imaginary part of the polarizability gives information about the possible excitations of the electron gas.

For the noninteracting electron gas, the dissipative response is given by the imaginary part of Eq. (6.18) above,

$$\mathrm{Im}\,\chi_e(\mathbf{q},\omega) = -\frac{2\pi e^2}{V}\sum_{\mathbf{k}}[f^0(\varepsilon_{\mathbf{k}}) - f^0(\varepsilon_{\mathbf{k+q}})]\delta(\varepsilon_{\mathbf{k}} - \varepsilon_{\mathbf{k+q}} + \hbar\omega). \tag{6.22}$$

Hence, electromagnetic energy can be dissipated by the excitation of particle-hole pairs of energy $\hbar\omega$ and momentum $\mathbf{q}$. Let us investigate Eq. (6.22) in more detail for zero temperature and $\omega > 0$.[1] Then the difference $f^0(\varepsilon_{\mathbf{k}}) - f^0(\varepsilon_{\mathbf{k+q}})$ is one if $\mathbf{k}$ is inside the Fermi sphere

[1] The case $\omega < 0$ follows from the relation $\chi_e^{\mathrm{R}}(\mathbf{q},\omega) = \chi_e^{\mathrm{R}}(-\mathbf{q},-\omega)$.

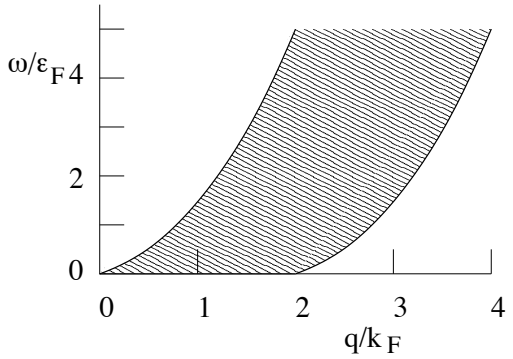

Figure 6.2: Support of the imaginary part of the polarizability $\chi_e(\mathbf{q}, \omega)$ for a noninteracting electron gas.

and $\mathbf{k} + \mathbf{q}$ is outside the Fermi sphere, and zero otherwise. Taking a parabolic dispersion relation, $\varepsilon_{\mathbf{k}} = \hbar^2 k^2/2m$, the delta function then implies $\omega = q^2/2m\hbar + \mathbf{k} \cdot \mathbf{q}/m\hbar$. In general, one has $|\mathbf{k} \cdot \mathbf{q}| \leq mvq/\hbar$, where $v = \hbar k/m$ is the velocity for an electron with wavenumber $\mathbf{k}$. Since $\mathbf{k}$ is inside the Fermi sphere, one has $v \leq v_F$, so that the momentum and frequency range where $\operatorname{Im} \chi_e$ is nonzero is given by

$$\frac{q^2}{2m\hbar} - v_F q < \omega < \frac{q^2}{2m\hbar} + v_F q. \tag{6.23}$$

The support of $\operatorname{Im} \chi_e$ is shown in Fig. 6.2.

6.2 polarizability function for a dirty metal

How do electrons in a disordered metal respond to a change in the potential?

At high frequencies or small wavelengths, we do not expect that the disorder will play an important role. Hence, for high frequencies or small wavelength we expect that the polarizability function χ_e is given by the results obtained in the previous section. However, at low frequencies or large wavelengths, impurity scattering becomes important and should affect the way the electron density responds to a change of the potential.

As before, let us first examine the Boltzmann equation. Looking at linear response only, we write $f = f^0 + f^1$. For Gaussian white noise, the Boltzmann equation reads

$$(\partial_t + \mathbf{v}_{\mathbf{k}} \cdot \partial_{\mathbf{r}} - (e/\hbar)\partial_{\mathbf{r}}\phi \cdot \partial_{\mathbf{k}})\, f_{\mathbf{k}}(\mathbf{r}, t) = -\frac{1}{\tau}\left(f_{\mathbf{k}}(\mathbf{r}, t) - \overline{f}_{\mathbf{k}}(\mathbf{r}, t)\right) \tag{6.24}$$

where $\overline{f}$ is the average of $f_{\mathbf{k}}$ over all directions of $\mathbf{k}$, see Eq. (5.22). Linearizing the Boltzmann equation and Fourier transforming with respect to $\mathbf{r}$ and t, we find

$$f^1_{\mathbf{k}}(\mathbf{q},\omega) = \frac{\overline{f_{\mathbf{k}}}(\mathbf{q},\omega) + i\tau(e/\hbar)\mathbf{v}_{\mathbf{k}}\cdot\mathbf{q}(\partial_\varepsilon f^0_{\mathbf{k}})\phi(\mathbf{q},\omega)}{1 + i\tau\mathbf{v}_{\mathbf{k}}\cdot\mathbf{q} - i\omega\tau}. \tag{6.25}$$

Upon performing an angular average one finds a self-consistent equation for $\overline{f}$. Since the effect of impurities is important only if $\omega\tau \ll 1$ and $ql \ll 1$, where $l = \tau v_F$ is the mean free path, we can expand the denominator in Eq. (6.25) for small q and ω, which greatly simplifies the calculation. Upon performing the angular average, the leading terms in Eq. (6.25) cancel. Solving for $\overline{f}$ from the remaining sub-leading terms, we find

$$\overline{f}_{\mathbf{k}}(\mathbf{q},\omega) = -e\frac{Dq^2}{Dq^2 - i\omega}(-\partial_\varepsilon f^0_{\mathbf{k}})\phi(\mathbf{q},\omega), \tag{6.26}$$

where $D \equiv v_F^2\tau/3$ is the so-called "diffusion constant". Hence, we conclude

$$\chi_e(\mathbf{q},\omega) = -\frac{2e^2}{V}\sum_{\mathbf{k}}\frac{Dq^2}{Dq^2 - i\omega}(-\partial_\varepsilon f^0_{\mathbf{k}}). = -\frac{2e^2\nu Dq^2}{Dq^2 - i\omega}, \tag{6.27}$$

where ν is the density of states at the Fermi surface.

To see what this result means, it is useful to perform a Fourier transform to time t and coordinate $\mathbf{r}$. For the density response to a sudden increase of the potential $\delta\phi(\mathbf{r},t) = \delta(\mathbf{r}-\mathbf{r}')\theta(t)\delta\phi$ we find from Eq. (6.27)

$$\delta\rho_e(\mathbf{r},t) = -2e^2\nu\left[\delta(\mathbf{r}-\mathbf{r}') - \left(\frac{\pi}{Dt}\right)^{3/2} e^{-|\mathbf{r}-\mathbf{r}'|^2/4Dt}\right]\delta\phi. \tag{6.28}$$

This result has a very simple interpretation: the change in the potential at $\mathbf{r} = \mathbf{r}'$ creates a density profile that spreads diffusively.[2]

The behavior of the polarizability in the limit that both the frequency ω and the wavevector q are taken to zero is singular. It depends on which of those is taken to zero first. If the frequency is taken to zero first, we essentially look at the response to a static potential. In that case, the fact that the electron motion is slowed down by the impurities plays no

[2]Note that the Drude conductivity is a function of the diffusion coefficient as well,

$$\sigma_{\alpha\beta}(\omega) = 2e^2\nu D\delta_{\alpha\beta}.$$

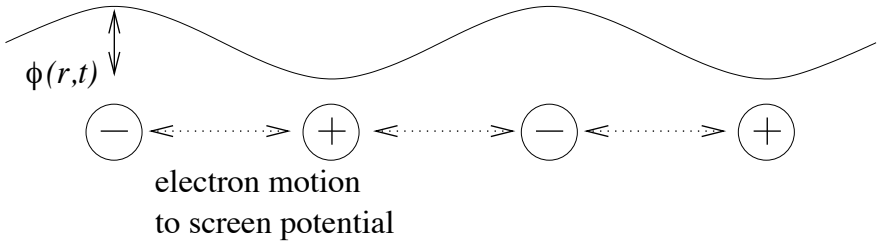

Figure 6.3: The electrons move periodically in order to screen an external time-dependent potential. It depends on the frequency of the potential whether the electron gas can sustain this periodic motion in the presence of disorder.

role. Sooner or later they'll adjust their density profile to accomodate the external potential, $\chi_e = -2e^2\nu$. This response to an external potential is referred to as "Thomas-Fermi screening". On the other hand, if the wavenumber q is taken to zero first, the presence of the impurities does not allow the electrons to travel between the minima and maxima of the external potential within one period $1/\omega$, see Fig. 6.3. Hence, the charge density does not adjust itself, $\chi_e = 0$.

Can the same result be obtained using the diagrammatic method? Repeating the calculations of Sec. 6.1, we find that the polarizability function χ_e is equal to

$$\chi_e(\mathbf{q}, i\Omega_n) = \frac{2Te^2}{V} \sum_{\mathbf{k},\mathbf{k}',m} \mathcal{G}_{\mathbf{k}+\mathbf{q},\mathbf{k}'+\mathbf{q}}(i\omega_m + i\Omega_n)\mathcal{G}_{\mathbf{k}',\mathbf{k}}(i\omega_m), \tag{6.29}$$

where the Green function $\mathcal{G}$ is calculated in the presence of the exact impurity potential. We will be interested in the impurity averaged polarizability function $\langle\chi_e\rangle$. For the disorder, we use the model of Gaussian white noise, see Sec. 5.5. Evaluating the average, we limit ourselves to the ladder diagrams shown in Fig. 6.4. The middle part of these diagrams is a geometric series, and can be summed up separately. The result is called the "diffusion propagator" or "diffusion" D shown in Fig. 6.5,

$$\mathcal{D}(\mathbf{q}; i\omega_m, i\omega_m + i\Omega_n) = \left[1 - \frac{1}{2\pi\nu\tau V} \sum_{\mathbf{k}'} \langle\mathcal{G}_{\mathbf{k}'+\mathbf{q}}(i\omega_m + i\Omega_n)\rangle\langle\mathcal{G}_{\mathbf{k}'}(i\omega_m)\rangle\right]^{-1}. \tag{6.30}$$

We can replace the summation over $\mathbf{k}'$ by an integration over the energy $\xi = \varepsilon_{\mathbf{k}'} - \mu$ and the angle θ between $\mathbf{k}'$ and $\mathbf{q}$. We are interested in wavevectors $q \ll k_F$, so that we can expand

$$\varepsilon_{\mathbf{k}+\mathbf{q}} = \varepsilon_{\mathbf{k}} + v_F q \cos\theta. \tag{6.31}$$

Since the main contribution of the ξ-integration comes from a window of width $\sim \hbar/\tau$ around

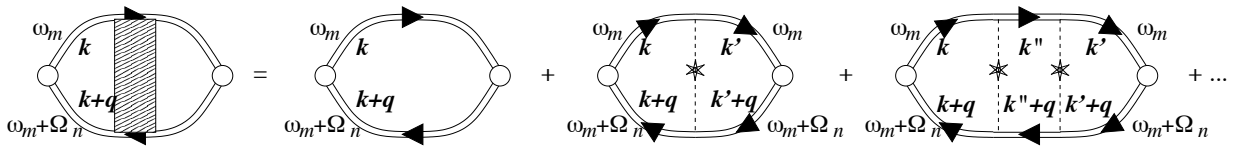

Figure 6.4: Diagrammatic representation of ladder series for the polarizability function is a disordered non-interacting electron gas.

the Fermi energy, we can assume a constant density of states ν for the entire integration range. The result of the ξ-integration depends on the position of the Matsubara frequencies $i\omega_m + i\Omega_n$ and $i\omega_m$ with respect to the real axis. If they are on the same side of the real axis, the integration over the energy ξ vanishes, and one finds $D = 1$. If $\omega_m + \Omega_n > 0$ whereas $\omega_m < 0$, the ξ-integration is finite, and one has

$$\begin{aligned} \frac{1}{2\pi\nu\tau V}\sum_{\mathbf{k}'}\langle\mathcal{G}_{\mathbf{k}'+\mathbf{q}}(i\omega_m + i\Omega_n)\rangle\langle\mathcal{G}_{\mathbf{k}'}(i\omega_m)\rangle &= \frac{1}{2}\int_{-1}^{1} d\cos\theta \frac{1}{1+\Omega_n\tau + iv_F q\tau\cos\theta} \\ &= 1 - \Omega_n\tau - Dq^2\tau, \end{aligned} \tag{6.32}$$

where, in the last equality, we expanded for low frequencies, $i\Omega_n \to \omega \ll 1/\tau$ and for long wavelengths Similarly, for $\omega_m + \Omega_n < 0$ and $\omega_m > 0$, one finds

$$\frac{1}{2\pi\nu\tau V}\sum_{\mathbf{k}'}\langle\mathcal{G}_{\mathbf{k}'+\mathbf{q}}(i\omega_m + i\Omega_n)\rangle\langle\mathcal{G}_{\mathbf{k}'}(i\omega_m)\rangle = 1 + \Omega_n\tau - \frac{1}{3}v_F^2 q^2\tau^2. \tag{6.33}$$

We thus conclude that for $|\Omega_n|\tau \ll 1$, $qv_F\tau \ll 1$, one has

$$\mathcal{D}(\mathbf{q}; i\omega_m, i\omega_m + i\Omega_n) = \begin{cases} 1 & \text{if } \omega_m + \Omega_n > 0,\ \omega_m > 0, \\ 1/[\tau(Dq^2 + \Omega_n)] & \text{if } \omega_m + \Omega_n > 0,\ \omega_m < 0, \\ 1/[\tau(Dq^2 - \Omega_n)] & \text{if } \omega_m + \Omega_n < 0,\ \omega_m > 0, \\ 1 & \text{if } \omega_m + \Omega_n < 0,\ \omega_m < 0, \end{cases} . \tag{6.34}$$

Performing the analytical continuation $i\omega_m \to \varepsilon \pm i\eta$, $i\omega_m + i\Omega_n \to \varepsilon + \omega \pm i\eta$, we refer to the four cases listed in Eq. (6.34) as retarded-retarded, retarded-advanced, advanced-retarded, and advanced-advanced,

$$\begin{aligned} D^{\mathrm{RR}}(\mathbf{q},\omega) &= 1, \\ D^{\mathrm{AR}}(\mathbf{q},\omega) &= 1/[\tau(Dq^2 - i\omega)], \\ D^{\mathrm{RA}}(\mathbf{q},\omega) &= 1/[\tau(Dq^2 + i\omega)], \\ D^{\mathrm{AA}}(\mathbf{q},\omega) &= 1. \end{aligned} \tag{6.35}$$

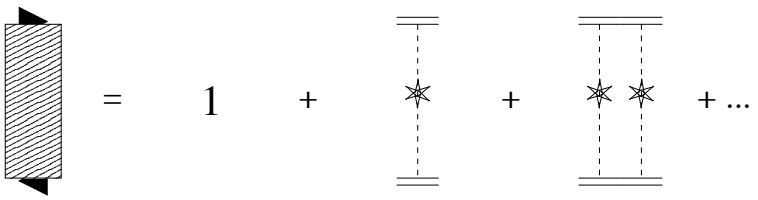

Figure 6.5: Diagrammatic representation of the diffusion propagator.

The propagators $D^{\rm RA}$ and $D^{\rm AR}$ contain the denominator $Dq^2 \pm i\omega$, which is the kernel of the diffusion equation. For that reason, they are referred to as the "diffusion propagator": $D^{\rm RA}$ and $D^{\rm AR}$ are Green functions of the diffusion equation. If no confusion is possible we'll refer to the retarded-advanced propagator $D^{\rm RA}$ simply by D. The advanced-retarded propagator is found by complex conjugation.

In terms of the diffusion propagator, the polarizability reads

$$\chi_e(\mathbf{q}, i\Omega_n) \;=\; \frac{2Te^2}{V}\sum_{\mathbf{k},m}\langle\mathcal{G}_{\mathbf{k+q}}(i\omega_m + i\Omega_n)\rangle\langle\mathcal{G}_{\mathbf{k}}(i\omega_m)\rangle\mathcal{D}(\mathbf{q}; i\omega_m, i\omega_m + i\Omega_n). \quad (6.36)$$

The calculation of χ_e differs in an essential way from the calculation of the diffusion propagator, since Eq. (6.36) involves both a summation over Matsubara frequencies ω_m and a summation over wavevectors $\mathbf{k}$. The summation over ω_m, which needs to be performed first, can be done as in Sec. 5.6. Replacing the summation over Matsubara frequencies by an integration in the complex plane and deforming the contours as in Fig. 5.12, and performing the analytical continuation $i\Omega_n \to \omega + i\eta$, we find

$$\begin{aligned}\chi_e^{\rm R}(\mathbf{q},\omega) \;=\; & \frac{e^2}{2\pi i V}\int d\xi \tanh(\xi/2T)\sum_{\mathbf{k}} \\ & \times\left[\langle G^{\rm R}_{\mathbf{k}}(\xi)\rangle\langle G^{\rm R}_{\mathbf{k+q}}(\xi+\omega)\rangle D^{\rm RR}(\mathbf{q},\omega) - \langle G^{\rm A}_{\mathbf{k}}(\xi)\rangle\langle G^{\rm R}_{\mathbf{k+q}}(\xi+\omega)\rangle D^{\rm AR}(\mathbf{q},\omega)\right. \\ & \left. + \langle G^{\rm A}_{\mathbf{k}}(\xi-\omega)\rangle\langle G^{\rm R}_{\mathbf{k+q}}(\xi)\rangle D^{\rm AR}(\mathbf{q},\omega) - \langle G^{\rm A}_{\mathbf{k}}(\xi-\omega)\rangle\langle G^{\rm A}_{\mathbf{k+q}}(\xi)\rangle D^{\rm AA}(\mathbf{q},\omega)\right].\end{aligned}$$

For the first and fourth terms between the brackets, the diffuson propagator $D^{\rm RR} = D^{\rm AA} = 1$. For the second and third term, we write $D^{\rm AR} = 1 + (D^{\rm AR} - 1)$. Then there is a contribution from all four terms between brackets, which is identical to that calculated in Eq. (5.62), and a contribution from the remaining part of the second and third term between brackets. Adding both terms and making use of the limits $qv_F\tau \ll 1$, $\omega\tau \ll 1$ and $\varepsilon_F\tau \gg 1$, we find

$$\chi_e^{\rm R}(\mathbf{q},\omega) \;=\; -2e^2\nu - \frac{e^2}{2\pi i V\tau(Dq^2 - i\omega)}\int d\xi\left(\tanh\frac{\xi}{2T} - \tanh\frac{\xi+\omega}{2T}\right)$$

$$\begin{aligned} & \times \sum_{\mathbf{k}} \langle G^{\rm A}_{\mathbf{k}}(\xi)\rangle \langle G^{\rm R}_{\mathbf{k}+\mathbf{q}}(\xi+\omega)\rangle \\ = & -2e^2\nu - \frac{2e^2\nu i\omega}{Dq^2 - i\omega} \\ = & -\frac{2e^2\nu Dq^2}{Dq^2 - i\omega}, \end{aligned} \tag{6.37}$$

in agreement with Eq. (6.27).

6.3 Weak localization

Our calculation of the conductivity in Ch. 5 was done to leading order in the impurity concentration. The leading contribution consisted of diagrams without crossed impurity lines. Diagrams that have impurity lines are a factor $1/\epsilon_F\tau$ smaller. However, as we'll show here, such diagrams can have a singular temperature dependence in one and two dimensions, actually diverging in the limit of zero temperature. The singularity arises from the diffusive electron motion we considered in the previous section.

The leading correction in powers of $1/\epsilon_F\tau$ is given by the so-called "maximally crossed" diagrams.[3] The maximally crossed diagrams are shown in Fig. 6.6. They can be represented in terms of the renormalized current vertex (see Sec. 5.6) and the so-called cooperon propagator. The cooperon is a series of ladder diagrams, similar to the diffusion propagator we encountered in the previous section. However, unlike for the diffuson, where the difference of the momenta is constant throughout the ladder, for the cooperon the sum of the momenta is constant throughout the ladder, see Fig. 6.6. The cooperon propagator derives its name from its close resemblance to the electron-electron correlation function that describes the superconducting instability.

The cooperon propagator reads

$$\mathcal{C}(\mathbf{q}; i\omega_m, i\omega_m + i\Omega_n) = \frac{\sum_{\mathbf{k}} \langle \mathcal{G}_{\mathbf{q}-\mathbf{k}}(i\omega_m + i\Omega_n)\rangle \langle \mathcal{G}_{\mathbf{k}}(i\omega_m)\rangle}{2\pi\nu V\tau - \sum_{\mathbf{k}} \langle \mathcal{G}_{\mathbf{q}-\mathbf{k}}(i\omega_m + i\Omega_n)\rangle \langle \mathcal{G}_{\mathbf{k}}(i\omega_m)\rangle}. \tag{6.38}$$

Performing the momentum summations, we find for $qv_F\tau \ll 1$ and $|\Omega_n|\tau \ll 1$

$$\mathcal{C}(\mathbf{q}; i\omega_m, i\omega_m + i\Omega_n) = \frac{1}{\tau(Dq^2 + |\Omega_n|)} \theta[(-\omega_m)(\omega_m + \Omega_n)]. \tag{6.39}$$

[3] Don't be confused by the word "maximally crossed". These diagrams, in fact, have the smallest number of crossed impurity lines of all the diagrams that remain after calculation of the Drude conductivity.

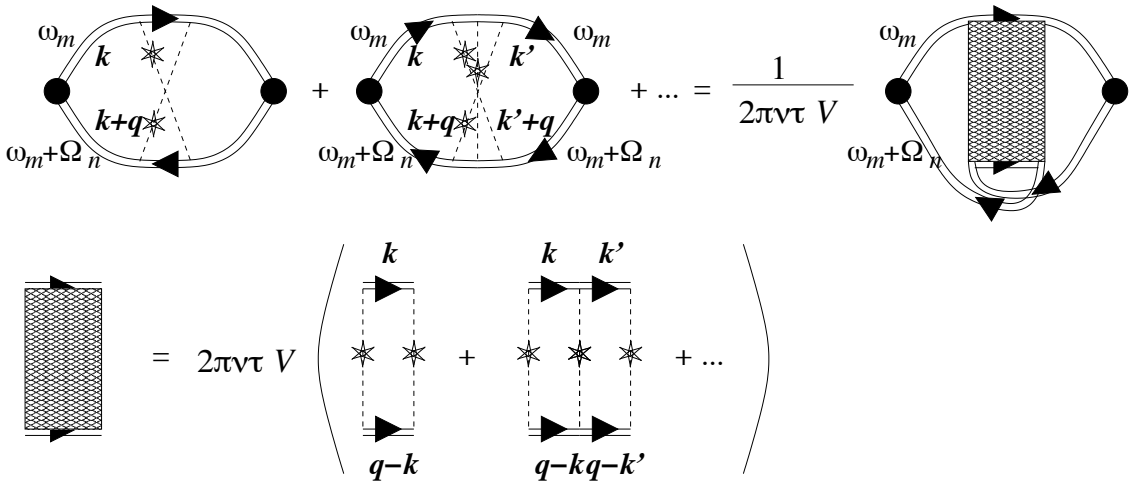

Figure 6.6: Diagrammatic representation of maximally crossed diagrams that contribute to the conductivity (top). The double lines represent the disorder averaged Green function; the solid dots refer to the renormalized current vertex, see Fig. 5.10. The maximally crossed diagrams can be represented in terms of the cooperon propagator (right and below).

The expression is formally identical to the corresponding expression for the diffusion propagator. However, you have to keep in mind that for the Cooperon $\mathbf{q}$ is the sum of the momenta, whereas for the diffuson $\mathbf{q}$ is the difference of the momenta.

For the current-current correlator, the diagrams of Fig. 6.6 imply a correction

$$\begin{aligned}\delta\Pi_{\alpha\beta}(\mathbf{q}\to 0, i\Omega_n) &= \frac{2e^2T}{m^2V^2}\sum_{\mathbf{k},\mathbf{k}'} k_\alpha k'_\beta \sum_m \langle\mathcal{G}_{\mathbf{k}}(i\omega_m)\rangle\langle\mathcal{G}_{\mathbf{k}}(i\omega_m+i\Omega_n)\\ &\quad\times\frac{\hbar}{2\pi\nu\tau}\mathcal{C}(\mathbf{k}+\mathbf{k}';i\omega_m,i\omega_m+i\Omega_n)\langle\mathcal{G}_{\mathbf{k}'}(i\omega_m)\rangle\langle\mathcal{G}_{\mathbf{k}'}(i\omega_m+i\Omega_n)\rangle,\end{aligned} \tag{6.40}$$

The summation over m and the integrations over $\mathbf{k}$ and $\mathbf{k}'$ can be done as in the previous sections. Alternatively, we note that the Green functions have a very weak dependence on ω_m for $|\omega_m| < 1/\tau$, so that we may set $i\omega_n \to -i\eta$ in the arguments of the Green functions. Then summation over m gives nothing but a factor $n = \Omega_n/2\pi T$. Now the analytical continuation $i\Omega_n \to \omega + i\eta$ is possible, followed by division by ω and the limit $\omega \to 0$. Also, if we write $\mathbf{k}' = -\mathbf{k} + \mathbf{Q}$ and note that the mean contribution of the summation over $\mathbf{Q}$ comes from $\mathbf{Q}$ close to 0, we can ignore the $\mathbf{Q}$ dependence of the single-electron Green functions in Eq. (6.40). The remaining integration over $\mathbf{k}$ then gives

$$\frac{1}{V}\sum_{\mathbf{k}} k_\alpha(-k_\beta)\langle G^{\mathrm{R}}_{\mathbf{k},\mathbf{k}}(0)\rangle^2\langle G^{\mathrm{A}}_{\mathbf{k},\mathbf{k}}(0)\rangle^2 = 4\pi\nu\tau^3 k_F^2/d, \tag{6.41}$$

where d is the dimensionality of the conductor. Combining everything, we find

$$\delta\Pi^{\rm R}_{\alpha\beta}(\mathbf{q}\to 0,\omega) \;=\; \frac{2\tau e^2 k_F^2}{\pi d m^2 V}\sum_{\mathbf{Q}}\frac{i\omega}{DQ^2}. \tag{6.42}$$

Hence, using the general relation $D = v_F^2\tau/d$, we find that the correction to the conductivity reads

$$\begin{aligned}\delta\sigma_{\alpha\beta} &= -\frac{1}{i\omega}\delta\Pi^{\rm R}_{\alpha\beta}(\mathbf{q}\to 0,\omega)\Big|_{\omega\to 0}\\ &= -\frac{2\tau e^2 k_F^2}{\pi d m^2 V}\sum_{\mathbf{Q}}\frac{1}{DQ^2}\delta_{\alpha\beta}\\ &= -\frac{2e^2}{\pi V}\sum_{\mathbf{Q}}\frac{1}{Q^2}\delta_{\alpha\beta}.\end{aligned} \tag{6.43}$$

In three dimensions, the summation over $\mathbf{Q}$ is divergent for large Q. The reason for the divergence is that the approximations we made cease to be valid for Q larger than the inverse mean free path $l = v_F\tau$. Truncating the summation for $Ql \sim 1$, we find

$$\delta\sigma \sim -\frac{e^2}{l}. \tag{6.44}$$

This correction to the conductivity is a factor $k_F l$ smaller than the Drude conductivity. Hence, for three dimensions, we conclude that the strategy of Sec. 5.6, where we kept diagrams without crossed lines only, is valid.

For two dimensions, the summation over $\mathbf{Q}$ is divergent both for large Q and for small Q. The divergence at large Q is removed by truncating the integration at $Q \sim 1/l$. The divergence at small Q, however, has an entirely different origin. Small Q correspond to large length scales, and on large length scales our description in terms of non-interacting electrons in a static and unbounded environment breaks down. In a real sample, electrons exit the sample through the contacts, or they loose their phase memory because of scattering from photons or phonons, or because of electron-electron interactions. That means that our description, in which such processes are not taken into account, breaks down at long time scales or long length scales. If we do not want to formulate a full microscopic theory that includes the contacts and decohering processes, we can simply cut off the momentum summation from below at $Q \sim \max(1/L, 1/L_\phi)$, where L is the system size and L_ϕ is the length scale at which the electrons loose their phase memory. Alternative, we keep the full momentum summation but replace the frequency $-i\omega$ in the Cooperon propagator by

$\max(1/\tau_{\rm esc}, 1/\tau_\phi)$, where $\tau_{\rm esc} = L^2/D$ is the time it takes to exit the sample through the contacts and $\tau_\phi = L_\phi^2/D$ is the dephasing time. In both cases we find[45]

$$\delta\sigma = \begin{cases} -(e^2/\pi^2)\ln[\min(L, L_\phi)/l], & \text{if } d = 2, \\ -(e^2/\pi)[\min(L, L_\phi) - l], & \text{if } d = 1. \end{cases} \tag{6.45}$$

These results are very important for our understanding of electron transport through disordered conductors. On the one hand, you verify that $\delta\sigma$ is, at first sight, a factor $k_F l$ smaller than the Drude conductivity. However, $\delta\sigma$ has an additional dependence on system size or temperature that leads to a divergence at large system sizes and low temperatures. (The dephasing length $L_\phi \to \infty$ if $T \to 0$.) Hence, we see that these small corrections become large in large samples at low temperatures, and that the conductivity becomes significantly smaller than the Drude conductivity because of the quantum correction $\delta\sigma$. In one and two dimensions, the correction $\delta\sigma$ we calculated is the first signature of the phenomenon of "Anderson localization", the statement that all "metals" in one and two dimensions become insulators at sufficiently low temperatures. For that reason, the correction $\delta\sigma$ is called "weak localization correction". Moreover, $\delta\sigma$ is very sensitive to the size of the conductor or the temperature (through the low-momentum cut-off) and, as we'll see soon, to the presence of a magnetic field, unlike the Drude conductivity σ, which has at most a weak dependence on these quantities.

At this point, it is important to stress what is meant by "two dimensions" and "one dimension" in the context of disordered conductors. The meaning is not that the electron gas has to be strictly two-dimensional or one-dimensional, as is the case, *e.g.,* in the two-dimensional electron gas formed at the interface in a semiconductor heterostructure, or in carbon nanotubes. What is meant is that the transverse sample direction (thickness of a film for a two-dimensional sample or thickness of a wire for a one-dimensional sample) is much smaller than the relevant large-length cut-off scales, such as L or L_ϕ.[6] In samples of

[4] In obtaining the numerical factor for $d = 1$ and for $d = 2$, we replaced ω by i/τ_ϕ in the diffuson propagator and used $\tau_\phi = L_\phi^2/D$ to express τ_ϕ in terms of L_ϕ.

[5] In three dimensions, the fact that we need to add a lower cut-off to the momentum integration has a minor effect. It simply amounts to the replacement of Eq. (6.44) by

$$\delta\sigma = -\frac{e^2}{2\pi^2}\left(\frac{1}{l} - \frac{1}{L_\phi}\right).$$

Yet, the temperature and magnetic-field dependence of the conductance correction is dominated by the low-momentum cut-off.

[6] Alternatively, and more appropriately, a sample is referred to as being in a reduced dimension if the time scale for transverse diffusion is small in comparison to the relevant large-time cut-off scales, such as the "dwell time", the time it takes to exit from the sample, or the "dephasing time" τ_ϕ. Whereas this definition

reduced dimension, the smallest wavevector in the transverse direction is $Q_\perp = 0$. The next wavevector is already so large that the corresponding length scale $2\pi/Q_\perp$ is larger than the low-wavevector cut-off. Although this does not mean that these wavevectors are excluded from the summation (6.43) — after all, they are likely to be smaller than the high-wavevector cut-off $1/l$ —, their contribution to $\delta\sigma$ is non-singular and independent of the sample size L, the dephasing length L_ϕ, or any other relevant experimental parameter.

The weak localization correction has a simple physical explanation. In a semiclassical picture, the electrons are described as wave packets that move along well defined trajectories, acquiring a phase as they move along. Hence, the electron propagation along a certain path is described by an amplitude, *i.e.*, by an intensity and a phase. The probability for an electron to go from one location in the sample to another location is proportional to the square of the amplitudes for all trajectories linking start and finish. Without quantum phase coherence, one would add intensities of all trajectories, not amplitudes. In other words, without quantum phase coherence, one squares the amplitudes first and then adds them. The difference between the two descriptions — add squared amplitudes or square added amplitudes — is "interference". Interference can be constructive or destructive. In most cases, the interference correction contains a sum over many terms with different phases, and averages to zero. However there is one exception: interference of trajectories that return to the point of departure. In this case, time-reversed trajectories acquire the same phase, and, hence, interfere constructively, see Fig. 6.7. Thus, the probability to return to the point of departure is enhanced by quantum interference. This also implies that the rate at which particles diffuse through the metal is decreased, which, in turn, leads to a reduction of the conductivity. This reduction is precisely what we calculated above!

The interference between time-reversed trajectories is described by the Cooperon propagator. Recall that the Cooperon propagator was most important precisely for the case of opposite momenta $\mathbf{k}$ and $\mathbf{k}'$.

In this picture, the cut-offs needed for the calculation of the weak localization correction are more transparent. The large momentum cut-off corresponds to the break down of diffusion theory at length scales below the mean free path. Indeed, since one needs impurity scattering in order to return to the point of departure, there is a minimal length for such a trajectory. Also, the interference correction exists only if the electrons keep their phase memory along the trajectory and if the electrons return to the point of departure at all. This explains the cut-off at low momenta at $1/L_\phi$ or $1/L$, respectively.

---

is the same as the length-based definition given in the text for samples with a simple geometry and extended contacts, it can more readily be generalized to samples of arbitrary shape and to samples with point contacts or tunneling contacts. In particular, it allows for the definition of a "zero dimensional" sample: a sample in which the time it takes to diffuse through the entire sample is small in comparison to all other relevant time scales.

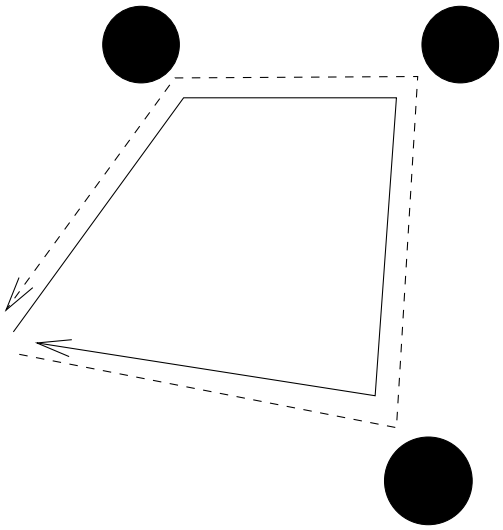

Figure 6.7: Constructive interference of two time-reversed trajectories returning to the point of departure.

In a magnetic field B, time-reversed trajectories acquire a phase difference equal to 2π times the enclosed flux Φ divided by the flux quantum $\Phi_0 = hc/e$. If the typical flux accumulated by a trajectory that ventures a distance L away from the point of departure is denotes $\Phi(L)$, trajectories of length L such that $\Phi(L) > \Phi_0$ do not contribute to the interference. Hence, in a magnetic field, we should impose a lower momentum cutoff at $Q \sim 1/l_m$, where l_m is the so-called magnetic length, defined using the criterion $\Phi(l_m) = \Phi_0$. If l_m is smaller than the dephasing length L_ϕ and the system size, the dephasing length L_ϕ should be replaced by L_B in Eq. (6.45). Hence, for large magnetic fields, the weak localization correction to the conductivity is suppressed. In a three-dimensional sample or in a two-dimensional sample with the magnetic field perpendicular to the plane of the sample, the typical area swept out for a trajectory that ventures a distance L away from the point of departure is of order L^2, hence $l_m \sim (\Phi_0/B)^{1/2}$. In a film of thickness a with the magnetic field in the plane of the film or in a wire of thickness a, this typical area is La, hence $l_m \sim \Phi_0/Ba$.

6.4 Formulation in real space

In Sec. 6.2 we saw that the diffuson is equal to the pole of the diffusion equation. We arrived at this conclusion from an analysis in momentum representation, which, in principle, is valid

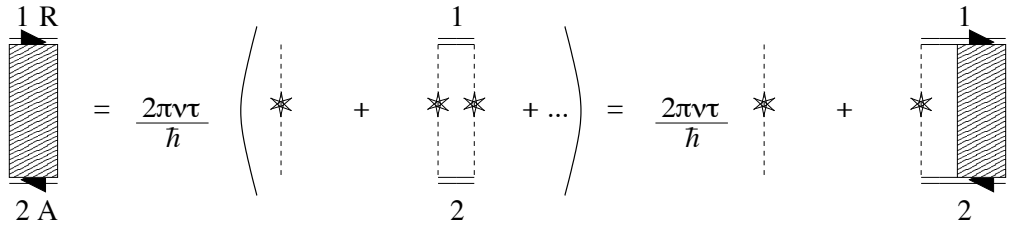

Figure 6.8: Defining equation for the diffusion propagator.

for a bulk system only. For finite-sized systems or for inhomogeneous systems, a description in real space is more useful. In this section, we rederive the results of Sec. 6.2 using the coordinate and time representation.

Before embarking on a diagrammatic calculation in coordinate representation, let us recall the expressions for the impurity averaged Green function,

$$\begin{aligned}\langle G^{\mathrm{R}}(\mathbf{r},\mathbf{r}';\omega)\rangle &= -\frac{m}{2\pi\hbar|\mathbf{r}-\mathbf{r}'|}e^{i(k_F+\omega/v_F)|\mathbf{r}-\mathbf{r}'|-|\mathbf{r}-\mathbf{r}'|/2l},\\ \langle G^{\mathrm{A}}(\mathbf{r},\mathbf{r}';\omega)\rangle &= -\frac{m}{2\pi\hbar|\mathbf{r}-\mathbf{r}'|}e^{-i(k_F+\omega/v_F)|\mathbf{r}-\mathbf{r}'|-|\mathbf{r}-\mathbf{r}'|/2l}.\end{aligned} \tag{6.46}$$

Fourier transforming to time, one has

$$\begin{aligned}\langle G^{\mathrm{R}}(\mathbf{r},\mathbf{r}',t,t')\rangle &= -\frac{m}{2\pi\hbar|\mathbf{r}-\mathbf{r}'|}e^{ik_F|\mathbf{r}-\mathbf{r}'|-|\mathbf{r}-\mathbf{r}'|/2l}\delta(t-t'-|\mathbf{r}-\mathbf{r}'|/v_F),\\ \langle G^{\mathrm{A}}(\mathbf{r},\mathbf{r}';t,t')\rangle &= -\frac{m}{2\pi\hbar|\mathbf{r}-\mathbf{r}'|}e^{-ik_F|\mathbf{r}-\mathbf{r}'|-|\mathbf{r}-\mathbf{r}'|/2l}\delta(t'-t-|\mathbf{r}-\mathbf{r}'|/v_F).\end{aligned} \tag{6.47}$$

We also recall the averaging rule for the Gaussian white noise potential,

$$\langle U(\mathbf{r})U(\mathbf{r}')\rangle = \frac{\hbar}{2\pi\nu\tau}\delta(\mathbf{r}-\mathbf{r}'), \tag{6.48}$$

where τ is the elastic mean free time and ν is the density of states per spin direction. Equations (6.46) and (6.47) are valid in three dimensions; similar results can be obtained in one and two dimensions. Throughout this discussion we assume weak disorder, $k_F l \gg 1$, where $l = v_F/\tau$ is the elastic mean free path.

Starting point of our discussion is the diagrammatic expression for the diffusion propagator, which we repeat in Fig. 6.8. In principle, the diffusion propagator has four coordinate and four time arguments. However, because of the special structure of the Gaussian white noise average, the spatial arguments are pairwise equal. Hence, we may write the arguments

of the diffusion propgator as $D(\mathbf{r},\mathbf{r}';t_1,t_1';t_2,t_2')$. With this notation, using the coordinate and time representation, the defining expression in Fig. 6.8 reads

$$\begin{aligned} D(\mathbf{r},\mathbf{r}';t_1,t_1';t_2,t_2') &= \delta(\mathbf{r}-\mathbf{r}')\delta(t_1-t_1')\delta(t_2-t_2') + \frac{1}{2\pi\nu\tau\hbar}\int d\mathbf{r}''dt_1''dt_2''\langle G^{\mathrm{R}}(\mathbf{r},t_1;\mathbf{r}'',t_1'')\rangle \\ &\quad \times D(\mathbf{r}'',\mathbf{r}';t_1'',t_1';t_2'',t_2')\langle G^{\mathrm{A}}(\mathbf{r}'',t_2'';\mathbf{r},t_2)\rangle \end{aligned} \tag{6.49}$$

Because of the delta-function time dependence of the impurity-averaged Green functions, the solution $D(\mathbf{r},\mathbf{r}';t_1,t_1';t_2,t_2')$ of Eq. (6.49) will be proportional to $\delta(t_1-t_1'+t_2'-t_2)$. In coordinate representation, the disorder-averaged Green functions are short ranged, see Eq. (6.46). Anticipating that D will be a slowly varying function of it arguments (apart from the delta-function dependence noted above), one might be tempted to replace the product of single-electron Green functions by a delta functions in space and in time. In that case, one finds

$$\frac{1}{2\pi\nu\tau\hbar}\langle G^{\mathrm{R}}(\mathbf{r},t_1;\mathbf{r}'';t_1'')\rangle\langle G^{\mathrm{A}}(\mathbf{r}'',t_2'';\mathbf{r},t_2)\rangle = \delta(\mathbf{r}-\mathbf{r}'')\delta(t_1-t_1'')\delta(t_2-t_2''). \tag{6.50}$$

Using Eq. (6.50) for the product of single-electron Green functions, the diffusion propagator cancels from Eq. (6.49). Hence, we need to go beyond the simple delta-function approximation used in Eq. (6.50). Taking the spatial and temporal dependence of the Green functions into account to leading order, one has

$$\begin{aligned} \frac{1}{2\pi\nu\tau\hbar}\langle G^{\mathrm{R}}(\mathbf{r},t_1;\mathbf{r}'';t_1'')\rangle\langle G^{\mathrm{A}}(\mathbf{r}'',t_2'';\mathbf{r},t_2)\rangle &= (1+D\tau\partial_{\mathbf{r}}^2-\tau(\partial_{t_1}+\partial_{t_2})) \\ &\quad \times \delta(\mathbf{r}-\mathbf{r}'')\delta(t_1-t_1'')\delta(t_2-t_2''), \end{aligned} \tag{6.51}$$

where $D=(1/3)v_F^2\tau$ is the diffusion constant.[7] Note that the temporal derivatives appear as a sum, so that there is not contribution from the delta function $\delta(t_1-t_1'+t_2'-t_2)$ in the diffusion propagator. In this notation, the diffusion propagator satisfies the equation

$$\left(-D\partial_{\mathbf{r}}^2+\partial_{t_1}+\partial_{t_2}\right)D(\mathbf{r},\mathbf{r}';t_1,t_1';t_2,t_2') = \frac{1}{\tau}\delta(\mathbf{r}-\mathbf{r}')\delta(t_1-t_1')\delta(t_2-t_2') \tag{6.52}$$

This is precisely the diffusion equation. Note that Eq. (6.52) contains a derivative to the sum t_1+t_2 only. Hence, in solving Eq. (6.52) one can consider all time differences and the sum $t_1'+t_2'$ as parameters. For a bulk system, Fourier transform of Eq. (6.52) gives $D(\mathbf{q};\omega)=[\tau(Dq^2+i\omega)]^{-1}$, in agreement with the results of Sec. 6.2.

[7] Equation (6.51) is derived "under the integral sign", considering the integral of $\langle\mathcal{G}(\mathbf{r},t_1;\mathbf{r}'';t_1'')\rangle\langle\mathcal{G}(\mathbf{r}'',t_2'';\mathbf{r},t_2)\rangle$ times an arbitrary function $f(\mathbf{r}'',t_1'',t_2'')$ over $\mathbf{r}''$, t_1'', and t_2''. Expanding the function f in a Taylor series around $\mathbf{r}''=\mathbf{r}$, $t_1''=t_1$, and $t_2''=t_2$ then gives the desired result.

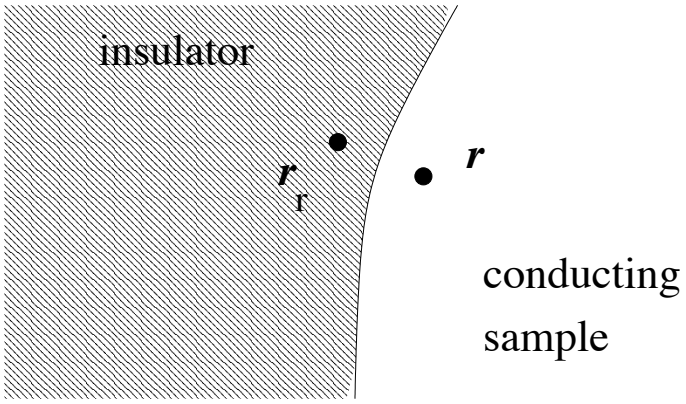

Figure 6.9: Relative positions of a point $\mathbf{r}$ close to the sample boundary and its mirror image $\mathbf{r}_{\rm r}$. For the derivation of the boundary conditions for the diffusion propagator, the point $\mathbf{r}$ is chosen well within a mean free path from the boundary, but much further away than a Fermi wavelength.

The boundary conditions for the diffuson propagator can be obtained in a similar way. If we fix the point $\mathbf{r}'$ to be inside the sample, the boundary conditions are found by taking the correct form of the disorder averaged single-electron Green functions at the sample boundary. Since the wavefunctions have to vanish at the sample boundary, you verify that one has

$$\langle G(\mathbf{r},\mathbf{r}'')\rangle = \langle G(\mathbf{r},\mathbf{r}'')\rangle_{\rm bulk} - \langle \mathcal{G}(\mathbf{r}_{\rm r},\mathbf{r}'')\rangle_{\rm bulk}, \tag{6.53}$$

where $\mathbf{r}_{\rm r}$ is the mirror image of $\mathbf{r}$ in the sample boundary, see Fig. 6.9, and the subscript "bulk" indicates the expression for the average Green function deep inside the sample, see Eqs. (6.46) and (6.47) above. Since we are interested in spatial variations of the diffusion propagator on length scales of the mean free path l and beyond, we take the point $\mathbf{r}$ such that its distance from the boundary is much smaller than the mean free path l but much larger than the Fermi wavelength $\lambda_F = 2\pi/k_F$. Then, using Eq. (6.47), we find

$$\frac{1}{2\pi\nu\tau\hbar}\langle G^{\rm R}(\mathbf{r},t_1;\mathbf{r}'',t_1')\rangle\langle G^{\rm A}(\mathbf{r}'',t_2'';\mathbf{r},t_2)\rangle \;=\; (1+Dv_F^{-1}\hat{n}\cdot\partial_{\mathbf{r}})\delta(\mathbf{r}-\mathbf{r}'')\delta(t_1-t_1'')\delta(t_2-t_2''), \tag{6.54}$$

where $\hat{n}$ is the outward oriented unit vector normal to the sample boundary. Hence, using Eq. (6.49), we conclude that, at the sample boundary, the diffusion propagator must satisfy the boundary condition

$$\hat{n}\cdot\partial_{\mathbf{r}} D(\mathbf{r},\mathbf{r}';t_1,t_1';t_2,t_2') = 0. \tag{6.55}$$

Similarly, at points where the sample is connected to a perfect conductor, one has the boundary condition

$$D(\mathbf{r},\mathbf{r}';t_1,t_1';t_2,t_2') = 0. \tag{6.56}$$

The boundary condition (6.55) describes the fact that, at a boundary with an insulator, the current density is zero, whereas the boundary condition (6.56) describes the fact that, at a boundary with a perfect conductor, the particle accumulation must vanish.

In the presence of a vector potential $\mathbf{A}$ and a scalar potential ϕ that vary on a spatial and temporal scales slow compared to the mean free path and the mean free time, the retarded and advanced Green functions (6.46) acquire an extra factor $\exp[-ie\phi|\mathbf{r}-\mathbf{r}'| + i(e\mathbf{A}/c\hbar)\cdot(\mathbf{r}-\mathbf{r}')]$ and $\exp[ie\phi|\mathbf{r}-\mathbf{r}'| + i(e\mathbf{A}/c\hbar)\cdot(\mathbf{r}-\mathbf{r}')]$, respectively. The effect of these factors is to replace the derivatives in Eq. (6.52) and (6.55) by covariant derivatives. Hence, we find

$$\left[-D\left(\partial_{\mathbf{r}} - \frac{ie}{\hbar c}(\mathbf{A}(\mathbf{r},t_1)-\mathbf{A}(\mathbf{r},t_2))\right)^2 + \partial_{t_1} + \partial_{t_2} + ie\phi(\mathbf{r},t_1) - ie\phi(\mathbf{r},t_2)\right] \times D(\mathbf{r},\mathbf{r}';t_1,t_1';t_2,t_2') = \frac{1}{\tau}\delta(\mathbf{r}-\mathbf{r}')\delta(t_1-t_1')\delta(t_2-t_2'), \tag{6.57}$$

whereas the derivative $\partial_{\mathbf{r}}$ in the boundary condition (6.55) is replaced by the covariant derivative $\partial_{\mathbf{r}} - (ie/\hbar c)(\mathbf{A}(\mathbf{r},t_1)-\mathbf{A}(\mathbf{r},t_2))$.

The same considerations apply to the Cooperon. Using the space and time representation, the defining equation for the Cooperon reads

$$\begin{aligned} C(\mathbf{r},\mathbf{r}';t_1,t_1';t_2,t_2') &= \delta(\mathbf{r}-\mathbf{r}')\delta(t_1-t_1')\delta(t_2-t_2') + \frac{1}{2\pi\nu\tau\hbar}\int d\mathbf{r}''dt_1''dt_2''\langle G^{\mathrm{R}}(\mathbf{r},t_1;\mathbf{r}'',t_1'')\rangle \\ &\quad\times\langle G^{\mathrm{A}}(\mathbf{r},t_2;\mathbf{r}'',t_2'')\rangle C(\mathbf{r}'',\mathbf{r}';t_1'',t_1';t_2'',t_2') \end{aligned} \tag{6.58}$$

From this equation, one concludes that the Cooperon propagator $C(\mathbf{r},\mathbf{r}';t_1,t_1';t_2,t_2')$ is proportional to $\delta(t_1-t_1'+t_2-t_2')$. Replacing the product of retarded and advanced Green functions by the appropriate sum of a delta functions and derivatives of delta functions, one finds that the Cooperon then satisfies the equation

$$\left[-D\left(\partial_{\mathbf{r}} - \frac{ie}{\hbar c}(\mathbf{A}(\mathbf{r},t_1)+\mathbf{A}(\mathbf{r},t_2))\right)^2 + \partial_{t_1} - \partial_{t_2} + ie\phi(\mathbf{r},t_1) - ie\phi(\mathbf{r},t_2)\right] \times C(\mathbf{r},\mathbf{r}';t_1,t_1';t_2,t_2') = \frac{1}{\tau}\delta(\mathbf{r}-\mathbf{r}')\delta(t_1-t_1')\delta(t_2-t_2'), \tag{6.59}$$

The boundary conditions are the same as those for the diffuson propagator. In the presence of a magnetic field, the differential operator $\partial_{\mathbf{r}}$ is replaced by the covariant derivative $\partial_{\mathbf{r}} -$

$(ie/\hbar c)(\mathbf{A}(\mathbf{r},t_1)+\mathbf{A}(\mathbf{r},t_2))$. Note that Eq. (6.59) contains a derivative to the time difference $t_1 - t_2$. In solving Eq. (6.52) one can consider all time sums and the difference $t_1' - t_2'$ as parameters.

A time-independent magnetic field, which is represented by a time-independent vector potential, has no effect on the diffuson, see Eq. (6.57). This is understandable, since the diffusion propagator, which governs the diffusive spreading of charge in a disordered metal, should not be affected by the presence of a magnetic field. On the other hand, the Cooperon, which contains information about the interference of time-reversed trajectories, depends strongly on a magnetic field. How strong this dependence is one can see by realizing that Eq. (6.59) is formally equivalent to the defining equation for the imaginary-time Green function of a particle of mass $\hbar/D$ and charge $2e$. This mass is much smaller than the electron mass if the disorder is weak, $k_F l \gg 1$, so that the effect of a magnetic field is unusually strong. A very small magnetic field will significantly affect the Cooperon propagator and destroy the interference leading to weak localization.

6.5 Random matrix theory

Now let us look at an isolated piece of a disordered conductor of finite size. We are interested in the density of states in the conductor. Since the sample has a finite size, the density of states will be a sum of Dirac delta functions,

$$\mathcal{N}(\omega) = 2\sum_{\mu} \delta(\omega - \varepsilon_\mu), \tag{6.60}$$

where μ labels the eigenvalues of the single-electron Hamiltonian (without spin) and the factor two accounts for spin degeneracy.

The positions of the energy levels ε_μ and, hence, the density of states, will depend on the precise impurity configuration. As before, we'll take a statistical approach, and calculate the probability distribution of the density of states.

Calculation of the average is straightforward, $\langle \mathcal{N} \rangle = 2\nu V$, where V is the volume of the sample. The more interesting question is that of the fluctuations of the density of states, which is described by the function

$$\mathcal{R}(\omega_1 - \omega_2) = \langle \mathcal{N}(\omega_1)\mathcal{N}(\omega_2)\rangle - \langle \mathcal{N}(\omega_1)\rangle\langle \mathcal{N}(\omega_2)\rangle. \tag{6.61}$$

In order to calculate $\mathcal{R}$, we first express the density of states in terms of the electron Green functions,

$$\mathcal{N}(\omega) = \frac{1}{\pi i}\int d\mathbf{r}[G^{\mathrm{A}}(\mathbf{r},\mathbf{r};\omega) - G^{\mathrm{R}}(\mathbf{r},\mathbf{r};\omega)]. \tag{6.62}$$

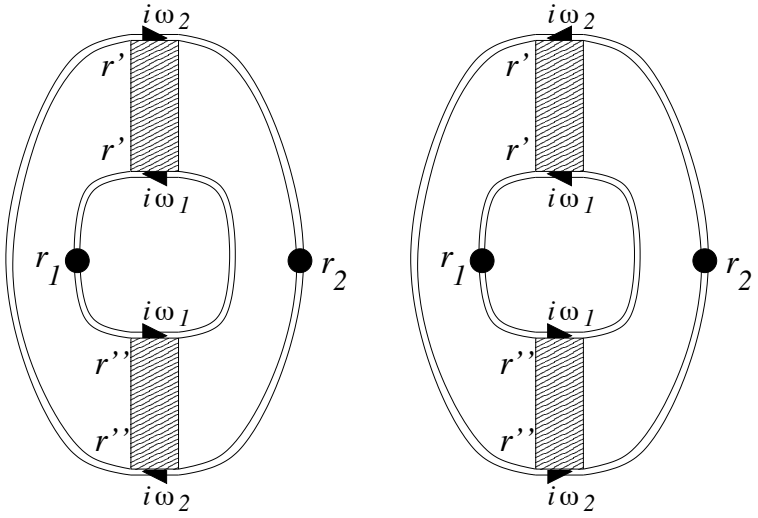

Figure 6.10: Diagrams contributing to the fluctuations of the density of states in a disordered metal grain.

With this expression, $\mathcal{R}(\omega_1 - \omega_2)$ can be calculated with the help of diagrammatic perturbation theory. The relevant diagrams for $\mathcal{R}(\omega_1 - \omega_2)$ are shown in Fig. 6.10. (Note that the diagrams without any lines connecting the inner and outer electron lines contribute to the average of the density of states and not to the fluctuations.)

After substitution of Eq. (6.62) into Eq. (6.61), we distinguish four contributions to the density of states fluctuations. Performing the same calculation as the one leading to Eq. (6.50), one finds that the contributions involving two retarded Green functions or two advanced Green functions are smaller than the contributions involving one retarded and one advanced Green function by a factor $k_F l \gg 1$. Hence, we conclude

$$\mathcal{R}(\omega_1 - \omega_2) = \frac{2}{\pi^2}\mathrm{Re} \int d\mathbf{r}_1 d\mathbf{r}_2 \langle G^{\mathrm{R}}(\mathbf{r}_1, \mathbf{r}_1, \omega_1) G^{\mathrm{A}}(\mathbf{r}_2, \mathbf{r}_2, \omega_2)\rangle. \tag{6.63}$$

Making use of the auxiliary results

$$\begin{aligned} G^{\mathrm{R}}(\mathbf{r}_1, \mathbf{r}', \omega_1) G^{\mathrm{R}}(\mathbf{r}'', \mathbf{r}_1, \omega_1) G^{\mathrm{A}}(\mathbf{r}', \mathbf{r}'', \omega_2) &= -2\pi i \nu \tau^2 \delta(\mathbf{r}' - \mathbf{r}_1)\delta(\mathbf{r}'' - \mathbf{r}_1) \\ G^{\mathrm{R}}(\mathbf{r}_1, \mathbf{r}', \omega_1) G^{\mathrm{R}}(\mathbf{r}'', \mathbf{r}_1, \omega_2) G^{\mathrm{A}}(\mathbf{r}'', \mathbf{r}', \omega_2) &= -2\pi i \nu \tau^2 \delta(\mathbf{r}' - \mathbf{r}_1)\delta(\mathbf{r}'' - \mathbf{r}_1), \end{aligned} \tag{6.64}$$

we find that, according to the diagrams of Fig. 6.10,

$$\mathcal{R}(\omega_1 - \omega_2) = \frac{2\tau^2}{\pi^2}\,\mathrm{Re} \int d\mathbf{r} d\mathbf{r}' [D^{\mathrm{RA}}(\mathbf{r}, \mathbf{r}'; \omega_1, \omega_2) D^{\mathrm{RA}}(\mathbf{r}', \mathbf{r}; \omega_1, \omega_2)$$

$$+ C^{\rm RA}(\mathbf{r},\mathbf{r}';\omega_1,\omega_2)C^{\rm RA}(\mathbf{r}',\mathbf{r};\omega_1,\omega_2)]. \tag{6.65}$$

We now calculate the density of states correlator at energy ω_1 and vector potential $\mathbf{A}_1$ and at energy ω_2 and vector potential $\mathbf{A}_2$. Hereto, we write the diffuson and cooperon propagators as a sum over eigenmodes of the diffusion equation,

$$-D\left[\partial_{\mathbf{r}} + \frac{ie}{\hbar c}(\mathbf{A}_1 - (\pm)\mathbf{A}_2)\right]^2 \phi_{m\pm}(\mathbf{r}) \;=\; \gamma_{m\pm}\phi_{m\pm}(\mathbf{r}), \tag{6.66}$$

where the ϕ_m are properly normalized eigenfunctions and the γ_m are the corresponding eigenvalues,

$$D^{\rm RA}(\mathbf{r},\mathbf{r}';\omega_1,\omega_2) \;=\; \frac{1}{\tau}\sum_m \frac{\phi_{m+}(\mathbf{r})\phi_{m+}(\mathbf{r}')^*}{\gamma_{m+} - i(\omega_1-\omega_2)}, \tag{6.67}$$

$$C^{\rm RA}(\mathbf{r},\mathbf{r}';\omega_1,\omega_2) \;=\; \frac{1}{\tau}\sum_m \frac{\phi_{m-}(\mathbf{r})\phi_{m-}(\mathbf{r}')^*}{\gamma_{m-} - i(\omega_1-\omega_2)}. \tag{6.68}$$

Substituting this into Eq. (6.65) we find

$$\mathcal{R}(\omega_1-\omega_2) = \frac{2}{\pi^2}{\rm Re}\sum_m \left(\frac{1}{(\gamma_{m+}-i(\omega_1-\omega_2))^2} + \frac{1}{(\gamma_{m-}-i(\omega_1-\omega_2))^2}\right). \tag{6.69}$$

This result, which was first obtained by Altshuler and Shklovskii [Sov. Phys. JETP **64**, 127 (1986)], is a key result in the study of spectral statistics in small disordered conductors. Let us look at it in more detail. First, we consider the case in which there is no magnetic field. Then, the cooperon and diffuson contributions are equal. Finding an exact expression for $\mathcal{R}(\omega_1-\omega_2)$ requires solving the diffusion equation, which may be difficult in a sample with an irregular shape. However, we can make three general statements: First, all γ_m are non-negative. Second the smallest eigenvalue of the diffusion equation is $\gamma_0 = 0$. Third, the second smallest eigenvalue γ_1 is of order D/L^2, where L is the sample size. (The length L is the longest dimension of the sample for a sample with an anisotropic shape.) The smallest eigenvalue γ_1 in the absence of a magnetic field is known as the "Thouless energy", $E_{\rm Th}$. Hence, if $|\omega_1-\omega_2| \ll E_{\rm Th}$ the sum in Eq. (6.69) is dominated by the $m=0$ term, and one has

$$\mathcal{R}(\omega_1-\omega_2) = -\frac{4}{\pi^2(\omega_1-\omega_2)^2} \quad \text{if no magnetic field.} \tag{6.70}$$

Notice that this result is completely universal: it does not depend on sample size, sample shape, or disorder concentration.

If, on the other hand, there is a finite magnetic field, the lowest eigenvalue γ_{0-} for the cooperon propagator is nonzero. For small magnetic fields, one can find γ_{0-} using perturbation theory,

$$\gamma_{0-} = \frac{4De^2}{\hbar^2 c^2} \int d\mathbf{r} |\mathbf{A}|^2 \sim \left(\frac{\Phi e}{hc}\right)^2 \frac{E_{\rm Th}}{\delta}, \tag{6.71}$$

where $\delta = 1/\nu V$ is the mean spacing between energy levels and the vector potential $\mathbf{A}$ is taken in the London gauge ($\partial_{\mathbf{r}} \cdot \mathbf{A} = 0$ inside the sample and $\hat{n} \cdot \partial_{\mathbf{r}} \mathbf{A} = 0$ on the sample boundary, where $\hat{n}$ is the unit vector perpendicular to the sample boundary). Equation (6.71) is valid as long as $\gamma_{0-} \ll E_{\rm Th}$. Hence, for magnetic fields for which $\gamma_{0-} \gg |\omega_1 - \omega_2|$, the cooperon contribution to the density of states fluctuations is suppressed, and one finds

$$\mathcal{R}(\omega_1 - \omega_2) = -\frac{2}{\pi^2(\omega_1 - \omega_2)^2} \quad \text{with magnetic field.} \tag{6.72}$$

The results (6.70) and (6.72) are divergent if $\omega_1 - \omega_2 \to 0$. This divergence appears because of a level's "self correlation": Looking at the definitions (6.60) and (6.61), one sees that the correlator $\mathcal{R}(\omega_1 - \omega_2)$ contains the singular term

$$\begin{aligned} \mathcal{R}_{\rm self}(\omega_1 - \omega_2) &= 4 \sum_\mu \left[\langle \delta(\omega_1 - \varepsilon_\mu) \delta(\omega_2 - \varepsilon_\mu) \rangle - \langle \delta(\omega_1 - \varepsilon_\mu) \rangle \langle \delta(\omega_2 - \varepsilon_\mu) \rangle \right] \\ &= \frac{4}{\delta} \delta(\omega_1 - \omega_2) - \frac{4}{\delta^2}. \end{aligned} \tag{6.73}$$

The origin of the divergence in our diagrammatic calculation is that the diagrammatic perturbation theory breaks down when the energy difference $\omega_1 - \omega_2$ becomes comparable to the spacing $\delta = V/\nu$ between energy levels in the sample and thus fails to resolve the delta-function correlations of Eq. (6.73). One way to cure this problem is to give all levels a finite width γ, which regularizes the divergence arising from the self correlations. This amounts to replacing Eqs. (6.70) and (6.72) by

$$\begin{aligned} \mathcal{R}(\omega) &= \frac{4}{\pi^2 \beta} \mathrm{Re} \frac{1}{(\gamma - i\omega)^2} \\ &= \frac{4}{\pi^2 \beta} \frac{\gamma^2 - \omega^2}{(\gamma^2 + \omega^2)^2}, \end{aligned} \tag{6.74}$$

where $\beta = 2$ with a magnetic field and $\beta = 1$ without a field. Using field-theoretic methods, Efetov has been able to calculate the exact correlation function $\mathcal{R}(\omega)$ down to $\omega = 0$ [Adv. Phys. **32**, 53 (1983)]. Without magnetic field he found

$$\mathcal{R}(\omega) = -\frac{4}{\pi^2} \frac{\sin^2(\omega\pi/\delta)}{\omega^2} - \frac{4}{\pi^2} \frac{\partial}{\partial \omega} \left[\left(\frac{\sin(\omega\pi/\delta)}{\omega} \right) \int_{\delta/\pi}^{\infty} dx \frac{\sin(\omega x)}{x} \right] \quad \text{for } \omega \neq 0. \tag{6.75}$$

With a magnetic field, only the first term on the r.h.s. of Eq. (6.75) is kept. Note that Eq. (6.75) simplifies to our results (6.70) and (6.72) if $|\omega| \gg \delta$.

One striking consequence of the correlator (6.70) and (6.72) is that the spectrum is *rigid*. This means that the fluctuations of the number of levels $N(\omega_2, \omega_1)$ in a certain energy interval $\omega_1 < \omega < \omega_2$ increases slower with $|\omega_1 - \omega_2|$ than $|\omega_1 - \omega_2|^{1/2}$. (Fluctuations proportional to $|\omega_1 - \omega_2|^{1/2}$ are expected if the levels were distributed as uncorrelated random numbers.) Indeed, one finds

$$\begin{aligned} \mathrm{var}\, N(\omega_2, \omega_1) &= \int_{\omega_1}^{\omega_2} d\omega d\omega' \mathcal{R}(\omega - \omega') \\ &\sim \frac{4}{\pi^2 \beta} \ln \frac{(\omega_1 - \omega_2)^2}{\delta^2}, \end{aligned} \tag{6.76}$$

where we used the regularized result (6.74) with $\gamma \sim \delta$ to cut off the divergence of $\mathcal{R}(\omega)$ at small ω.

The universality of the spectral fluctuations for energies below the Thouless energy is more general than the case of a disordered conductor of arbitrary shape we considered here. In fact, one finds the same spectral fluctuations for the energy levels in a ballistic conductor with an irregular shape, for the resonances in a heavy nucleus, and for the eigenvalues of a hermitian matrix with randomly chosen elements.[8] In these cases, the only relevant input is the average spacing between levels δ and the symmetry of the system: without a magnetic field, time-reversal symmetry is present, whereas with a magnetic field, time-reversal symmetry is broken. For hermitian matrices, the presence or absence of time-reversal symmetry corresponds to real or complex matrix elements. Mathematically, random matrices are much easier to deal with than disordered conductors. The study of eigenvalues and eigenvectors of random matrices has grown into a field of its own, called "random matrix theory". In fact, the label "random matrix theory" is also used to describe the universal aspect of spectral statistics of disordered metals and heavy nuclei within an energy window of width $\ll E_{\mathrm{Th}}$. You can find more about the mathematical aspects of the theory of random matrices in the book *Random matrices* by M.L. Mehta (Academic, New York, 1991).

[8] For a ballistic conductor, the Thouless energy is $E_{\mathrm{Th}} \sim v_F/L$, whereas for a random matrix of size N one has $E_{\mathrm{Th}} \sim N\delta$. For a ballistic conductor, $\mathcal{R}(\omega_1 - \omega_2)$ for $|\omega_1 - \omega_2| \ll v_F/L$ does not depend on the precise sample shape as long as the shape is irregular, whereas for a random matrix $\mathcal{R}(\omega_1 - \omega_2)$ does not depend on the distribution of the matrix elements if $|\omega_1 - \omega_2| \ll N\delta$. For a ballistic sample, the universality of spectral statistics has the status of a conjecture, although there is extensive numerical evidence.

6.6 Exercises

Exercise 6.1: Tunneling density of states

In this exercise we consider two pieces of metal that are weakly coupled by a tunnel barrier, see Fig. 6.11. The two pieces of metal are labeled A and B. In the tunneling Hamiltonian formalism, the total Hamiltonian H is written as

$$H = \hat{H}_A + \hat{H}_B + \hat{H}_{AB}, \tag{6.77}$$

where $\hat{H}_A$ and $\hat{H}_B$ operate on states of each system separately, with creation and annihilation operators $c^\dagger_{A\mu}$, $c_{A\mu}$, and $c^\dagger_{B\nu}$, $c_{B\nu}$ for the single-electron states in A and B, and $\hat{H}_{AB}$ is a tunneling Hamiltonian $\hat{H}_{AB}$ that describes the coupling between the two systems,

$$\hat{H}_{AB} = \sum_{\nu\mu} (T_{\mu\nu} c^\dagger_{A\mu} c_{B\nu} + T^*_{\nu\mu} c^\dagger_{B\nu} c_{A\mu}), \tag{6.78}$$

where, in principle, the indices μ and ν refer to any choice of an orthogonal basis for the single-electron states in the two systems A and B. The tunnel matrix elements $T_{\mu\nu}$ are complex number numbers that depend on the extension of the single-electron wavefunctions in A and B into the insulating region between them. In general, the tunnel matrix elements are exponentially small in the separation between A and B.

The current through the tunnel barrier follows from the rate of change of the charge Q_A in metal A (or metal B) as

$$I = \frac{\partial Q_A}{\partial t} = i[H, Q_A]_-, \quad Q_A = -e \sum_\mu c^\dagger_{A,\mu} c_{A,\mu}. \tag{6.79}$$

Substituting Eqs. (6.77) and (6.78) for H, one finds that only the tunneling Hamiltonian contributes to the commutator, and that

$$I = ie \sum_{\mu\nu} (T_{\mu\nu} c^\dagger_{A\mu} c_{B\nu} - T^*_{\nu\mu} c^\dagger_{B\nu} c_{A\mu}). \tag{6.80}$$

The current through the tunnel barrier is linear in the tunneling matrix elements $T_{\nu\mu}$. In order to calculate I to lowest (second) order in the tunneling matrix elements, it is sufficient to calculate the (change of the) current to linear response in the tunneling matrix elements. The Kubo formula then gives

$$I(t) = \int_{-\infty}^{\infty} dt' C^{\rm R}_{I,H_{AB}}(t,t'), \tag{6.81}$$

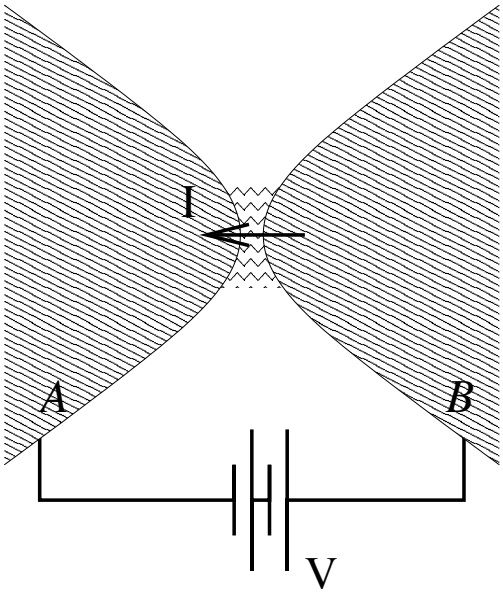

Figure 6.11: Setup for tunnel spectroscopy. Two metals, labeled A and B, are separated by an insulating material, e.g., an oxide or simply vacuum. A battery maintains a finite difference between the chemical potentials of A and B.

where the correlation function $C^{\mathrm{R}}_{I,H_{AB}}$ is defined as

$$C^{\mathrm{R}}_{I,H_{AB}}(t,t') = -i\theta(t-t')\langle[I(t),\hat{H}_{AB}(t')]_-\rangle. \tag{6.82}$$

Here, the thermal equilibrium average $\langle\ldots\rangle$ and the time-dependence of the tunneling Hamiltonian $\hat{H}_{AB}$ are taken with respect to the Hamiltonian $\hat{H}_A + \hat{H}_B$ only, i.e., without inclusion of the tunneling Hamiltonian $\hat{H}_{AB}$.

In the average (6.82), the two systems are completely separated. Hence, in thermal equilibrium, their chemical potentials μ_A and μ_B need not be equal. In fact, it is only if $\mu_B - \mu_A = eV \neq 0$ that a nonzero current flows between the reservoirs. Even in the presence of the tunneling current, a quasi equilibrium in which $\mu_B - \mu_A = eV \neq 0$ can be maintained with the help of a battery, as long as the contacts between the battery and the metals A and B have a much smaller resistance than the tunnel barrier between A and B.

(a) Calculate the correlator $C_{I,H_{AB}}$ and show that the tunneling current can be written

$$I = -e\int\frac{d\omega}{2\pi}\sum_{\mu\nu}|T_{\mu\nu}|^2 A_{A,\mu}(\omega)A_{B,\nu}(\omega+eV)\left(n_F(\omega+eV)-n_F(\omega)\right), \tag{6.83}$$

where $n_F(\omega) = 1/(1+\exp((\omega-\mu)/T))$ is the Fermi distribution function. Be sure that your derivation makes no specific assumptions about the Hamiltonians $\hat{H}_A$ and $\hat{H}_B$! Equation (6.83) is valid both with and without electron-electron interactions.

(b) If metal B has a spectral density that is more or less constant,

$$\sum_\nu |T_{\mu\nu}|^2 A_{B,\nu}(\omega) \approx \text{const.}, \tag{6.84}$$

show that the tunneling current can be used as a direct measurement of the spectral density of metal A. This method of measuring the spectral density is known as "tunnel spectroscopy".

Exercise 6.2: Polarizability function

In this exercise, we consider the polarizability function for the non-interacting electron gas at zero temperature

$$\begin{aligned} \chi_e^0(\mathbf{q},\omega) &= -\frac{2e^2}{V}\sum_{\mathbf{k}} \frac{\theta(\mu-\varepsilon_{\mathbf{k}+\mathbf{q}}) - \theta(\mu-\varepsilon_{\mathbf{k}})}{\omega - \varepsilon_{\mathbf{k}+\mathbf{q}} + \varepsilon_{\mathbf{k}} + i\eta} \\ &= \frac{2e^2}{V}\sum_{\mathbf{k}<k_F}\left[\frac{1}{\omega-\varepsilon_{\mathbf{k}+\mathbf{q}}+\varepsilon_{\mathbf{k}}+i\eta} - \frac{1}{\omega-\varepsilon_{\mathbf{k}}+\varepsilon_{\mathbf{k}-\mathbf{q}}+i\eta}\right]. \end{aligned} \tag{6.85}$$

(a) Perform the summation over $\mathbf{k}$ to show that the real part of χ_e is

$$\operatorname{Re}\chi_e(\mathbf{q},\omega) = -2\nu e^2\left(f(x,x_0)+f(x,-x_0)\right), \tag{6.86}$$

where ν is the density of states at the Fermi level per spin direction and per unit volume, $x = q/2k_F$, $x_0 = \omega/4\varepsilon_F$, and

$$f(x,x_0) = \frac{1}{4} + \frac{(1-(x_0/x-x)^2)}{8x}\ln\left|\frac{x+x^2-x_0}{x-x^2+x_0}\right|.$$

(b) The expressions for $\operatorname{Im}\chi_e$ are somewhat more complicated. Show that if $q < 2k_F$ and $\omega \geq 0$ one finds

$$\operatorname{Im}\chi_e(\mathbf{q},\omega) = -\frac{\pi\nu e^2}{8x}\begin{cases} 4x_0/x & \text{if } 0 < x_0 < x-x^2, \\ (1-(x_0/x-x)^2) & \text{if } x-x^2 < x_0 < x+x^2, \\ 0 & \text{if } x_0 > x+x^2. \end{cases} \tag{6.87}$$

The dimensionless quantities x and x_0 were defined above. On the other hand, if $q > 2k_F$, one finds

$$\mathrm{Im}\,\chi_e(\mathbf{q},\omega) \;=\; -\frac{\pi\nu e^2}{8x}\begin{cases} (1-(x_0/x-x)^2) & \text{if } x^2-x<x_0<x^2+x, \\ 0 & \text{if } 0<x_0<x^2-x \\ & \text{or if } x_0>x+x^2. \end{cases} \tag{6.88}$$

Exercise 6.3: Conductivity from polarizability function

Whereas the polarizability function $\chi_e(\mathbf{q},\omega)$ measures the charge response to a time-dependent shift of the scalar potential, the conductivity $\sigma(\mathbf{q},\omega)$ measures the current response to a time-dependent electric field. However, charge and current are related, as well as electric field and scalar potential. Hence, one should be able to calculate the conductivity from the polarizability function.

Charge and current are related via the continuity relation, $\partial_t\rho_e + \partial_{\mathbf{r}}\mathbf{j} = 0$. Upon Fourier transformation, the continuity equation reads

$$\omega\rho_e(\mathbf{q},\omega) = \mathbf{q}\cdot\mathbf{j}(\mathbf{q},\omega).$$

The electric field and the scalar potential are related as

$$\mathbf{E}(\mathbf{q},\omega) = -i\mathbf{q}\phi(\mathbf{q},\omega).$$

(a) Express the longitudinal current component $q^{-2}\mathbf{q}(\mathbf{q}\cdot\mathbf{j})$ in terms of the polarizability function and the electric field $\mathbf{E}(\mathbf{q},\omega)$.

(b) For an isotropic system, we expect that the current density $\mathbf{j}$ is parallel to the electric field $\mathbf{E}$. For electric fields generated by a scalar potential, $\mathbf{E}$ is always parallel to $\mathbf{q}$. Use this, and your answer to (a) to calculate the dc conductivity σ. Take care to take the limits $\omega \to 0$ and $\mathbf{q} \to 0$ in the correct order!

(c) Derive a general relation between the polarizability $\chi_e(\mathbf{q},\omega)$ and the conductivity $\sigma(\mathbf{q},\omega)$.

Note that the restriction that $\mathbf{E}$ and $\mathbf{q}$ are parallel did not appear when the conductivity was calculated using the time-dependent vector potential.

Exercise 6.4: Magnetic-field dependence of weak localization

In the presence of a magnetic field, the expression we found for the weak-localization correction to the conductivity, Eq. (6.43), should be supplemented with a cut-off for small wavevectors $\mathbf{Q}$. In the text, we argued that this cut-off should be $Q \sim 1/l_m$, where l_m is the so-called magnetic length. In this exercise, you're asked to give a more rigorous calculation.

Starting point of our analysis is the expression of the conductivity correction in terms of the Cooperon propagator $C(\mathbf{Q}; i\omega_m, i\omega_m + i\Omega_n)$, which we write as

$$\delta\sigma = -2\frac{e^2 D\tau}{\pi V}\sum_{\mathbf{Q}} \mathcal{C}(\mathbf{Q}; 0, 0). \tag{6.89}$$

Shifting to coordinate representation and replacing the summation over the wavevector $\mathbf{Q}$ to an integration over space, we find

$$\delta\sigma = -2\frac{e^2 D\tau}{\pi V}\int d\mathbf{r} C(\mathbf{r}, \mathbf{r}; 0, 0). \tag{6.90}$$

In the presence of a magnetic field $\mathbf{B}$, the Cooperon propagator satisfies the differential equation (6.59). With time-independent vector and scalar potentials and after Fourier transforming to time, one finds

$$-D(\partial_{\mathbf{r}} - \frac{2ie}{\hbar c}\mathbf{A}(\mathbf{r}))^2 C(\mathbf{r}, \mathbf{r}'; 0, 0) = \frac{1}{\tau}\delta(\mathbf{r} - \mathbf{r}'). \tag{6.91}$$

This equation is formally equivalent to the defining equation for the Green function of a single particle of charge $2e$ and mass $\hbar^2/2D$ in a magnetic field. The eigenfunctions of that problem are known: they are the Landau level wavefunctions $\phi_{n,\alpha,q_\parallel}$. These wavefunctions are labeled by the Landau level index $n = 0, 1, 2, \ldots$, the wavenumber $q_\parallel$ parallel to the direction of the magnetic field, and the degeneracy index α. At a fixed value of $q_\parallel$, the index α can take $2eBA/hc$ values, where A is the sample cross section perpendicular to the magnetic field.

(a) Show that the solution of Eq. (6.91) can be written as

$$C(\mathbf{r}, \mathbf{r}'; 0, 0) = \frac{1}{\tau}\sum_{n,\alpha,q_\parallel} \frac{\phi_{n,\alpha,q_\parallel}(\mathbf{r})\phi^*_{n,\alpha,q_\parallel}(\mathbf{r}')}{Dq_\parallel^2 + \Omega_B(n + 1/2)}, \tag{6.92}$$

where $\Omega_B = 4DeB/c\hbar$ is the cyclotron frequency for a particle of mass $\hbar^2/2D$. Note that no regularization of the denominator is needed.

(b) Derive an expression for the weak localization correction to the conductivity.

(c) Consider a metal film of thickness a. You may assume $D/a^2 \gg \Omega_B$, so that the film is effectively two-dimensional. Discuss the magnetic-field dependence of the weak-localization for the case that the magnetic field is perpendicular to the plane of the film and for the case that the magnetic field is parallel to the plane of the film.

Exercise 6.5: Kubo formula for conductance

The response of a bulk sample to an applied electric field is characterized by the conductivity. However, for a sample of finite size, one measures the conductance, the coefficient of proportionality between the total current I flowing through a cross section of the sample and the total voltage drop V over the sample.

In order to derive a relation between the total current I and the voltage drop V, we introduce a coordinate system $(\xi, \xi_\perp)$, such that ξ is parallel with the electric field lines and $\xi_\perp$ is parallel with the equipotential lines, see Fig. 6.12. The current can then be written as an integral of the current density,

$$I(\xi) = \int d\xi_\perp \hat{\xi} \cdot \mathbf{j}(\xi, \xi_\perp), \tag{6.93}$$

where $\hat{\xi}$ is the unit vector in the ξ-direction. We are interested in the dc conductance only. Then, current conservation implies that $I(\xi)$ does not depend on the choice of the cross section, i.e., $I(\xi)$ does not depend on ξ.

(a) Use the Kubo formula for the dc conductivity to express $I(\xi)$ in terms of an integral over the electric field $\mathbf{E}(\xi', \xi'_\perp)$.

(b) Use current conservation to show that the conductance G can be written as

$$G = \lim_{\omega \to 0} \mathrm{Re}\, \frac{i}{\omega} C^{\mathrm{R}}_{II}(\omega), \tag{6.94}$$

where C^{R}_{II} is the retarded current-current correlation function,

$$C^{\mathrm{R}}_{II}(t) = -i\theta(t)\langle [I(t), I(0)]_- \rangle. \tag{6.95}$$

The current can be calculated among an arbitrary cross section along the sample.

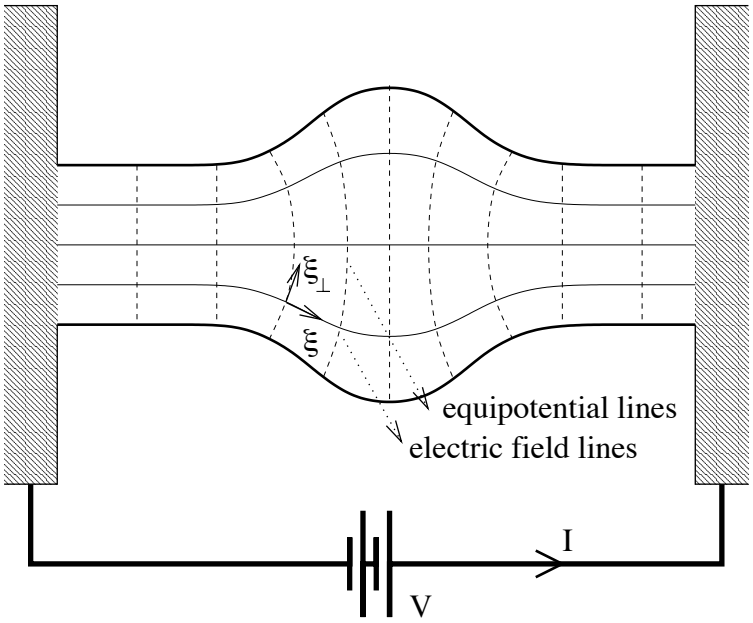

Figure 6.12: Schematic of a conductance measurement. In the derivation of the Kubo formula for the conductance one uses a coordinate system where the coordinate ξ points along the electric field and the coordinate $\xi_\perp$ points along equipotential lines.

(c) Discuss when the relation $G = \sigma A/L$ is true for a sample of cross section A and length L.

(d) Use the Kubo formula (6.94) to calculate the conductance of a one-dimensional wire without impurities.

Exercise 6.6: Weak localization and kinetic equation

One can study the effects of weak localization using the kinetic equation. In that approach, the effect of impurity scattering is described through a correction to the self energy $\underline{\Sigma}$, which is then used to calculate the collision integral. You may find it helpful to re-read Sec. 5.3 before proceeding with this exercise. This exercise is based on Sec. IV of the review *Quantum field-theoretical methods in transport theory of metals* by Rammer and Smith [Rev. Mod. Phys. **58**, 323 (1986)].

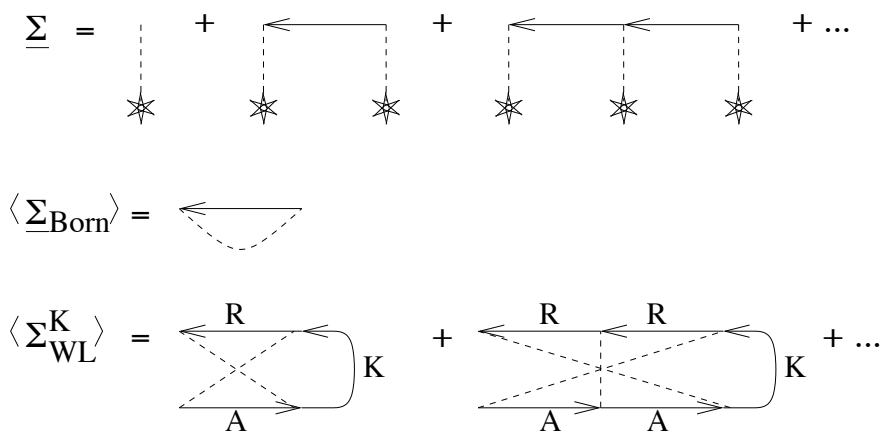

Figure 6.13: Top: Diagrammatic representation of the self energy $\underline{\Sigma}$ for impurity scattering. Middle: Leading contribution to the disorder-averaged self energy. Bottom: Maximally crossed diagrams contributing to the Keldysh component of $\langle\underline{\Sigma}\rangle$.

(a) With impurity scattering, the self-energy $\underline{\Sigma}$ is given by the Born series shown in Fig. 6.13. Show that the Born series shown in the top panel of Fig. 6.13 implies the following matrix structure for the nth order contribution to the self energy

$$\underline{\Sigma}^{(n)} = U \begin{pmatrix} (G^{0\mathrm{R}}U)^{n-1} & \sum_{p=1}^{n-1}(G^{0\mathrm{R}}U)^{p-1}G^{0\mathrm{K}}U(UG^{0\mathrm{A}}U)^{n-p-1} \\ 0 & (G^{0\mathrm{A}}U)^{n-1} \end{pmatrix}. \tag{6.96}$$

In Sec. 3.3 you showed how the leading contribution $\langle\underline{\Sigma}_{\mathrm{Born}}\rangle$ to the disorder-averaged self energy, shown in the middle panel of Fig. 6.13, gave rise to the collision term in the Boltzmann equation and, hence, to the Drude conductivity of a disordered metal. Here we consider a contribution to the Keldysh component $\langle\Sigma^{\mathrm{K}}_{\mathrm{WL}}\rangle$ that involves a maximally crossed diagram, see the bottom panel of Fig. 6.13. Clearly, the maximally crossed part of the diagram is nothing but the Cooperon propagator.

(b) Show that the weak-localization correction to the self energy $\langle\Sigma^{\mathrm{K}}_{\mathrm{WL}}\rangle$ can be expressed in terms of the Cooperon propagator $C(\mathbf{r},\mathbf{r}';t_1,t_1';t_2,t_2')$ and the Keldysh Green function $G^{0\mathrm{K}}$ in the absence of impurity scattering as

$$\langle\Sigma^{\mathrm{K}}_{\mathrm{WL}}(\mathbf{r},t;\mathbf{r}',t')\rangle \;=\; \frac{\hbar}{2\pi\nu\tau}\int dt_2 dt_1' C(\mathbf{r},\mathbf{r}';t,t_1';t_2,t')G^{\mathrm{K}}(\mathbf{r}',t_1';\mathbf{r},t_2). \tag{6.97}$$

Here we made the expression self-consistent by including the effect of impurity scattering on G^{K}.

(c) Why does one consider maximally crossed diagrams for the Keldysh component of the self energy only?

(d) In order to study the effect of the self energy contribution $\langle \underline{\Sigma}_{\rm WL} \rangle$ on the kinetic equation, one should shift to a mixed representation with respect to time and space coordinates. Write down the expression you derived under (b) in terms of the mixed representation.

(e) Now consider the kinetic equation (5.18) in the gradient approximation. Consider the case of a uniform and time-independent electric field. As before, we drop the real parts of the self energy and the Green function from the equation, so that one obtains,

$$-e\mathbf{E}\cdot\partial_{\mathbf{k}} G^{\rm K} = i\langle \Sigma^{\rm K}(G^{\rm R}-G^{\rm A}) - i(\Sigma^{\rm R}-\Sigma^{\rm A})G^{\rm K}. \tag{6.98}$$

Note that the self-energy only affects the right-hand side of the equation, which is the collision term. Instead of calculating the collision term explicitly, one can find the effect of weak localization on the linear conductivity from the solution of the full equation (6.98). In linear response in $\mathbf{E}$, the Keldysh Green function on the l.h.s. can be replaced by the equilibrium Green function, which is unaffected by impurity scattering. [In any case, there is no weak-localization correction to $G^{\rm K}$ in equilibrium, because in equilbrium $G^{\rm K}$ is proportional to the spectral density.] Hence, the net effect of $\langle \underline{\Sigma}_{\rm WL} \rangle$ on the right-hand side of Eq. (6.98) must be zero. If the effect of weak localization is small in comparison to that of classical impurity scattering, show that one then finds that weak localization causes the following small correction to $\langle G^{\rm K} \rangle$,

$$\langle G^{\rm K}_{\rm WL} \rangle = \frac{G^{\rm R}-G^{\rm A}}{\Sigma^{\rm R}-\Sigma^{\rm A}} \langle \Sigma^{\rm K}_{\rm WL} \rangle = 2\pi\tau\nu \langle \Sigma^{\rm K}_{\rm WL} \rangle/\hbar. \tag{6.99}$$

(f) Now calculate the effect of weak localization on the current density.

Chapter 7

The interacting electron gas

Sofar we have discussed electrons mainly as if they were non-interacting particles. This is a huge simplification of reality that turns out to work remarkably well. In this chapter we include electron-electron interactions into our theory and uncover part of the picture why it is that the approximation of noninteracting electrons is as good as it is.

In our theoretical description, we'll consider a general electron-electron interaction Hamiltonian of the form

$$\hat{H} = \hat{H}_0 + \hat{H}_1, \tag{7.1}$$

where $\hat{H}_0$ is the "unperturbed" Hamiltonian, which we assume to be quadratic in fermion or boson creation and annihilation operators, whereas $\hat{H}_1$ is the perturbation. The Hamiltonian $\hat{H}_1$ will include the effect of electron-electron interactions, which, in the most general case, read

$$\hat{H}_1 = \frac{1}{2} \sum_{\nu\nu',\mu\mu'} V_{\nu\mu,\nu'\mu'} \hat{\psi}^\dagger_\nu \hat{\psi}^\dagger_\mu \hat{\psi}_{\mu'} \hat{\psi}_{\nu'}. \tag{7.2}$$

Here the indices μ, ν, μ', and ν' label a complete set of single-electron states and $V_{\nu\mu,\nu'\mu'}$ is the corresponding matrix element. For electrons, the fermion statistics is taken care by the anticommutation relations of the creation and annihilation operators $\hat{\psi}^\dagger$ and $\hat{\psi}$. Depending on the problem of interest, the effects of impurity scattering may be included in $\hat{H}_0$ or as an additional term in $\hat{H}_1$.

Of course, the true microscopic electron-electron interaction is the Coulomb interaction. Using a representation in real space, the Coulomb interaction Hamiltonian reads

$$\hat{H}_1 = \frac{1}{2} \sum_{\sigma_1,\sigma_2} \int d\mathbf{r}_1 \int d\mathbf{r}_2 \frac{e^2}{4\pi\epsilon_0 |\mathbf{r}_1 - \mathbf{r}_2|} \hat{\psi}^\dagger_{\sigma_1}(\mathbf{r}_1) \hat{\psi}^\dagger_{\sigma_2}(\mathbf{r}_2) \hat{\psi}_{\sigma_2}(\mathbf{r}_2) \hat{\psi}_{\sigma_1}(\mathbf{r}_1). \tag{7.3}$$

In momentum space, the Coulomb interaction reads

$$\hat{H}_1 = \frac{1}{2V} \sum_{\sigma_1,\sigma_2} \sum_{\mathbf{k}_1,\mathbf{k}_2} \sum_{\mathbf{q}} V_{\mathbf{q}} \hat{\psi}^\dagger_{\mathbf{k}_1+\mathbf{q},\sigma_1} \hat{\psi}^\dagger_{\mathbf{k}_2-\mathbf{q},\sigma_2} \hat{\psi}_{\mathbf{k}_2,\sigma_2} \hat{\psi}_{\mathbf{k}_1,\sigma_1}, \tag{7.4}$$

where

$$V_{\mathbf{q}} = \int d\mathbf{r} \frac{e^2}{4\pi\epsilon_0 r} e^{-i\mathbf{q}\cdot\mathbf{r}} = \frac{e^2}{\epsilon_0 q^2}. \tag{7.5}$$

One important aspect of the Coulomb interaction is its long range. As a matter of fact, the energy required to charge a system is infinite! That is the reason why all objects are electrically neutral. In most cases, charge neutrality is maintained by the positive charge density of the ion lattice, but charge neutrality can also be maintained by the charge on objects that are near the sample of interest, but that are not a part of it, such as nearby pieces of metal or condensator plates.

7.1 Perturbation theory

The effect of electron-electron interactions can be accounted for by means of a perturbative expansion in the interaction Hamiltonian $\hat{H}_1$. This perturbative expansion can be organized using diagrammatic rules, in exactly the same way as the perturbation expansion for impurity scattering could be organized using the diagrammatic technique, see chapter 4.

In this section, we present the rules for the specific case of the calculation of a single-particle imaginary time Green function, and then discuss the same calculation in the framework of the real-time formalism. The extension to more complicated correlation functions is straightforward.

7.1.1 Imaginary-time formalism

Recall that the single particle imaginary time Green function can be expressed as a thermal average over the non-interacting Hamiltonian $\hat{H}_0$,

$$\mathcal{G}_{\sigma_1,\sigma_2}(\mathbf{r}_1,\tau_1;\mathbf{r}_2,\tau_2) = -\frac{\langle T_\tau e^{-\int_0^{1/T} \hat{H}_1(\tau')d\tau'} \hat{\psi}_{\sigma_1}(\mathbf{r}_1,\tau_1)\hat{\psi}^\dagger_{\sigma_2}(\mathbf{r}_2,\tau_2)\rangle_0}{\langle T_\tau e^{-\int_0^{1/T} \hat{H}_1(\tau')d\tau'}\rangle_0}. \tag{7.6}$$

Here operators are represented in the interaction picture. As before, the Green function is calculated in a series in $\hat{H}_1$. Each term in the series can be represented by a Feynman diagram. The diagrammatic representation of the interaction (7.2) is as in figure 7.1: it

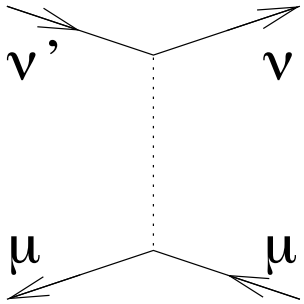

Figure 7.1: Diagrammatic representation of an interaction vertex

consists of four fermion lines connected by a dotted line.[1] Each interaction line carries the weight $-V_{\mu\nu;\mu'\nu'}$ appropriate to the representation that is used, the minus sign arising from the minus sign in the exponent of the evolution operator in Eq. (7.6). For the Coulomb interaction in coordinate representation, the interaction involves one particle at coordinate $\mathbf{r}$ and one particle at coordinate $\mathbf{r}'$ and has weight is $-e^2/4\pi\epsilon_0|\mathbf{r}-\mathbf{r}'|$. For the Coulomb interaction in momentum representation, the Coulomb interaction scatters electrons in momentum states $\mathbf{k}$ and $\mathbf{k}'$ to momentum states $\mathbf{k}+\mathbf{q}$ and $\mathbf{k}'-\mathbf{q}$, respectively, and has weight $-V_{\mathbf{q}}/V$. The factor $1/V$ follows from the normalization of the Fourier transform of the Coulomb interaction, see Eq. (7.4).

The diagrammatic rules for a perturbation $\hat{H}_1$ that includes interactions are the same as those for the case of impurity scattering we discussed in chapter 4. There are two additional rules, specific for the case of interactions,

1. The interaction Hamiltonian $\hat{H}_1$ involves four creation and annihilations operators at the same time. In order to ensure that creation operators are always kept in front of annihilation operators, one adds a positive infinitesimal η to their imaginary times,

$$\hat{H}_1(\tau) = \frac{1}{2}\sum_{\nu\nu',\mu\mu'} V_{\nu\mu,\nu'\mu'}\hat{\psi}^\dagger_\nu(\tau+\eta)\hat{\psi}^\dagger_\mu(\tau+\eta)\hat{\psi}_{\mu'}(\tau)\hat{\psi}_{\nu'}(\tau). \tag{7.7}$$

   With this convention, the time ordering operator T_τ guarantees that $\hat{\psi}^\dagger(\tau)$ always appears in front of $\hat{\psi}(\tau)$.

2. With interactions, connected diagrams may include closed particle loops, see, e.g., Fig. 7.2. For fermions, each loop corresponds to an odd permutation of the creation and annihilation operators in the perturbation expansion, and hence carries a weight -1.

[1] In the literature, the dotted line is often replaced by a wiggly line.

As before, all internal times are integrated over, all internal spin indices are summed over, and all internal coordinates or momenta are integrated over or summed over, depending on the representation that is used in the calculation. You verify that combinatorial factors conspire in such a way that (i) all disconnected diagrams cancel between numerator and denominator and (ii) one has to sum over topologically different diagrams only, with the same weight for each diagram, up to a factor -1 for each fermion loop. You can find a detailed proof of these rules in the book by Abrikosov, Gorkov, and Dzyaloshinski.

One often studies a generalization of the interaction (7.7), in which the "instantaneous" interaction is replaced by a time-dependent interaction (although the time dependence is in imaginary time),

$$\int d\tau \hat{H}_1(\tau) \rightarrow \frac{1}{2}\int d\tau d\sigma V_{\nu\mu,\nu'\mu'}(\tau-\sigma)\hat{\psi}^\dagger_\nu(\tau+\eta)\hat{\psi}^\dagger_\mu(\sigma+\eta)\hat{\psi}_{\mu'}(\sigma)\hat{\psi}_{\nu'}(\tau). \tag{7.8}$$

In this notation, the original interaction corresponds to $V_{\nu\mu,\nu'\mu'}(\tau-\sigma) = V_{\nu\mu,\nu'\mu'}\delta(\tau-\sigma)$. We refer to $V_{\nu\mu,\nu'\mu'}(\tau-\sigma)$ as the "interaction propagator". The usefulness of an interaction propagator that depends on an imaginary time difference will be shown later, when we consider screening. With the time dependence included, the interaction progagator has the same arguments as an imaginary time Green function. Since the interaction propagator relates the interaction of *densities*, we take it to be a periodic function of the imaginary time difference $\tau-\sigma$, with period $\hbar/T$.

All diagrams for the single particle Green function, up to second order in the Coulomb interaction, are shown in Fig. 7.2. The second, fourth, fifth, eleventh, twelfth, and thirteenth diagram in the figure have an odd number of fermion loops and, hence, receive an extra factor -1. The first three terms in the expansion of the single-particle Green function read

$$\begin{aligned}
\mathcal{G}_{\sigma,\sigma'}(\mathbf{r},\tau;\mathbf{r}',\tau') &= \mathcal{G}^0_\sigma(\mathbf{r},\tau;\mathbf{r}',\tau')\delta_{\sigma,\sigma'} \\
&\quad - \int_0^{1/T} d\tau_1 d\tau_2 \sum_{\sigma_1}\int d\mathbf{r}_1 \int d\mathbf{r}_2 \mathcal{G}^0_\sigma(\mathbf{r},\tau;\mathbf{r}_1,\tau_1)(-V(\mathbf{r}_1,\mathbf{r}_2;\tau_1-\tau_2)) \\
&\quad \times \mathcal{G}^0_{\sigma_1}(\mathbf{r}_2,\tau_2;\mathbf{r}_2,\tau_2+\eta)\mathcal{G}^0_\sigma(\mathbf{r}_1,\tau_1;\mathbf{r}',\tau')\delta_{\sigma,\sigma'} \\
&\quad + \int_0^{1/T} d\tau_1 d\tau_2 \int d\mathbf{r}_1 \int d\mathbf{r}_2 \mathcal{G}^0_\sigma(\mathbf{r},\tau;\mathbf{r}_1,\tau_1)(-V(\mathbf{r}_1,\mathbf{r}_2;\tau_1-\tau_2)) \\
&\quad \times \mathcal{G}^0_\sigma(\mathbf{r}_1,\tau_1;\mathbf{r}_2,\tau_2+\eta)\mathcal{G}^0_\sigma(\mathbf{r}_2,\tau_2;\mathbf{r}',\tau')\delta_{\sigma,\sigma'},
\end{aligned} \tag{7.9}$$

if the coordinate representation is used, whereas in momentum representation the first three diagrams read

$$\mathcal{G}_{\mathbf{k}\sigma;\mathbf{k}'\sigma'}(\tau;\tau') = \mathcal{G}^0_{\mathbf{k}\sigma}(\tau;\tau')\delta_{\sigma,\sigma'}\delta_{\mathbf{k},\mathbf{k}'}$$

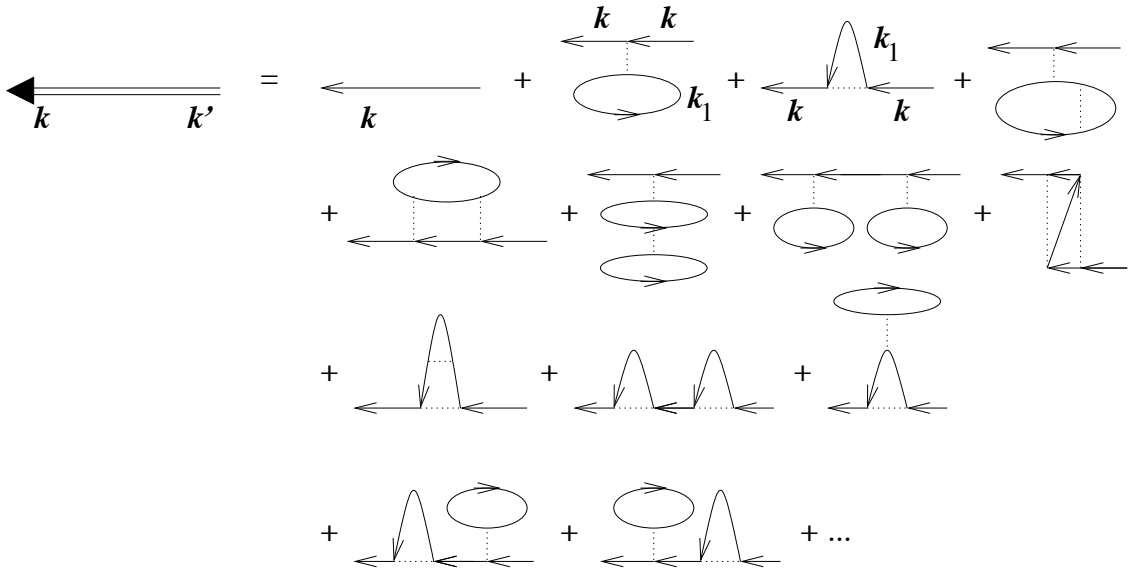

Figure 7.2: Diagrammatic representation of all diagrams for the single particle Green function, up to second order in the Coulomb interaction. The Coulomb interaction lines are drawn dotted.

$$
\begin{aligned}
&- \frac{1}{V}\int_0^{1/T} d\tau_1 d\tau_2 \sum_{\sigma_1}\sum_{\mathbf{k}_1} \mathcal{G}^0_{\mathbf{k}\sigma}(\tau;\tau_1)(-V_0(\tau_1-\tau_2)) \\
&\times \mathcal{G}^0_{\mathbf{k}_1\sigma_1}(\tau_2;\tau_2+\eta)\mathcal{G}^0_{\mathbf{k}\sigma}(\tau_1;\tau')\delta_{\sigma,\sigma'}\delta_{\mathbf{k},\mathbf{k}'} \\
&+ \frac{1}{V}\int_0^{1/T} d\tau_1 d\tau_2 \sum_{\mathbf{k}_1} \mathcal{G}^0_{\mathbf{k}\sigma}(\tau;\tau_1)(-V_{\mathbf{k}-\mathbf{k}_1}(\tau_1-\tau_2)) \\
&\times \mathcal{G}^0_{\mathbf{k}_1\sigma}(\tau_1;\tau_2+\eta)\mathcal{G}^0_{\mathbf{k}\sigma}(\tau_2;\tau')\delta_{\sigma,\sigma'}\delta_{\mathbf{k},\mathbf{k}'}. \qquad (7.10)
\end{aligned}
$$

Note that the interaction matrix element that appears in the integrations depends on the distance $\mathbf{r}_1 - \mathbf{r}_2$ only (if the coordinate representation is used) or on the transferred momentum $\mathbf{k} - \mathbf{k}_1$ (if the momentum representation is used). Also note that the Coulomb interaction does not flip spins, so that spin needs to be conserved separately at each end of an interaction line. We used the generalized version of the interaction, see Eq. (7.8) above. For a standard interaction Hamiltonian, the time-dependence of the interaction potential $V(\tau_1 - \tau_2)$ is proportional to $\delta(\tau_1 - \tau_2)$.

In order to deal with the integrations over imaginary time, it is advantageous to make a Fourier transform to imaginary time, i.e., to write

$$
\mathcal{G}_{\sigma,\sigma'}(\mathbf{r},\tau;\mathbf{r}',\tau') \;=\; T\sum_n \mathcal{G}_{\sigma,\sigma}(\mathbf{r},\mathbf{r}';i\omega_n)e^{-i\omega_n(\tau-\tau')},
$$

$$\mathcal{G}_{\mathbf{k}\sigma;\mathbf{k}'\sigma'}(\tau;\tau') \;=\; T\sum_n \mathcal{G}_{\mathbf{k}\sigma;\mathbf{k}'\sigma'}(i\omega_n)e^{-i\omega_n(\tau-\tau')}, \tag{7.11}$$

where the ω_n are the fermionic of bosonic Matsubara frequencies. Each internal integration over imaginary time for each interaction vertex gives $1/T$ times a Kronecker delta for the Matsubara frequencies. Since an interaction vertex carries only one internal time, this implies that only the sum of the four Matsubara frequencies is conserved at each interaction line, not the Matsubara frequencies of the individual fermions or bosons participating in the interaction.[2] In other words, at interaction vertices a Matsubara frequency difference can be "transferred" between particles. Note that a "transferred" Matsubara frequency difference is of the boson type if it is transferred between bosons and bosons or fermions and fermions, and of fermion type if it is transferred between a boson and a fermion. Since the Coulomb interaction is instantaneous, the weight of the Coulomb interaction lines do not depend on the Matsubara frequency that is transferred at the interaction line. All remaining intermediate Matsubara frequencies that are not fixed by the conservation rules are summed over; normalization requires an extra factor T for each summation over Matsubara frequencies, in accordance with Eq. (7.11).

To illustrate the use of Matsubara frequencies, we rewrite Eq. (7.10) using Matsubara frequencies,

$$\begin{aligned} G_{\mathbf{k}\sigma;\mathbf{k}'\sigma'}(i\omega_n) &= G^0_{\mathbf{k}\sigma}(i\omega_n)\delta_{\sigma,\sigma'}\delta_{\mathbf{k},\mathbf{k}'} \\ &\quad - \frac{T}{V}\sum_{\sigma_1}\sum_m\sum_{\mathbf{k}_1} G^0_{\mathbf{k}\sigma}(i\omega_n)(-V_0(i0))G^0_{\mathbf{k}_1\sigma_1}(i\omega_m)e^{i\eta\omega_m}G^0_{\mathbf{k}\sigma}(i\omega_n)\delta_{\sigma,\sigma'}\delta_{\mathbf{k},\mathbf{k}'} \\ &\quad + \frac{T}{V}\sum_{\mathbf{k}_1}\sum_m G^0_{\mathbf{k}\sigma}(i\omega_n)(-V_{\mathbf{k}-\mathbf{k}_1}(i\omega_n - i\omega_m))G^0_{\mathbf{k}_1\sigma}(i\omega_m)e^{i\eta\omega_m}G^0_{\mathbf{k}\sigma}(i\omega_n)\delta_{\sigma,\sigma'}\delta_{\mathbf{k},\mathbf{k}'}. \end{aligned} \tag{7.12}$$

The factors $\exp(i\eta\omega_m)$ were added to account for the infinitesimal time difference in the intermediate Green functions, cf. Eqs. (7.10) and (7.11). Note that in the case of an interaction potential, the Fourier transform $V(i\Omega_m)$ does not depend on the frequency Ω_m.

Looking at all the indices and summations that appear in Eq. (7.12), it becomes useful to group all these indices together into one "four-vector" that includes the momentum, the spin, and the Matsubara frequency,

$$k = (\mathbf{k}, \sigma, i\omega_n).$$

[2]The statement that the sum of the four Matsubara frequencies is conserved means that the sum of the Matsubara frequencies of the two outgoing particles equals the sum of the Matsubara frequencies of the incoming particles at the interaction vertex.

Then the symbol

$$\sum_k = \frac{T}{V}\sum_{\mathbf{k}}\sum_{\sigma}\sum_{n}$$

will denote summation over the momentum $\mathbf{k}$, the spin σ, and the Matsubara frequency ω_n and includes the appropriate normalization factors.

7.1.2 Real-time formalism

For the real-time formalism, the expression for the Green function is given by Eq. (2.56), where $\hat{H}_1$ is the interaction Hamiltonian. If the contour language is used, the diagrammatic rules are precisely the same as in the case of the imaginary time formalism, except for two minor differences:

1. The meaning of the infinesimal η is such that $t+\eta$ is further along the contour than t. This preserves the correct ordering of operators evaluated at equal times.

2. The interaction propagator gets a factor i, instead of a minus sign, which is a consequence of the fact that the real-time Green functions are defined with a factor $-i$, whereas the imaginary-time Green function carry a factor -1.

With these rules, the diagrammatic expansion of the single-particle Green function is the same as shown in Fig. 7.2. Calculating the Green function up to first order in the interaction, we find

$$\begin{aligned} G_{\sigma,\sigma'}(\mathbf{r},t;\mathbf{r}',t') &= G^0_\sigma(\mathbf{r},t;\mathbf{r}',t')\delta_{\sigma,\sigma'} \\ &\quad - \frac{1}{\hbar}\sum_{\sigma_1}\int d\mathbf{r}_1 d\mathbf{r}_2 \int_{\mathrm{c}} dt_1 dt_2 G^0_\sigma(\mathbf{r},t;\mathbf{r}_1,t_1)(iV(\mathbf{r}_1-\mathbf{r}_2;t_1,t_2)) \\ &\quad \times G^0_{\sigma_1}(\mathbf{r}_2,t_2;\mathbf{r}_2,t_2+\eta)G^0_\sigma(\mathbf{r}_1,t_1;\mathbf{r}',t')\delta_{\sigma,\sigma'} \\ &\quad + \frac{1}{\hbar}\int d\mathbf{r}_1 d\mathbf{r}_2 \int_{\mathrm{c}} dt_1 dt_2 G^0_\sigma(\mathbf{r},t;\mathbf{r}_1,t_1)(iV(\mathbf{r}_1-\mathbf{r}_2;t_1,t_2)) \\ &\quad \times G^0_\sigma(\mathbf{r}_1,t_1;\mathbf{r}_2,t_2+\eta)G^0_\sigma(\mathbf{r}_2,t_2;\mathbf{r}',t')\delta_{\sigma,\sigma'}. \end{aligned} \tag{7.13}$$

The Green function $G^0_{\sigma_1}(\mathbf{r}_2,t_2;\mathbf{r}_2,t_2+\eta)$ from the third line of Eq. (7.13) is always a lesser Green function, because of the presence of the infinitesimal η.

In the real-time formalism, the interaction propagator V depends on two contour points t_1 and t_2, and is assumed to have the same causal structure as a contour-ordered Green function. This condition makes the replacement of an instantaneous interaction potential by an interaction propagator is not entirely straightforward. At first sight, one is tempted to

set $V(t_1 - t_2) \propto \pm\delta(t_1 - t_2)$ if t_1 and t_2 are both on the upper (+) or lower (−) branch on the Keldysh contour, and zero otherwise. Indeed, with this choice the integration over t_2 in Eq. (7.13) gives one, and the Green function $G^0_\sigma(\mathbf{r}_1, t_1; \mathbf{r}_2, t_2 + \eta)$ from the fifth line of Eq. (7.13) becomes a lesser Green function. That is precisely what it should be, since a lesser Green function represents an electron density, as is appropriate for an interaction correction. However, this simple choice for the interaction propagator does not have the causal structure of a true real-time propagator. To see this, one shifts to the matrix notation, in which V has the form

$$\underline{V}(t_1 - t_2) = \begin{pmatrix} V^{\rm R}(t_1 - t_2) & V^{\rm K}(t_1 - t_2) \\ V^{\rm Z}(t_1 - t_2) & V^{\rm A}(t_1 - t_2) \end{pmatrix} = V \begin{pmatrix} \delta(t_1 - t_2) & 0 \\ 0 & \delta(t_1 - t_2) \end{pmatrix}.$$

Without regularization, it is not clear that the advanced and retarded components are zero for $t_1 < t_2$ and $t_1 > t_2$, respectively. You verify that the correct regularization, which gives a lesser Green function in the fifth line of Eq. (7.13) and which obeys the conditions that $V^{\rm R}(t_1 - t_2) = 0$ for $t_1 < t_2$, $V^{\rm A}(t_1 - t_2) = 0$ for $t_1 > t_2$, and $V^{\rm Z}(t_1 - t_2) = 0$ for all t_1, t_2 is[3]

$$\begin{aligned} \underline{V}(t_1 - t_2) &= \begin{pmatrix} V^{\rm R}(t_1 - t_2) & V^{\rm K}(t_1 - t_2) \\ V^{\rm Z}(t_1 - t_2) & V^{\rm A}(t_1 - t_2) \end{pmatrix} \\ &= V \begin{pmatrix} \delta(t_1 - t_2 - \eta) & \delta(t_1 - t_2 + \eta) - \delta(t_1 - t_2 - \eta) \\ 0 & \delta(t_1 - t_2 + \eta) \end{pmatrix}. \end{aligned} \tag{7.14}$$

With this choice of the interaction propagator, the infinitesimal η can be dropped from the Green function $G^0_{\sigma,\sigma}(\mathbf{r}_1, t_1; \mathbf{r}_2, t_2 + \eta)$ in the fifth line of Eq. (7.13). (In the general case that $V(t_1 - t_2)$ has a true time dependence, the times t_1 and t_2 are different and addition or subtraction of the infinitesimal η is irrelevant.)

Equation (7.13) is written in the contour language: the arguments t and t' of the Green function, as well as the integration variables t_1 and t_2 represent points on the Keldysh contour. It is customary to switch to the matrix representation, in which the contour-ordered Green function is represented by a 2×2 matrix as in Eq. (2.61),

$$\underline{G} = \begin{pmatrix} G^{\rm R} & G^{\rm K} \\ 0 & G^{\rm A} \end{pmatrix}. \tag{7.15}$$

[3] In contour language, Eq. (7.14) corresponds to

$$\begin{aligned} V_{11}(t_1, t_2) &= V\delta(t_1 - t_2 + \eta), \\ V_{12}(t_1, t_2) &= V\delta(t_1 - t_2 + \eta) - V\delta(t_1 - t_2 - \eta), \\ V_{21}(t_1, t_2) &= 0, \\ V_{22}(t_1, t_2) &= -V\delta(t_1 - t_2 - \eta). \end{aligned}$$

Here the subscripts 1 and 2 refer to contour points on the upper and lower branches of the Keldysh contour, respectively.

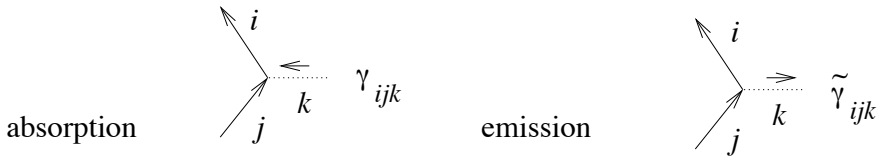

Figure 7.3: Diagrammatic rules for interaction Coulomb vertices.

In the matrix notation, the arguments t, t', as well as the integration variables t_1 and t_2, are simple times, not contour points. Switching to the notation (2.61), one then finds

$$\begin{aligned}
\underline{G}_{\sigma,\sigma'}(\mathbf{r},t;\mathbf{r}',t') &= \underline{G}^0_\sigma(\mathbf{r},t;\mathbf{r}',t')\delta_{\sigma,\sigma'} \\
&- \frac{1}{\hbar}\sum_{\sigma_1}\int d\mathbf{r}_1 d\mathbf{r}_2 \int dt_1 dt_2 \underline{G}^0_\sigma(\mathbf{r},t;\mathbf{r}_1,t_1)\underline{G}^0_\sigma(\mathbf{r}_1,t_1;\mathbf{r}',t')\delta_{\sigma,\sigma'} \\
&\times \left(iV(\mathbf{r}_1-\mathbf{r}_2;t_1,t_2)^{\mathrm{R}}\right) G^{0<}_{\sigma_1}(\mathbf{r}_2,t_2;\mathbf{r}_2,t_2) \\
&+ \frac{1}{\hbar}\sum_{mn}\int d\mathbf{r}_1 d\mathbf{r}_2 \int dt_1 dt_2 \underline{G}^0_\sigma(\mathbf{r},t;\mathbf{r}_1,t_1)\gamma_m \underline{G}^0_\sigma(\mathbf{r}_1,t_1;\mathbf{r}_2,t_2) \\
&\times \tilde{\gamma}_n \underline{G}^0_\sigma(\mathbf{r}_2,t_2;\mathbf{r}',t')(iV(\mathbf{r}_1-\mathbf{r}_2;t_1,t_2)_{mn})\delta_{\sigma,\sigma'},
\end{aligned} \tag{7.16}$$

where the indices m and n now refer to the matrix structure (7.15) and

$$\gamma_1 = \tilde{\gamma}_2 = \frac{1}{\sqrt{2}}\begin{pmatrix} 1 & 0 \\ 0 & 1 \end{pmatrix}, \quad \gamma_2 = \tilde{\gamma}_1 = \frac{1}{\sqrt{2}}\begin{pmatrix} 0 & 1 \\ 1 & 0 \end{pmatrix}. \tag{7.17}$$

The matrix manipulations that lead to Eq. (7.16) can be summarized in terms of a general diagrammatic rules: the vertices with the interaction propagator carry a matrix γ or $\tilde{\gamma}$, see Fig. 7.3. Unlike in the imaginary-time formalism or in the contour language, the interaction lines need to have a direction if the representation (7.15) is used. However, the final results do not depend on the direction of the assigned direction and the direction of the interaction propagator has no physical meaning at this point.

Once the matrix structure has been laid out, Fourier transform to time and space coordinates is straightforward.

$$\begin{aligned}
\underline{G}_{\mathbf{k}\sigma;\mathbf{k}'\sigma'}(\omega) &= \underline{G}^0_{\mathbf{k}\sigma}(\omega)\delta_{\sigma,\sigma'}\delta_{\mathbf{k},\mathbf{k}'} \\
&- \frac{1}{2\pi V}\sum_{\sigma_1}\int d\omega' \sum_{\mathbf{k}_1} \underline{G}^0_{\mathbf{k}\sigma}(\omega)\underline{G}^0_{\mathbf{k}\sigma}(\omega)\delta_{\sigma,\sigma'}\delta_{\mathbf{k},\mathbf{k}'}\left(iV_0(0)^{\mathrm{R}}\right) G^{0<}_{\mathbf{k}_1\sigma_1}(\omega') \\
&+ \frac{1}{2\pi V}\int d\omega' \sum_{\mathbf{k}_1}\sum_{m,n} \underline{G}^0_{\mathbf{k}\sigma}(\omega)\gamma_m \underline{G}^0_{\mathbf{k}_1\sigma}(\omega')\tilde{\gamma}_n \underline{G}^0_{\mathbf{k}\sigma}(\omega)\delta_{\sigma,\sigma'}\delta_{\mathbf{k},\mathbf{k}'}(iV_{\mathbf{k}-\mathbf{k}_1}(\omega-\omega')_{mn}).
\end{aligned} \tag{7.18}$$

In this case, we can simplify the notation by writing symbolically $k = (\mathbf{k}, \sigma, \omega)$, and

$$\sum_k = \frac{1}{2\pi V} \sum_{\mathbf{k}} \sum_{\sigma} \int d\omega.$$

7.2 Self energy and Hartree Fock approximation

An important approximate method to treat the effect of interactions is the Hartree Fock approximation. In the Hartree Fock approximation, the electron-electron is replaced by an effective potential, which is then determined self-consistently. Replacing the interaction by a potential is a very useful approximation, because potentials can be dealt with on the single-particle level.

If the interaction is replaced by an effective potential, the Hamiltonian is quadratic in electron creation and annihilation operators. This means that Wick's theorem holds for this Hamiltonian. The principle of the Hartree Fock approximation is that the interaction Hamiltonian is replaced with a Hamiltonian that is quadratic in electron creation and annihilation operators in a way that respects Wick's theorem,[4]

$$\begin{aligned} \hat{H}_1^{\mathrm{HF}} &= \frac{1}{2} \sum V_{\nu\mu,\nu'\mu'} \left(\hat{\psi}_\nu^\dagger \hat{\psi}_{\nu'} \langle \hat{\psi}_\mu^\dagger \hat{\psi}_{\mu'} \rangle + \hat{\psi}_\mu^\dagger \hat{\psi}_{\mu'} \langle \hat{\psi}_\nu^\dagger \hat{\psi}_{\nu'} \rangle - \langle \hat{\psi}_\mu^\dagger \hat{\psi}_{\mu'} \rangle \langle \hat{\psi}_\nu^\dagger \hat{\psi}_{\nu'} \rangle \right) \\ &\quad - \frac{1}{2} \sum V_{\nu\mu,\nu'\mu'} \left(\hat{\psi}_\nu^\dagger \hat{\psi}_{\mu'} \langle \hat{\psi}_\mu^\dagger \hat{\psi}_{\nu'} \rangle + \hat{\psi}_\mu^\dagger \hat{\psi}_{\nu'} \langle \hat{\psi}_\nu^\dagger \hat{\psi}_{\mu'} \rangle - \langle \hat{\psi}_\mu^\dagger \hat{\psi}_{\nu'} \rangle \langle \hat{\psi}_\nu^\dagger \hat{\psi}_{\mu'} \rangle \right). \end{aligned} \tag{7.19}$$

Here, the first line corresponds to what is known as the "Hartree Hamiltonian", whereas the second line is the "Fock Hamiltonian". If the labels μ and ν refer to different particles, the Fock contribution is zero; for indistinguishable particles, however, the Fock contribution is important. The averages $\langle \hat{\psi}_\mu^\dagger \hat{\psi}_{\mu'} \rangle$ are to be regarded as parameters in the Hartree-Fock Hamiltonian that should be calculated self-consistently at the end of the calculation.

In a non-magnetic translationally invariant system, any average of the form $\langle \hat{\psi}_{\mathbf{k}\sigma}^\dagger \hat{\psi}_{\mathbf{k}'\sigma'} \rangle$ should be nonzero only if $\mathbf{k} = \mathbf{k}'$ and $\sigma = \sigma'$. Denoting

$$n_{\mathbf{k}\sigma} = \langle \hat{\psi}_{\mathbf{k}\sigma}^\dagger \hat{\psi}_{\mathbf{k}\sigma} \rangle, \tag{7.20}$$

the Hartree-Fock Hamiltonian in a translationally invariant system can be written

$$H^{\mathrm{HF}} = \hat{H}_0 + \hat{H}_1^{\mathrm{HF}} = \sum_{\mathbf{k}\sigma} \varepsilon_{\mathbf{k}\sigma}^{\mathrm{HF}} \hat{\psi}_{\mathbf{k}\sigma}^\dagger \hat{\psi}_{\mathbf{k}\sigma}, \tag{7.21}$$

[4]You verify that any average of the Hamiltonian $\hat{H}_1^{\mathrm{HF}}$ is the same as that of the original interaction Hamiltonian $\hat{H}_1$ if the Wick theorem were to be used.

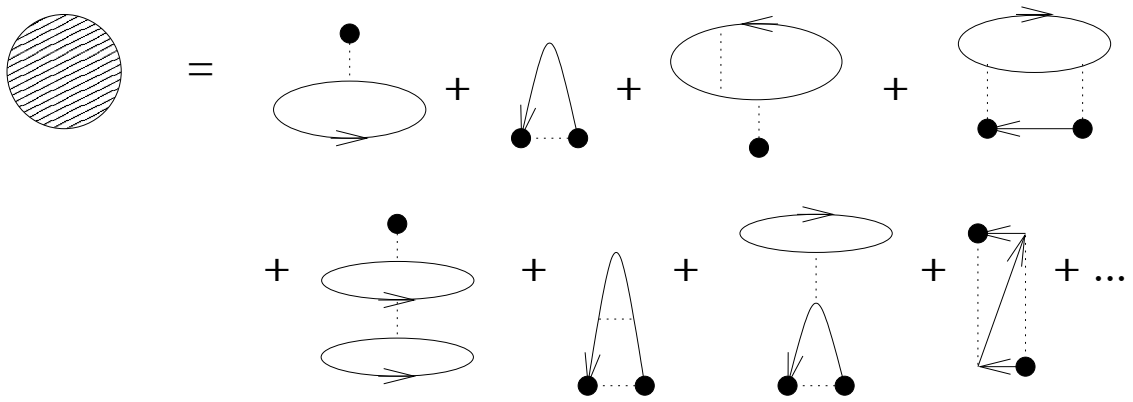

Figure 7.4: Diagrammatic expansion of the self energy, up to second order in the Coulomb interaction.

where the Hartree Fock energy is given by

$$\varepsilon^{\rm HF}_{\mathbf{k}\sigma} = \varepsilon_{\mathbf{k}} + \sum_{\mathbf{k}'\sigma} (V_0 - \delta_{\sigma\sigma'} V_{\mathbf{k}-\mathbf{k}'}) n_{\mathbf{k}'\sigma'}. \tag{7.22}$$

Note that the Hartree-Fock energies $\varepsilon^{\rm HF}_{\mathbf{k}\sigma}$ depend on the occupation numbers $n_{\mathbf{k}'\sigma'}$ which, in turn, depend self-consistently on the Hartree-Fock energies $\varepsilon^{\rm HF}_{\mathbf{k}\sigma}$.

The Hartree Fock approximation can be given a diagrammatic interpretation by consider the concept of a "self energy". In previous chapters, we saw that this concept was very useful in order to organize the summation of a diagrammatic perturbation series for a disorder-averaged Green function. The same is true for interacting electrons.

As in the case of impurity diagrams, we call a diagram "irreducible" if it cannot be cut in two by removal of a single fermion line. In Fig. 7.2, the seventh, tenth, twelfth, and thirteenth diagrams are not irreducible. The self-energy is defined as the sum over all all irreducible diagrams without the two external fermion lines, see Fig. 7.4. With this definition of the self energy, the single-particle Green function obeys the Dyson equation

$$G_{k,k'} = G^0_{k,k'} + \sum_{k_1,k_2} G^0_{k,k_1} \Sigma_{k_1,k_2} G_{k_2,k'}. \tag{7.23}$$

In the real-time formalism, Σ is a 2×2 matrix and matrix multiplication is implied. Note that, in contrast to the case of the disorder average we studied before, the self energy $\Sigma_{k,k'}$ does not need to be diagonal in the four-vectors k, k'.

A perturbative expansion for the self energy is shown in Fig. 7.4. The first two diagrams of Fig. 7.4 have our special attention: The interaction line can be seen as an effective "impurity

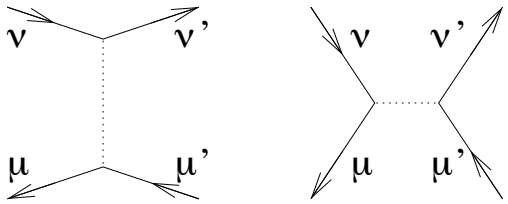

Figure 7.5: Interaction vertex and exchanged interaction vertex.

line". In other words, it can be represented by an effective potential. This is particularly clear for the first diagram, which is known as the "Hartree" diagram. For the second diagram, which is known as the "Fock diagram", you should consider the fermion line as being part of the "effective impurity".

At first sight, the Hartree and Fock diagrams appear to be rather different. However, they are related by simple exchange of particles participating in the interaction! To understand this, look at the effect of exchange on the basic interaction vertex, see Fig. 7.5. It is precisely this exchange operation that maps the Hartree diagram into the Fock diagram and vice versa.

Let us calculate what these two contributions to the self energy are. We use the imaginary-time formalism. Calculation of the Hartree diagram gives, *cf.* Eq. (7.12),

$$\Sigma^{\rm H}_{\mathbf{k}\sigma}(i\omega_n) \;=\; -\frac{T}{V}\sum_{\mathbf{k}'}\sum_{\sigma'}\sum_{m}(-V_0)\mathcal{G}^0_{\mathbf{k}'\sigma'}(i\omega_m)e^{i\eta\omega_m}. \tag{7.24}$$

The factor $\exp(i\eta\omega_m)$ arose because we take the creation operator in the interaction Hamiltonian at an infinitesimally larger imaginary time than the annihilation operator. Performing the summation over the Matsubara frequency ω_m and the momentum $\mathbf{k}$, we find

$$\Sigma^{\rm H} \;=\; V_0\sum_{\mathbf{k}\sigma} n^0_{\mathbf{k}\sigma} = V_0 n, \tag{7.25}$$

where n is the particle density. Similarly, calculation of the Fock diagram gives, *cf.* Eq. (7.12),

$$\begin{aligned}\Sigma^{\rm F}_{\mathbf{k}\sigma}(i\omega_n) &= \frac{T}{V}\sum_{\mathbf{k}'}\sum_{\sigma'}\sum_{m}(-V_{\mathbf{k}-\mathbf{k}'}\delta_{\sigma\sigma'})\mathcal{G}_{\mathbf{k}'\sigma'}(i\omega_m)e^{i\eta\omega_m}\\ &= -\frac{1}{V}\sum_{\mathbf{k}'}V_{\mathbf{k}-\mathbf{k}'}n^0_{\mathbf{k}'\sigma}.\end{aligned} \tag{7.26}$$

Here, there is no summation over spin, because spin is conserved throughout the diagram. In the real-time formalism, the self-energy is given by Eqs. (7.25) and (7.26), multiplied by the 2×2 unit matrix.

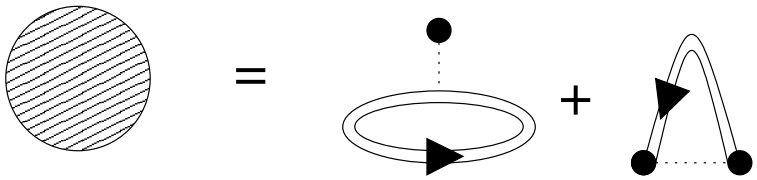

Figure 7.6: Diagrammatic representation of the Hartree-Fock approximation. The self energy is expressed in terms of the full single-particle Green function, which, in turn, depends on the self energy as in Fig. 5.7.

Looking at these results, we first note that the Hartree and Fock corrections to the self energy are real: they correspond to a shift of the particle's energy, but the particle's lifetime remains infinite. The results (7.25) and (7.26) are almost identical to the correction to the single particle-energy in the Hartree-Fock approximation. The only difference is the absence of self-consistency in Eqs. (7.25) and (7.26): in those equations, the occupation numbers $n_{\mathbf{k}\sigma}$ are calculated in the non-interacting ground state. Self-consistency can be achieved if the single-particle Green function $\mathcal{G}^0$ in the Hartree and Fock diagrams is replaced by the full Green function $\mathcal{G}$, see Fig. 7.6. In that case one recovers precisely the Hartree-Fock equation (7.22). You easily verify that, because of the self-consistency condition, the Hartree-Fock approximation includes all diagrams of Fig. 7.4 with the exception of the fourth and the eighth diagrams of that figure.

Note that, formally, the Hartree self energy is divergent. In practice, the negative charge of the electrons is balanced by the positive charge of the lattice ions, and there is no contribution from the $\mathbf{q} = 0$ mode of the interaction. Hence, for a translationally invariant system, the Hartree contribution to the self energy can be neglected.

7.3 Dielectric response

Interactions profoundly modify the electronic response to an external potential. This phenomenon is known as "screening". Screening is described by the polarizability function χ_e, which was defined in Sec. 6.1. The polarizability function expresses the induced charge density as a function of the external potential,

$$\rho_{\rm ind}(\mathbf{q},\omega) = \chi_e^{\rm R}(\mathbf{q},\omega)\phi_{\rm ext}(\mathbf{q},\omega). \tag{7.27}$$

Below, we'll calculate the polarizability function using the Green function formalism. However, for long-wavelength and low frequency perturbations, one can use the Boltzmann

equation to find χ_e. Starting from the Fourier transformed linearized Boltzmann equation,

$$(-i\omega + i\mathbf{v_k}\cdot\mathbf{q})f^1_{\mathbf{k}}(\mathbf{q},\omega) - i(e/\hbar)\phi(\mathbf{q},\omega)\mathbf{q}\cdot\partial_{\mathbf{k}}f^0_{\mathbf{k}} = 0, \tag{7.28}$$

with $\phi(\mathbf{q},\omega) = \phi_{\rm ext}(\mathbf{q},\omega) + \phi_{\rm ind}(\mathbf{q},\omega)$ equal to the total electrostatic potential, we find that the presence of an external potential perturbation $\phi_{\rm ext}$ causes the response

$$f^1_{\mathbf{k}}(\mathbf{q},\omega) = -\frac{e\mathbf{q}\cdot\mathbf{v_k}(\phi_{\rm ext}(\mathbf{q},\omega)+\phi_{\rm ind}(\mathbf{q},\omega)}{\hbar(\mathbf{q}\cdot\mathbf{v_k}-\omega)}(-\partial_{\varepsilon_{\mathbf{k}}}f^0(\varepsilon_{\mathbf{k}})). \tag{7.29}$$

In order to eleminate $\phi_{\rm ind}$ from this equation, we multiply by $2e/V$ and sum over $\mathbf{k}$, with the result

$$\begin{aligned}
\rho_{\rm ind}(\mathbf{q},\omega) &= \frac{2e}{V}\sum_{\mathbf{k}} f^1_{\mathbf{k}}(\mathbf{q},\omega) \\
&= -\frac{2e^2}{V\hbar}\sum_{\mathbf{k}}\frac{\mathbf{q}\cdot\mathbf{v_k}}{\mathbf{q}\cdot\mathbf{v_k}-\omega}(-\partial_{\varepsilon_{\mathbf{k}}}f^0(\varepsilon_{\mathbf{k}}))(\phi_{\rm ext}(\mathbf{q},\omega)+\phi_{\rm ind}(\mathbf{q},\omega)) \\
&= \chi^{0R}_e(\mathbf{q},\omega)(\phi_{\rm ext}(\mathbf{q},\omega)+\phi_{\rm ind}(\mathbf{q},\omega)),
\end{aligned} \tag{7.30}$$

where χ^{0R} is the polarizability function of the non-interacting electron gas. Of course, this equation could have been derived without use of the Boltzmann equation. It simply expresses that the response of the interacting electron gas to the potential $\phi_{\rm ext}$ is the same as the response of the non-interacting electron gas to the total potential $\phi_{\rm ext}+\phi_{\rm ind}$. Using

$$\phi_{\rm ind}(\mathbf{q},\omega) = \frac{1}{\epsilon_0 q^2}\rho_{\rm ind}(\mathbf{q},\omega), \tag{7.31}$$

we find finally

$$\chi^{\rm R}_e(\mathbf{q},\omega) = \frac{\chi^{0R}_e(\mathbf{q},\omega)}{1-\chi^{0R}_e(\mathbf{q},\omega)/\epsilon_0 q^2}. \tag{7.32}$$

Before we study the properties of χ_e in more detail, we show how the polarizability function can be derived in the Green function formalism. In the Green function formalism, χ_e is calculated as the retarded charge density autocorrelation function, which is obtained as the analytical continuation of the temperature charge density autocorrelation function

$$\begin{aligned}
\chi_e(\mathbf{q},\tau) &= -\frac{1}{V}\langle T_\tau \rho_{e,\mathbf{q}}(\tau)\rho_{e,-\mathbf{q}}(0)\rangle \\
&= -\frac{e^2}{V}\sum_{\mathbf{k}\sigma}\sum_{\mathbf{k}'\sigma'}\langle T_\tau \hat\psi^\dagger_{\mathbf{k},\sigma}(\tau+\eta)\hat\psi_{\mathbf{k}+\mathbf{q},\sigma}(\tau)\hat\psi^\dagger_{\mathbf{k}'+\mathbf{q},\sigma'}(\eta)\hat\psi_{\mathbf{k}',\sigma'}(0)\rangle.
\end{aligned} \tag{7.33}$$

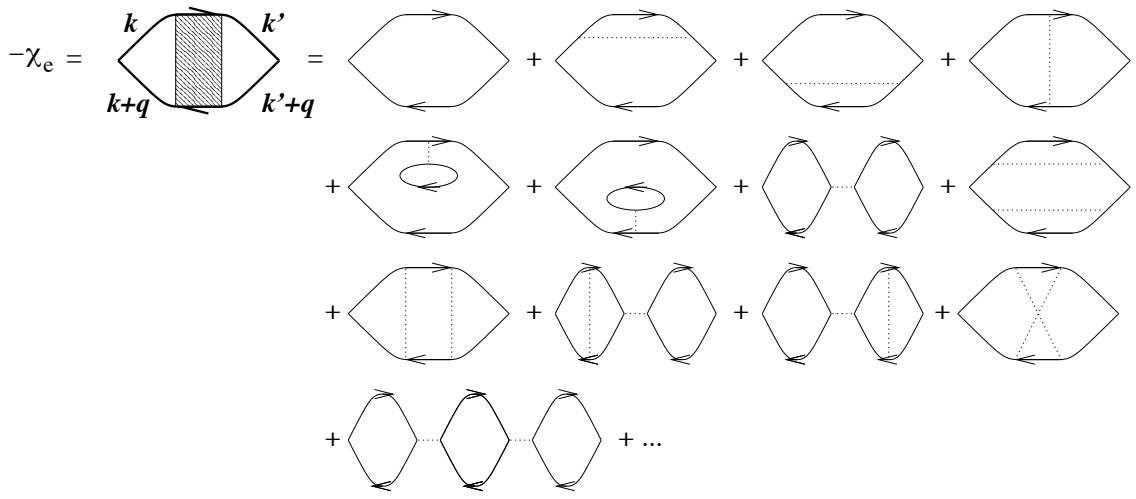

Figure 7.7: Diagrammatic expansion of the polarizability function χ_e. The figure contains all diagrams to first order in the interaction and a subset of the diagrams to second order in the interaction.

Diagrammatically, this function is obtained as in Fig. 7.7. We can organize the diagrammatic expansion as we did previously when we looked at the single-particle Green function. A polarization diagram is called "reducible" if the two end points can be separated by cutting a single interaction line. For example, of the diagrams in Fig. 7.7, the seventh, ninth, tenth, eleventh, and thirteenth diagrams are reducible. All other diagrams are irreducible in this sense. Defining the irreducible polarizability function as (minus) the sum over all irreducible diagrams, we can write the polarizability function as

$$\chi_e(\mathbf{q}, i\Omega_n) = \frac{\chi_e^{\rm irr}(\mathbf{q}, i\Omega_n)}{1 - V_{\mathbf{q}}\chi_e^{\rm irr}(\mathbf{q}, i\Omega_n)/e^2}. \tag{7.34}$$

The diagrammatic series for $\chi_e^{\rm irr}$ is as in Fig. 7.8. In the so-called "random phase approximation" (RPA), one only keeps the zeroth order diagram for $\chi_e^{\rm irr}$, which is the polarizability function for the noninteracting electron gas. After analytical continuation to real frequencies, one finds

$$\chi_e^{\rm RPA}(\mathbf{q}, \omega) = \frac{\chi_e^{0R}(\mathbf{q}, \omega)}{1 - V_{\mathbf{q}}\chi_e^{0}(\mathbf{q}, \omega)/e^2}, \tag{7.35}$$

which is the same as we obtained from the Boltzmann equation previously.

We can now use our result for the polarizability function to discuss the dielectric response function

$$\epsilon^{-1}(\mathbf{q}, \omega) = 1 + V_{\mathbf{q}}\chi_e^{\rm R}(\mathbf{q}, \omega)/e^2. \tag{7.36}$$

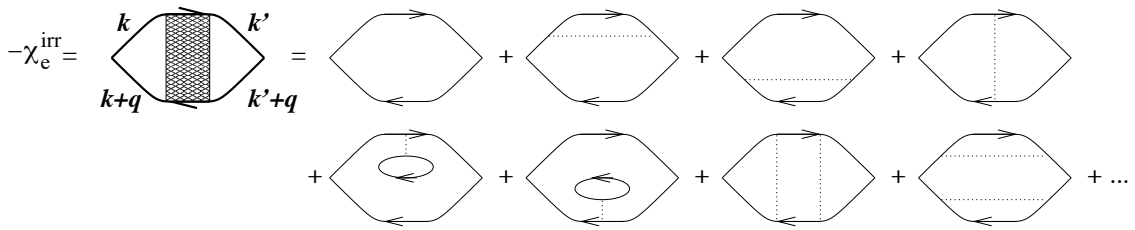

Figure 7.8: Diagrammatic expansion of the irreducible part $\chi_e^{\rm irr}$ of the polarizability function. The figure contains all diagrams to first order in the interaction and a subset of the diagrams to second order in the interaction.

Substituting the RPA result (7.35), we find

$$\epsilon^{-1}(\mathbf{q},\omega) = \left[1 - \chi_e^{0R}(\mathbf{q},\omega)V_{\mathbf{q}}/e^2\right]^{-1}. \tag{7.37}$$

The polarizability function of the non-interacting electron gas was calculated in Ex. 6.2. In the static limit, $\omega \to 0$, the result is

$$\chi_e^0(\mathbf{q},0) = -\nu\left[1 + \left(\frac{k_F}{q} - \frac{q}{4k_F}\right)\ln\left|\frac{2k_F+q}{2k_F-q}\right|\right], \tag{7.38}$$

where $\nu = mk_F/2\pi^2$ is the density of states at the Fermi level. Hence,

$$\epsilon^{-1}(\mathbf{q},0) = \left[1 + \frac{e^2k_Fm}{2\epsilon_0q^2\pi^2}\left[1 + \left(\frac{k_F}{q} - \frac{q}{4k_F}\right)\ln\left|\frac{2k_F+q}{2k_F-q}\right|\right]\right]^{-1}. \tag{7.39}$$

The long wavelengths limit of Eq. (7.39) is the Thomas-Fermi dielectric function,

$$\epsilon(\mathbf{q},0) = 1 + \frac{k_s^2}{q^2}, \tag{7.40}$$

where $k_s^2 = me^2k_F/\pi^2\epsilon_0$ is the inverse Thomas-Fermi screening length.

An important feature of the RPA result for the static dielectric response function is that it is singular at $q = 2k_F$. This has a number of physical consequences, akin to the Friedel oscillations we discussed in an earlier chapter.

For large frequencies $\omega \gg qv_F$, the polarizability function χ_0 can be expanded as

$$\begin{aligned}\chi_0^{\rm R}(\mathbf{q},\omega) &= \frac{k_F^3q^2}{3\pi^2m\omega^2}\left(1 + \frac{3}{5}\left(\frac{qv_F}{\omega}\right)^2\right)\\ &= \frac{nq^2}{m\omega^2}\left(1 + \frac{3}{5}\left(\frac{qv_F}{\omega}\right)^2\right),\end{aligned} \tag{7.41}$$

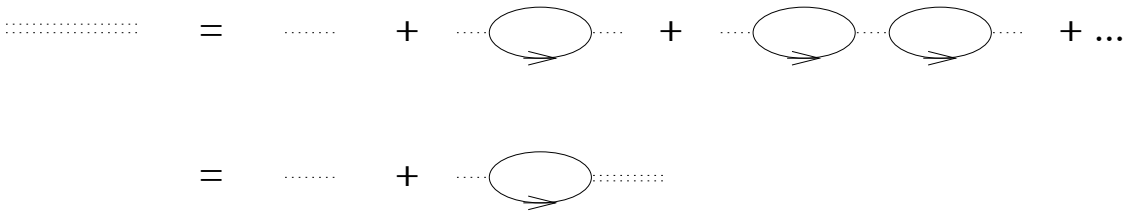

Figure 7.9: Diagrammatic representation of the effective interaction in the random phase approximation.

where $n = k_F^3/3\pi$ is the density of electrons. Substituting this into the dielectric response function gives

$$\varepsilon^{-1}(\mathbf{q},\omega) = \left[1 - \frac{ne^2}{m\epsilon_0\omega^2}\left(1 + \frac{3}{5}\left(\frac{qv_F}{\omega}\right)^2\right)\right]^{-1}. \tag{7.42}$$

Just as the dielectric response function gives the interaction the electron gas to an external charge, it also gives the response of the electron gas to itself. In other words, it describes how the electron-electron interaction is modified by the presence of other electrons. The effective electron-electron interaction is then simply $V_{\mathbf{q}}\varepsilon^{-1}(\mathbf{q}, i\Omega_n)$. In the RPA approximation, this corresponds to

$$V_{\mathbf{q}}^{\mathrm{RPA}}(i\Omega_n) = \frac{V_{\mathbf{q}}}{1 - \chi_e^0(\mathbf{q}, i\Omega_n)V_{\mathbf{q}}} = \frac{e^2}{\epsilon_0 q^2 - \chi_{e\mathbf{q}}^{0\mathrm{R}}(i\Omega_n)}. \tag{7.43}$$

Diagrammatically, the effective interaction is calculated as in Fig. (7.9). Again, the "random phase approximation" consists of taking the non-interacting polarizability function for "polarization bubbles" in the diagrammatic expansion.

Note that the effective interaction has a nontrivial time dependence. Because of that, we call the effective interaction "retarded". Now you understand why we went through the trouble of defining the diagrammatic rules for the general case of a time-dependent interaction instead of simply restricting ourselves to an instantaneous interaction potential: if the effective interaction is used as the building block for a diagrammatic expansion, the interaction lines carry a true time dependence.

For small momentum and energy exchange, we can replace the polarizability χ^0 by its value at $\mathbf{q} = 0$,

$$\chi_{e,\mathbf{q}\to 0}^{0\mathrm{R}}(i\Omega_n \to 0) = -2\nu e^2, = -\epsilon_0 k_s^2, \tag{7.44}$$

where ν is the density of states at the Fermi level, per spin direction and per unit volume, and k_s is the inverse Thomas-Fermi screening length introduced previously. Then the effective

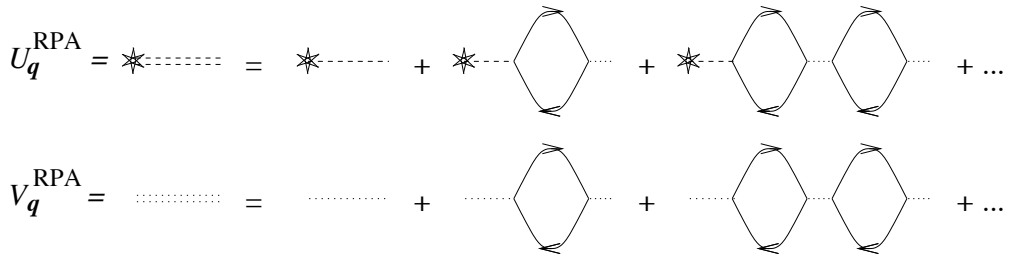

Figure 7.10: Diagrammatic representations of impurity potential and screened Coulomb interaction in the RPA approximation.

Coulomb interaction in the limit of small $\mathbf{q}$ and ω reads

$$V_{\mathbf{q}}^{\mathrm{RPA}}(i\Omega_n) = \frac{e^2}{\epsilon_0(q^2+k_s^2)} \quad \text{if } \mathbf{q},\, \Omega_n \to 0. \tag{7.45}$$

The quantity $1/k_s$ is known as the "Thomas-Fermi screening length". The singularity of the Coulomb interaction at large wavelengths is cut off by the screening of the interaction by the electron gas. The Thomas-Fermi screening potential is found when we use the limiting form of Eq. (7.45) for all momenta and frequencies. In that case, the screened Coulomb interaction is instantaneous and has the spatial dependence of the Yukawa potential,

$$V^{\mathrm{TF}}(\mathbf{r}) = \frac{e^2}{4\pi\epsilon_0 r} e^{-k_s r}. \tag{7.46}$$

Note, however, that true RPA screened interaction we derived above, however, has a different from on short length scales and, more importantly, is retarded (*i.e.*, it depends on frequency).

At this point, it is important to make a comment on the effect of impurities in the metal. The impurities are charged objects — otherwise they would hardly interact with the electrons. However, in our previous treatment, we have modeled impurities with a short-range potential. Now we see why that was correct: the impurity potential is screened by the electron gas, so that

$$U_{\mathbf{q}} \to U_{\mathbf{q}} + U_{\mathbf{q}}\chi_e^{\mathrm{R}}(\mathbf{q},0)V_{\mathbf{q}}. \tag{7.47}$$

Diagrammatically, the screening of the impurity potential and of the Coulomb interaction in the RPA approximation can be represented in striking similarity, see Fig. 7.10.

The "random phase approximation" may seem rather ad-hoc: one decides to sum a subset of diagrams, and to ignore all others. In fact, this is not true. One can show that the RPA becomes exact in the limit of a high density of electrons. This is what we now show.

In defining the relative importance of interactions, one introduces the so-called "gas parameter" r_s, which is a dimensionless parameter measuring the density of the electron gas. The parameter r_s is defined in terms of the electron number density n as

$$a_0 r_s = (4\pi n/3)^{-1/3}. \tag{7.48}$$

A sphere of radius $a_0 r_s$ contains precisely one electron on average. Using the relation $n = k_F^3/3\pi^2$, we can rewrite this as

$$r_s = (9\pi/4)^{1/3}(a_0 k_F)^{-1}. \tag{7.49}$$

A low gas parameter corresponds to a high density of electrons. The gas parameter also relates the Fermi wavenumber k_F and the inverse Thomas-Fermi screening length k_s,

$$k_s^2 = \frac{4}{\pi}\frac{k_F}{a_0} = k_F^2 r_s \left(\frac{16}{3\pi^2}\right)^{2/3}. \tag{7.50}$$

The importance of the electron density for a perturbation expansion in the Coulomb interaction follows from the observation that the gas parameter is proportional to the ratio of typical Coulomb interaction for neighboring electrons, which is of order $e^2/\epsilon_0 k_F$, and the electronic kinetic energy, which is $\hbar^2 k_F^2/2m$. Hence, at high electron densities the main contribution to the electron's energy is kinetic.

For realistic metals, r_s is between 1.5 and 6. That is not really small. Hence, our small-r_s expansion is an idealized theory, and we should expect that some of our quantitative conclusions cannot be trusted.

In order to see which diagrams are important in the limit of high density, we need two observations.

- First, we consider a diagram contribution to the self energy to nth order in the Coulomb interaction. In order to estimate its dependence on the gas parameter r_s, we measure energy and temperature in units of the Fermi energy, which is $\propto k_F^2$. Then, noting that every nth order diagram has n integrations over internal momenta (there are $2n-1$ fermion lines and $n-1$ constraints from the interaction lines) and that it contains $2n-1$ fermion Green functions, we find that

  $$\Sigma^{(n)}/\varepsilon_F \propto r_s^n. \tag{7.51}$$

  (The summations over internal Matsubara frequencies do not contribute to this estimate, since, for each internal Matsubara frequency, the diagram carries a factor T.)

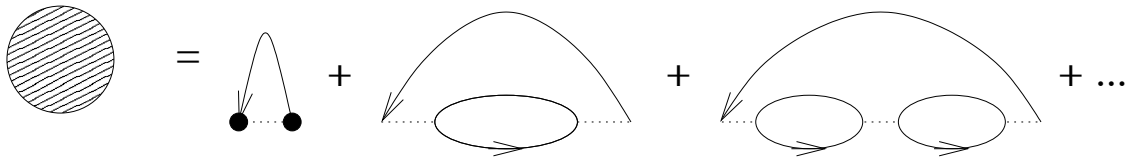

Figure 7.11: Diagrammatic representation of the random phase approximation for the self energy in a translationally invariant system.

- Second, we note that the Coulomb potential is singular: for small transferred momentum $\mathbf{q}$, the Coulomb potential diverges $V_q \propto q^{-2}$. The role of these divergences is stronger if the same momentum $\mathbf{q}$ is transferred more than once, i.e., if there is more than one interaction vertex with precisely the same momentum transfer. Hence, we conclude that those diagrams with the maximal number of identical transferred momenta have the largest contribution.

With these two observations, we can identify the leading diagrams in the limit of high electron density. Namely, for each set of diagrams with the same largest number of identical transferred momenta, the diagram of minimal order in the interaction potential dominates for small r_s. These are precisely the diagrams one retains in the "random phase approximation".

Note that the random phase approximation does not treat the direct interaction and the exchange interaction on the same footing: performing the same transformation as in Fig. 7.5 on the diagrams of Fig. 7.6 leads to different contributions to the self energy. The reason that these contributions are left out in the present calculation is that they are less singular. In the next chapter we consider the effects of a short-range interaction, for which it is essential that exchange and direct interactions are treated equally.

We close this section with a calculation of the self energy in the random phase approximation. For the self energy, the random phase approximation corresponds to retaining the diagrams shown in Fig. 7.11. If we sum the entire RPA series for the self energy, we find

$$\Sigma^{\mathrm{RPA}}_{\mathbf{k}}(i\omega_n) = -\frac{T}{V}\sum_{\mathbf{k}'}\sum_{m}\frac{V^{\mathrm{RPA}}_{\mathbf{k}-\mathbf{k}'}(i\omega_n - i\omega_n)e^{i\eta\omega_m}}{(i\omega_m - \varepsilon_{\mathbf{k}'} + \mu)}. \tag{7.52}$$

Unlike the Hartree-Fock self energy, the self energy in the random phase approximation depends on frequency.

7.4 Plasmon modes

For some frequency/wavelength combinations, the dielectric response function can vanish. Then, there is an induced charge density without an external one! Such a situation is referred

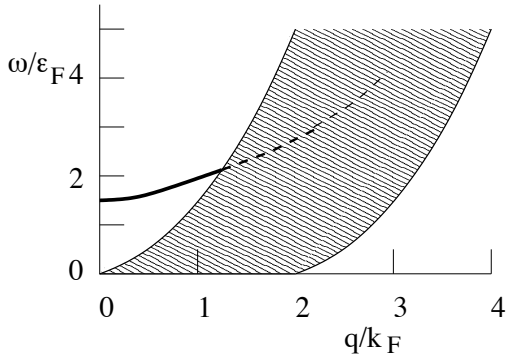

Figure 7.12: Plasmon dispersion relation (thick curve) together with the support of $\mathrm{Im}\,\epsilon$. Plasmon modes are strongly damped (Landau damping) if $\mathrm{Im}\,\epsilon \neq 0$.

to as a "collective mode" of the electron gas. It is a motion that can sustain itself without external input.

In principle, the dielectric response function is complex. In those cases, the occurrence of zeroes is unlikely. However, there are regions of (q, ω) space where ϵ is real. In such regions, long-lived collective excitations can be expected. The support of the imaginary part of the polarizability function of the noninteracting electron gas (which equals the support of $\mathrm{Im}\,\epsilon^{-1}$) was shown in Fig. 6.2. Based on that figure, we expect collective excitations in the region of finite frequencies and long wavelengths. In this parameter regime, the dielectric response function is given by Eq. (7.42) above. We see that, indeed, there are zeroes, given by the dispersion relation

$$\omega(\mathbf{q}) = \omega_p + \frac{3q^2 v_F^2}{10\omega_p}, \quad \omega_p^2 = \frac{ne^2}{m\epsilon_0}. \tag{7.53}$$

The frequency ω_p is known as the "plasma frequency" and the corresponding collective modes are known as "plasma oscillations" or "plasmons". The plasmon modes are long-lived as long as the dielectric response function remains real. At the point when the dispersion curve (7.53) enters that region of (q, ω) space where ϵ^{-1} is complex, the zeroes of ϵ at real frequency ω and wavevector q cease to exist. In this case, one can still find zeroes of ϵ at complex frequencies. These correspond to damped collective modes. The damping that arises from the fact that ϵ is complex is called "Landau damping".

The plasmon dispersion relation is shown schematically in Fig. 7.12, together with the support of $\mathrm{Im}\,\epsilon(q, \omega)$.

7.5 Free energy

What do the interactions imply for the free energy of the electron gas? At first sight, the free energy cannot be calculated using the Green function method — after all, it is not a Green function. However, there is a nice technical trick that allows us to apply the Green function formalism to the calculation of the free energy.

In this trick, the interaction Hamiltonian $\hat{H}_1$ is multiplied by a "coupling constant" λ,

$$\hat{H}(\lambda) = \hat{H}_0 + \lambda \hat{H}_1. \tag{7.54}$$

Hence, $\hat{H}(0)$ corresponds to the unperturbed Hamiltonian $\hat{H}_0$ whereas $H(\hat{1})$ corresponds to the full Hamiltonian $\hat{H}_0 + \hat{H}_1$. For this Hamiltonian, the Free energy becomes a function of λ

$$F(\lambda) = -T \ln Z(\lambda), \quad Z(\lambda) = \mathrm{tr}\, e^{-(\hat{H}_0 + \lambda \hat{H}_1)/T}. \tag{7.55}$$

Taking a derivative to λ, we find

$$\frac{\partial F(\lambda)}{\partial \lambda} = \frac{\mathrm{tr}\, \hat{H}_1 e^{-(\hat{H}_0 + \lambda \hat{H}_1)/T}}{\mathrm{tr}\, e^{-(\hat{H}_0 + \lambda \hat{H}_1)/T}} = \frac{1}{\lambda} \langle \lambda \hat{H}_1 \rangle_\lambda \tag{7.56}$$

where the brackets $\langle \ldots \rangle_\lambda$ denote a thermal average with respect to the Hamiltonian $\hat{H}(\lambda)$. Integrating Eq. (7.56) from $\lambda = 0$ to $\lambda = 1$ we find the free energy difference ΔF between the full Hamiltonian $\hat{H}_0 + \hat{H}_1$ and the unperturbed Hamiltonian $\hat{H}_0$,

$$\Delta F = \int_0^1 d\lambda \frac{1}{\lambda} \langle \lambda \hat{H}_1 \rangle_\lambda. \tag{7.57}$$

Hence, if we know the average $\langle \lambda \hat{H}_1 \rangle_\lambda$ for all λ, we can find the change in the free energy. This average is nothing but a Green function!

Rewriting $\hat{H}_1$ as

$$\hat{H}_1 = \frac{1}{2V} \sum_{\sigma_1, \sigma_2} \sum_{\mathbf{k}_1, \mathbf{k}_2, \mathbf{q}} V_{\mathbf{q}} \hat{\psi}^\dagger_{\mathbf{k}_1 + \mathbf{q}, \sigma_1} \hat{\psi}_{\mathbf{k}_1, \sigma_1} \hat{\psi}^\dagger_{\mathbf{k}_2 - \mathbf{q}, \sigma_2} \hat{\psi}_{\mathbf{k}_2, \sigma_2} - \frac{1}{2} n \sum_{\mathbf{q}} V_{\mathbf{q}}, \tag{7.58}$$

we can express the average $\langle \hat{H}_1 \rangle$ as

$$\begin{aligned} \langle \hat{H}_1 \rangle &= -\frac{1}{2e^2} \lim_{\tau \uparrow 0} \sum_{\mathbf{q}} V_{\mathbf{q}} \chi_e(\mathbf{q}, \tau) - \frac{1}{2} n \sum_{\mathbf{q}} V_{\mathbf{q}}, \\ &= -\frac{T}{2e^2} \sum_{\mathbf{q}} \sum_n e^{-i\Omega_n \eta} V_{\mathbf{q}} \chi_e(\mathbf{q}, i\Omega_n) - \frac{1}{2} n \sum_{\mathbf{q}} V_{\mathbf{q}}, \end{aligned} \tag{7.59}$$

where χ_e is the polarizability function. Within the random phase approximation we can use Eq. (7.35) for χ_e, replace $V_{\mathbf{q}}$ by $\lambda V_{\mathbf{q}}$ and perform the integration to λ. The result is

$$F - F_0 = \frac{T}{2} \sum_{\mathbf{q}} \sum_n e^{i\Omega_n \eta} \ln\left(1 - V_{\mathbf{q}} \chi_e^0(\mathbf{q}, i\Omega_n)/e^2\right) - \frac{1}{2} n \sum_{\mathbf{q}} V_{\mathbf{q}}. \tag{7.60}$$

We can perform the summation over n writing $F - F_0$ as a contour integral in the complex plane and shifting the contours to the real axis,

$$F - F_0 \;=\; \sum_{\mathbf{q}} \int_{-\infty}^{\infty} \frac{d\xi}{4\pi} \coth(\xi/2T) \mathrm{Im} \ln\left(\epsilon(\mathbf{q}, \xi)\right) - \frac{1}{2} n \sum_{\mathbf{q}} V_{\mathbf{q}}. \tag{7.61}$$

Here we used Eq. (7.37) to express the argument of the logarithm in terms of the RPA dielectric response function.

Evaluation of this expression for the Free energy is not entirely straightforward. Some insight into the physics of Eq. (7.61) is obtained if we look at the contribution from the plasmons. Using Eq. (7.42) for the dielectric response function $\epsilon(\mathbf{q}, \omega)$ near the plasmon branch $\omega \approx \omega_p(\mathbf{q}) \gg q v_F$ at low wavenumber, we find

$$\mathrm{Im} \ln \epsilon(\mathbf{q}, \omega) = \begin{cases} 0 & \text{if } |\omega| > \omega_p(\mathbf{q}), \\ \pi & \text{if } q v_F \ll \omega < \omega_p(\mathbf{q}), \\ -\pi & \text{if } -\omega_p(\mathbf{q}) < \omega \ll -q v_F. \end{cases} \tag{7.62}$$

We then see that each plasmon mode with $v_F q \ll \omega_p(\mathbf{q})$ has a contribution

$$\begin{aligned} \delta F_{\mathbf{q}} \;&=\; \frac{1}{2} \int^{\omega_p(\mathbf{q})} d\xi \coth(\xi/2T) \\ &=\; T \ln(\sinh(\omega_p/2T)) - \text{const}, \end{aligned} \tag{7.63}$$

where the additional constant reflects the contribution from the integration close to $\xi = 0$ where the approximation (7.62) does not hold. The first term on the r.h.s. of Eq. (7.63) represents the free energy of a plasmon mode at wavevector $\mathbf{q}$, while the additional constant represents the contribution from low energy particle-hole excitations to the free energy.

In the literature (e.g., the book by Bruus and Flensberg or Mahan's book), one can find a result for the ground state energy as an expansion for small gas parameter r_s,

$$E - E_0 = \left(-\frac{0.916}{r_s} + 0.0622 \ln r_s - 0.094 \right) \mathrm{Ry}. \tag{7.64}$$

In the same units, the ground state energy of the non-interacting electron gas is $(2.21/r_s^2)$ Ry. The unit Ry, for Rydberg, corresponds to $e^2/2a_0 \approx 13.6$ eV. Higher-order terms in the small-r_s expansion of the ground state have been calculated. However, for those terms, one needs to go beyond the RPA approximations.

7.6 Interactions and disorder

The fact that dynamics in a dirty metal is diffusive, rather than ballistic, for time scales longer than the mean free time τ and length scales longer than the mean free path $l = v_F\tau$, has important consequences for the screening of the Coulomb interaction: since it is more difficult to move charge around, the electron gas has a reduced capacity to screen time-dependent potentials. The relevant frequency for the time dependence is not the ballistic frequency $v_F q$ (as it is in the response of a clean electron gas), but the diffusive one, $\omega \sim Dq^2$, where $1/q \gg l$ is the length scale that the system is probed at. Qualitatively, the effect of disorder on the screened Coulomb interaction can be seen from Fig. 6.3. In order to screen a time-dependent potential with frequency ω and wavevector q, the electrons need to move a distance $\sim 1/q$ in a time $\sim 1/\omega$. As long as $\omega \ll Dq^2$ the electron gas can accommodate such a displacement, and Thomas-Fermi screening theory applies. If, however, $\omega \gg Dq^2$ the electron gas cannot follow the potential, and screening is absent.

The reduced screening capability is seen quantitatively in the RPA calculation of the dielectric function of the interacting electron gas, which now becomes

$$\epsilon^{\rm RPA}(\mathbf{q}, i\Omega_n) = 1 + \frac{k_s^2}{q^2}\frac{Dq^2}{|\Omega_n| + Dq^2}, \tag{7.65}$$

where $k_s^2 = 2\nu e^2/\epsilon_0$ is the Thomas-Fermi wavenumber. Similarly, the effective electron-electron interaction becomes

$$\begin{aligned} V_{\mathbf{q}}^{\rm RPA}(i\Omega_n) &= \frac{e^2}{\epsilon_0 q^2 \epsilon^{\rm RPA}(\mathbf{q}, i\Omega_n)} \\ &= \frac{e^2}{\epsilon_0}\left(q^2 + k_s^2\frac{Dq^2}{|\Omega_n| + Dq^2}\right)^{-1}. \end{aligned} \tag{7.66}$$

For $|\omega| \ll Dq^2$ the effect of the disorder is negligible, whereas for $\omega \gg Dq^2$ the Coulomb interaction is essentially unscreened. This is different from the case of a clean metal, where Thomas-Fermi screening breaks down at the much higher frequency $\omega \sim v_F q$.

One example where the modified screening capability of electrons plays a role is the so-called "zero bias anomaly" in the tunneling density of states. The density of states can be measured by a tunneling experiment, in which electrons from a reference conductor with known (and constant) spectral density tunnel into the sample, see Fig. 7.13. Indeed, as shown in Ex. 6.1, the current I through a tunneling barrier contacting the sample at position $\mathbf{r}$ is proportional to the spectral density,

$$\frac{\partial I(\mathbf{r}, eV)}{\partial V} \propto \frac{1}{4T}\int_{-\infty}^{\infty} d\xi A(\mathbf{r}, \xi) \sum_{\pm} \frac{1}{\cosh^2[(\xi \pm eV)/2T]}. \tag{7.67}$$

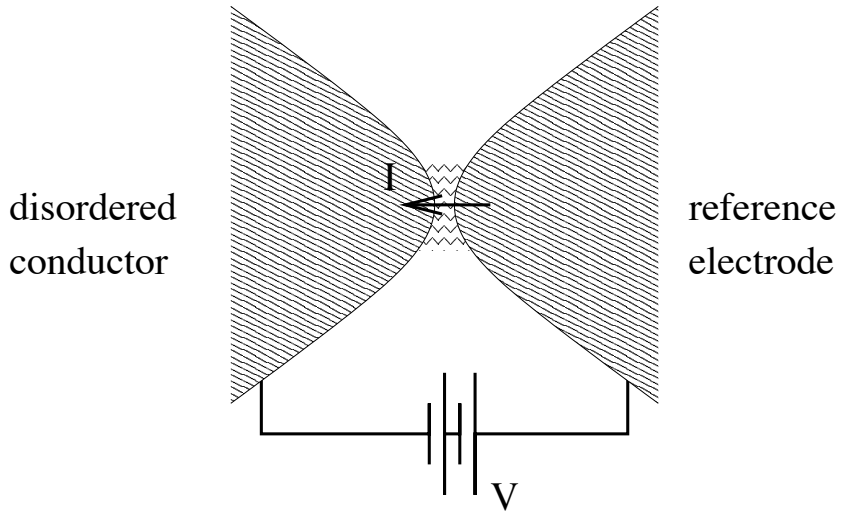

Figure 7.13: Tunnel spectroscopy setup for a measurement of the spectral density of a disordered conductor.

(At zero temperature, this simplifies to $\partial I/\partial V \propto A(\mathbf{r}, eV)$.)

For a non-interacting electron gas, the spectral density is essentially energy independent, hence the tunnel current is proportional to the applied bias voltage V and independent of the temperature T. For the disordered interacting electron gas, the situation is more complicated. When an electron tunnels into the sample, it charges the sample locally. For a cloud that is bigger than the mean free path l, dispersion of the charge cloud is a slow process, which is determined by the diffusive motion of the electrons. Until the energy of the charge cloud, which is a sum of kinetic and the Coulomb energy contributions, has dropped below the bias voltage eV or the temperature T, the electron that tunnels into the metal has to exist in a virtual state. The prolonged existence in a virtual state suppresses the tunneling current or, in other words, the density of states. At low voltages and low temperatures, the suppression should be maximal, the tunneling density of states being an increasing function of V and T for small voltages and low temperatures.

A particularly illuminating qualitative picture of how interactions affect the density of states and the conductivity in disordered metals is given by Aleiner, Altshuler, and Gershenson [Waves in Random Media **9**, 201 (1999)]. As we have seen in Ch. 4, the electron density near an impurity will show oscillations with wavevector $2k_F$. Because electrons are interacting, they see an oscillating potential $\phi(\mathbf{r})$ with wavevector $2k_F$. These oscillations strongly modify the scattering properties of the impurity. The modification is strongest near the Fermi energy because of the resonant scattering off the oscillating potential. Modified

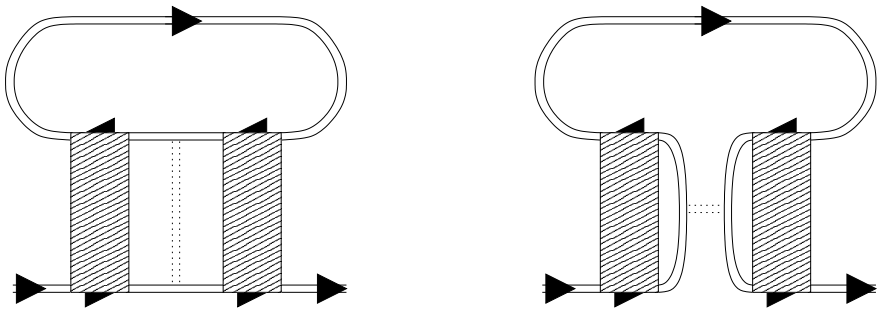

Figure 7.14: Lowest order corrections to the single-particle Green function in a disordered interacting electron gas. Left: Hartree diagram, right: Fock diagram. The shaded blocks represent the diffusion propagator, see Fig. 6.5.

scattering properties include a modified scattering phase shift, and, hence, a modified impurity contribution to the density of states and a modified scattering rate. Below, we focus on the effect of interactions on the density of states, using diagrammatic perturbation theory.[5] A simple calculation illustrating interaction effects on transport is given in Ex. 7.5.

Our calculation of the density of states follows the original work of Altshuler and Aronov [Sov. Phys. JETP **50**, 968 (1979)] and Altshuler, Aronov, and Lee [Phys. Rev. Lett. **44**, 1288 (1980)]. To lowest order in the interaction, this correction is given by Hartree and Fock diagrams. The diffusive electron motion is reflected in the presence of the diffusion ladders around the interaction line, which, in turn, represents the effective interaction of Eq. (7.66) above. The two relevant diagrams for the correction to the single-particle Green function are shown in Fig. 7.14.[6]

We consider the Fock diagram first. The correction to the single-electron Green function shown in Fig. 7.14 reads

$$\begin{aligned}\delta\langle\mathcal{G}_{\mathbf{k},\mathbf{k}}(i\omega_n)\rangle &= \frac{T}{V}\sum_{\mathbf{q}}\sum_{m}\langle\mathcal{G}^0_{\mathbf{k},\mathbf{k}}(i\omega_n)\rangle^2\mathcal{D}(\mathbf{k},i\omega_n;\mathbf{k}+\mathbf{q},i\omega_m)^2 \\ &\quad\times(-V_{\mathbf{q}}(i\omega_n-i\omega_m))\langle\mathcal{G}^0_{\mathbf{k}+\mathbf{q},\mathbf{k}+\mathbf{q}}(i\omega_m)\rangle. \qquad (7.68)\end{aligned}$$

[5] A non-perturbative semiclassical theory of the density of states has been formulated by Shytov and Levitov [JETP Lett. **66**, 214 (1997)].

[6] There are two additional diagrams containing cooperons instead of diffusons. These diagrams involve interactions at high momentum transfers, unlike the Fock diagram shown in the figure, which is dominated by interactions at low momenta. For that reason, the appropriate effective interaction in these diagrams is more complicated than the RPA interaction $V^{\rm RPA}$ that is used in the calculation below. For details, see the article *Electron-electron interaction in disordered conductors*, by B.L. Altshuler and A.G. Aronov, in the book *Electron-electron interactions in disordered systems*, edited by A.L. Efros and M. Pollak (North-Holland, 1985).

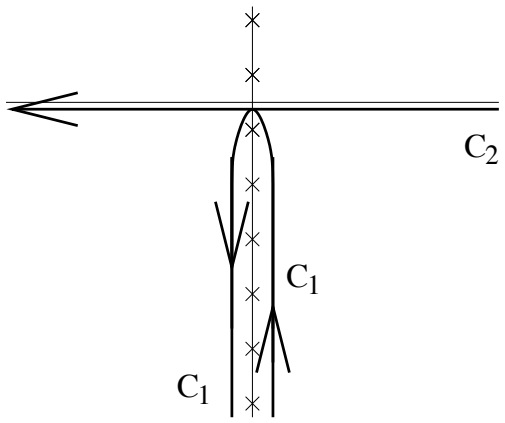

Figure 7.15: Integration contour for the calculation of the zero-bias anomaly to the tunneling density of states.

The correction to the spectral density is found as

$$\begin{aligned}\delta A(\mathbf{r},\omega) &= -4\mathrm{Im}\,\delta G^{\mathrm{R}}(\mathbf{r},\mathbf{r};\omega) \\ &= -\frac{4T}{V^2}\mathrm{Im}\sum_{\mathbf{k},\mathbf{q}}\sum_m \langle \mathcal{G}^0_{\mathbf{k},\mathbf{k}}(i\omega_n)\rangle^2 \mathcal{D}(\mathbf{k},i\omega_n;\mathbf{k}+\mathbf{q},i\omega_m)^2 \\ &\quad \times (-V_{\mathbf{q}}(i\omega_n - i\omega_m))\langle \mathcal{G}^0_{\mathbf{k}+\mathbf{q},\mathbf{k}+\mathbf{q}}(i\omega_m)\rangle\big|_{i\omega_n\to\omega+i\eta}\,. \end{aligned} \tag{7.69}$$

where the extra factor two accounts for spin degeneracy.

Since the diffusion propagator is divergent for small momentum transfers, the main contribution to the integration in Eq. (7.68) comes from small $\mathbf{q}$. For these momenta, we can use the screened interaction of Eq. (7.66).

A singular contribution to the density of states can come from the pole of the diffusion propagator at small momentum and frequency. For the case $\omega_n > 0$, this pole exists for $\omega_m < 0$ only. Replacing the summation over ω_m by an integration in the complex plane, deforming the integration contour as in Fig. 7.15, and performing the analytical continuation $i\omega_n \to \omega + i\eta$ we find

$$\begin{aligned}\delta A(\mathbf{r},\omega) &= \mathrm{Im}\,\frac{1}{V^2\pi i}\sum_{\mathbf{k},\mathbf{q}}\int_{-\infty}^{\infty} d\xi\,\tanh(\xi/2T)\langle \mathcal{G}^{0\mathrm{R}}_{\mathbf{k},\mathbf{k}}(\omega)\rangle^2 \frac{1}{(Dq^2+i\xi-i\omega)^2\tau^2} \\ &\quad \times (-V_{\mathbf{q}}(\omega-\xi+i\eta))\langle \mathcal{G}^{0\mathrm{A}}_{\mathbf{k}+\mathbf{q},\mathbf{k}+\mathbf{q}}(\xi)\rangle. \end{aligned} \tag{7.70}$$

Since the main dependence on ω and $\mathbf{q}$ comes from the pole of the diffusion operator, we

set $\mathbf{q} = 0$ and $\omega = \xi$ in the arguments of the Green functions in Eq. (7.70). Performing the summation over $\mathbf{k}$ and shifting integration variables $\xi \to \omega - \xi$ we then find

$$\delta A(\mathbf{r}, \omega) = -\mathrm{Im}\, \frac{2\nu}{V} \sum_{\mathbf{q}} \int_{-\infty}^{\infty} d\xi \tanh\left(\frac{\xi - \omega}{2T}\right) \frac{V_{\mathbf{q}}(\xi + i\eta)}{(Dq^2 - i\xi)^2}. \tag{7.71}$$

In three dimensions, the summation over $\mathbf{q}$ and the integration over ξ are, in fact, divergent for large $\mathbf{q}$ and large ξ. The divergence is not physical, since our approximations break down when $v_F q\tau$ and $\omega\tau$ become of order unity. In order to arrive at a meaningful result that describes the temperature and energy dependence of the density of states, we subtract δA in the limit $\omega \to 0$, $T \to 0$ (limits taken in this order). In Eq. (7.71) this amounts to the replacement of $\tanh[(\xi - \omega)/2T]$ by $\tanh[(\xi - \omega)/2T] - \mathrm{sign}\,(\xi)$. For the interaction, we substitute the screened Coulomb interaction in the presence of disorder, Eq. (7.66) above. First performing the remaining summation over $\mathbf{q}$, one finds

$$\begin{aligned} \delta A(\mathbf{r}, \omega) &= -\mathrm{Im}\, \frac{1}{4\pi D^{3/2}} \int_{-\infty}^{\infty} d\xi \left(\tanh \frac{\xi - \omega}{2T} - \mathrm{sign}\,(\xi)\right) \\ &\quad \times \left[\frac{1}{\sqrt{-i\xi}} - \frac{1}{\sqrt{Dk_s^2 - i\xi}}\right]. \end{aligned} \tag{7.72}$$

We omit the second term between the square brackets, which gives a vanishing contribution to the spectral density if $\omega, T \ll Dk_s^2$. For the remaining integration, we find

$$\delta A(\mathbf{r}, \omega) = -\frac{T^{1/2}}{\pi\sqrt{2}(\hbar D)^{3/2}} f(\omega/T), \tag{7.73}$$

where

$$f(x) = \int_0^{\infty} \frac{dy}{2y^{1/2}} \left(\frac{\sinh y}{\cosh y + \cosh x} - 1\right). \tag{7.74}$$

Asymptotically, the function $f(x)$ behaves as

$$\begin{aligned} f(x) &\approx -\sqrt{x} - \frac{\pi^2}{24} x^{-3/2} \quad \text{if } x \gg 1, \\ f(x) &\approx -1.072 \quad \text{if } x \ll 1. \end{aligned} \tag{7.75}$$

You verify that, indeed, $\delta A \to 0$ if we take the limit $\omega \to 0$, followed by $T \to 0$.

For two dimensional samples and one dimensional samples, the calculation of the density of states is very similar. The first difference is that the Coulomb interaction has a different

form in one and two dimensions,

$$V_{\mathbf{q}}(i\Omega_n) = \begin{cases} (e^2/2\epsilon_0)\left[q + (e^2/\epsilon_0)\nu\frac{Dq^2}{|\Omega_n|+Dq^2}\right]^{-1} & \text{if } d=2, \\ (e^2/\epsilon_0)\left[-\frac{4\pi}{\ln(q^2a^2)} + 2(e^2/\epsilon_0)\nu\frac{Dq^2}{|\Omega_n|+Dq^2}\right]^{-1} & \text{if } d=1. \end{cases} \tag{7.76}$$

Here ν is the density of states per spin direction and per unit area (in two dimensions) or unit length (in one dimension), whereas a is the thickness or radius of the sample. In quasi two-dimensional samples, $\nu = \nu_3 a$, where ν_3 is the three-dimensional density of states. With this modification, the calculation proceeds as in the three dimensional case.

In two dimensions, the final integration over ξ and summation over $\mathbf{q}$ is logarithmically divergent. Performing the summation over $\mathbf{q}$ first and truncating the ξ-integration at $\xi \sim 1/\tau$, we find

$$\begin{aligned} \delta A(\mathbf{r},\omega) &= \frac{1}{4\pi D}\int_0^\infty \frac{d\xi}{\xi}\ln\frac{\xi}{De^2\nu/\epsilon_0}\left(\tanh\frac{\xi+\omega}{2T} + \tanh\frac{\xi-\omega}{2T}\right) \\ &\approx -\frac{1}{4\pi D}\left[\ln\frac{\max(\omega,T)}{D^2(e^2/\epsilon_0)\nu^2\tau}\right]\ln\left[\tau\max(\omega,T)\right]. \end{aligned} \tag{7.77}$$

Similarly, in the one-dimensional case one has

$$\delta A(\mathbf{r},\omega) = -\frac{ak_s}{2\sqrt{2\pi TD}}\left[\ln\frac{Dk_s^2}{\max(\omega,T)}\right]^{-1/2}\int_0^\infty \frac{dy}{y^{3/2}}\frac{\sinh y}{\cosh y + \cosh(\omega/T)}, \tag{7.78}$$

where k_s is the three-dimensional Thomas-Fermi wavenumber.

The contribution from the Hartree diagram is similar. The transferred momentum $\mathbf{q}$ in interaction factor of the Hartree diagram does not have to be small for the momentum in the diffusion propagators to be small. Since the Hartree diagram involves large momentum exchanges in the interaction matrix element, the precise magnitude depends on the details of the short-range part of the Coulomb interaction. In that case we cannot use the simple screened form (7.66) above, but need information about the microscopic details of the sample. For the discussion here, we limit ourselves to the statement that the energy and temperature dependence of δA is still the same as that of Eq. (7.73), whereas the prefactor depends on sample details. For details of this calculation we refer to the article *Electron-electron interaction in disordered conductors*, by B.L. Altshuler and A.G. Aronov, in the book *Electron-electron interactions in disordered systems*, edited by A.L. Efros and M. Pollak (North-Holland, 1985).

7.7 Exercises

Exercise 7.1: Coulomb interactions in two dimensions

In certain materials, such as a quantum well at the interface of the semiconductors GaAs and GaAlAs, the electrons are confined to two spatial dimensions only.

For such a system, the non-interacting part of the Hamiltonian can be written

$$\hat{H}_0 = \sum_{\mathbf{k}\sigma} \varepsilon_{\mathbf{k}\sigma} \hat{\psi}^\dagger_{\mathbf{k}\sigma} \hat{\psi}_{\mathbf{k}\sigma}, \tag{7.79}$$

where the summation over wavevectors $\mathbf{k}$ is restricted to wavevectors in the plane of the two-dimensional electron gas. The creation operator $\hat{\psi}^\dagger_{\mathbf{k}\sigma}$ creates an electron with spin σ and orbital wavefunction

$$\hat{\psi}_{\mathbf{k}}(\mathbf{r}, z) = \frac{1}{A^{1/2}} e^{i\mathbf{k}\cdot\mathbf{r}} \zeta(z), \tag{7.80}$$

where $\mathbf{r}$ is the coordinate in the plane of the two-dimensional electron gas, and z is the transverse coordinate, and A is the area of the two-dimensional electron gas. For most practical purposes, the function $\zeta(z)$ can be approximated by the delta function $\delta(z)$.

The interaction between the electrons in the two-dimensional electron gas is the three-dimensional Coulomb interactions,

$$V(\mathbf{r}) = \frac{1}{4\pi\epsilon_0\epsilon_r |\mathbf{r}|}. \tag{7.81}$$

The relative permittivity ϵ_r appears because the two-dimensional electron gas is not surrounded by vacuum, but by a semiconducting material. For this system, write down the interaction Hamiltonian for the Coulomb interaction using the momentum representation. Find an explicit expression for the Coulomb-interaction matrix element $V_{\mathbf{q}}$ in two dimensions.

Exercise 7.2: Four-vertex formalism

Abrikosov, Gorkov, and Dzyaloshinski discuss a different diagrammatic formalism to describe electron-electron interactions. The diagrams for the direct and the exchange interaction are combined into one diagram, as shown in Fig. 7.16.

Discuss the diagrams contributing to the self-energy to second order in the interaction using this formalism. Also discuss the Hartree-Fock approximation. Does the simplest four-vertex formulation of an effective interaction agree with the RPA approximation? Why (not)?

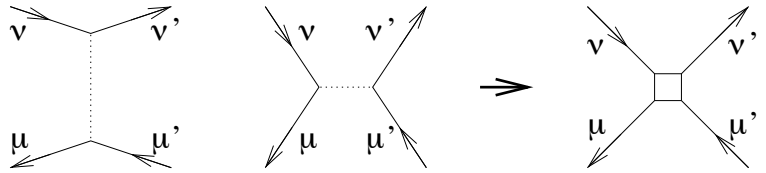

Figure 7.16: Diagrammatic representation of both the direct and exchange parts of the electron-electron interaction, following the notation of the book by Abrikosov, Gorkov, and Dzyaloshinski.

Exercise 7.3: Plasma oscillations

It is possible to find the plasma frequency ω_p from simple classical considerations. Consider an electron gas in a rectangular box of length L_x and cross section A. Since the mass of the ions is much larger than the mass of the electrons, the ions can be treated as an inert positive background charge that compensates the charge of the electrons. The electron gas can be set in oscillating motion by translating it a distance δx in the x-direction, leaving the ion background fixed. Show that the frequency of this oscillation is precisely the plasma frequency ω_p.?

Exercise 7.4: Plasma oscillations in two dimensions

In this exercise we return to the case of a two-dimensional electron gas that exists at a quantum well in a semiconductor heterostructure.

(a) Calculate the dielectric response function $\epsilon(\mathbf{q}, \omega)$ for a two-dimensional electron gas in the RPA approximation.

(b) From the zeroes of the dielectric response function, calculate the dispersion relation of plasma oscillations in the two-dimensional electron gas. Discuss for what wavenumbers plasma oscillations are damped by Landau damping (excitation of particle/hole pairs).

(c) Calculate the screened Coulomb interaction in a two-dimensional electron gas in the RPA approximation.

(d) Show that, at small wavevectors $q \ll k_F$ and low frequencies $\hbar\omega \ll \varepsilon_F$ the screened interaction is given by

$$V_{\mathbf{q}}^{\mathrm{RPA}} = \frac{e^2}{2\epsilon_0\epsilon_r(q + k_s)}, \tag{7.82}$$

where k_s is the two-dimensional Thomas-Fermi screening wavenumber. Calculate k_s for the case of a GaAs/GaAlAs heterostructure, for which the effective electron mass is $m^* = 0.067m$, relative permittivity $\epsilon_r = 13$, and electron density $n = 10^{15}$ m^{-2}. How does it compare to the Fermi wavelength for this system?

Exercise 7.5: Interacting wire with impurity

In this exercise you'll consider a one-dimensional wire with an impurity at $x = 0$. The impurity is characterized by its transmission amplitude t. Here you'll calcualte how t is modified by the presence of interactions. This exercise is based on the article *Tunneling in one-dimensional non-Luttinger electron liquid* by Matveev, Yue, and Glazman [Phys. Rev. Lett. **71**, 3351 (1993)].

Without interactions, the retarded Green function for the wire reads

$$\begin{aligned} G^{0\mathrm{R}}(x,x';\omega) &= \frac{1}{i\hbar v_k}\left[te^{ik(x-x')}\theta(x) + (e^{ik|x-x'|} + re^{-ik(x+x')})\theta(-x)\right] \quad \text{if } x' < 0, \\ G^{0\mathrm{R}}(x,x';\omega) &= \frac{1}{i\hbar v_k}\left[te^{-ik(x-x')}\theta(-x) + (e^{ik|x-x'|} + re^{ik(x+x')})\theta(x)\right] \quad \text{if } x' > 0, \end{aligned} \tag{7.83}$$

see Ex. 4.5. Here r and t are the "reflection amplitude" and "transmission amplitude" of the impurity, and k is the positive solution of $\varepsilon_k - \mu = \omega$. The corresponding wavefunctions are

$$\begin{aligned} \phi^0_k(x) &= \theta(-x)(e^{ikx} + re^{-ikx}) + \theta(x)te^{ikx}, \\ \phi^0_{-k}(x) &= \theta(-x)te^{-ikx} + \theta(x)(e^{-ikx} + re^{ikx}). \end{aligned} \tag{7.84}$$

The transmission amplitude t gives information about the conductance of the wire. The goal of this exercise is to find how the interactions change the transmission amplitude t. We'll restrict ourselves to the case of "spinless electrons".

(a) The lowest order in perturbation theory corresponds to the Hartree-Fock approximation, but without the self-consistency condition. Because the Hartree-Fock approximation interactions are described by means of an effective "potential" U, it will be sufficient to find the wavefunctions ϕ_k and ϕ_{-k} in the presence of this potential. Show that the wavefunction ϕ_k satisfies the equation

$$\phi_k(x) = \phi^0_k(x) + \int dy G^{0\mathrm{R}}_k(x,y) \int dz U(y,z)\phi_k(z), \tag{7.85}$$

where the potential $U(x,y)$ is the sum of Hartree and Fock contributions,

$$U(x,y) = U_{\rm H}(x)\delta(x-y) - U_{\rm F}(x,y), \tag{7.86}$$

which read

$$\begin{aligned} U_{\rm H}(x) &= \int dy V(x-y)\langle\hat{\psi}^\dagger(y)\hat{\psi}(y)\rangle \\ &= \frac{1}{2\pi}\int dk' f(\varepsilon_{k'})\int dy V(x-y)(|\phi_{k'}(y)|^2 + |\phi_{-k'}(y)|^2), \qquad (7.87) \\ U_{\rm F}(x,y) &= V(x-y)\langle\hat{\psi}^\dagger(y)\hat{\psi}(x)\rangle \\ &= \frac{1}{2\pi}\int dk' f(\varepsilon_{k'})V(x-y)(\phi^*_{k'}(y)\phi_{k'}(x) + \phi^*_{-k'}(y)\phi_{-k'}(x)). \qquad (7.88) \end{aligned}$$

Here V is the interaction potential.

If we are interested in the lowest order perturbation theory in V only, we can replace the wavefunctions ϕ by ϕ^0 in the r.h.s. of Eq. (7.85) and in Eqs. (7.87) and (7.88).

(b) Show that the interactions modify the transmission amplitude as $t \to t + \delta t$, where

$$\begin{aligned} \delta t &= \frac{1}{i\hbar v_k}\int dy \left[t(1+re^{2ik|y|})U_{\rm H}(y) + (\theta(y)(e^{-iky} + re^{iky}) + \theta(-y)te^{-iky}) \right. \\ &\quad \left. \times \int dz\, U_{\rm F}(y,z)(\theta(-z)(e^{ikz} + re^{-ikz}) + \theta(z)te^{ikz}) \right]. \end{aligned} \tag{7.89}$$

(c) The Hartree and Fock potentials contain an integration over all wavenumbers k' for which states are occupied. We first calculate the shift $\delta t(k')$ from the states with wavevector k' and then integrate over k'. Calculating $\delta t(k')$ you'll find a non-singular contribution, together with a contribution that is singular as $k \to k'$. We're interested in the singular contribution only, because that contribution will determine the temperature dependence of δt. Show that the singular contribution reads

$$\begin{aligned} \delta t(k') &= \frac{1}{2\hbar v_k(k-k')}|r|^2 t(V_{-2k} + V_{2k} - 2V_0) \\ &= \frac{1}{2\hbar v_k(k-k')}(1-|t|^2)t(V_{-2k} + V_{2k} - 2V_0), \end{aligned} \tag{7.90}$$

where V_q is the Fourier transform of the interaction potential.

(d) The total change δt is now found upon multiplication of $\delta t(k')$ by $f(\varepsilon_{k'})/2\pi$, followed by integration over k'. You may cut off the logarithmic divergence at small k' at $k - k' \simeq \kappa$, where $1/\kappa$ is of the order of the Fermi wavelength or the spatial range of the potential V, whichever is larger. Calculate δt and discuss its asymptotic properties for low temperatures and electrons close to the Fermi surface.

Transport at low temperatures corresponds to the limit $k \to k_F$, $T \to 0$. In this limit, the first-order perturbation theory shift to the transmission amplitude is logarithmically divergent. This situation is reminiscent of the Kondo problem, where one finds that the rate for scattering off a magnetic impurity diverges logarithmically upon lowering the temperature. For the Kondo problem, good insight could be obtained by Anderson's "poor man's scaling" method. In this approach, the cut-off κ is gradually decreased, leading to an effective theory with a smaller cut-off κ. This procedure can be repeated until $\kappa \sim \max(|k - k_F|, T/v_F)$. In the language of perturbation theory, "poor man's scaling" amounts to summing up the most divergent contributions to δt in each order of perturbation theory.

(e) Calculate the shift to the transmission amplitude t that arises from taking into account only states with $k_F - \kappa < k' < k_F - (\kappa + d\kappa)$, with $d\kappa$ negative, and write your result in the form of a differential equation that expresses $dt/d\kappa$ in terms of t and κ.

(f) Solve the differential equation you find under (e) to find how the effective zero temperature transmission amplitude depends on $|k - k_F|$ for $k - k_F| \to 0$. Express your answer in terms of the transmission amplitude t_0 at a reference cut-off κ_0.

The result you find in (f) is very interesting: For a repulsive interaction, you find that $t \to 0$ if $k \to k_F$ at zero temperature, irrespective of the "bare" value of t for k far away from k_F. Hence, even the weakest impurity will turn a one-dimensional wire into an insulator at low temperatures. Moreover, you find that t approaches zero as a power law of $|k - k_F|$, with an exponent that depends on the interaction. Such power laws are typical of one-dimensional interacting metals. We return to this issue when we discuss the "Luttinger Liquid" description of one-dimensional metals.

Chapter 8

Magnetism

In this chapter we study the magnetic excitations in a solid. We start with a calculation of the magnetic susceptibility χ, which is the coefficient of proportionality between the spin polarization induced by a magnetic field and the magnetic field $\mathbf{h}$. The susceptibility not only tells us how easy it is to magnetize a solid, it also points to the onset of a magnetic phase. This happens at the point where the susceptibility diverges. A divergent susceptibility signals an instability: a spin polarization is formed for arbitrarily weak magnetic field.

The magnetic instability is governed by a competition between two effects. On the one hand, the kinetic energy of the electrons is minimal if there is no net spin polarization, because then all energy levels $\varepsilon_{\mathbf{k}}$ can be doubly occupied. On the other hand, the short-range part of the electron-electron interaction favors a magnetic state. This is because electrons with the same spin have a strongly reduced repulsion since the Pauli principle already guarantees that they are spatially separated.

We first consider the susceptibility for a gas of interacting electrons with a parabolic dispersion ("free electrons"). This is the example that we studied in detail in the previous chapters. A calculation within the RPA approximation shows that electron-electron interactions enhance χ, but also that they do not lead to a divergence. In other words, for free electrons, the competition between kinetic energy and interaction energy always favors the kinetic energy, and, hence, forbids a spontaneous spin polarization.

The picture is different once the ionic lattice is taken into account. Band structure effects turn out to be crucial for the occurrence of a ferromagnetic instability. In a narrow band, the kinetic energy cost for polarizing electron spins is strongly reduced, and a magnetic instability becomes possible. Depending on the material one looks at, one may have a ferromagnetic instability (uniform magnetization) or a spin-wave material (nonuniform magnetization). One example of a spin-wave material is an antiferromagnet, where the spin polarization has opposite direction on neighboring lattice sites.

8.1 Magnetic susceptibility

In order to make the above picture more quantitative, we consider an electron gas in the presence of a magnetic field $\mathbf{h}$. We are interested in the spin density $\mathbf{s}(\mathbf{r})$,

$$s_\alpha(\mathbf{r}) = \frac{1}{2}\sum_{\sigma,\sigma'} \hat{\psi}^\dagger_\sigma(\mathbf{r})(\sigma_\alpha)_{\sigma,\sigma'}\hat{\psi}_{\sigma'}(\mathbf{r}), \quad \alpha = x, y, z, \tag{8.1}$$

where σ_α is the Pauli matrix. The response of a magnetic material to an applied magnetic field is characterized by the magnetic susceptibility $\chi(\mathbf{r}, t; \mathbf{r}', t')$, which relates the change in spin density at position $\mathbf{r}$ and time t to the magnetic field at position $\mathbf{r}'$ and time t',

$$\delta s_\alpha(\mathbf{r}, t) = \sum_\beta \int d\mathbf{r}' \int dt' \chi_{\alpha\beta}(\mathbf{r}, t; \mathbf{r}', t')h_\beta(\mathbf{r}', t'). \tag{8.2}$$

Note that $\chi_{\alpha\beta}$ is a tensor: in principle, a magnetic field $\mathbf{h}$ can cause a spin density in a different direction than the direction of $\mathbf{h}$. The magnetic field $\mathbf{h}$ enters into the Hamiltonian through the Zeeman coupling,

$$\hat{H}_1 = -\frac{\hbar}{2}\mu_B g \int d\mathbf{r}\mathbf{h}(\mathbf{r}, t) \cdot \mathbf{s}(\mathbf{r}), \tag{8.3}$$

where $\mu_B = e\hbar/2mc$ is the Bohr magneton and $g = 2$ the electron g factor. For electrons, it also enters the Hamiltonian through the kinetic energy $(1/2m)(\mathbf{p} - e\mathbf{A}/c)^2$. We neglect the role of the vector potential in the discussion below.

According to the Kubo formula, the spin susceptibility is equal to the retarded spin-spin correlation function,

$$\chi_{\alpha\beta}(\mathbf{r}, t; \mathbf{r}', t') = i\frac{\mu_B g}{2}\theta(t - t')\langle[s_\alpha(\mathbf{r}, t), s_\beta(\mathbf{r}', t')]_-\rangle. \tag{8.4}$$

Note the absence of a minus sign on the r.h.s. of Eq. (8.4) because of the minus sign in front of the magnetic field in the expression (8.3) for the Zeeman energy. We may perform a Fourier transform to find the susceptibility in frequency representation,

$$\delta s_\alpha(\mathbf{r}, \omega) = \sum_\beta \int d\mathbf{r}' \chi_{\alpha\beta}(\mathbf{r}, \mathbf{r}'; \omega)h_\beta(\mathbf{r}', \omega), \tag{8.5}$$

where

$$\chi_{\alpha\beta}(\mathbf{r}, \mathbf{r}'; \omega) = i\frac{\mu_B g}{2}\int_0^\infty dt e^{i\omega t}\langle[s_\alpha(\mathbf{r}, t), s_\beta(\mathbf{r}', 0)]_-\rangle. \tag{8.6}$$

For a spatially homogeneous system, we may perform one further Fourier transform to the coordinate $\mathbf{r}$, which gives a susceptibility $\chi_{\alpha\beta}(\mathbf{q},\omega)$,

$$\chi_{\alpha\beta}(\mathbf{q},\omega) = \frac{1}{V}\int d\mathbf{r}d\mathbf{r}' e^{-i\mathbf{q}\cdot(\mathbf{r}-\mathbf{r}')}\chi_{\alpha\beta}(\mathbf{r},\mathbf{r}';\omega). \tag{8.7}$$

For the calculation of $\chi_{\alpha\beta}(\mathbf{q},\omega)$ it is useful to write the spin density in terms of the plane wave basis,

$$\chi_{\alpha\beta}(\mathbf{q};t,t') = i\theta(t-t')\frac{\mu_B g}{2V}\langle[s_{\mathbf{q},\alpha}(t), s_{-\mathbf{q},\beta}(t')]_-\rangle, \tag{8.8}$$

where

$$s_{\mathbf{q},\alpha} = \frac{1}{2}\sum_{\mathbf{k},\sigma,\sigma'}\hat{\psi}^\dagger_{\mathbf{k},\sigma}(\sigma_\alpha)_{\sigma,\sigma'}\hat{\psi}_{\mathbf{k}+\mathbf{q},\sigma'}. \tag{8.9}$$

In practice, the x and y labels of the tensor $\chi_{\alpha\beta}$ are often replaced by labels "+" and "−", referring to the linear combinations

$$s_\pm = s_1 \pm i s_2. \tag{8.10}$$

These combinations are expressed in terms of raising and lowering operators for the spin, which are much easier to calculate. In particular, we have the susceptibility

$$\chi_{-+}(\mathbf{r},t;\mathbf{r}',t') = i\frac{\mu_B g}{2}\theta(t-t')\langle[s_-(\mathbf{r},t), s_+(\mathbf{r}',t')]_-\rangle. \tag{8.11}$$

The susceptibility χ_{-+} is known as the "transverse" susceptibility, while χ_{zz} is known as the "longitudinal" susceptibility. For an isotropic system, the tensor $\chi_{\alpha\beta}$ is proportional to the unit tensor. In that case one has

$$\chi_{\alpha\beta} = \frac{1}{2}\delta_{\alpha\beta}\chi_{-+}, \quad \alpha,\beta = x,y,z. \tag{8.12}$$

A calculation of the susceptibility for non-interacting electrons is very similar to the calculation of the polarizability that we discussed in Sec. 6.1. One finds

$$\chi_{-+}(\mathbf{q},t) \;=\; i\frac{\mu_B g}{2V}\theta(t)\sum_{\mathbf{k},\mathbf{k}'}\langle[\hat{\psi}^\dagger_{\mathbf{k},\downarrow}(t)\hat{\psi}_{\mathbf{k}+\mathbf{q},\uparrow}(t), \hat{\psi}^\dagger_{\mathbf{k}',\uparrow}(0)\hat{\psi}_{\mathbf{k}'-\mathbf{q},\downarrow}(0)]_-\rangle. \tag{8.13}$$

Diagrammatically, the susceptibility for non-interacting electrons can be represented by the diagram shown in Fig. 8.1. The white dots are spin vertices. For the transverse susceptibility χ_{-+}, they enforce that the ingoing and outgoing spins have different sign, see Fig. 8.1.

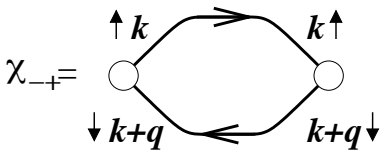

Figure 8.1: Diagrammatic representation of the transverse spin susceptibility χ_{-+} for non-interacting electrons.

As a matter of fact, we can find χ_{-+} without doing a calculation if we compare Eqs. (8.13) and the expression for the polarizability of the non-interacting electron gas, Eq. (6.18). We then immediately conclude

$$\chi^0_{-+}(\mathbf{q},\omega) = -\frac{\mu_B g}{2V}\sum_{\mathbf{k}} \frac{n_F(\varepsilon_{\mathbf{k}}-\mu) - n_F(\varepsilon_{\mathbf{k}+\mathbf{q}}-\mu)}{\varepsilon_{\mathbf{k}} - \varepsilon_{\mathbf{k}+\mathbf{q}} + \omega + i\eta}, \tag{8.14}$$

where n_F is the Fermi function and η is a positive infinitesimal.

In the limit $\mathbf{q} \to 0, \omega \to 0$ of a static and uniform magnetic field, one has $\chi_{-+} \to \nu\mu_B g/2$, where ν is the density of states per unit volume and per spin direction. This result is known as the "Pauli susceptibility". The Pauli susceptibility accounts for the fact that it costs a finite kinetic energy to have a finite spin density. The value of the Pauli susceptibility then follows from the competition of the magnetic energy gain (proportional to the spin density and the magnetic field) and the kinetic energy loss (proportional to the square of the spin density).

The imaginary part of the susceptibility $\chi^0(\mathbf{q},\omega)$ characterizes energy dissipation through magnetic excitations. The support of the imaginary part of χ^0 is the same as that of the imaginary part of the polarizability of the non-interacting electron gas, see Fig. 6.2.

For the interacting electron gas, we can use the diagrammatic theory to compute the susceptibility. Some diagrams are shown in Fig. 8.2. They can be rearranged in three steps. First, we incorporate all interaction lines that connect the upper or lower fermion line to itself into single-particle Green functions. Second, we replace the interaction by the screened interaction by inserting any number of "bubbles" into the interaction. Below, the single-electron Green function will be calculated using the Hartree-Fock approximation, the effective interaction in the RPA. Third, we write the diagram in terms of a "vertex correction" as in Sec. 5.6, see Fig. 8.2. The renormalized vertex, which is indicated by a black dot, then contains all contributions from interaction lines that connect the upper and lower fermion lines.

In the spirit of the RPA approximation, we keep only "ladder" diagrams for the vertex correction, see Fig. 8.3. In this approximation, the calculation has become very similar to

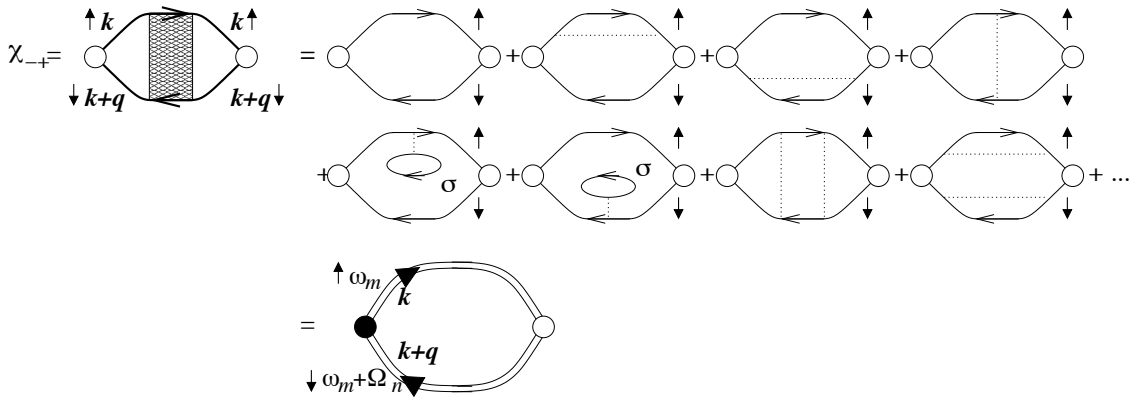

Figure 8.2: Diagrammatic representation of the contributions to the transverse spin susceptibility χ_{-+} for interacting electrons, up to second order in the interaction. The arrows indicate the spin direction, while "σ" denotes an additional summation over spin. Note that spin is conserved throughout the upper and lower fermion lines.

that of the current-current correlation function of Sec. 5.6. Denoting the renormalized vertex by $\Gamma(\mathbf{k}, i\omega_m; \mathbf{k}+\mathbf{q}, i\omega_m + i\Omega_n)$ and the screened interaction by $V^{\rm eff}_{\mathbf{q}}(i\Omega_n)$, we have

$$\begin{aligned}\Gamma(\mathbf{k}, i\omega_m; \mathbf{k}+\mathbf{q}, i\omega_m + i\Omega_n) &= 1 - \frac{T}{V}\sum_{\mathbf{k}'}\sum_{p} \mathcal{G}_{\mathbf{k}'\uparrow,\mathbf{k}'\uparrow}(i\omega_p)\mathcal{G}_{\mathbf{k}'+\mathbf{q}\downarrow,\mathbf{k}'+\mathbf{q}\downarrow}(i\omega_p + i\Omega_n) \\ &\quad \times V^{\rm eff}_{\mathbf{k}-\mathbf{k}'}(i\omega_m - i\omega_p)\Gamma(\mathbf{k}', i\omega_p; \mathbf{k}'+\mathbf{q}, i\omega_p + i\Omega_n). \quad (8.15)\end{aligned}$$

Note that the effective interaction depends on the Matsubara frequency difference $i\omega_m - i\omega_p$, in contrast to the bare interaction which is frequency independent. Then, in terms of the renormalized vertex, the spin susceptibility is calculated as

$$\begin{aligned}\chi^{\rm RPA}_{-+}(\mathbf{q}, i\Omega_n) &= -\frac{T\mu_B g}{2V}\sum_{\mathbf{k}}\sum_{m} \Gamma(\mathbf{k}, i\omega_m; \mathbf{k}+\mathbf{q}, i\omega_m + i\Omega_n) \\ &\quad \times \mathcal{G}_{\mathbf{k}\uparrow,\mathbf{k}\uparrow}(i\omega_m)\mathcal{G}_{\mathbf{k}+\mathbf{q}\downarrow,\mathbf{k}+\mathbf{q}\downarrow}(i\omega_m + i\Omega_n). \quad (8.16)\end{aligned}$$

The analytical continuation $i\Omega_n \to \omega + i\eta$ is done as in Sec. 5.6. The result is

$$\begin{aligned}\chi_{-+}(\mathbf{q}, \omega + i\eta) &= -\frac{\mu_B g}{8\pi i V}\int d\xi \tanh(\xi/2T)\sum_{\mathbf{k}} \\ &\quad \times \big[\Gamma^{\rm RR}(\mathbf{k}, \xi; \mathbf{k}+\mathbf{q}, \xi+\omega)G^{\rm R}_{\mathbf{k}\uparrow,\mathbf{k}\uparrow}(\xi)G^{\rm R}_{\mathbf{k}+\mathbf{q}\downarrow,\mathbf{k}+\mathbf{q}\downarrow}(\xi+\omega) \\ &\quad - \Gamma^{\rm AR}(\mathbf{k}, \xi; \mathbf{k}+\mathbf{q}, \xi+\omega)G^{\rm A}_{\mathbf{k}\uparrow,\mathbf{k}\uparrow}(\xi)G^{\rm R}_{\mathbf{k}+\mathbf{q}\downarrow,\mathbf{k}+\mathbf{q}\downarrow}(\xi+\omega)\end{aligned}$$

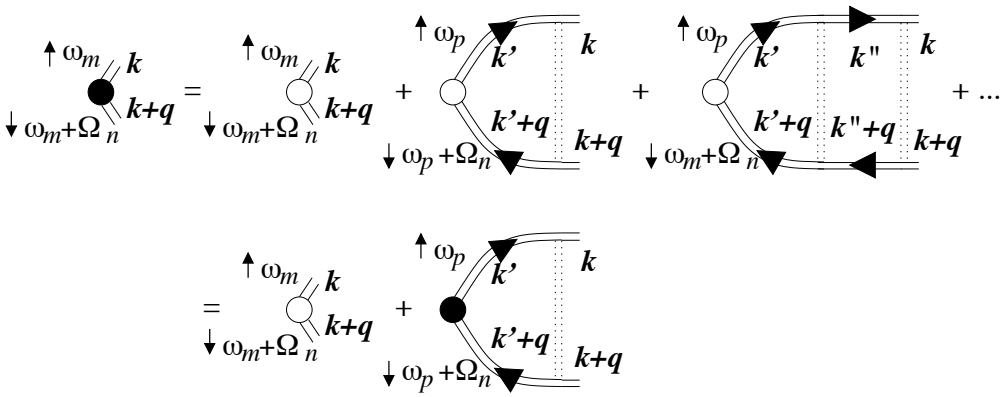

Figure 8.3: Diagrammatic representation of the RPA approximation for the transverse spin susceptibility χ_{-+}.

$$\begin{aligned} &+ \Gamma^{\mathrm{AR}}(\mathbf{k}, \xi - \omega; \mathbf{k}+\mathbf{q}, \xi) G^{\mathrm{A}}_{\mathbf{k}\uparrow,\mathbf{k}\uparrow}(\xi - \omega) G^{\mathrm{R}}_{\mathbf{k}+\mathbf{q}\downarrow,\mathbf{k}+\mathbf{q}\downarrow}(\xi) \\ &- \Gamma^{\mathrm{AA}}(\mathbf{k}, \xi - \omega; \mathbf{k}+\mathbf{q}, \xi) G^{\mathrm{A}}_{\mathbf{k}\uparrow,\mathbf{k}\uparrow}(\xi - \omega) G^{\mathrm{A}}_{\mathbf{k}+\mathbf{q}\downarrow,\mathbf{k}+\mathbf{q}\downarrow}(\xi) \big] \, . \end{aligned} \tag{8.17}$$

For the full frequency and momentum dependent screened interaction, the RPA equation for the renormalized vertex cannot be solved in closed form. Here, we'll adopt the Thomas-Fermi approximation and replace the screened interaction by the interaction at $\mathbf{q} = 0$, $\omega = 0$,

$$V^{\mathrm{TF}}_{\mathbf{q}}(i\Omega_n) \approx \frac{e^2}{\epsilon_0 k_s^2}, \tag{8.18}$$

where $k_s^2 = 2\nu e^2/\epsilon_0$ is the Thomas-Fermi wavenumber. This approximation corresponds to a delta-function interaction in real space, $V^{\mathrm{TF}}(\mathbf{r}) \approx (2\nu)^{-1}\delta(\mathbf{r})$. With this approximation, calculation of the renormalized vertex is straightforward, and we find the simple result

$$\begin{aligned} &\Gamma(\mathbf{k}, i\omega_m; \mathbf{k}+\mathbf{q}, i\omega_m + i\Omega_n) \\ &\quad = \left[1 + \frac{T}{2\nu V} \sum_{\mathbf{k}'} \sum_{p} \mathcal{G}_{\mathbf{k}'\uparrow,\mathbf{k}'\uparrow}(i\omega_p) \mathcal{G}_{\mathbf{k}'+\mathbf{q}\downarrow,\mathbf{k}'+\mathbf{q}\downarrow}(i\omega_p + i\Omega_n) \right]^{-1} . \end{aligned} \tag{8.19}$$

The summation in the denominator has the same expression as the susceptibility for non-interacting electrons, the only difference being that the single-electron Green functions have been replaced by their values in the interacting electron liquid. In other words, this is the susceptibility for the interacting electron liquid without vertex renormalization. Using the

Hartree-Fock approximation for the single-particle Green function, we write

$$\begin{aligned}\chi^{0,\mathrm{HF}}_{-+}(\mathbf{q},i\Omega_n) &= -\frac{\mu_B g T}{2V}\sum_{\mathbf{k}}\sum_m \mathcal{G}_{\mathbf{k}\uparrow,\mathbf{k}\uparrow}(i\omega_m)\mathcal{G}_{\mathbf{k}+\mathbf{q}\downarrow,\mathbf{k}+\mathbf{q}\downarrow}(i\omega_m+i\Omega_n)\\ &= -\frac{\mu_B g}{2V}\sum_{\mathbf{k}}\frac{n_F(\varepsilon^{\mathrm{HF}}_{\mathbf{k},\uparrow}-\mu)-n_F(\varepsilon^{\mathrm{HF}}_{\mathbf{k}+\mathbf{q},\downarrow}-\mu)}{\varepsilon^{\mathrm{HF}}_{\mathbf{k},\downarrow}-\varepsilon^{\mathrm{HF}}_{\mathbf{k}+\mathbf{q},\uparrow}+i\Omega_n},\end{aligned} \tag{8.20}$$

so that we can express the full transverse susceptibility in the Thomas-Fermi approximation as

$$\chi^{\mathrm{TF}}_{-+}(\mathbf{q},\omega)=\frac{\chi^{0,\mathrm{HF}}_{-+}(\mathbf{q},\omega)}{1-\frac{1}{\nu\mu_B g}\chi^{0,\mathrm{HF}}_{-+}(\mathbf{q},\omega)}. \tag{8.21}$$

For a uniform static magnetic field, one has $\chi^{0,\mathrm{HF}}_{-+}(0,0)=\nu\mu_B g/2$, where the density of states ν should be interpreted as the "density of poles" of the full Green function, i.e., the density of Hartree-Fock energy levels. Since this is the same density of states as the one that occurs in the screened interaction, one has

$$\chi^{\mathrm{TF}}_{-+}(0,0)=\nu\mu_B g. \tag{8.22}$$

We conclude that, according to the Thomas-Fermi approximation, in an interacting electron gas the electron-electron interactions increase the spin susceptibility by a factor two compared to the case of the non-interacting electron gas.[1]

The enhancement of the susceptibility by the interactions follows from the fact that the repulsive interaction between the electrons is lowered if a finite spin density is created. After all, the Pauli principle forbids that electrons of the same spin are at the same location, so that they have a smaller electrostatic repulsion. The interaction energy gain is proportional to the square of the spin density, so that the net energy cost for polarizing the system is reduced with respect to the case of non-interacting electrons.

If the interaction energy gain is larger than the kinetic energy cost, a spin polarization will form spontaneously. This instability is known as the "Stoner instability". We see that for the standard case of a parabolic band the Stoner instability does not occur. The situation becomes different once the precise band structure of the material is taken into account. The next section discusses a simple model for this.

[1]The Thomas-Fermi approximation is not quantitatively correct. A more correct treatment of the RPA approximation which takes into account the momentum dependence of the effective interaction gives

$$\chi^{\mathrm{RPA}}_{-+} = \frac{\nu\mu_B g}{2-(2/3\pi^2)^{2/3}r_s\ln(1+(3\pi^2/2)^{2/3}/r_s)},$$

see Ex. 8.1.

8.2 Hubbard model

The approximations of the previous subsection are appropriate for the standard parabolic band of free electrons. In real materials, the electrons occupy bands, and the band structure needs to be taken into account for a calculation of the magnetic susceptibility. A simple model to take the band structure into account is the "Hubbard model".

For the construction of the Hubbard model, we consider electrons in an energy band with Bloch energies $\varepsilon_{\mathbf{k}}$ described by the Hamiltonian

$$\hat{H}_0 = \sum_{\mathbf{k}} \varepsilon_{\mathbf{k}} \hat{\psi}^\dagger_{\mathbf{k}} \hat{\psi}_{\mathbf{k}}. \tag{8.23}$$

For such a band, wavefunctions can be represented in the basis of Wannier wavefunctions at lattice site $\mathbf{r}_i$,

$$\phi_i(\mathbf{r}) = N^{-1/2} \sum_{\mathbf{k}} e^{i\mathbf{k}\cdot\mathbf{r}_i} \hat{\psi}_{\mathbf{k}}(\mathbf{r}), \tag{8.24}$$

where the summation is restricted to wavevectors in the first Brillouin zone and N is the number of lattice sites. The Wannier wavefunctions at different lattice sites are orthogonal.

The Coulomb interaction can be written in terms of the basis of Wannier wavefunctions. The corresponding matrix elements are

$$V_{ij,i'j'} = \int d\mathbf{r}_1 d\mathbf{r}_2 \phi^*_i(\mathbf{r}_1) \phi^*_j(\mathbf{r}_2) V^{\text{eff}}(\mathbf{r}_1 - \mathbf{r}_2) \phi_{j'}(\mathbf{r}_2) \phi_{i'}(\mathbf{r}_1), \tag{8.25}$$

where V^{eff} is the screened Coulomb interaction. The approximation of the Hubbard model consists in neglecting all interaction matrix elements except for the matrix element $U = V_{iiii}$. The justification for this approximation is that the screened interaction is short range, while the Wannier wavefunctions are mainly localized at one lattice site. This approximation leads to the interaction Hamiltonian

$$\hat{H}_1 = U/2 \sum_{i\sigma\sigma'} n_{i\sigma} n_{i\sigma'}, \tag{8.26}$$

where $n_{i\sigma} = \hat{\psi}^\dagger_{i\sigma} \hat{\psi}_{i\sigma}$ is the Wannier number operator and

$$\hat{\psi}_{i\sigma} = N^{-1/2} \sum_{\mathbf{k}} \hat{\psi}^\dagger_{\mathbf{k}\sigma} e^{i\mathbf{k}\cdot\mathbf{r}_i} \tag{8.27}$$

is the Wannier annihilation operator.

The interaction Hamiltonian can be further simplified if we use $n_{i\sigma}^2 = n_{i\sigma}$, so that

$$\hat{H}_1 = U \sum_i n_{i\uparrow} n_{i\downarrow} + (U/2) \sum_i (n_{i\uparrow} + n_{i\downarrow}). \tag{8.28}$$

The second term is nothing but a shift of the chemical potential and will be neglected. Fourier transforming the first term in Eq. (8.28) we then arrive at

$$\hat{H}_1 = \frac{U}{N} \sum_{\mathbf{k},\mathbf{k}',\mathbf{q}} \hat{\psi}^\dagger_{\mathbf{k},\uparrow} \hat{\psi}_{\mathbf{k}+\mathbf{q},\uparrow} \hat{\psi}^\dagger_{\mathbf{k}',\downarrow} \hat{\psi}_{\mathbf{k}'-\mathbf{q},\downarrow}. \tag{8.29}$$

Let us now calculate the spin susceptibility for the Hubbard model. The calculation proceeds along the same lines as that of the previous section. The only differences are that, for the Hubbard model, the wavevector summation is restricted to the first Brillouin zone, and that the strength of the interaction is set independently by the interaction constant U. The result for the transverse susceptibility is

$$\chi_{-+}(\mathbf{q},\omega) = \frac{\chi^{0,\mathrm{HF}}_{-+}(\mathbf{q},\omega)}{1 - \frac{2U}{\mu_B g} \chi^{0,\mathrm{HF}}_{-+}(\mathbf{q},\omega)}, \tag{8.30}$$

where

$$\chi^{0,\mathrm{HF}}_{-+}(\mathbf{q},\omega) = \frac{\mu_B g}{2N} \sum_{\mathbf{k}} \frac{n_F(\varepsilon^{\mathrm{HF}}_{\mathbf{k},\uparrow} - \mu) - n_F(\varepsilon^{\mathrm{HF}}_{\mathbf{k}+\mathbf{q},\downarrow} - \mu)}{\varepsilon^{\mathrm{HF}}_{\mathbf{k}+\mathbf{q},\downarrow} - \varepsilon^{\mathrm{HF}}_{\mathbf{k},\uparrow} + \omega + i\eta}. \tag{8.31}$$

For the Hubbard model, the Hartree-Fock energy levels have a very simple connection to the bare energy levels $\varepsilon_{\mathbf{k}}$,

$$\varepsilon^{\mathrm{HF}}_{\mathbf{k}\sigma} = \varepsilon_{\mathbf{k}} + U\bar{n}_{-\sigma}, \quad \bar{n}_\sigma = \frac{1}{N} \sum_{\mathbf{k}} n_F(\varepsilon^{\mathrm{HF}}_{\mathbf{k}\sigma}) \rangle. \tag{8.32}$$

In the absence of a spontaneous magnetization, the levels of electrons with spin up and spin down experience the same uniform shift, which can be incorporated into the chemical potential. In particular, this implies that the support of the imaginary part of $\chi^{0,\mathrm{HF}}_{-+}$ and, hence, of the imaginary part of χ^{TF}_{-+}, is the same as that of $\chi^0 - +$, which is shown in Fig. 6.2. In the presence of a spontaneous magnetization, the Hartree-Fock energy levels for electrons with spin up and spin down experience different shifts. We return to this case in Sec. 8.5.

As before, the limit of large wavelength and low frequency has $\chi^{0,\mathrm{HF}}_{-+}(0,0) = \nu\mu_B g/2$, where ν is the density of states per spin direction and per lattice site. Hence

$$\chi^{\mathrm{TF}}_{-+}(0,0) = \frac{\nu\mu_B g/2}{1 - U\nu}. \tag{8.33}$$

We can use these results to find the interaction correction to the Free energy for the Hubbard model. Repeating the analysis of Sec. 7.5, we find the result

$$F - F_0 = \int_{-\infty}^{\infty} \frac{d\xi}{4\pi} \sum_{\mathbf{q}} \coth(\xi/2T) \mathrm{Im}\, \ln(1 - 2U\chi^{0,\mathrm{HF}}(\mathbf{q}, \xi)/\mu_B g). \tag{8.34}$$

This result may be analyzed using the detailed expressions for $\chi^{0,\mathrm{HF}}$ of Ex. 6.2. For low temperatures, the main contribution comes from frequencies around $\omega = 0$, and one finds that the specific heat is enhanced close to the Stoner instability,

$$C_V \propto -T \ln(1 - U\nu). \tag{8.35}$$

This is to be compared to the usual specific heat of the noninteracting electron gas, which is proportional to νT.

8.3 The Stoner instability

As long as the interaction constant U is small enough, the susceptibility remains finite. A finite susceptibility implies that it requires a finite value of the magnetic field $\mathbf{h}$ to create a spin polarization. However, if the interaction strength increases, the susceptibility increases. If the static susceptibility $\chi(\mathbf{q}, 0)$ diverges, an instability occurs, and a spontaneous magnetization will form.

From our general result (8.30) for the Hubbard model we find that the instability criterion is[2]

$$U = U_c(\mathbf{q}) = \mu_B g / 2\chi^{0,\mathrm{HF}}(\mathbf{q}, 0). \tag{8.36}$$

This is the Stoner criterion.

For zero wavevector $\mathbf{q} = 0$, the Stoner criterion describes the ferromagnetic instability, which occurs at critical interaction strength $U\nu = 1$. For a parabolic band, the instability occurs first at $\mathbf{q} = 0$, since $\chi^{0,\mathrm{HF}}(\mathbf{q}, 0)$ is a monotonously decreasing function of $|\mathbf{q}|$, cf. Ex. 6.2. However, in the presence of a more complicated band structure, instabilities at finite wavenumbers are also possible. An instability at finite $\mathbf{q}$ leads to the formation of a so-called "spin density wave" state, as was first pointed out by Overhauser [Phys. Rev. **128**, 1437 (1962)]. As an example, we consider the band

$$\varepsilon_{\mathbf{k}} = -2t \sum_{\alpha=x,y,z} \cos k_\alpha a, \tag{8.37}$$

[2]For finite frequencies, the denominator of Eq. (8.30) is generally complex, so that one can rule out the existence of zeroes. Physically, one expects the instability to happen at zero frequency, since an instability at nonzero frequency corresponds to a time-dependent polarization, which is damped. Response at nonzero frequencies is studied in a later section.

which corresponds to electrons on a simple cubic lattice with lattice constant a and hopping amplitude t, see Ex. 8.7. For this band, there is a competition between the ferromagnetic instability at wavevector $\mathbf{q} = 0$ and an antiferromagnetic instability at wavevector $\mathbf{q} = \mathbf{q}_A = (\pi/a)(1,1,1)$ at the far corner of the first Brillouin zone. You verify that one has

$$\chi^{0,\mathrm{HF}}(\mathbf{q}_A, 0) = -\frac{\mu_B g}{2} \int_{-6t}^{\mu} d\xi \frac{\nu(\xi)}{\xi}. \tag{8.38}$$

For chemical potentials close to the band edges $\pm 6t$, the instability occurs at wavevector $\mathbf{q} = 0$, while for a chemical potential μ close to the band center at $\varepsilon = 0$, the instability occurs at $\mathbf{q} = \mathbf{q}_A$. For this simple cubic band structure, one has $\chi^{0,\mathrm{HF}}(\mathbf{q}_A, 0) \to \infty$ as $\mu \to 0$, so that the antiferromagnetic instability occurs already for arbitrarily small repulsive interaction!

Note that for interaction strength $U > U_c$, our expression (8.30) for the spin susceptibility in the Thomas Fermi approximation is, again, finite. However, this result is unphysical, since, for $U > U_c$ the ground state has a spontaneous spin polarization (or a spin-density wave state). Hence, we conclude that Eq. (8.30) is valid for all $U < \min_{\mathbf{q}} U_c(\mathbf{q})$, whereas a state with spontaneous magnetization is formed for $U > U_c$. A description of the ferromagnetic state is given in Sec. 8.5 below.

8.4 Neutron scattering

Neutrons have spin 1/2. The neutron spins interact with the spins of electrons in a solid through the magnetic dipole interaction. Hence, the neutron scattering cross section is sensitive to the magnetic structure of a solid.

The inelastic scattering cross section $d^2\sigma/d\Omega d\omega$ tells us the amount of scattered neutrons that emerge from the sample at a given energy $\hbar\omega$ and solid angle Ω. In order to describe the scattering of slow neutrons, we start from the first Born approximation for the neutron scattering cross section,[3]

$$\frac{d^2\sigma}{d\Omega d\omega} = \frac{1}{2} \sum_{f,\sigma_f,\sigma_i} \frac{k'}{k} \left(\frac{M}{2\pi}\right)^2 \left\langle |\langle \mathbf{k}'\sigma_f, f|H'|\mathbf{k}\sigma_i, i\rangle|^2 \right\rangle \delta(\omega + E_i - E_f), \tag{8.39}$$

where σ_f and σ_i denote the outgoing and incoming spin states of the neutron, $\mathbf{k}$ is the wavevector of the incoming neutron, $\mathbf{k}'$ is the wavevector of the outgoing neutron, M is the

[3]This result is derived in standard texts on quantum mechanics, e.g., *Quantum Mechanics*, by A. Messiah, North-Holland (1961).

reduced mass of the neutron, i and f refer to initial state and final state, respectively, H' is the interaction between the neutron and the target, and the outer brackets $\langle \ldots \rangle$ indicate a thermal average over the initial states i of the target. The prefactor $1/2$ is added since we average over the possible incoming spin states. For the interaction between an electron and a neutron we take the first quantization form[4]

$$H' = V_0(\mathbf{r}_n - \mathbf{r}) + V_1(\mathbf{r}_n - \mathbf{r})\mathbf{s}_n \cdot \mathbf{s}, \tag{8.40}$$

where $\mathbf{r}_n$ and $\mathbf{s}_n$ are the position and spin of the neutron, while $\mathbf{r}$ and $\mathbf{s}$ are the position and spin of the electron. Using the second quantization language for the electrons, H' can be rewritten as

$$H' = \int d\mathbf{r} V_0(\mathbf{r}_n - \mathbf{r}) n(\mathbf{r}) + \mathbf{s}_n \cdot \int d\mathbf{r} V_1(\mathbf{r}_n - \mathbf{r}) \mathbf{s}(\mathbf{r}), \tag{8.41}$$

where $n(\mathbf{r})$ and $\mathbf{s}(\mathbf{r})$ are the second quantization operators for the electron number density and spin density. Writing $\mathbf{q} = \mathbf{k} - \mathbf{k}'$, we then find

$$\begin{aligned} \langle \mathbf{k}'\sigma_f, f|H'|\mathbf{k}\sigma_i, i\rangle &= \int d\mathbf{r}_n d\mathbf{r} e^{-i\mathbf{q}\cdot\mathbf{r}_n} V_0(\mathbf{r}_n - \mathbf{r}) \delta_{\sigma_f,\sigma_i} \langle f|n(\mathbf{r})|i\rangle \\ &\quad + \frac{1}{2}\sum_\alpha \int d\mathbf{r}_n d\mathbf{r} e^{-i\mathbf{q}\cdot\mathbf{r}_n} V_1(\mathbf{r}_n - \mathbf{r}) (\sigma_\alpha)_{\sigma_f\sigma_i} \langle f|s(\mathbf{r})|i\rangle \\ &= V_{0\mathbf{q}} \langle f|\rho_\mathbf{q}|i\rangle \delta_{\sigma_f,\sigma_i} + \frac{V_{1\mathbf{q}}}{2} \sum_\alpha (\sigma_\alpha)_{\sigma_f\sigma_i} \langle f|s_{\mathbf{q}\alpha}|i\rangle, \end{aligned} \tag{8.42}$$

where $V_{0\mathbf{q}}$ and $V_{1\mathbf{q}}$ are the Fourier transforms of V_0 and V_1, respectively. Next, we write the delta function in Eq. (8.39) as an integration over time, absorb the factors $\exp(iE_i t)$ and $\exp(-iE_f t)$ into a time-shift of the operators n and $\mathbf{s}$, and perform the summation over final states. The result is[5]

$$\frac{d^2\sigma}{d\Omega d\omega} = \left(\frac{M}{2\pi}\right)^2 \frac{k'}{2\pi k} \times \int dt e^{i\omega t} \left[|V_{0\mathbf{q}}|^2 \langle n_{-\mathbf{q}}(0) n_\mathbf{q}(t)\rangle + \frac{|V_{1\mathbf{q}}|^2}{4} \langle \mathbf{s}_{-\mathbf{q}}(0) \cdot \mathbf{s}_\mathbf{q}(t)\rangle \right].$$

The spin-spin correlation function appearing in the spin-dependent part of the inelastic neutron scattering cross section is nothing but a "greater Green function". For an isotropic system, it can be written in terms of the spin raising and lowering operators s_+ and s_-,

$$\langle \mathbf{s}_{-\mathbf{q}}(0) \cdot \mathbf{s}_\mathbf{q}(t)\rangle = \frac{3}{2} \langle s_{-,-\mathbf{q}}(0) s_{+,\mathbf{q}}(t)\rangle. \tag{8.43}$$

[4]For more details: see L.D. Landau and E.M. Lifschitz, *Quantum mechanics, non-relativistic theory*, Addison and Wesley (1958).

[5]See, e.g., the book by Doniach and Sondheimer for details.

Using the general relation (2.49) between Green functions, the Fourier transform with respect to time can be written in terms of the imaginary part of the retarded spin density correlation function,

$$\int dt e^{i\omega t} \langle \mathbf{s}_{-\mathbf{q}}(0) \cdot \mathbf{s}_{\mathbf{q}}(t) \rangle = \frac{3}{2\mu_B g} \frac{\mathrm{Im}\, \chi^{\mathrm{R}}_{-+}(\mathbf{q}, \omega)}{1 - e^{-\hbar\omega/T}}. \tag{8.44}$$

The minus-sign in the denominator appears because χ is a correlation function of spin densities, which are even in fermion creation and annihilation operators.

The approach to the instability point leads to a strong enhancement of the neutron scattering cross section. For small $\mathbf{q}$ and ω and a parabolic band, one has (cf. Ex. 6.2)

$$\mathrm{Im}\, \chi^{R}_{-+}(\mathbf{q}, \omega) = \frac{\pi \mu_B g \omega / 8 q v_F}{(1 - U\nu)^2 + (U\pi\omega/4qv_F)^2}. \tag{8.45}$$

Thus, as the ferromagnetic instability is approached, inelastic neutron scattering is strongly enhanced for low frequencies. The physical origin of the enhanced neutron scattering rate at low temperatures is the slowing down of spin relaxation at the approach of the Stoner instability.

8.5 The ferromagnetic state

Beyond the instability point a spontaneous magnetization forms. In principle, the magnetization can point in any direction, although, for each sample, a specific direction will be selected. Here, we assume that the magnetization points in the positive z-direction.

The main difference between the ferromagnetic state and the paramagnetic state is that, in a ferromagnet, the Hartree-Fock energy levels are different for up spins and down spins, see Eq. (8.32). For the Hubbard model, the difference between levels for spin up and spin down does not depend on the wavevector,

$$\Delta = \varepsilon^{\mathrm{HF}}_{\mathbf{k}\downarrow} - \varepsilon^{\mathrm{HF}}_{\mathbf{k}\uparrow} = U(\bar{n}_\uparrow - \bar{n}_\downarrow). \tag{8.46}$$

The existence of the gap Δ implies that electrons with spin up have a larger Fermi momentum than electrons with spin down, see Fig. 8.4, which, in turn reflects the fact that there is a net spin polarization. The electrons with spin parallel to the magnetization direction are referred to as "majority electrons", whereas those with opposite to the magnetization direction are called "minority electrons".

One can calculate Δ self-consistently from the requirement that the total number of particles does not change upon the formation of the magnetic moment. Together with Eq. (8.32), one can then solve for the energy gap Δ. Nontrivial solutions exist for $U\nu > 1$ only.

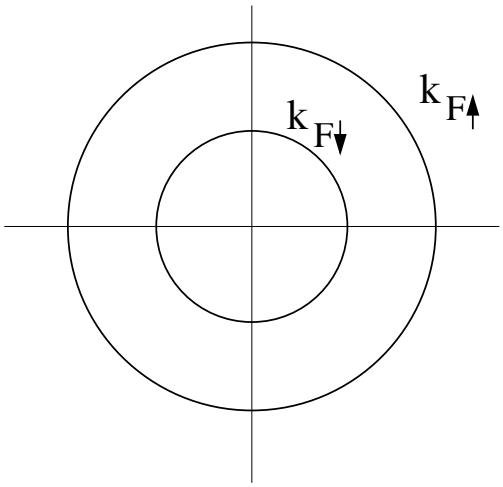

Figure 8.4: Support of the imaginary part of χ_{-+} for a ferromagnet and spin wave dispersion.

The difference between Hartree-Fock energy levels for different spin directions leads to a modification of the expression for the transverse spin susceptibility,

$$\chi_{-+}^{0,\mathrm{HF}}(\mathbf{q},\omega) = -\frac{\mu_B g}{2N}\sum_{\mathbf{k}} \frac{n_F(\varepsilon^{\mathrm{HF}}_{\mathbf{k},\uparrow}-\mu) - n_F(\varepsilon^{\mathrm{HF}}_{\mathbf{k}+\mathbf{q},\downarrow}-\mu)}{\varepsilon_{\mathbf{k}} - \varepsilon_{\mathbf{k}+\mathbf{q}} - \Delta + \omega + i\eta}. \tag{8.47}$$

The support of the imaginary part of $\chi^{0,\mathrm{HF}}$ and, hence, of χ, is affected by the appearance of the gap Δ: The imaginary part of χ_{-+} is nonzero if there are excitations of pairs of a particle and a hole of opposite spin. Such excitations are called "Stoner excitations". The existence of the gap Δ implies that Stoner excitations at $\mathbf{q} = 0$ require an energy Δ. Zero frequency Stoner excitations require q to be at least equal to the difference between the Fermi momenta of electrons with spin up and spin down. Repeating the arguments of Sec. 6.1, we can find an expression for the support of $\mathrm{Im}\,\chi_{-+}$ in the, for a ferromagnet, somewhat unrealistic case of a parabolic band. For positive ω one finds that, at zero temperature, $\mathrm{Im}\,\chi_{-+}$ is nonzero for

$$-v_F q + \frac{\Delta}{\hbar} + \frac{q^2}{2m\hbar} < \omega < v_F q + \frac{\Delta}{\hbar} + \frac{q^2}{2m\hbar}. \tag{8.48}$$

This support is shown in Fig. 8.5.

Substitution into Eq. (8.30) then yields for $\mathbf{q} \to 0$

$$\chi_{-+}(\mathbf{q}\to 0,\omega) = \left(\frac{g\mu_B}{2}\right)\frac{\Delta}{U\omega}. \tag{8.49}$$

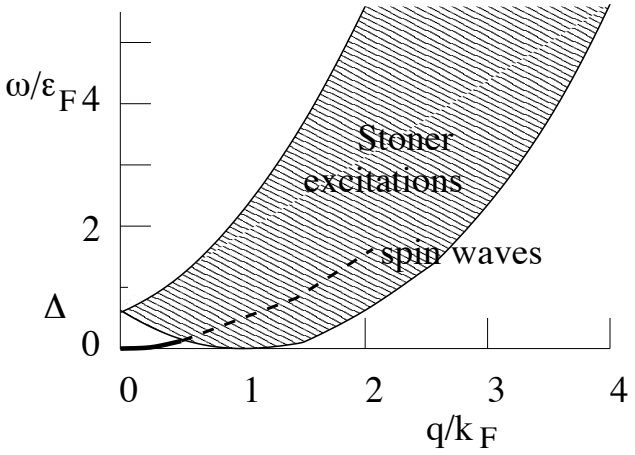

Figure 8.5: Support of the imaginary part of χ_{-+} for a ferromagnet and spin wave dispersion.

The pole of χ as $\omega \to 0$ corresponds to a uniform rotation of the magnetization. This collective excitation has zero frequency because no energy is required for such a uniform rotation. At finite wavevector $\mathbf{q}$, the transverse spin susceptibility χ_{-+} has a pole at frequencies $\omega = Dq^2$, where D is a proportionality constant. Such an excitation is known as a "spin wave". Spin waves are virtually undamped for small wavenumbers. At larger wavenumbers, the spin wave branch enters into the region of the (q, ω) plane where χ_{-+} is complex. Then, spin waves can decay by excitation of "Stoner excitations", a pair of a particle and a hole of opposite spin, see Fig. 8.5.

The fact that spin waves exist at low frequencies if $\mathbf{q} \to 0$ is guaranteed by the rotation symmetry of the ferromagnetic state. A uniform rotation of all spins does not cost energy, and, hence, a long-wavelength spin wave has energy proportional to q^2. Quite generally, low-lying collective modes whose existence is guaranteed by a continuous symmetry of the problem are referred to as "Goldstone modes".

8.6 The transition to a magnetic insulator

In Sec. 8.2 we considered the interaction term in the Hubbard model as a perturbation. Without interactions, the electrons are delocalized. In our treatment, the interaction does not change that; the main effect of interactions is to change the spin susceptibility, and, eventually, beyond the Stoner instability, to create a gap Δ between the self-consistent energy levels of electrons with spin up and spin down.

This perturbative picture should remain correct as long as the interaction energy is small compared to the band width. In this section, the opposite case is investigated, when the band width is small compared to the interaction strength U. This is called the "atomic limit" of the Hubbard model.

In the atomic limit, the coordinate representation is preferred over the momentum representation. Fourier transforming the non-interacting part of the Hamiltonian, Eq. (8.23) above, we find

$$\hat{H}_0 = \sum_{ij,\sigma} t(\mathbf{r}_i - \mathbf{r}_j)\hat{\psi}^\dagger_{i\sigma}\hat{\psi}_{j\sigma}, \tag{8.50}$$

where $\hat{\psi}_{i\sigma}$ is the annihilation operator for an electron with spin σ in Wannier wavefunction $\phi_i(\mathbf{r})$. The interaction Hamiltonian is

$$\hat{H}_1 = U\sum_i n_{i\uparrow}n_{i\downarrow}, \tag{8.51}$$

which is the first term on the r.h.s. of Eq. (8.28) above. The indices "0" and "1" refer to the non-interacting and interacting parts of the Hamiltonian, respectively. As we discussed above, in the atomic limit the Hamiltonian $\hat{H}_1$ is, in fact, dominant.

The problem of studying the full Hamiltonian $\hat{H}_0 + \hat{H}_1$ has proven extremely difficult. Whereas an exact solution has been obtained in one dimension, in two and three dimensions no more than a few limiting are fully understood. In order to make progress, we now make use of the fact that the interaction U is much larger than the band width. Hereto, we write

$$\hat{H}_0 = \hat{H}_{00} + \hat{H}_{01}, \tag{8.52}$$

where

$$\hat{H}_{00} = \sum_{i,\sigma} t(0)\hat{\psi}^\dagger_{i\sigma}\hat{\psi}_{i\sigma}, \quad \hat{H}_{01} = \sum_{i\neq j,\sigma} t(\mathbf{r}_i - \mathbf{r}_j)\hat{\psi}^\dagger_{i\sigma}\hat{\psi}_{j\sigma}, \tag{8.53}$$

and consider $\hat{H}_{01}$ as a perturbation. (Note that $\hat{H}_{00}$ cannot be considered a perturbation, since $t(0)$ determines the position of the band, not the band width.)

Below, we are interested in the retarded single-particle Green function,

$$G_{ij,\sigma}(t) = -i\theta(t)\langle[\hat{\psi}_{i\sigma}(t), \hat{\psi}^\dagger_{j\sigma}(0)]_+\rangle. \tag{8.54}$$

Recall that the poles of the single-particle Green function contain information about the particle-like excitations of the system. Since the "unperturbed" Hamiltonian $\hat{H}_{00} + \hat{H}_1$ is not quadratic in the fermion creation/annihilation operators, the diagrammatic perturbation theory we used in the previous chapters cannot be employed to calculate $G_{ij,\sigma}$. Instead, we

have to calculate Green functions using the equation of motion approach. An illustration of the equation of motion approach for the calculation of phonon Green functions was given in Sec. 2.6 above.

Let us first calculate the single-particle Green function in the absence of the perturbation $\hat{H}_{01}$. In that case, one has

$$\partial_t G_{ij,\sigma}(t) = -i\delta(t)\langle[\hat{\psi}_{i\sigma}(t), \hat{\psi}^\dagger_{j\sigma}(0)]_+\rangle - i\theta(t)\langle[\partial_t\hat{\psi}_{i\sigma}(t), \hat{\psi}^\dagger_{j\sigma}(0)]_+\rangle. \tag{8.55}$$

Using the equation of motion for the annihilation operator $\hat{\psi}_{i\sigma}(t)$,

$$\partial_t\hat{\psi}_{i\sigma}(t) \;=\; -it(0)\hat{\psi}_{i\sigma}(t) - iUn_{i,-\sigma}\hat{\psi}_{i\sigma}(t), \tag{8.56}$$

we find

$$(-i\partial_t + t(0))\, G_{ij,\sigma}(t) \;=\; -\delta(t)\delta_{ij} - (-i)U\theta(t)\langle[n_{i,-\sigma}(t)\hat{\psi}_{i\sigma}(t), \hat{\psi}^\dagger_{j\sigma}(0)]_+\rangle. \tag{8.57}$$

Repeating the same procedure for the Green function that appeared at the r.h.s. of Eq. (8.57), we find

$$\begin{aligned}
&\partial_t\left[-i\theta(t)\langle[n_{i,-\sigma}(t)\hat{\psi}_{i\sigma}(t), \hat{\psi}^\dagger_{j\sigma}(0)]_+\rangle\right] = \\
&= -i\delta(t)\langle[n_{i,-\sigma}(t)\hat{\psi}_{i\sigma}(t), \hat{\psi}^\dagger_{j\sigma}(0)]_+\rangle - t(0)\theta(t)\langle[n_{i,-\sigma}(t)\hat{\psi}_{i\sigma}(t), \hat{\psi}^\dagger_{j\sigma}(0)]_+\rangle \\
&\quad - U\theta(t)\langle[n_{i,-\sigma}(t)^2\hat{\psi}_{i\sigma}(t), \hat{\psi}^\dagger_{j\sigma}(0)]_+\rangle \\
&= -i\delta(t)\delta_{ij}\langle n_{i,-\sigma}\rangle - i(t(0)+U)\left[-i\theta(t)\langle[n_{i,-\sigma}(t)\hat{\psi}_{i\sigma}(t), \hat{\psi}^\dagger_{j\sigma}(0)]_+\rangle\right].
\end{aligned}$$

After Fourier transforming and substitution into Eq. (8.57), we find

$$G_{ij,\sigma}(\varepsilon) = \frac{(1-\langle n_{i,-\sigma}\rangle)\delta_{ij}}{\varepsilon - t(0) + i\eta} + \frac{\langle n_{i,-\sigma}\rangle\delta_{ij}}{\varepsilon - t(0) - U + i\eta}. \tag{8.58}$$

In a paramagnetic state, the expectation value $\langle n_{i,-\sigma}\rangle = n/2$, where n is the electron number density.

The result (8.58) has a very simple interpretation: If an electron of spin $-\sigma$ is present at a site, an added electron with spin σ has energy $t(0)+U$, so that its retarded Green function is $G_{ii,\sigma}(\varepsilon) = 1/(\varepsilon - t(0) - U + i\eta)$. If no electron of spin $-\sigma$ is present, the Green function is $G_{ii,\sigma}(\varepsilon) = 1/(\varepsilon - t(0) + i\eta)$. The probability that an electron of spin $-\sigma$ is present is $\langle n_{i,-\sigma}\rangle$, hence Eq. (8.58).

Once the hopping term $\hat{H}_{01}$ is included, the equation of motion for the Green function can no longer be truncated. However, following Hubbard, one can make the following "guess"

for the result. It should be pointed out, however, that this guess has no formal justification; nevertheless, as you'll see below, it conveys a compelling picture of how the system behaves. The single-electron Green function (8.58) can be interpreted as the inverse of $\varepsilon - \Sigma_i$, where Σ_i is a measure of the energy of an electron at site i, including the interaction modifications. Without interactions, the Green function of the electron would be $G_{\mathbf{k},\sigma} = 1/(\varepsilon - \varepsilon_{\mathbf{k}} + i\eta)$, where

$$\varepsilon_{\mathbf{k}} = t(0) + \sum_{i \neq j} e^{-i\mathbf{k}\cdot(\mathbf{r}_i - \mathbf{r}_j)} t(\mathbf{r}_i - \mathbf{r}_j). \tag{8.59}$$

Note that we switched to the momentum representation. With interactions, we replace $\varepsilon - t(0)$ by $(G_{ii,\sigma}(\varepsilon))^{-1}$. Hence, we find

$$G^{\mathrm{H}}_{\mathbf{k}\sigma} = \frac{1}{(G_{ii\sigma}(\varepsilon))^{-1} - (\varepsilon_{\mathbf{k}} - t(0)) + i\eta}. \tag{8.60}$$

Let us now consider the positions of the poles of the Green function $G^{\mathrm{H}}_{\mathbf{k}\sigma}$. They are at the solutions of the equation

$$(\varepsilon - t(0))(\varepsilon - t(0) - U) = (\varepsilon_{\mathbf{k}} - t(0))(\varepsilon - t(0) - U(1 - n/2)). \tag{8.61}$$

You verify that for $n \to 0$ or $U \to 0$ one recovers the Bloch band $\varepsilon = \varepsilon_{\mathbf{k}}$. You also verify that for the limit of very small bandwidth $\max|\varepsilon_{\mathbf{k}} - t(0)| \ll U$ the solutions approach the on-site energies $t(0)$ and $t(0) + U$ of the Hubbard model in the atomic limit. The effect of the inter-site hopping is to change the N-fold degenerate solutions $\varepsilon = t(0)$ and $\varepsilon = t(0) + U$ into narrow bands around $t(0)$ and $t(0) + U$. For $\max|\varepsilon_{\mathbf{k}} - t(0)| \ll U$ these bands are given by

$$\varepsilon = t(0)(n/2) + \varepsilon_{\mathbf{k}}(1 - n/2), \quad \varepsilon = t(0)(1 - n/2) + U + \varepsilon_{\mathbf{k}}(n/2). \tag{8.62}$$

A schematic picture of these bands is shown in Fig. 8.6.

In general, the two bands may overlap. An exception is the case that n is close to 1. The case $n = 1$ is known as "half filling", since it amounts to half of the maximum possible number of electrons in the system. At $n = 1$, the two bands are always separated, although one may question whether this result is realistic for small U. Since the lowest band is fully filled at $n = 1$, there is an excitation gap, and the system becomes an insulator. In this case, the excitation gap is referred to as "Coulomb gap" and the insulating state is known as a "Mott insulator".

8.7 Heisenberg model

The Heisenberg model gives a description for an insulating magnet. The magnetization arises from the alignment of local magnetic moments, not from the shift of Fermi levels for

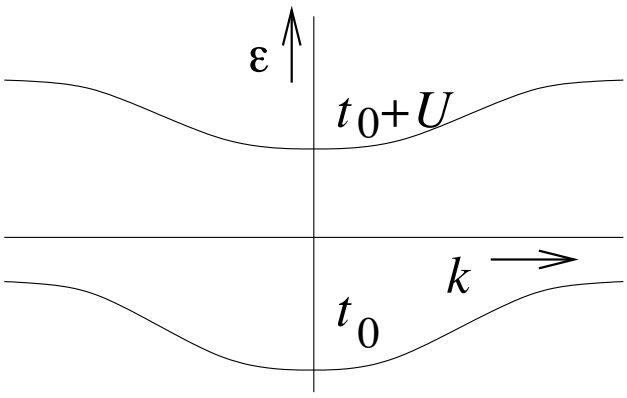

Figure 8.6: Schematic picture of the two energy bands for the Hubbard model for the case that the interaction U is much larger than the bandwidth.

"majority" and "minority" electrons.[6]

The Heisenberg model is described by the Hamiltonian

$$\begin{aligned}\mathcal{H}_{\rm Heis} &= \sum_{ij\,\rm nn} J\mathbf{s}_i\cdot\mathbf{s}_j \\ &= \sum_{ij\,\rm nn} J(s_i^x s_j^x + s_i^y s_j^y + s_i^z s_j^z) \qquad (8.63)\\ &= \sum_{ij\,\rm nn} J\left(\frac{1}{2}s_i^+ s_j^- + \frac{1}{2}s_i^- s_j^+ + s_i^z s_j^z\right). \qquad (8.64)\end{aligned}$$

In writing (8.64), we consider a lattice whose sites are labeled with the index i, the summation is over nearest neighbor pairs i and j on this lattice only, and $\mathbf{s}_i$ denotes the spin 1/2 operator at site i. In principle, one can include next-nearest neighbor interactions, etc., in the Hamiltonian (8.64). The spin operators commute for different sites, and obey the usual spin commutation relations on the same sites. Thus, in terms of the spin raising and lowering operators,

$$[s_i^-, s_j^z] = \delta_{ij}s_i^-, \quad [s_i^+, s_j^z] = -\delta_{ij}s_i^+ \quad [s_i^+, s_j^-] = 2\delta_{ij}s_i^z \qquad (8.65)$$

$$[s_i^x, s_j^y] = i\delta_{ij}s_i^z, \text{ and cyclic.} \qquad (8.66)$$

We will take the quantum Heisenberg model as a starting point here; the Heisenberg model with antiferromagnetic coupling ($J > 0$) can be derived from the Hubbard model at half filling, with nearest-neighbor hopping and large positive U, see exercise 8.7.

[6]Parts of this section are based on lecture notes by W. van Saarloos, Leiden, 1996.

In the literature, sometimes an anisotropic version of the Heisenberg model (8.64) is studied,

$$\begin{aligned}\mathcal{H}^{\text{anis}}_{\text{Heis}} &= \sum_{ij\,\text{nn}} \left[J_\perp(s^x_i s^x_j + s^y_i s^y_j) + J_z s^z_i s^z_j\right] \\ &= \sum_{ij\,\text{nn}} \left[\frac{J_\perp}{2}(s^+_i s^-_j + s^-_i s^+_j) + J_z s^z_i s^z_j\right]. \end{aligned} \tag{8.67}$$

Clearly, in this case the model is not invariant under arbitrary rotations of the spins, but is invariant for rotations of the spins about the z-axis.[7]

Despite its simplicity, the Heisenberg model is difficult to study analytically. One reason that is of interest to us, is that Wick's theorem does not hold for the Heisenberg model. Hence, we cannot rely on the diagrammatic perturbation theory.

An important question of interest for the Heisenberg model is when and how a magnetic phase is formed. This question is in the realm of the theory of phase transitions and critical phenomena, and we will not discuss it here. Instead, we will assume that a low-temperature magnetic phase exists, and aim at a description of the possible excitations of the system in the low-temperature magnetic phase and the high-temperature paramagnetic phase. We will carry out this program in detail for the ferromagnetic Heisenberg model, for which the low-temperature magnetic phase is the fully polarized phase. For the antiferromagnetic Heisenberg model, this question is much more difficult, as the precise nature of the antiferromagnetic phase is not known.

Let us now turn to the isotropic ferromagnetic ($J < 0$) Heisenberg model (8.64) in absence of a field to introduce the concept of spin-waves in more detail. The case of the ferromagnetic Heisenberg model is particularly simple — but somewhat a-typical — in that the order parameter associated with the broken symmetry, the total magnetization, is also a conserved quantity. (This is sometimes referred to as an *exact spontaneously broken symmetry.*)
Since the total spin $\mathbf{S}$ commutes with $\mathcal{H}_{\text{Heis}}$, we can diagonalize the Hamiltonian in each subspace of eigenvalues of the operator S^z. Let $|+\rangle$ denote the state with all the spins pointing up, so that $S^z|+\rangle = (N/2)|+\rangle$, where N is the total number of spins. The state $|+\rangle$ is the ground state of $\mathcal{H}_{\text{Heis}}$ if $J < 0$, although it is not the only possible ground state. In

[7] In passing, we note that for $J_\perp = 0$, $\mathcal{H}^{\text{anis}}_{\text{Heis}}$ reduces to the celebrated Ising model, which plays a central role in the theory of critical phenomena. Unlike the Heisenberg model, the Ising model does not have a continuous symmetry, and, as a result, the Ising model has no Goldstone modes. On a bipartite lattice, the antiferromagnetic Ising model at zero magnetic field is equivalent to the ferromagnetic Ising model. This result does not extend to the Heisenberg model; the ferromagnetic and antiferromagnetic Heisenberg models are fundamentally different.

fact, all states obtained from $|+\rangle$ by multiple operation of the total spin lowering operator,

$$S^- = \sum_i s_i^- \tag{8.68}$$

are ground states of the Heisenberg Hamiltonian as well. For a hypercubic lattice in d dimensions, the ground state energy is $E_0 = dNJ/4$.

Since the ground state of the ferromagnetic Heisenberg model is so simple, some low-lying excitations, the spin waves — can be determined exactly. A spin-wave state with wavevector $\mathbf{q}$ is created by the operator $S_\mathbf{q}^-$ operating on the fully polarized state $|+\rangle$, with

$$S_\mathbf{q}^- = N^{-1/2} \sum_i e^{i\mathbf{q}\cdot\mathbf{r}_i} s_i^-. \tag{8.69}$$

You verify that a state with a single spin wave is an exact eigenstate of the Heisenberg Hamiltonian $\mathcal{H}_{\rm Heis}$, at energy $E_0 + \hbar\omega_\mathbf{q}$, where E_0 is the ground state energy and

$$\hbar\omega_\mathbf{q} = \frac{|J|}{2} \sum_\delta (1 - e^{i\mathbf{q}\cdot\delta}), \tag{8.70}$$

where the vector δ is summed over all nearest-neighbor directions in the lattice. For small $\mathbf{q}$, the energy $\omega_\mathbf{q}$ increases proportional to q^2. Note that, for $\mathbf{q} \to 0$, the state $S_\mathbf{q}^-|+\rangle = |\mathbf{q}\rangle$ approaches the uniformly rotated state $S^-|+\rangle$ continuously, and therefore we expect the excitation energy $\hbar\omega_\mathbf{q}$ of this mode to vanish continuously as $\mathbf{q} \to 0$. This again illustrates that the appearance of such "low lying modes" or "Goldstone modes" for $\mathbf{q}$ small is a general phenomenon when a continuous symmetry is broken.

The spin-wave state $|\mathbf{q}\rangle$ is a collective mode; it describes a delocalized state with many spin excitations involved. For small $\mathbf{q}$, it describes a slow rotation of the spins about the z-axis. To make this more explicitly, one can calculate the expectation value of the transverse spin correlation in the state $|\mathbf{q}\rangle$,

$$\langle \mathbf{q}| s_i^x s_j^x + s_i^y s_j^y |\mathbf{q}\rangle = \frac{1}{N} \cos[\mathbf{q}\cdot(\mathbf{i} - \mathbf{j})]. \tag{8.71}$$

Spin waves do interact: the two-spin wave state $S_{\mathbf{q}_1}^- S_{\mathbf{q}_2}^-|+\rangle$ is not an exact eigenstate of the Hamiltonian (8.64). On the other hand, spin-wave interactions are small if the number of excited spin wave modes is small. Then, the spin waves can be considered independent boson modes, their distribution being given by the Bose-Einstein distribution function. The picture of independent spin wave modes leads to the Bloch $T^{3/2}$ law for the temperature dependence

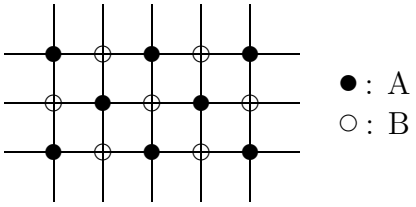

Figure 8.7: An example of a bipartite lattice. Every neighbor of the A sublattice is a site on the B sublattice, and vice versa.

of the low-temperature magnetization in three dimensions, $\langle S_z(T)\rangle - \langle S_z(T=0)\rangle \propto T^{3/2}$.[8] For one and two dimensions, the density of states of low-energy spin waves is higher than in three dimensions; there is no regime of a small number of excited spin waves, leading to a breakdown of the ferromagnetic state in one and two dimensions.

Within the Green function approach, these conclusions can be arrived at if we look at the retarded transverse spin-spin correlation function,

$$R^R_{ij}(t) = -i\theta(t)\langle[s^-_i(t), s^+_j(0)]_-\rangle, \tag{8.72}$$

which is the Heisenberg-model equivalent of the transverse spin susceptibility χ_{-+} we studied previously. (Note that the correlation function contains a commutator of spin operators, since spin operators satisfy commutation relations.) The function $R^R_{ij}(t)$ describes the response of the spin polarization to a magnetic field, where both the response and the field are perpendicular to the z axis, which is presumed to be the direction of spontaneous magnetization. The poles of the correlation function corresponds to the collective modes. Further, the spin-spin correlation function is related to the average magnetization through the relation

$$\lim_{t\downarrow 0} R^R_{ij}(t) = 2i\langle s^z\rangle\delta_{ij}. \tag{8.73}$$

In order to calculate the transverse spin-spin correlation function, we consider its equation of motion

$$\frac{\partial}{\partial t}R^R_{ij}(t) = 2i\delta(t)\langle s^z_i\rangle - \theta(t)\sum_l \langle J_{li}[s^-_l(t)s^z_i(t) - s^z_l(t)s^-_i(t), s^+_j(0)]_-\rangle, \tag{8.74}$$

where we defined $J_{li} = J$ if l and i are nearest neighbor sites and $J_{li} = 0$ otherwise. In order to close this equation of motion, we replace the operator $s^z_i(t)$ by the average $\langle s^z\rangle \equiv \langle s^z_i\rangle$ in

[8] See, e.g., *Solid State Physics*, by N. W. Ashcroft and N. D. Mermin, Saunders (1976), and the discussion below.

the ferromagnetic state,[9]

$$\frac{\partial}{\partial t}R_{ij}^R(t) = 2i\delta(t)\langle s_i^z\rangle - i\langle s^z\rangle \sum_l J_{li}(R_{lj}^R(t) - R_{ij}^R(t)). \tag{8.75}$$

The justification for this approximation is that, in the ferromagnetic state, fluctuations of s_i^z around its average are small. Moreover, since Eq. (8.75) contains a sum over nearest neighbors, only the sum of s_i^z over nearest neighbors is important. In high dimensions, the summation over nearest neighbors leads to an even further reduction of fluctuations, and one expects the approximation $s_i^z \approx \langle s^z\rangle$ to continue to hold outside the almost fully polarized ferromagnetic state. Solving Eq. (8.75) by means of a Fourier transform, we find

$$R_{\mathbf{k}}(\omega) = -\frac{2\langle s^z\rangle}{\omega + \omega_{\mathbf{k}} + i\eta}, \tag{8.76}$$

where

$$\omega_{\mathbf{k}} = \langle s^z\rangle J \sum_\delta (1 - e^{-i\mathbf{k}\cdot\delta}), \tag{8.77}$$

the summation being over all nearest-neighbor vectors δ. Note that this solution satisfies the relation (8.73).

For zero temperature, $\langle s^z\rangle = s$, and we recover the spin-wave dispersion relation (8.70). For finite temperatures, the spin-wave frequencies depend on the average spin polarization $\langle s^z\rangle$, which, in turn, is a function of the temperature T. In order to determine $\langle s^z\rangle$, we use the "greater" correlation function,

$$R_{ij}^>(t) = -i\langle s_i^-(t)s_j^+(0)\rangle, \tag{8.78}$$

for which one has

$$R_{ii}^>(0) = -is(s+1) + i\langle s^z(s^z+1)\rangle. \tag{8.79}$$

In keeping with the approximations we made previously, we neglect fluctuations of s_z and set

$$R_{ii}^>(0) \approx -is(s+1) + i\langle s^z\rangle(\langle s^z\rangle + 1). \tag{8.80}$$

We calculate $R_{ij}^>(t)$ from the retarded correlation function (8.76) using the general relation (2.49),

$$\begin{aligned} R_{\mathbf{k}}^>(\omega) &= 2i\frac{\operatorname{Im} R_{\mathbf{k}}^R(\omega)}{1 - e^{-\hbar\omega/T}} \\ &= 4\pi i\frac{\langle s^z\rangle\delta(\omega + \omega_{\mathbf{k}})}{1 - e^{-\hbar\omega T}}. \end{aligned} \tag{8.81}$$

[9]This approximation is the equivalent of the Weiss molecular field approximation, see, e.g, *Statistical and Thermal Physics*, F. Reif, Mc Graw Hill, 1965.

Performing the inverse Fourier transform, we then find

$$R_{ii}^{>}(0) = -\frac{2i}{N}\sum_{\mathbf{k}} \frac{1}{e^{\hbar\omega_{\mathbf{k}}/T}-1}, \tag{8.82}$$

from which we derive the self-consistency equation

$$s(s+1) - \langle s^z\rangle(\langle s^z\rangle + 1) = \langle s^z\rangle \frac{2}{N}\sum_{\mathbf{k}} \frac{1}{e^{\hbar\omega_{\mathbf{k}}/T}-1}. \tag{8.83}$$

In the limit $T \to 0$ the r.h.s. vanishes in three dimensions and above, recovering the solution $\langle s^z\rangle = s$ at $T = 0$. For one and two spatial dimensions, the r.h.s. does not vanish as $T \to 0$, implying the breakdown of the ferromagnetic state by spin wave generation, as we discussed previously. For low temperatures and three dimensions, one find $\langle s^z(T=0)\rangle - \langle s^z(T)\rangle \propto T^{3/2}$, which is the Bloch $T^{3/2}$ law mentioned previously.

The self-consistent relation could be used to find the Curie temperature, the highest temperature at which the spontaneous magnetization exists. However, close to the Curie temperature, spin fluctuations are abundant, and the approximation $s_i^z \to \langle s^z\rangle$ we made in the derivation of Eq. (8.83) is not justified in systems with low dimensionality.

We now turn to the antiferromagnetic Heisenberg model $J > 0$. Classically, an antiferromagnetic state is possible only if the lattice is bipartite: it can be separated in sublattices A and B such that all nearest neighbors of a site in lattice A belong to lattice B and vice versa, see Fig. 8.7. If the lattice is not bipartite, the antiferromagnet is "frustrated", and a completely different physical picture arises, which we do not discuss here. The classical antiferromagnetic ground state is a state in which spins on one sublattice point "up", whereas spins on the other sublattice point "down". This state is known as the "Néel state". Intuitively, we expect that the Néel state is the ground state of the quantum antiferromagnetic Heisenberg model as well. However, the Néel state is not an exact eigenstate of $\mathcal{H}_{\text{Heis}}$![10] Nevertheless the true ground state has strong antiferromagnetic correlations reminiscent of this state.

Even though the classical Néel state is not the exact ground state, it does suggest a definition of the antiferromagnetic "order parameter", which takes the role of the magnetization for the ferromagnetic Heisenberg model. Let us consider a hypercubic lattice with lattice spacing a in d dimensions and let a reference spin on sublattice A point up; then the so called "staggered magnetization" is defined as

$$M_i^{\text{AF}} = \begin{cases} \langle s_i^z\rangle & \text{if } \mathbf{r}_i \text{ in sublattice } A, \\ -\langle s_i^z\rangle & \text{if } \mathbf{r}_i \text{ in sublattice } B \end{cases}. \tag{8.84}$$

[10]The classical Néel state is the ground state of $\mathcal{H}_{\text{Heis}}^{\text{anis}}$ with $J_z > 0$ and $J_\perp = 0$, but not of the model with $J_\perp \neq 0$.

In the classical Néel state, this order parameter is 1/2 for all sites.

This choice of the order parameter may be justified for a Heisenberg model with spin $s \gg 1/2$. The larger the spin s is, the more "classical" the behavior of the model becomes, as the commutation relations (and hence fluctuations) become less important. In the classical limit, we can represent the spins by vectors on a sphere of radius s. In this $s \to \infty$ classical limit, the ground state of the antiferromagnetic Heisenberg model consists of vectors pointing in opposite directions on the two sublattices. In this limit, (8.84) is a good order parameter, whose value approaches s for s large.

In recent years, there has been a lot of research on the properties of quantum antiferromagnets, in particular in $d = 2$. Research on two-dimensional antiferromagnets was motivated to a large extent by the discovery of high temperature superconductors, which are obtained by doping compounds which are layered insulating quantum antiferromagnets. The consensus, based on many large scale numerical simulations, is that the ground state of the two dimensional Heisenberg model with spin 1/2 does have antiferromagnetic order, but that the order parameter (8.84) is reduced from the classical Néel value 1/2 to about 0.34.

In the ferromagnetic case, the order parameter was a conserved quantity and as a result a single spin wave state $|\mathbf{q}\rangle$ was an exact eigenstate of the Hamiltonian. In the present case, the staggered order parameter (8.84) is not a conserved quantity, and the spin wave analysis can not be performed exactly (after all, the ground state is not known exactly either!), so we have to resort to an approximate treatment. In order to understand the nature of the approximation better, it will turn out to be useful to look at the Heisenberg model for the case of large spin s. Since we expect the ground state to get closer to the classical Néel state for large s, increasing s gives us a way to get a controlled approximation.

As in the case of a ferromagnet, to analyze spin waves we need to consider states where one spin is flipped. Since the ground state is not explicitly known, it is more convenient to use (in the Heisenberg picture) the equation of motion for the spin flip operator. Using the commutation relations (8.65) (which are also valid for arbitrary spin s), we get

$$\frac{\partial s_{\mathbf{i}}^-}{\partial t} = \frac{1}{i\hbar}[s_{\mathbf{i}}^-, \mathcal{H}_{\text{Heis}}] = \frac{J}{i\hbar} \sum_{\delta} \left(s_{\mathbf{i}}^- s_{\mathbf{i}+\delta}^z - s_{\mathbf{i}+\delta}^- s_{\mathbf{i}}^z \right). \tag{8.85}$$

As before, the sum over δ is a sum over the nearest neighbor vectors on the quadratic ($d = 2$) or cubic ($d = 3$) lattice.

For large s, spin waves consist of minor distortions of the Néel state, with the z-component of the spin slightly reduced from its maximal value $+s$ on the A sublattice, and slightly increased from its minimal value $-s$ on the B sublattice. To a good approximation, we can then write in (8.85) $s_{\mathbf{i}}^z|\text{ground state}\rangle \approx \pm s|\text{ground state}\rangle$ depending on whether $\mathbf{r}_i$ is on the

A or B sublattice. Using the notation

$$|\mathbf{i}\rangle_A = s_{\mathbf{i}}^-|\text{ground state}\rangle \qquad \text{for } \mathbf{r}_i \text{ in sublattice } A, \tag{8.86}$$

$$|\mathbf{i}\rangle_B = s_{\mathbf{i}}^+|\text{ground state}\rangle \qquad \text{for } \mathbf{r}_i \text{ in sublattice } B, \tag{8.87}$$

we then get from (8.85)

$$\begin{aligned} \frac{\partial}{\partial t}|\mathbf{i}\rangle_A &= \frac{J}{i\hbar}\left(-2ds|\mathbf{i}\rangle_A - s\sum_\delta |\mathbf{i}+\delta\rangle_B\right), \\ \frac{\partial}{\partial t}|\mathbf{i}\rangle_B &= \frac{J}{i\hbar}\left(\ \ 2ds|\mathbf{i}\rangle_B + s\sum_\delta |\mathbf{i}+\delta\rangle_A\right). \end{aligned} \tag{8.88}$$

Since the two sublattices are distinct, we now have two coupled equations, instead of one in the case of a ferromagnet. The equations for the spin waves can be solved by introducing Fourier transforms,

$$|\mathbf{q}\rangle_A = N_A^{-1/2}\sum_{\mathbf{i}\in A} e^{i\mathbf{q}\cdot\mathbf{i}}|\mathbf{i}\rangle_A, \quad |\mathbf{q}\rangle_B = N_B^{-1/2}\sum_{\mathbf{i}\in B} e^{i\mathbf{q}\cdot\mathbf{i}}|\mathbf{i}\rangle_B. \tag{8.89}$$

Writing the temporal evolution of these modes as $e^{-i\omega_{\mathbf{q}}t}$, we then get from (8.88) the dispersion relation

$$\begin{vmatrix} \hbar\omega_{\mathbf{q}} + 2dsJ & 2dsJ\gamma_{\mathbf{q}} \\ -2dsJ\gamma_{\mathbf{q}} & \hbar\omega_{\mathbf{q}} - 2dsJ \end{vmatrix} = 0, \quad \gamma_{\mathbf{q}} = \frac{1}{2d}\sum_\delta e^{i\mathbf{q}\cdot\delta}. \tag{8.90}$$

Solution of Eq. (8.90) yields

$$\hbar\omega_{\mathbf{q}} = 2dsJ\sqrt{1-\gamma_{\mathbf{q}}^2}. \tag{8.91}$$

By expanding $\gamma_{\mathbf{q}}$ for small q, we find that long wavelength antiferromagnetic spin waves have a *linear* dispersion

$$\omega_q \approx 2sJq\sqrt{d}, \quad q \ll 1. \tag{8.92}$$

This linear dispersion is reminiscent of that of acoustic phonons in a crystal. The difference between the quadratic dispersion of ferromagnetic spin waves and the linear dispersion of the antiferromagnetic spin waves — the Goldstone modes of the antiferromagnet — can be traced to the fact that in the first case, the order parameter itself is conserved. This is rather exceptional, and indeed Goldstone modes usually have a linear dispersion.

Our earlier discussion implies that (8.92) is a good approximation for large s. Although the estimate of the spin wave velocity $c = sJ\sqrt{2d}/\hbar$ may not be that accurate for spin 1/2, the linearity of the antiferromagnetic spin wave dispersion is a robust feature that is not affected by the approximations made.

In closing this section, we note that the present analysis may be extended to a systematic $1/s$ expansion for quantities like the spin wave velocity and the order parameter. Quantum mechanical fluctuations are more and more suppressed as s increases. Intuitively, this becomes clear from the fact that for $s = 1/2$, the operators s_i^+ or s_i^- lead to a local reversion of the spin, and hence tends to locally make the order parameter of the wrong sign. For large s, these operators just reduce the z-component of the spin slightly — they do not lead to a complete spin reversal.

8.8 Exercises

Exercise 8.1: Spin susceptibility

The Thomas-Fermi approximation (8.22) for the spin susceptibility in an interacting electron gas is not correct. It neglects the structure of the interaction on the scale of the Fermi wavelength. A better approximation is made when the full Thomas-Fermi screened interaction is used,

$$V_{\mathbf{q}}^{\mathrm{RPA}}(i\omega_n) = \frac{e^2}{\epsilon_0(q^2 + k_s^2)} \quad \text{if } \mathbf{q},\, \omega_n \to 0,$$

see Eq. (7.45). Hence, the momentum-dependence of the screened interaction is taken into account, but retardation effects are neglected.

(a) Argue that, in the limit $\mathbf{q} \to 0$, the renormalized vertex $\Gamma(\mathbf{k}, i\omega_m; \mathbf{k}+\mathbf{q}, i\omega_m + i\Omega_n)$ of Eq. (8.15) does not depend on the direction of the wavevector $\mathbf{k}$ or on the energy ω_m.

(b) Since $\Gamma(\mathbf{k}, i\omega_m; \mathbf{k}+\mathbf{q}, i\omega_m + i\Omega_n)$ of Eq. (8.15) does not depend on the direction of the wavevector $\mathbf{k}$, the effective interaction $V^{\mathrm{eff}}_{\mathbf{k}-vk'}$ in the vertex equation (8.15) may be integrated over the directions of $\mathbf{k}'$. Show that the integrated interaction is

$$V^{\mathrm{eff}}_{\mathbf{k},\mathbf{k}'} = \frac{e^2}{4\epsilon_0 k k'} \ln \frac{k_s^2 + (k+k')^2}{k_s^2 + (k-k')^2}. \tag{8.93}$$

(c) Argue that the renormalized vertex is determined by the effective interaction at the Fermi level. From here, derive the result

$$\chi_{-+}^{\mathrm{RPA}} = \frac{\nu \mu_B g}{2 - (2/3\pi^2)^{2/3} r_s \ln(1 + (3\pi^2/2)^{2/3}/r_s)}. \tag{8.94}$$

(d) Can you explain this result qualitatively in the limits $r_s \ll 1-$ and $r_s \gg 1$?

Exercise 8.2: Specific heat

Verify Eq. (8.35) for the low-temperature specific heat of the Hubbard model close to the Stoner instability. For your verification is is sufficient if you find the order of magnitude of the proportionality constant in Eq. (8.35). You do not need to find precise numerical coefficients.

Exercise 8.3: Ferromagnet with parabolic dispersion relation

In this exercise we consider the Hubbard model, with a parabolic dispersion of the band energies $\varepsilon_{\mathbf{k}}$. This model is somewhat unrealistic, but it allows us to calculate many quantities in closed form.

(a) Using the Hartree-Fock energy levels, show that the spin polarization

$$\zeta = \frac{\bar{n}_\uparrow - \bar{n}_\downarrow}{\bar{n}_\uparrow + \bar{n}_\downarrow} \tag{8.95}$$

obeys the equation

$$U \left(\frac{n}{9\pi^4}\right)^{1/3} \frac{2m\zeta}{\hbar^2} = (1+\zeta)^{2/3} - (1-\zeta)^{2/3}. \tag{8.96}$$

Here $n = \bar{n}_\uparrow + \bar{n}_\downarrow$ is the total electron density. Find a relation between ζ and the energy gap Δ.

(b) Analyze Eq. (8.95) and find for what values of the Hubbard interaction strength U a spontaneous spin polarization is formed.

(c) Show that, if the Hubbard interaction strength U is further increased, a full polarization is achieved, $\zeta = \pm 1$. This situation is known as a half metal.

(d) Calculate the transverse spin susceptibility χ_{-+} for low frequencies and long wavelengths. What is the spin-wave dispersion that you find from your answer?

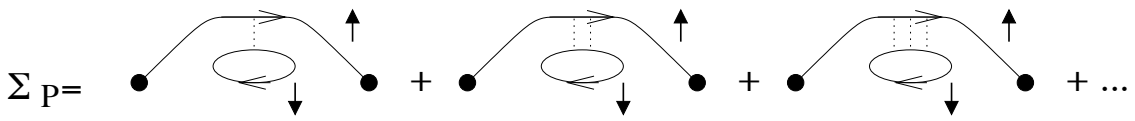

Figure 8.8: Singular contribution to the electron self energy at the Stoner instability.

Exercise 8.4: Self-energy correction

Close to the Stoner instability point there are important corrections to the self energy that are not included in the Hartree-Fock approximation. One of the leading corrections is shown in Fig. 8.8.

(a) Calculate the contribution to the self energy shown in Fig. 8.8 for the Hubbard model.

(b) Discuss how the self-energy correction you calculated under (a) affects the electron effective mass m^* and the density of states at the Fermi level.

Exercise 8.5: Coulomb gap

In this exercise, we consider the ansatz (8.58) for the single particle Green function of the Hubbard model. The Green function not only contains information about the possible single-particle excitations through its poles, but also through the spectral weight of each pole.

(a) Find the spectral weights for the case of large U, $U \gg \max|\varepsilon_{\mathbf{k}} - t(0)|$, for which you can use Eqs. (8.62) for the poles of the Green function.

(b) Do the same for the case of small U, $U \ll \max|\varepsilon_{\mathbf{k}} - t(0)|$. Formulate your answer for the case $n \ll 1$ and $n = 1$ separately.

Exercise 8.6: Bloch $T^{3/2}$ law

Derive the Bloch $T^{3/2}$ law for the magnetization of a three-dimensional ferromagnet from Eq. (8.83).

Exercise 8.7: Antiferromagnetic Heisenberg model from large-U Hubbard model at half filling

In this exercise we consider the Hubbard model with nearest neighbor hopping,

$$\mathcal{H}_{\text{Hub}} = -t \sum_{ij\,\text{nn},\sigma} \left(\hat{\psi}^\dagger_{i\sigma} \hat{\psi}_{j\sigma} + \hat{\psi}^\dagger_{j\sigma} \hat{\psi}_{i\sigma} \right) + U \sum_i n_{i\uparrow} n_{i\downarrow}. \tag{8.97}$$

(a) When $U = 0$, the Hubbard model describes non-interacting electrons, and we can explicitly determine the single electron energies $\varepsilon_{\mathbf{k}}$. Show that these are given by Eq. (8.37) above.

Because of the Pauli principle, there can not be more than two electrons per site. Let us from now on consider half filling, i.e. the case where there is one electron per site. Moreover, we consider the limit of large positive U ($U \gg t$). Then it is energetically very unfavorable to have two electrons on the same site — in other words the low energy sector of the Hilbert space is the one where all sites are occupied by one electron. Our strategy now will be to project onto this part of Hilbert space of singly occupied sites.

What will the interactions look like? Well, the operator $n_{i\uparrow} n_{i\downarrow}$ only counts whether a site is doubly occupied, therefore it does not depend on the absolute spin direction. Therefore, the effective spin interaction will only depend on the *relative* spin orientation, in other words, it will be of the Heisenberg type $\mathbf{s}_i \cdot \mathbf{s}_j$.

Furthermore the interaction will be antiferromagnetic. Physically, this can be seen as follows. Virtual excitations to states in which one site is doubly occupied involve the hop of an electron to a neighboring site and back (see the figure); in the intermediate state, there is an extra energy U associated with the double occupancy.

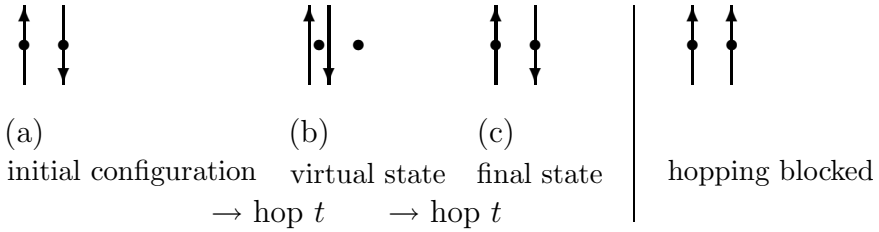

(b) Argue that, with these considerations, the large-U Hubbard model at half filling reduces to an antiferromagnetic Heisenberg model with interaction $J = 2t^2/U$.

The range over which the antiferromagnetic phase exists as a function of the ratio U/t and doping of the Hubbard model, is still under active investigation.

Chapter 9

Phonons and Electron-phonon interaction

In the previous chapters we have looked at the dynamics of electrons in a metal. In this chapter, we'll consider the lattice ions, their mutual interaction, and the interaction between lattice ions and electrons. Just like the presence of the electron gas modifies the electron-electron interaction, and leads to an effective, or "screened" interaction, the presence of the ionic lattice and the interaction between electrons and phonons causes a modification of the electron-electron interaction. This phonon-modified interaction is attractive, and is the root cause for superconductivity.

9.1 Normal modes

We consider the dynamics of the atoms of a lattice. The atoms interact via a potential $\mathcal{V}(\{\mathbf{x}_i\})$ that depends on the location $\mathbf{x}_i$ of all atoms $i = 1, \ldots, N$. Each atom has an equilibrium position $\mathbf{r}_i$. For small displacements $\mathbf{u}_i = \mathbf{x}_i - \mathbf{r}_i$ from equilibrium, the Hamiltonian for the lattice atoms can be expanded in a series in the displacements $\mathbf{u}_i$. The first order term in the expansion vanishes, since the potential $\mathcal{V}$ is a minimum at the equilibrium positions of the atoms. If we truncate the expansion at the second order, we have

$$H = \sum_{i=1}^{N} \frac{\mathbf{p}_i^2}{2M} + \frac{1}{2} \sum_{i,j} \sum_{\alpha\beta} u_{i\alpha} u_{j\beta} V_{\alpha;\beta}(\mathbf{r}_i, \mathbf{r}_j), \tag{9.1}$$

where the numbers $V_{\alpha;\beta}(\mathbf{r}_i, \mathbf{r}_j)$ are derivatives of the potential $\mathcal{V}$ at the equilibrium positions $\mathbf{r}_i$, $\mathbf{r}_j$,

$$V_{\alpha;\beta}(\mathbf{r}_i, \mathbf{r}_j) = \partial_{x_{i\alpha}} \partial_{x_{j\beta}} \mathcal{V}(\{\mathbf{r}_i\}). \tag{9.2}$$

The displacement and momentum operators $\mathbf{u}_i$ and $\mathbf{p}_j$ have canonical commutation relations,

$$[p_{i\alpha}, p_{j\beta}]_- = [u_{i\alpha}, u_{j\beta}]_- = 0 \tag{9.3}$$

$$[p_{i\alpha}, u_{j\beta}]_- = -i\hbar\delta_{\alpha\beta}\delta_{ij}. \tag{9.4}$$

For an infinite lattice or for a lattice with periodic boundary conditions, the real numbers $V_{\alpha;\beta}(\mathbf{r}_i, \mathbf{r}_j))$ depend on the difference $\mathbf{r}_i - \mathbf{r}_j$ only. Inversion symmetry implies $V_{\alpha;\beta}(\mathbf{r}_i - \mathbf{r}_j) = V_{\alpha;\beta}(\mathbf{r}_j - \mathbf{r}_i)$, and, since derivatives can be taken in any order, $V_{\alpha;\beta}(\mathbf{r}_i - \mathbf{r}_j) = V_{\beta;\alpha}(\mathbf{r}_i - \mathbf{r}_j)$. The approximation (9.1) in which the Hamiltonian of the lattice atoms is truncated after the quadratic term in the displacements is known as the "harmonic approximation".

The Hamiltonian (9.1) can be brought to diagonal form by a suitable basis transformation. We construct this basis transformation in two steps. First, we perform a Fourier transform with respect to the lattice coordinate $\mathbf{r}_i$ and define

$$\mathbf{p}_\mathbf{k} = \frac{1}{\sqrt{N}} \sum_j e^{i\mathbf{k}\cdot\mathbf{r}_j} \mathbf{p}_j \tag{9.5}$$

$$\mathbf{u}_\mathbf{k} = \frac{1}{\sqrt{N}} \sum_j e^{-i\mathbf{k}\cdot\mathbf{r}_j} \mathbf{u}_j. \tag{9.6}$$

Here and below, the wavevector $\mathbf{k}$ is in the first Brillouin zone of the reciprocal lattice. After Fourier transform, the operators $\mathbf{p}_\mathbf{k}$ and $\mathbf{u}_\mathbf{k}$ still obey canonical commutation relations,

$$[p_{\mathbf{k}\alpha}, p_{\mathbf{k}'\beta}]_- = [u_{\mathbf{k}\alpha}, u_{\mathbf{k}'\beta}]_- = 0 \tag{9.7}$$

$$[p_{\mathbf{k}\alpha}, u_{\mathbf{k}'\beta}]_- = -i\hbar\delta_{\alpha\beta}\delta_{\mathbf{k}\mathbf{k}'}. \tag{9.8}$$

The momenta and displacements corresponding to opposite wavevectors $\mathbf{k}$ and $-\mathbf{k}$ are related by hermitian conjugation, $\mathbf{p}_\mathbf{k} = \mathbf{p}^\dagger_{-\mathbf{k}}$ and $\mathbf{u}_\mathbf{k} = \mathbf{u}^\dagger_{-\mathbf{k}}$. Note that the total number of degrees of freedom has not changed upon Fourier transform.

In terms of these new variables, the Hamiltonian reads

$$H = \sum_\mathbf{k} \sum_{\alpha,\beta} \left(\frac{1}{2M} p_{\mathbf{k}\alpha} p_{\beta,-\mathbf{k}} + \frac{1}{2} V_{\alpha\beta,\mathbf{k}} u_{\mathbf{k}\alpha} u_{\beta,-\mathbf{k}} \right), \tag{9.9}$$

where

$$V_{\alpha\beta,\mathbf{k}} = \frac{1}{N} \sum_{i,j} e^{i\mathbf{k}\cdot(\mathbf{r}_i - \mathbf{r}_j)} V_{\alpha;\beta}(\mathbf{r}_i - \mathbf{r}_j). \tag{9.10}$$

The 3×3 matrix $V_\mathbf{k}$ is symmetric because $V_{\alpha;\beta}(\mathbf{r})$ is symmetric and real because $V_{\beta;\alpha}(\mathbf{r}) = V_{\alpha;\beta}(-\mathbf{r})$. Moreover, $V_{\alpha\beta,\mathbf{k}} = V_{\alpha\beta,-\mathbf{k}}$. Since the matrix $V_\mathbf{k}$ is real and symmetric, it is

diagonalized by three real and orthogonal eigenvectors. We denote the eigenvectors as $v^\lambda_{\mathbf{k}\alpha}$, $\lambda = 1, 2, 3$, and the corresponding eigenvalues as $M\omega^2_{\mathbf{k}\lambda}$. Then we can introduce normal modes

$$p^\lambda_{\mathbf{k}} = \sum_\alpha v^\lambda_{\mathbf{k}\alpha} p_{\mathbf{k}\alpha}, \tag{9.11}$$

$$u^\lambda_{\mathbf{k}} = \sum_\alpha v^\lambda_{\mathbf{k}\alpha} u_{\mathbf{k}\alpha}, \tag{9.12}$$

that bring H into diagonal form,

$$H = \sum_{\mathbf{k},\lambda} \left(\frac{1}{2M} p^\lambda_{\mathbf{k}} p^\lambda_{-\mathbf{k}} + \frac{1}{2} M\omega^2_{\mathbf{k}\lambda} u^\lambda_{\mathbf{k}} u^\lambda_{-\mathbf{k}} \right). \tag{9.13}$$

One verifies that the normal mode operators $p^\lambda_{\mathbf{k}}$ and $u^\lambda_{\mathbf{k}}$ still obey canonical commutation relations.

The Hamiltonian (9.13) represents $3N$ harmonic oscillator modes. One can write the normal mode Hamiltonian in terms of phonon creation and annihilation operators,

$$b^\lambda_{\mathbf{k}} = u^\lambda_{\mathbf{k}} \sqrt{\frac{M\omega_{\mathbf{k}\lambda}}{2\hbar}} + i p^\lambda_{-\mathbf{k}} \sqrt{\frac{1}{2M\omega_{\mathbf{k}\lambda}\hbar}}, \tag{9.14}$$

$$b^{\lambda\dagger}_{\mathbf{k}} = u^\lambda_{-\mathbf{k}} \sqrt{\frac{M\omega_{\mathbf{k}\lambda}}{2\hbar}} - i p^\lambda_{\mathbf{k}} \sqrt{\frac{1}{2M\omega_{\mathbf{k}\lambda}\hbar}}, \tag{9.15}$$

that obey the commutation rules

$$\begin{aligned} \left[b^\lambda_{\mathbf{k}}, b^{\lambda'}_{\mathbf{k}'} \right]_- &= \left[b^{\lambda\dagger}_{\mathbf{k}}, b^{\lambda'\dagger}_{\mathbf{k}'} \right]_- \\ &= 0, \\ \left[b^\lambda_{\mathbf{k}}, b^{\lambda'\dagger}_{\mathbf{k}'} \right]_- &= \delta_{\mathbf{k}\mathbf{k}'} \delta_{\lambda\lambda'}. \end{aligned} \tag{9.16}$$

In terms of the new operators $b^{\lambda\dagger}_{\mathbf{k}}$ and $b^\lambda_{\mathbf{k}}$, the Hamiltonian reads

$$H = \sum_{\mathbf{k}\lambda} \hbar\omega_{\mathbf{k}\lambda} \left(b^{\lambda\dagger}_{\mathbf{k}} b^\lambda_{\mathbf{k}} + \frac{1}{2} \right). \tag{9.17}$$

Since the operators $b^{\lambda\dagger}_{\mathbf{k}}$ and $b^\lambda_{\mathbf{k}}$ satisfy creation and annihilation operators for bosons, the Hamiltonian (9.17) is interpreted as describing "phonons", quantized lattice vibrations with boson statistics. With or without such interpretation, what is important for us is that the

Hamiltonian (9.17) is diagonal, so that any average of displacements and momenta of lattice atoms can be calculated straightforwardly once it is expressed in terms of the operators $b_{\mathbf{k}}^{\lambda\dagger}$ and $b_{\mathbf{k}}^{\lambda}$. For this, it is important to have an expression for the inverse of the normal-mode transformation we just derived,

$$u_{j\alpha} = \frac{1}{\sqrt{N}} \sum_{\mathbf{k}\lambda} e^{i\mathbf{k}\cdot\mathbf{r}_j} v_{\mathbf{k}\alpha}^{\lambda} \sqrt{\frac{\hbar}{2M\omega_{\mathbf{k}\lambda}}} \left(b_{\mathbf{k}}^{\lambda} + b_{-\mathbf{k}}^{\lambda\dagger} \right), \tag{9.18}$$

$$p_{j\alpha} = \frac{1}{\sqrt{N}} \sum_{\mathbf{k}\lambda} e^{-i\mathbf{k}\cdot\mathbf{r}_j} v_{\mathbf{k}\alpha}^{\lambda} \sqrt{\frac{M\hbar\omega_{\mathbf{k}\lambda}}{2}} \left(ib_{\mathbf{k}}^{\lambda\dagger} - ib_{-\mathbf{k}}^{\lambda} \right). \tag{9.19}$$

Since the phonon Hamiltonian is nothing but the Hamiltonian of $3N$ harmonic harmonic oscillators, phonon Green functions can easily be derived from the harmonic oscillator Green functions, see Sec. 2.6.

For phonons one defines Green functions with respect to the displacement operators $u_{i\alpha}$. The phonon temperature Green function then reads

$$\mathcal{D}_{i\alpha;j\beta}(\tau_1;\tau_2) = -\langle T_\tau [u_{i\alpha}(\tau_1) u_{j\beta}(\tau_2)] \rangle. \tag{9.20}$$

For phonons, $\mathcal{D}$ is real, since u and H are real. According to Eq. (2.19), this implies

$$\mathcal{D}_{i\alpha;j\beta}(\tau) = \mathcal{D}_{i\alpha;j\beta}(-\tau). \tag{9.21}$$

Similarly, one defines phonon retarded, advanced, time-ordered, greater, and lesser Green functions.

Calculation of the temperature Green function then yields, for $0 \le \tau \le \hbar/T$,

$$\mathcal{D}_{i\alpha;j\beta}(\tau) = -\sum_{\mathbf{k}\lambda} \left(\frac{\hbar}{2MN\omega_{\mathbf{k}\lambda}} \right) v_{\alpha}^{\lambda} v_{\beta}^{\lambda} e^{i\mathbf{k}\cdot(\mathbf{r}_i - \mathbf{r}_j)} \left(\frac{e^{\omega_{\mathbf{k}\lambda}\tau}}{e^{\hbar\omega_{\mathbf{k}\lambda}/T} - 1} + \frac{e^{-\omega_{\mathbf{k}\lambda}\tau}}{1 - e^{-\hbar\omega_{\mathbf{k}\lambda}/T}} \right). \tag{9.22}$$

It is easily verified that $\mathcal{D}_{i\alpha;j\beta}(0) = \mathcal{D}_{i\alpha;j\beta}(\hbar/T)$, so that this result can be extended periodically to the entire imaginary time axis. Fourier transform to the imaginary time τ yields

$$\mathcal{D}_{i\alpha;j\beta}(i\Omega_n) = -\sum_{\mathbf{k}\lambda} \left(\frac{\hbar}{MN} \right) v_{\alpha}^{\lambda} v_{\beta}^{\lambda} e^{i\mathbf{k}\cdot(\mathbf{r}_i - \mathbf{r}_j)} \frac{1}{\omega_{\mathbf{k}\lambda}^2 + \Omega_n^2}. \tag{9.23}$$

Similarly, for the retarded and advanced Green functions, one finds

$$D_{i\alpha;j\beta}^{\mathrm{R}}(t) = -\theta(t) \sum_{\mathbf{k}\lambda} \left(\frac{\hbar}{MN\omega_{\mathbf{k}\lambda}} \right) v_{\alpha}^{\lambda} v_{\beta}^{\lambda} e^{i\mathbf{k}\cdot(\mathbf{r}_i - \mathbf{r}_j)} \sin(\omega_{\mathbf{k}\lambda} t), \tag{9.24}$$

$$D_{i\alpha;j\beta}^{\mathrm{A}}(t) = \theta(-t) \sum_{\mathbf{k}\lambda} \left(\frac{\hbar}{MN\omega_{\mathbf{k}\lambda}} \right) v_{\alpha}^{\lambda} v_{\beta}^{\lambda} e^{i\mathbf{k}\cdot(\mathbf{r}_i - \mathbf{r}_j)} \sin(\omega_{\mathbf{k}\lambda} t). \tag{9.25}$$

Performing a Fourier transform to time, we have

$$D^{\rm R}_{i\alpha;j\beta}(\omega) = \sum_{\mathbf{k}\lambda}\left(\frac{\hbar}{2MN\omega_{\mathbf{k}\lambda}}\right)v^\lambda_\alpha v^\lambda_\beta e^{i\mathbf{k}\cdot(\mathbf{r}_i-\mathbf{r}_j)}\left(\frac{1}{\omega-\omega_{\mathbf{k}\lambda}+i\eta}-\frac{1}{\omega+\omega_{\mathbf{k}\lambda}+i\eta}\right). \quad (9.26)$$

Finally, the phonon time-ordered Green function is

$$D_{i\alpha;j\beta}(t) = -i\sum_{\mathbf{k}\lambda}\left(\frac{\hbar}{2MN\omega_{\mathbf{k}\lambda}}\right)v^\lambda_\alpha v^\lambda_\beta e^{i\mathbf{k}\cdot(\mathbf{r}_i-\mathbf{r}_j)}\left(\langle n_{\mathbf{k}\lambda}\rangle e^{i\omega_{\mathbf{k}\lambda}|t|}+\langle n_{\mathbf{k}\lambda}+1\rangle e^{-i\omega_{\mathbf{k}\lambda}|t|}\right), \quad (9.27)$$

where $\langle n_{\mathbf{k}\lambda}\rangle = 1/(\exp(\hbar\omega_{\mathbf{k}\lambda}/T)-1)$ is the occupation number.

The spectral density can now be found by taking the imaginary part of $D^{\rm R}(\omega)$,

$$A_{i\alpha;j\beta}(\omega) = 2\pi\sum_{\mathbf{k}\lambda}\left(\frac{\hbar}{2MN\omega_{\mathbf{k}\lambda}}\right)v^\lambda_\alpha v^\lambda_\beta e^{i\mathbf{k}\cdot(\mathbf{r}_i-\mathbf{r}_j)}\left(\delta(\omega-\omega_{\mathbf{k}\lambda})-\delta(\omega+\omega_{\mathbf{k}\lambda})\right). \quad (9.28)$$

As an application of the use of Green functions for phonons, olne may again consider inelastic neutron scattering. The relevant quantity to calculate in such a scattering experiment is the differential cross section, the amount of scattered neutrons that emerge from the sample at a given energy $\hbar\omega$ and solid angle Ω.

Starting point of the analysis is, as in Sec. 8.4, the expression for the differential scattering cross section,

$$\frac{d^2\sigma}{d\Omega d\omega} = \sum_f \frac{k'}{k}\left(\frac{M}{2\pi}\right)^2\left\langle|\langle\mathbf{k}',f|H'|\mathbf{k},i\rangle|^2\right\rangle\delta(\omega+E_i-E_f), \quad (9.29)$$

where $\mathbf{k}$ is the wavevector of the incoming neutron, $\mathbf{k}'$ is the wavevector of the outgoing neutron, M is the reduced mass of the neutron, i and f refer to initial state and final state, respectively, H' is the interaction between the neutron and the target, and the outer brackets $\langle\ldots\rangle$ indicate a thermal average over the initial states i of the target.

Equation (9.29) can be rewritten as

$$\frac{d^2\sigma}{d\Omega d\omega} = \frac{k'}{2\pi k}\left(\frac{M}{2\pi}\right)^2|V_{\mathbf{q}}|^2\int_{-\infty}^{\infty}dt e^{i\omega t}F(\mathbf{q},t), \quad (9.30)$$

where $\mathbf{q}=\mathbf{k}-\mathbf{k}'$ and the correlation function $F(\mathbf{q},t)$ is defined as

$$F(\mathbf{q},t) = \sum_{j,l}e^{i\mathbf{q}\cdot(\mathbf{r}_l-\mathbf{r}_j)}\left\langle e^{-i\mathbf{q}\cdot\mathbf{u}_j(t)}e^{i\mathbf{q}\cdot\mathbf{u}_l(0)}\right\rangle. \quad (9.31)$$

In Eq. (9.31), the summation is over the lattice sites j and l and the operators $\mathbf{u}_j(t)$, $\mathbf{u}_l(0)$ are the corresponding displacements of the lattice atoms in the Heisenberg picture. The equilibrium positions of the lattice atoms are denoted $\mathbf{r}_j$ and $\mathbf{r}_l$. In Eq. (9.30), $V_{\mathbf{q}}$ is the Fourier transform of the potential that describes how a neutron scatters off a single atom. The combined effect of many atoms in a vibrating lattice is described by the correlation function $F(\mathbf{q},t)$.

For small $\mathbf{q}$, we now write

$$F(\mathbf{q},t) = \sum_{j,l} e^{i\mathbf{q}\cdot(\mathbf{r}_l-\mathbf{r}_j)} \left\langle e^{-i\mathbf{q}\cdot(\mathbf{u}_j(t)-\mathbf{u}_l(0))+\frac{1}{2}[\mathbf{q}\cdot\mathbf{u}_j(t),\mathbf{q}\cdot\mathbf{u}_l(0)]_-} \right\rangle, \tag{9.32}$$

where the expression in the exponent is correct up to corrections of order q^3. In order to perform the thermal average, we use the *cumulant expansion*,[1] and obtain

$$F(\mathbf{q},t) = \sum_{j,l} e^{i\mathbf{q}\cdot(\mathbf{r}_l-\mathbf{r}_j)-\frac{1}{2}\langle(\mathbf{q}\cdot\mathbf{u}_j(t))^2\rangle-\frac{1}{2}\langle(\mathbf{q}\cdot\mathbf{u}_l(0))^2\rangle+\langle(\mathbf{q}\cdot\mathbf{u}_j(t))(\mathbf{q}\cdot\mathbf{u}_l(0))\rangle}, \tag{9.33}$$

again up to corrections of order q^3 in the exponent.[2]

The second and third terms in the exponent do not depend on j, l, or t; they form an overall prefactor known as the Debije-Waller factor. Writing the Debije-Waller factor as e^{-2W}, we may calculate W from the time-ordered phonon Green function

$$W = \frac{i}{2} \sum_{\alpha\beta} q_\alpha q_\beta \lim_{t\downarrow 0} D_{j\alpha;j\beta}(t). \tag{9.34}$$

Substituting the exact result (9.27) for the time-ordered Green function, we obtain

$$W = \sum_{\mathbf{k}\lambda} \sum_{\alpha\beta} \left(\frac{\hbar}{4MN\omega_{\mathbf{k}\lambda}} \right) q_\alpha q_\beta v_\alpha^\lambda v_\beta^\lambda \coth(\hbar\omega_{\mathbf{k}\lambda}/2T). \tag{9.35}$$

We further expand F in the fourth term of the exponent, and separate F into an elastic and inelastic contribution,

$$F(\mathbf{q},t) \;=\; F^{\rm el}(\mathbf{q},t) + F^{\rm inel}(\mathbf{q},t) \tag{9.36}$$

[1] According to the cumulant expansion, any average of the form $\langle\exp(A)\rangle$ can be calculated as

$$\langle e^A\rangle = \exp\left(\langle A\rangle + \tfrac{1}{2}\mathrm{var}\, A + \ldots\right),$$

where $\mathrm{var}\, A = \langle A^2\rangle - \langle A\rangle^2$ is the variance (i.e., the second cumulant) and the dots indicate higher cumulants. If the probability distribution of A is Gaussian, the first two terms in the cumulant expansion are sufficient.

[2] In fact, Eqs. (9.32) and (9.33) are exact because the Hamiltonian is quadratic in the displacements $\mathbf{u}_i$, $i = 1,\ldots,N$.

with

$$F^{\rm el}(\mathbf{q},t) = e^{-2W}\sum_{j,l} e^{i\mathbf{q}\cdot(\mathbf{r}_l-\mathbf{r}_j)} \tag{9.37}$$

$$F^{\rm inel}(\mathbf{q},t) = e^{-2W}\sum_{j,l} e^{i\mathbf{q}\cdot(\mathbf{r}_l-\mathbf{r}_j)}\sum_{\alpha\beta} q_\alpha q_\beta \langle u_{j\alpha}(t)u_{l\beta}(0)\rangle. \tag{9.38}$$

Fourier transform of $F^{\rm el}$ gives a term proportional to $\delta(\omega)$ in the scattering cross section, corresponding to elastic scattering from the lattice without the excitation of phonons. Fourier transform of $F^{\rm inel}$ gives

$$\int_{-\infty}^{\infty} dt e^{i\omega t} F^{\rm inel}(\mathbf{q},t) = ie^{-2W}\sum_{j,l} e^{i\mathbf{q}\cdot(\mathbf{r}_l-\mathbf{r}_j)}\sum_{\alpha\beta} q_\alpha q_\beta D^{>}_{j\alpha;l\beta}(\omega), \tag{9.39}$$

where $D^{>}_{j\alpha;l\beta}(\omega)$ is the phonon greater Green function. Using Eqs. (2.49) together with the exact result (9.28) to calculate $D^{>}_{j\alpha;l\beta}(\omega)$, we find

$$\begin{aligned}\int_{-\infty}^{\infty} dt e^{i\omega t} F^{\rm inel}(\mathbf{q},t) &= Ne^{-2W}\sum_{\mathbf{k}\lambda}\sum_{\alpha\beta} q_\alpha q_\beta v^\lambda_\alpha v^\lambda_\beta \frac{\pi\hbar e^{\omega/2T}}{2M\omega\sinh(\omega/2T)} \\ &\quad\times\left(\delta(\omega-\omega_{\mathbf{k}\lambda})-\delta(\omega+\omega_{\mathbf{k}\lambda})\right).\end{aligned} \tag{9.40}$$

9.2 Electron-phonon interaction

For a discussion of the phonon-mediated electron-electron interaction we first need to describe the interaction between electrons and phonons. We first describe the electron-phonon interaction in the normal-mode picture, and then switch to the jellium model.

Starting point is the potential the electrons feel from the lattice ions,

$$\hat{H}_{\rm lattice} = \int d\mathbf{r}\hat{n}(\mathbf{r})\sum_{j=1}^{N} V_{\rm ion}(\mathbf{r}-\mathbf{x}_j), \tag{9.41}$$

where the vector $\mathbf{x}_j$ runs over the positions of all ions in the lattice and $\hat{n}$ is the electron number density operator. Expanding $\hat{H}_{\rm lattice}$ around the equilibrium positions $\mathbf{x}_j = \mathbf{r}_j$, $j = 1,\ldots,N$, we have

$$\hat{H}_{\rm lattice} = \int d\mathbf{r} n(\mathbf{r})\sum_{j=1}^{N} V_{\rm ion}(\mathbf{r}-\mathbf{r}_j) - \int d\mathbf{r} n(\mathbf{r})\sum_{j=1}^{N}\mathbf{u}_j\cdot\partial_{\mathbf{r}} V_{\rm ion}(\mathbf{r}-\mathbf{r}_j). \tag{9.42}$$

Here $\mathbf{u}_j = \mathbf{x}_j - \mathbf{r}_j$ is the displacement of the jth lattice ion. The first term represents a static potential and gives rise to the electronic band structure. The second term depends on the actual ionic positions. It is the second term that leads to the electron-phonon interaction.

Fourier transforming the second term of Eq. (9.42), we find

$$\hat{H}_{\rm ep} = -\frac{i}{V}\sum_{\mathbf{k}\sigma}\sum_{\mathbf{q}\lambda}\left(\sqrt{\frac{N\hbar}{2M\omega_{\mathbf{q}\lambda}}}\mathbf{v}_{\mathbf{q}}^{\lambda}\cdot\mathbf{q}V_{\mathbf{q}}^{\rm ie}\right)\hat{\psi}_{\mathbf{k}+\mathbf{q},\sigma}^{\dagger}\hat{\psi}_{\mathbf{k},\sigma}(b_{\mathbf{q}}^{\lambda}+b_{-\mathbf{q}}^{\lambda\dagger}), \tag{9.43}$$

where $\hat{\psi}_{\mathbf{k}\sigma}$ is the annihilation operator for an electron with wavevector $\mathbf{k}$ and spin σ, $b_{\mathbf{q}}^{\lambda}$ the annihilation operator for a phonon with momentum $\mathbf{q}$ and polarization $\mathbf{v}_{\mathbf{q}}^{\lambda}$. In the derivation of Eq. (9.43) we used Eq. (9.18) to express the displacement $\mathbf{u}_j$ in terms of the phonon creation and annihilation operators $b_{\mathbf{q}}^{\lambda\dagger}$ and $b_{\mathbf{q}}^{\lambda}$.

At low temperatures, the phase space available for "umklapp processes", corresponding to a momentum transfer $\mathbf{q}$ outside the first Brillouin zone, is small. Moreover, the weight of umklapp processes is suppressed because of the q-dependence of the potential $V_{\mathbf{q}}^{\rm ie}$ for large q. Hence, we will restrict the summation over $\mathbf{q}$ to the first Brillouin zone.

In an isotropic material, the polarization vector $\mathbf{v}_{\mathbf{q}}^{\lambda}$ is either perpendicular or parallel to $\mathbf{q}$. The corresponding phonon states are labeled "transverse" and "longitudinal", respectively. From Eq. (9.43), we conclude that only longitudinal phonons interact with electrons. This is because the longitudinal phonons carry a charge density, whereas transverse phonons do not. If we want to simplify Eq. (9.43) to the case that we keep longitudinal phonons only, we must remind ourselves that in our original formulation of the phonon modes, we have chosen the same polarization vectors for opposite wavevectors, $\mathbf{v}_{\mathbf{q}}^{\lambda} = \mathbf{v}_{-\mathbf{q}}^{\lambda}$. Hence, if the longitudinal polarization $\mathbf{v}_{\mathbf{q}}$ points along $\mathbf{q}$, $\mathbf{v}_{-\mathbf{q}}$ points opposite to $-\mathbf{q}$. We resolve this problem by defining a function $\mathrm{sign}\,(\mathbf{q})$, which can take the values 1 or -1 and which is such that $\mathrm{sign}\,(\mathbf{q}) = -\mathrm{sign}\,(-\mathbf{q})$. Keeping longitudinal phonons only, the expression for the electron-phonon interaction then simplifies to

$$\hat{H}_{\rm ep} = -\frac{i}{V}\sum_{\mathbf{k}\sigma}\sum_{\mathbf{q}}\left(V_{\mathbf{q}}^{\rm ie} q\,\mathrm{sign}\,(\mathbf{q})\sqrt{\frac{N\hbar}{2M\omega_{\mathbf{q}}}}\right)\hat{\psi}_{\mathbf{k}+\mathbf{q},\sigma}^{\dagger}\hat{\psi}_{\mathbf{k},\sigma}(b_{\mathbf{q}}+b_{-\mathbf{q}}^{\dagger}). \tag{9.44}$$

where the creation and annihilation operators $b^{\dagger}$ and b refer to longitudinal phonons only.

The calculation of Green functions for a system of electrons and phonons proceeds in a way that is very similar to what we have seen in the previous chapters. Since our discussion of phonon Green functions there focused on the Green functions for the displacements rather than the phonon creation and annihilation operators, we rewrite the electron-phonon

Hamiltonian in the form

$$\hat{H}_{\rm ep} = \frac{1}{V}\sum_{\mathbf{k}\sigma}\sum_{\mathbf{q}} g_{\mathbf{q}}\hat{\psi}^{\dagger}_{\mathbf{k}+\mathbf{q},\sigma}\hat{\psi}_{\mathbf{k},\sigma}u_{\mathbf{q}}, \tag{9.45}$$

where $u_{\mathbf{q}}$ is a longitudinal displacement,

$$u_{\mathbf{q}} = \frac{\mathbf{q}}{q}\sqrt{\frac{\hbar}{2M\omega_{\mathbf{q}}}}(b_{\mathbf{q}} + b^{\dagger}_{\mathbf{q}}), \tag{9.46}$$

and $g_{\mathbf{q}}$ describes the strength of the electron-phonon coupling,

$$g_{\mathbf{q}} = -iN^{1/2}qV^{\rm ie}_{\mathbf{q}}\text{sign}\,(\mathbf{q}). \tag{9.47}$$

9.3 Jellium model for phonons

In Sec. 9.1 we saw that lattice ions perform vibrations around their equilibrium positions, the frequency of the vibrations being determined by the second derivative of the interaction between ions. However, this interaction is an "effective interaction", mediated by the electrons. Without electrons, the potential between lattice ions would be the Coulomb potential. As we have seen in the previous section, the long-range Coulomb potential does not allow for phonon-like low-frequency collective modes. Instead, the collective modes allowed by the Coulomb interaction are plasma modes, which have a finite frequency even for zero wavevector.

A description of the interaction between electrons and the lattice and the lattice dynamics itself is not straightforward. After all, in such a theory the electrons interact with lattice vibrations, that themselves exist by virtue of the existence of the electrons. A theory of phonon-mediated electron-electron interactions in which the phonon dispersion is, in turn, governed by the electron-mediated interaction between the lattice ions is a risky enterprise.

In order to circumvent such a "chicken and egg" problem, it is preferable to start from first principles, and use a description in which the only interaction is the Coulomb interaction, just like we did for the case of the electron gas. As a complete "ab-initio" treatment is impossible here — for that we'd have to find the lattice structure from first principles —, we use a simplified model for the ionic lattice. That simplified model is referred to as "jellium model". In the jellium model, the lattice is replaced by a positively charged ion "fluid" (or "jellium"). In such a model, the only difference between the ions and the electrons is the different ratios of mass density to charge density: the ion jellium has the same average charge density as the electron gas, but its mass density is a factor $\sim 10^5$ higher. A simplified jellium

description may be used, *e.g.*, if one is interested in long-wavelength phenomena, or if one only needs an order-of-magnitude estimate of the phonon contribution to a certain physical observable.

In the jellium model, we describe the lattice ions by means of their charge density $\rho_{\rm ion}(\mathbf{r})$, which is taken to be a continuous function of the coordinate $\mathbf{r}$. Let us first establish what the normal modes in the jellium model. Hereto, we first treat the electron gas as a negatively charged static background that neutralizes the positive charge of the ions. Of course, this is not a correct description of the electrons — they are much lighter than the ions and, hence, much more mobile, — but it serves to make an important point needed later on.

If the electrons are treated as a static negative background charge, any deviation from equilibrium $\delta\rho_{\rm ion} = \rho_{\rm ion} - \rho^0_{\rm ion}$ is associated with an electric field

$$\nabla \cdot E = \frac{1}{\epsilon_0}\delta\rho_{\rm ion}, \tag{9.48}$$

where ϵ_0 is the electric permittivity of vacuum. The electric field, in turn exerts a force field on the ions,

$$\mathbf{f} = \rho^0_{\rm ion}\mathbf{E}. \tag{9.49}$$

The ion charge density then satisfies the equation

$$M\frac{\partial^2}{\partial t^2}\delta\rho_{\rm ion} + \frac{Ze\rho^0_{\rm ion}}{\epsilon_0}\delta\rho_{\rm ion} = 0, \tag{9.50}$$

where M is the ionic mass and Ze is the charge on one ion. The excitations described by Eq. (9.50) all have the same energy — energy does not depend on wavevector! For sure, these excitations are not the phonons we studied in the previous section. The physical cause that the jellium excitations we found are not phonons is the long range of the Coulomb interaction. In fact, those excitations are nothing but the ion lattice equivalent of the "plasmon" excitations. They are an artefact of the approximations we used in order to derive Eq. (9.50); They do not exist for a real ion lattice.

In a real material, the long range Coulomb interaction between the ions is screened by the electrons. Since electrons are much lighter than the phonons, they react quickly to any change in the ion density. In fact, to a good approximation we can assume that the electrons follow the ion density instantaneously, maintaining charge neutrality throughout the material at all times. As a consequence, the energy price for a perturbation $\delta\rho_{\rm ion}$ of the ion density is not the Coulomb energy, but the kinetic energy cost of increasing or decreasing the electron density: If the ionic charge density is changed by an amount $\delta\rho_{\rm ion}$, the electronic charge density needs to be changed by $-\delta\rho_{\rm ion}$ in order to maintain charge neutrality. The energy cost associated with the change of electron density leads to a restoring force for the ions.

The easiest way to estimate that restoring force, is to view it as an "electron pressure". One easily shows that, for a free electron gas, the ground state energy for N electrons confined to a volume V is

$$E_e = \frac{\hbar^2 \left(3\pi^2 N\right)^{5/3}}{10\pi^2 m V^{2/3}}. \tag{9.51}$$

Hence, one argues that the electronic pressure equals

$$p_e = \frac{\hbar^2}{15\pi^2 m} \left(3\pi^2 \rho_e\right)^{5/3}. \tag{9.52}$$

The ionic motion is driven by the gradient of the electronic pressure p_e. This leads to a wave equation for $\delta\rho_{\rm ion}$,

$$M \frac{\partial^2}{\partial t^2} \delta\rho_{\rm ion} - \frac{2}{3} Z \varepsilon_F \nabla^2 \delta\rho_{\rm ion} = 0. \tag{9.53}$$

Solutions of Eq. (9.53) have a valid dispersion relation

$$\omega_{\mathbf{q}} = v_F q \sqrt{\frac{Zm}{3M}}. \tag{9.54}$$

Note that, in the jellium model, there is only one phonon mode per wavevector. For a real lattice, there are three phonon modes per wavevector: one longitudinal mode and two transverse modes. The two transverse modes are not present in the jellium model, because they do not correspond to a change of the charge density. Since the electrons interact with longitudinal phonons only, the absence of transverse normal modes in the jellium model is not a real problem.

We now present a more microscopic picture of how the conduction electrons determine the phonon dispersion relation. In our theory we'll consider the electron-phonon interaction as a perturbation. Without electron-phonon interaction, the phonons are the quantized oscillations of the ion jellium without electron screening, see Eq. (9.50) above. Such oscillations, which are the equivalent of plasma oscillations in the interacting electron gas, have frequency $\Omega_{\rm E}$

$$\Omega_{\rm E}^2 = \frac{Z^2 e^2 N}{\epsilon_0 M V} = \frac{Z e^2 n}{\epsilon_0 M}, \tag{9.55}$$

where n is the electron density. The frequency does not depend on the wavelength of the phonons, as in the Einstein model of lattice vibrations. Also, in the jellium one has longitudinal phonons only; transverse phonons, which do not correspond to a change in ion density, can not be described in a jellium model. Thus, the phonon Hamiltonian in the jellium model is

$$\hat{H}_{\rm phonon} = \sum_{\mathbf{q}} \hbar\Omega_{\rm E} (b_{\mathbf{q}}^\dagger b_{\mathbf{q}} + 1/2). \tag{9.56}$$

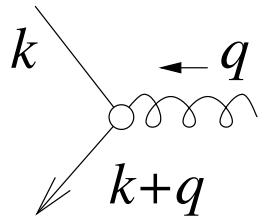

Figure 9.1: Diagrammatic representation of phonon line and of electron-phonon interaction vertex.

The relevant phonon Green function is defined with respect to the displacement operators $u_{\mathbf{q}}$. It is a harmonic oscillator Green function,

$$\mathcal{D}_{\mathbf{q}}(\tau) = -\langle T_\tau u_{\mathbf{q}}(\tau) u_{-\mathbf{q}}(0)\rangle, \quad \mathcal{D}^0_{\mathbf{q}}(i\Omega_n) = -\frac{1}{M(\Omega_n^2 + \Omega_{\rm E}^2)}. \tag{9.57}$$

The superscript "0" indicates that this phonon Green function is calculated without taking the electron gas into account.

In this first-principle jellium model, the interaction potential between electrons and ions is the Coulomb interaction. We thus set $V^{\rm ie}_{\mathbf{q}} = -Ze^2/\epsilon_0 q^2$ in Eq. (9.47),

$$g^0_{\mathbf{q}} = \frac{Ze^2 i}{\epsilon_0 q} N^{1/2} = i\sqrt{\frac{\Omega_{\rm E} M e^2}{\epsilon_0 q^2}}. \tag{9.58}$$

Diagrammatic rules for a combined electron-phonon system are quite similar to those of the previous chapters for electronic systems. We denote a correlation function of displacements with a "springy" line, see Fig. 9.1. The electron-phonon interaction is a vertex where a phonon line meets an incoming and outgoing electron line. Energy and momentum are conserved at the electron-phonon vertex. In the imaginary time formalism, each phonon line is represented by minus a phonon Green function, $-\mathcal{D}^0$; each electron-phonon vertex has weight $g^0_{\mathbf{q}}$. Note that $g^0_{-\mathbf{q}} = g^{0*}_{\mathbf{q}}$. If the real-time Keldysh formalism is used, the phonon line represents iD. The phonon lines are directed (although the final answer does not depend on the direction chosen). The vertices carry weight $g_{\mathbf{q}}$, multiplied by a 2×2 matrix in Keldysh space, see Sec. 7.1.

The first effect of the electron-phonon interaction is to modify the phonon Green function. Diagrams for the phonon Green function in the random phase approximation are shown in Fig. 9.2. In this diagram you recognize the electron polarizability function χ, which we calculate in the RPA approximation as well, see Eq. (7.35). We find

$$\mathcal{D}^{\rm RPA}_{\mathbf{q}}(i\Omega_n) \;=\; \frac{\mathcal{D}^0_{\mathbf{q}}(i\Omega_n)}{1 - \chi^{\rm RPA}_{\mathbf{q}}(i\Omega_n)\mathcal{D}^0_{\mathbf{q}}(i\Omega_n)|g^0_{\mathbf{q}}|^2/Ve^2}$$

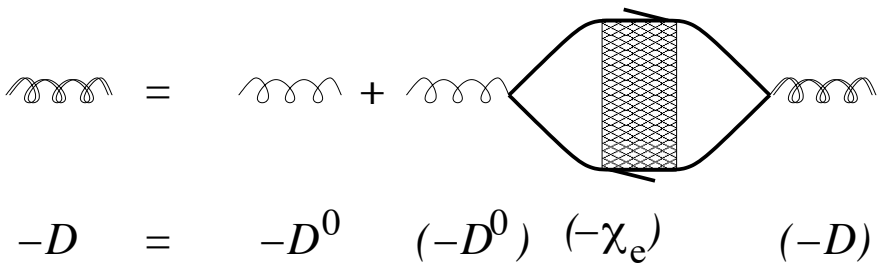

Figure 9.2: Diagrams for the effective phonon Green function $\mathcal{D}$.

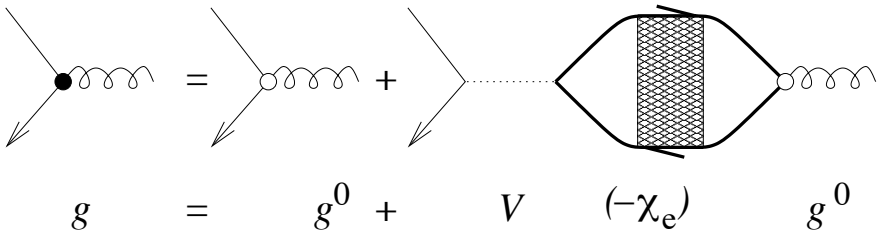

Figure 9.3: Diagrams for the effective electron-phonon interaction $g_{\mathbf{q}}$.

$$= -\frac{1}{M(\Omega_n^2+\omega_{\mathbf{q}}^2)}, \tag{9.59}$$

where

$$\omega_{\mathbf{q}}^2 = \frac{\Omega_{\rm E}^2}{\epsilon_{\mathbf{q}}^{\rm RPA}(i\Omega_n)} = \frac{Ze^2n}{\epsilon^{\rm RPA}\epsilon_0 M}. \tag{9.60}$$

Here we wrote the polarizability function in terms of the dielectric response function $\epsilon^{\rm RPA} = (1+V_{\mathbf{q}}\chi^{\rm RPA}/e^2)^{-1}$, where $V_{\mathbf{q}} = e^2/\epsilon_0 q^2$ denotes the electron-electron interaction. Substituting the Thomas-Fermi approximation (7.40) of the dielectric response function, we find, for small q,

$$\omega_{\mathbf{q}} = v_F q\sqrt{\frac{Zm}{3M}}, \tag{9.61}$$

which is the Bohm-Staver expression for the phonon dispersion, see Eq. (9.54). We thus arrive at the satisfactory conclusion that, once the electron-phonon interaction is taken into account, the phonon frequencies are renormalized from Ω to $\omega_{\mathbf{q}}$, where $\omega_{\mathbf{q}}$ is proportional to q for large wavelengths. Of course, we already reached the same conclusion in Eq. (9.54), based on macroscopic arguments.

Next, let us consider the electron-phonon interaction. This interaction is also modified by the presence of the electron gas. Instead of exciting a phonon directly, as is described by

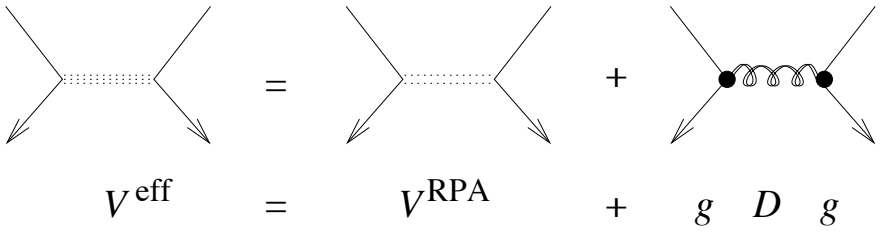

Figure 9.4: Diagrams for the effective electron-electron interaction $V_{\mathbf{q}}^{\rm eff}$.

the electron-phonon Hamiltonian (9.45), an electron may excite an electron-hole pair, which, in turn excites a phonon. Again using the random phase approximation, such processes can be described by the diagrams listed in Fig. 9.3. We thus find

$$\begin{aligned} g_{\mathbf{q}}^{\rm RPA}(i\Omega_n) &= g_{\mathbf{q}}^0(1+V_{\mathbf{q}}\chi_{\mathbf{q}}^{\rm RPA}/e^2) \\ &= \frac{g_{\mathbf{q}}^0}{\epsilon^{\rm RPA}(\mathbf{q},i\Omega_n)}. \end{aligned} \tag{9.62}$$

Let us now turn to the electron-electron interactions. A diagrammatic expression for the effective electron-electron interaction is shown in Fig. 9.4. The left diagram in Fig. 9.4 corresponds to interactions that do not involve the excitations of phonons. This is the RPA effective interaction we studied in Sec. 7.3. The right diagram contains all processes where a phonon is excited. Notice that the electron-phonon vertices are renormalized vertices of Eq. (9.62) and that the phonon propagator is the full renormalized propagator of Eq. (9.59). Combining everything, we find that the effective electron-electron interaction is

$$\begin{aligned} V_{\mathbf{q}}^{\rm eff}(i\Omega_n) &= \frac{V_{\mathbf{q}}}{\epsilon_{\mathbf{q}}^{\rm RPA}(i\Omega_n)} + g_{\mathbf{q}}^{\rm RPA}(i\Omega_n)g_{-\mathbf{q}}^{\rm RPA}(i\Omega_n)\mathcal{D}_{\mathbf{q}}^{\rm RPA}(i\Omega_n) \\ &= \frac{V_{\mathbf{q}}}{\epsilon_{\mathbf{q}}^{\rm RPA}(i\Omega_n)}\left(1-\frac{\omega_{\mathbf{q}}^2}{\Omega_n^2+\omega_{\mathbf{q}}^2}\right), \end{aligned} \tag{9.63}$$

where we have made use of the identity

$$g_{\mathbf{q}}^0 g_{-\mathbf{q}}^0 = M\omega_{\mathbf{q}}^2\varepsilon_{\mathbf{q}}^{\rm RPA}(i\Omega_n)V_{\mathbf{q}}. \tag{9.64}$$

Transforming to real frequencies, we finally obtain the phonon-mediated effective electron-electron interaction

$$V_{\mathbf{q}}^{\rm eff}(\omega) = \frac{V_{\mathbf{q}}}{\epsilon_{\mathbf{q}}^{\rm RPA}(\omega)}\frac{\omega^2}{\omega^2-\omega_{\mathbf{q}}^2}. \tag{9.65}$$

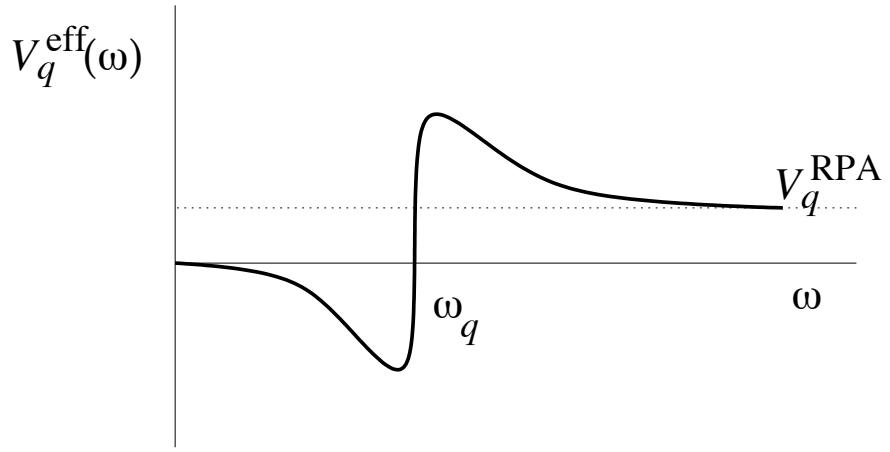

Figure 9.5: Sketch of the frequency dependence of the effective electron-electron interaction.

Using the Thomas-Fermi approximation for the dielectric response function, this simplifies to

$$V_{\mathbf{q}}^{\rm eff,\ TF}(\omega) = \frac{e^2\omega^2}{\epsilon_0(q^2+k_s^2)(\omega^2-\omega_{\mathbf{q}}^2)}. \tag{9.66}$$

In contrast to the RPA screened interaction, which hardly depended on frequency as long as $\omega \ll \epsilon_F$, the inclusion of electron-phonon interactions gives rise to a frequency dependence on a much smaller energy scale: $V^{\rm eff}$ depends on frequency on the scale $\omega_{\mathbf{q}}$, as sketched in Fig. 9.5. For large frequencies $\omega_{\mathbf{q}} \ll \omega$ the effect of the lattice is very small; $V^{\rm eff}$ is very close to $V^{\rm RPA}$. The effect of the lattice is most dramatic, however, for small frequencies, $\omega \ll \omega_{\mathbf{q}}$, where the effective electron-electron interaction becomes attractive, rather than repulsive.

What is the effect of the attractive interaction? At first sight, one is inclined to believe that the effect is small. After all, the interaction is attractive only in a very small frequency range, $\omega \lesssim \omega_D$, where the Debije frequency ω_D is the typical phonon frequency. Nevertheless, at low temperatures only electrons close to the Fermi level play a role. For these electrons interactions with small transferred energy are most important. It is precisely for those processes that the interaction is attractive.

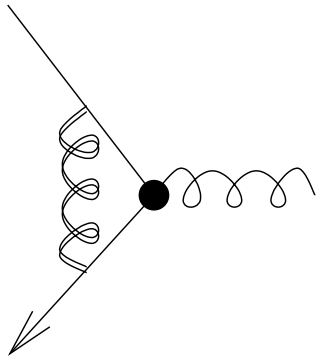

Figure 9.6: Diagram contribution to the renormalization of electron-phonon vertex by phonon scattering.

9.4 Exercises

Exercise 9.1: Phonon velocity in jellium model

Calculate the dispersion relation for phonons in the jellium model. What is the phonon velocity? This expression for the phonon disperson is known as the "Bohm-Staver law".

Exercise 9.2: Migdal's theorem

In principle, the electron-phonon vertex can also be renormalized by the repeated exchange of phonons, as, e.g., in the diagram of Fig. 9.6. (Note that the phonon line exchanged between the electrons is a renormalized phonon line.) Show that such diagrams are smaller than the diagrams without the exchange of a phonon by a large factor $\sim \sqrt{M/m}$, where M and m are ion and electron mass, respectively.

Chapter 10

Superconductivity

The electron-phonon interaction leads to an attractive effective electron-electron interaction. In this chapter we will review the consequence of the attractive interaction: an instability that leads to the superconducting state. We also dicuss the fundamentals of a Green function description of superconductors.

10.1 Cooper instability

What is the effect of an attractive interaction? In order to investigate the effect of a weak attractive interaction, we consider a cartoon version of the effective interaction we derived in the previous section.

The cartoon version, used since the original formulation of the theory of superconductivity by Bardeen, Cooper, and Schrieffer, reflects the fact that the attractive interaction exists for small energy transfers only, and combines it with our knowledge that only electrons near the Fermi surface play a role. With this motivation, we look at the interaction Hamiltonian

$$\hat{H}_{\rm ee} \;=\; -\frac{\lambda}{2V}\sum_{\mathbf{k}_1,\mathbf{k}_2,\mathbf{k}_3,\mathbf{k}_4}\sum_{\sigma_1,\sigma_2}\hat{\psi}^\dagger_{\mathbf{k}_1\sigma_1}\hat{\psi}^\dagger_{\mathbf{k}_2\sigma_2}\hat{\psi}_{\mathbf{k}_3\sigma_2}\hat{\psi}_{\mathbf{k}_4\sigma_1}\delta_{\mathbf{k}_1+\mathbf{k}_2,\mathbf{k}_3+\mathbf{k}_4}\theta(\mathbf{k}_1)\theta(\mathbf{k}_2)\theta(\mathbf{k}_3)\theta(\mathbf{k}_4), \tag{10.1}$$

where the function $\theta(\mathbf{k})$ is nonzero only for $|\varepsilon_{\mathbf{k}}-\mu|<\omega_{\rm D}$ and λ is a positive constant. Note that the interaction (10.1) is not the result of a formal manipulation starting from the effective phonon-mediated electron-electron interaction. Instead, it is merely a cartoon that is used because of its technical simplicity. In some respects, it is quite different than the effective phonon-mediated electron-electron interaction. The interaction (10.1) is instantaneous but velocity dependent (the interaction depends on $\varepsilon_{\mathbf{k}}$), whereas the true effective electron-

electron interaction is retarded. For the application we consider here, these differences are believed not to play an important role.

In some applications, it is useful to rewrite the interaction (10.1) in coordinate space. The interaction is local on length scales large compared to v_F/ω_D,

$$\hat{H}_{\rm ee} = -\frac{\lambda}{2}\sum_{\sigma_1,\sigma_2}\int d\mathbf{r}\hat{\psi}^\dagger_{\sigma_1}(\mathbf{r})\hat{\psi}^\dagger_{\sigma_2}(\mathbf{r})\hat{\psi}_{\sigma_2}(\mathbf{r})\hat{\psi}_{\sigma_1}(\mathbf{r}). \tag{10.2}$$

If the coordinate representation (10.2) is used, care must be taken that it is, in fact, the Fourier transformation of Eq. (10.1), and, thus, requires a momentum cut-off at momenta of order ω_D/v_F.[1]

The attractive interaction $\hat{H}_{\rm ee}$ leads to a new phase, the superconducting phase. In order to find the temperature or interaction strength at which this new phase starts to appear, we follow the road taken in our dicussion of magnetism, and search for a zero-frequency divergence of a response function. A diverging response function signals an instability: A finite response for no applied perturbation. In the case of a ferromagnet, the respone is the spin density, the perturbation is a magnetic field, and we found that for sufficiently strong interactions, the spin density in response to an applied magnetic field diverges. This divergence signalled the Stoner instability and the appearance of a ferromagnetic state. For the case of a superconductor, both the perturbation looks rather unphysical: We take

$$\hat{H}_1 = \int d\mathbf{r}(\Delta(\mathbf{r})\hat{\psi}^\dagger_\uparrow(\mathbf{r})\hat{\psi}^\dagger_\downarrow(\mathbf{r}) + \Delta^*(\mathbf{r})\hat{\psi}_\downarrow(\mathbf{r})\hat{\psi}_\uparrow(\mathbf{r})) \tag{10.3}$$

as the Hamiltonian of the perturbing 'field'. It is important that we use a grand canonical formulation, since the perturbation $\hat{H}_1$ does not conserve particle number. Indeed, the perturbation $\hat{H}_1$ is unphysical. It can not be a realistic perturbation in an experiment. But that is not the point! If we were to live in a world one did not know how to apply a magnetic field, one would consider the perturbation we looked at in Ch. 8 as unphysical. Yet, in such a world a theoretical physicist could stil ask the question what would happen if one were

[1] The exact Fourier transform of Eq. (10.1) has the form

$$\begin{aligned}\hat{H}_{\rm ee} &= \frac{\lambda}{2}\sum_{\sigma_1,\sigma_2}\int d\mathbf{r}\int d\mathbf{r}_1 d\mathbf{r}_2 d\mathbf{r}_3 d\mathbf{r}_4 \theta(\mathbf{r}-\mathbf{r}_1)\theta(\mathbf{r}-\mathbf{r}_2)\theta(\mathbf{r}-\mathbf{r}_3)\theta(\mathbf{r}-\mathbf{r}_4)\\ &\quad\times\hat{\psi}^\dagger_{\sigma_1}(\mathbf{r}_1)\hat{\psi}^\dagger_{\sigma_2}(\mathbf{r}_2)\hat{\psi}_{\sigma_2}(\mathbf{r}_3)\hat{\psi}_{\sigma_1}(\mathbf{r}_4),\end{aligned}$$

where

$$\theta(\mathbf{r}) = \frac{1}{V}\sum_{\mathbf{k}} e^{i\mathbf{k}\cdot\mathbf{r}}\theta(\mathbf{k}).$$

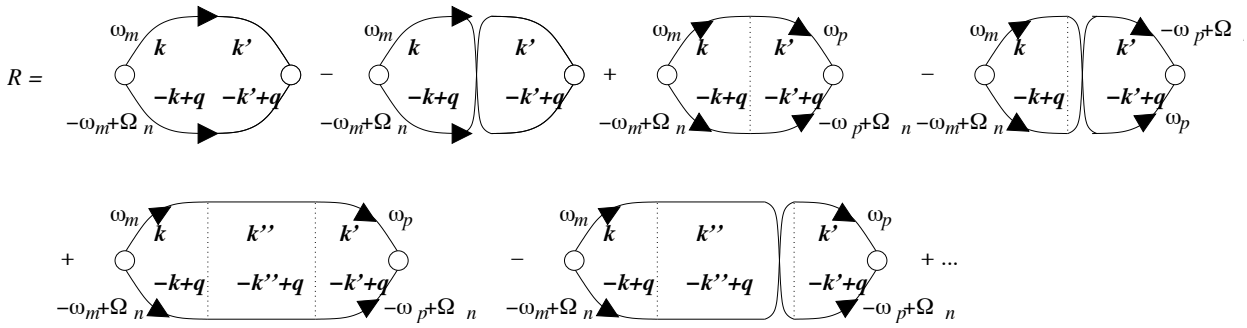

Figure 10.1: Ladder diagrams contributing to the Cooper correlator R of Eq. (10.8).

to apply a 'fictitous' magnetic field. Inevitably she/he would find that this field creates a finite spin density, that the spin density response diverges at the Stoner instability, and that there is a ferromagnetic state for interaction strengths beyond the critical value. Here we are equally justified in discussing the nonphysical perturbation $\hat{H}_1$. As soon as we find that it creates a diverging response, we know that we have discovered a new phase.

The response we look for is of the quantity

$$F^*(\mathbf{r}) = \langle \hat{\psi}^\dagger_\uparrow(\mathbf{r}) \hat{\psi}^\dagger_\downarrow(\mathbf{r}) \rangle. \tag{10.4}$$

The response of F^* to the perturbing field $\Delta(\mathbf{r})$ is easily found using the Kubo formula,

$$F^*(\mathbf{r},t) = \int dt' \int d\mathbf{r}' R^{\rm R}(\mathbf{r}-\mathbf{r}';t-t')\Delta^*(\mathbf{r}',t'), \tag{10.5}$$

where

$$R^{\rm R}(\mathbf{r}-\mathbf{r}',t-t') = -i\theta(t-t')\langle [\hat{\psi}^\dagger_\uparrow(\mathbf{r},t)\hat{\psi}^\dagger_\downarrow(\mathbf{r},t), \hat{\psi}_\downarrow(\mathbf{r}',t')\hat{\psi}_\uparrow(\mathbf{r}',t')]_- . \tag{10.6}$$

Here we omitted a contribution to the response that involves a commutator of four creation operators, which is nonzero in the non-interacting ground state. Fourier transforming and switching from the retarded correlation function to the temperature correlation function, we find

$$R_{\mathbf{q}}(\tau) = \sum_{\mathbf{k},\mathbf{k}'} R^{\downarrow\uparrow\uparrow\downarrow}_{\mathbf{k}\mathbf{k}'\mathbf{q}}(\tau), \tag{10.7}$$

$$R^{\sigma_1\sigma_2,\sigma_3\sigma_4}_{\mathbf{k},\mathbf{k}',\mathbf{q}}(\tau) = -\langle T_\tau \hat{\psi}_{-\mathbf{k}+\mathbf{q},\sigma_1}(\tau)\hat{\psi}_{\mathbf{k},\sigma_2}(\tau)\hat{\psi}^\dagger_{-\mathbf{k}'+\mathbf{q},\sigma_3}(0)\hat{\psi}^\dagger_{\mathbf{k}',\sigma_4}(0)\rangle. \tag{10.8}$$

We calculate the response function R using diagrammatic perturbation theory, taking the effective electron-electron interaction (10.1). The diagrams contributing to R are very

similar to the diagrams that contributed to the spin susceptibility in chapter 8. They are shown in Fig. 10.1. Note that there are contributions from the direct interaction and from the exchange interaction, which come with an extra minus sign. Summing the geometric series in Fig. 10.1, we find

$$\begin{aligned} R^{\sigma_1\sigma_2,\sigma_3\sigma_4}_{\mathbf{k},\mathbf{k}',\mathbf{q}}(i\Omega_n) &= (\delta_{\mathbf{k},\mathbf{k}'}\delta_{\sigma_1\sigma_3}\delta_{\sigma_2\sigma_4} - \delta_{\mathbf{k},\mathbf{q}-\mathbf{k}'}\delta_{\sigma_1\sigma_4}\delta_{\sigma_2\sigma_3}) \left(T\sum_m \mathcal{G}_{-\mathbf{k}+\mathbf{q}}(i\omega_m + i\Omega_n)\mathcal{G}_{\mathbf{k}}(-i\omega_m) \right) \\ &+ \frac{1}{V}\tilde{\lambda}(\delta_{\sigma_1\sigma_3}\delta_{\sigma_2\sigma_4} - \delta_{\sigma_1\sigma_4}\delta_{\sigma_2\sigma_3}) \left(T\sum_m \mathcal{G}_{-\mathbf{k}+\mathbf{q}}(-i\omega_m + i\Omega_n)\mathcal{G}_{\mathbf{k}}(i\omega_m) \right) \\ &\times \left(T\sum_p \mathcal{G}_{-\mathbf{k}'+\mathbf{q}}(-i\omega_p + i\Omega_n)\mathcal{G}_{\mathbf{k}'}(i\omega_p) \right). \end{aligned} \tag{10.9}$$

Here $\tilde{\lambda}$ is a renormalized interaction,

$$\tilde{\lambda} = \lambda \left[1 + \frac{T}{V}\lambda {\sum_{\mathbf{k}''}}' \sum_m \mathcal{G}_{\mathbf{k}''}(i\omega_m)\mathcal{G}_{-\mathbf{k}''+\mathbf{q}}(-i\omega_m + i\Omega_n) \right]^{-1}, \tag{10.10}$$

where the symbol $\sum'_{\mathbf{k}}$ denotes $\sum_{\mathbf{k}} \theta(\mathbf{k})\theta(-\mathbf{k}+\mathbf{q})$. Performing the Matsubara summations, we have

$$\begin{aligned} & T\sum_m \mathcal{G}_{-\mathbf{k}+\mathbf{q}}(-i\omega_m + i\Omega_n)\mathcal{G}_{\mathbf{k}}(i\omega_m) \\ &= T\sum_m \frac{1}{[-i\omega_m + i\Omega_n - (\varepsilon_{-\mathbf{k}+\mathbf{q}} - \mu)][i\omega_m - (\varepsilon_{\mathbf{k}} - \mu)]} \\ &= -\frac{1}{2}\frac{\tanh[(\varepsilon_{-\mathbf{k}+\mathbf{q}} - \mu)/2T] + \tanh[(\varepsilon_{\mathbf{k}} - \mu)/2T]}{\varepsilon_{\mathbf{k}} + \varepsilon_{-\mathbf{k}+\mathbf{q}} - 2\mu - i\Omega_n}. \end{aligned} \tag{10.11}$$

We perform the analytical continuation $i\Omega_n \to \omega + i\eta$ and consider the limit $\mathbf{q} \to 0$, $\omega \to 0$. Substituting Eq. (10.11) into the expression (10.10) for the effective interaction strength, replacing the momentum summation by an integration over energy, and integrating by parts, we find

$$\begin{aligned} \frac{1}{2V}\sum_{\mathbf{k}} \frac{\tanh[(\varepsilon_{\mathbf{k}} - \mu)/2T]}{\varepsilon_{\mathbf{k}} - \mu}\theta(\mathbf{k}) &= \nu \int_{-\hbar\omega_D}^{\hbar\omega_D} d\xi \frac{\tanh(\xi/2T)}{2\xi} \\ &= \nu \tanh\frac{\hbar\omega_D}{2T} \ln\frac{\hbar\omega_D}{2T} - \int_0^{\hbar\omega_D/2T} dx \frac{\ln x}{\cosh^2(x)}. \end{aligned} \tag{10.12}$$

The second term is convergent and approaches the value -0.81 as $T \to 0$, whereas the first term diverges logarithmically. We thus see that the denominator in Eq. (10.10) diverges if

$$1 = \lambda\nu(\ln(\hbar\omega_{\rm D}/2T) + 0.81), \quad \text{or} \quad T = T_c = 1.14\hbar\omega_{\rm D}e^{-1/\lambda\nu}. \tag{10.13}$$

It is important to realize that this divergence happens for an arbitrarily weak attractive interaction, provided the temperature is sufficiently low.

Of course, a divergence of $\tilde{\lambda}$ corresponds to a divergence of the correlation function R. The reason why we studied the correlation function R was precisely because of this divergence: a divergent correlation function is a signal of an instability. At high temperatures $T \gg T_c$, the response function $R_{\mathbf{q}}$ is finite, indicating a finite response to the perturbation $\Delta(\mathbf{r})$. Lowering the temperature, we see that the response to the fictitious field $\Delta(\mathbf{r})$ diverges upon approaching the critical temperature T_c. The divergence signals a phase transition to a state in which $F^*(\mathbf{r})$ acquires a nonzero value spontaneously.[2] This is the superconducting state. This important observation is the basis for the Green function description of the superconducting state of the next section.

The fact that the quantity F^* becomes nonzero in the superconducting phase has two consequences: First, the absolute value $|F^*|$ becomes nonzero, and, second, F^* acquires a phase. Upon rethinking this, the second statement may be more striking than the first one. After all, what determines the phase of F^*? For this, it is useful to again compare the normal-metal-superconductor phase transition to the normal-metal–ferromagnet transition we studied in the previous chapter. Upon passing the Stoner instability, the spin polarization acquired a finite magnitude, and a certain direction, although the Hamiltonian did not contain any preferred direction. The spin-rotational symmetry is broken spontaneously upon entering the ferromagnetic phase. In principle, the direction of the magnetization could be fixed by the addition of an infinitesimal magnetic field to the Hamiltonian. In the same way, the superconducting phase is a "broken symmetry phase". The quantity F^* acquires a phase, whereas the Hamiltonian does not contain a term that determines the phase of F^*. As in the case of the ferromagnet, the symmetry may be broken by a small perturbation, which has the form of the perturbation of Eq. (10.3).

10.2 Green's function description of a superconductor

In this section, we will derive an equation of motion for the superconductor Green functions. Hereto, we need the equation of motion for the creation and annihilation operators. Using

[2] If one would insist on a canonical formulation, the quantity that turns nonzero at the normal-metal–superconductor transition is $\langle N+2|\hat{\psi}^\dagger_{\mathbf{k}\uparrow}\hat{\psi}^\dagger_{\mathbf{k}\downarrow}|N\rangle$.

the coordinate representation (10.2) of the interaction Hamiltonian, we find

$$\begin{aligned}
\frac{\partial}{\partial\tau}\hat{\psi}_\sigma(\mathbf{r}) &= -(\hat{H}_0-\mu)\hat{\psi}_\sigma(\mathbf{r}) + \lambda\left[\sum_{\sigma'}\hat{\psi}^\dagger_{\sigma'}(\mathbf{r})\hat{\psi}_{\sigma'}(\mathbf{r})\right]\hat{\psi}_\sigma(\mathbf{r}) \\
\frac{\partial}{\partial\tau}\hat{\psi}^\dagger_\sigma(\mathbf{r}) &= (\hat{H}_0^*-\mu)\hat{\psi}^\dagger_\sigma(\mathbf{r}) - \lambda\hat{\psi}^\dagger_\sigma(\mathbf{r})\left[\sum_{\sigma'}\hat{\psi}^\dagger_{\sigma'}(\mathbf{r})\hat{\psi}_{\sigma'}(\mathbf{r})\right].
\end{aligned} \tag{10.14}$$

Here $\hat{H}_0^*$ is the complex conjugate of the Hamiltonian $\hat{H}_0$. Eventually, the repulsive part of the interaction at higher frequencies can be included into $\hat{H}_0$ as a self-consistent Hartree-Fock potential.

Slightly generalizing the arguments of the preceding section, we characterize the superconducting state by means of the standard Green function $\mathcal{G}_{\sigma\sigma'}(\mathbf{r},\tau;\mathbf{r}'\tau')$ and by the so-called "anomalous Green function"

$$\begin{aligned}
\mathcal{F}_{\sigma\sigma'}(\mathbf{r},\tau;\mathbf{r}',\tau') &= \langle T_\tau\hat{\psi}_\sigma(\mathbf{r},\tau)\hat{\psi}_{\sigma'}(\mathbf{r}',\tau')\rangle, \\
\mathcal{F}^+_{\sigma\sigma'}(\mathbf{r},\tau;\mathbf{r}',\tau') &= \langle T_\tau\hat{\psi}^\dagger_\sigma(\mathbf{r},\tau)\hat{\psi}^\dagger_{\sigma'}(\mathbf{r}',\tau')\rangle,
\end{aligned} \tag{10.15}$$

where $\hat{H}_0$ is the electron Hamiltonian without interactions. Note that the absence of a minus sign in the definition of the anomalous Green functions $\mathcal{F}$ and $\mathcal{F}^+$. Writing down the equation of motion for $\mathcal{G}$, we the find

$$\begin{aligned}
-\frac{\partial}{\partial\tau}\mathcal{G}_{\sigma\sigma'}(\mathbf{r},\mathbf{r}';\tau) &= \delta(\mathbf{r}-\mathbf{r}')\delta(\tau)\delta_{\sigma\sigma'} + \left(\hat{H}_0-\mu\right)\mathcal{G}_{\sigma\sigma'}(\mathbf{r},\mathbf{r}';\tau) \\
&\quad + \sum_{\sigma''}\lambda\left\langle T_\tau\hat{\psi}^\dagger_{\sigma''}(\mathbf{r},\tau)\hat{\psi}_{\sigma''}(\mathbf{r},\tau)\hat{\psi}_\sigma(\mathbf{r},\tau)\hat{\psi}^\dagger_{\sigma'}(\mathbf{r}',0)\right\rangle.
\end{aligned} \tag{10.16}$$

The imaginary-time arguments of the creation and annihilation operators in the last term on the r.h.s. of Eq. (10.17) should be increased by an infinitesimal amount in order to ensure the correct order under the time-ordering operation T_τ. Anticipating a description in terms of a self-consistent field (as in the Hartree-Fock approximation we discussed in Ch. 7), the average of a product of four creation and annihilation operators on the right hand side of Eq. (10.16) can be written as a product of two pair averages using Wick's theorem. Application of Wick's theorem results in three terms. Two of those are the Hartree and Fock terms we encountered before in Chapter 7. These can be absorbed into the Hartree and Fock self consistent potentials, which is included in the Hamiltonian $\hat{H}_0$. The third term involves the anomalous Green function $\mathcal{F}$,

$$\left\langle T_\tau\hat{\psi}^\dagger_{\sigma''}(\mathbf{r},\tau)\hat{\psi}_{\sigma''}(\mathbf{r},\tau)\hat{\psi}_\sigma(\mathbf{r},\tau)\hat{\psi}^\dagger_{\sigma'}(\mathbf{r}',0)\right\rangle \;\rightarrow\; \mathcal{F}_{\sigma''\sigma}(\mathbf{r},\tau+\eta;\mathbf{r},\tau)\mathcal{F}^+_{\sigma''\sigma'}(\mathbf{r},\tau;\mathbf{r}',0),$$

where η is a positive infinitesimal. Defining the field $\Delta_{\sigma\sigma'}(\mathbf{r})$ as[3]

$$\Delta_{\sigma\sigma'}(\mathbf{r}) = -\Delta_{\sigma'\sigma}(\mathbf{r}) = \lambda \mathcal{F}_{\sigma\sigma'}(\mathbf{r}, \tau + \eta; \mathbf{r}, \tau), \tag{10.17}$$

we arrive at the equation of motion

$$\begin{aligned} \left(-\frac{\partial}{\partial\tau} - (\hat{H}_0 - \mu)\right) \mathcal{G}_{\sigma\sigma'}(\mathbf{r}, \tau; \mathbf{r}', \tau') & \\ + \sum_{\sigma''} \Delta_{\sigma\sigma''}(\mathbf{r}) \mathcal{F}^{+}_{\sigma''\sigma'}(\mathbf{r}, \tau; \mathbf{r}', \tau') &= \delta(\mathbf{r} - \mathbf{r}')\delta(\tau - \tau'). \end{aligned} \tag{10.18}$$

Note that $\Delta(\mathbf{r})$ is antisymmetric in the spin indices. This reflects the fact that the superconducting instability exists for pairs of electrons with zero spin only. Similarly, one derives an equation of motion for the anomalous Green function,

$$\left(\frac{\partial}{\partial\tau} - (\hat{H}_0^* - \mu)\right) \mathcal{F}^{+}_{\sigma\sigma'}(\mathbf{r}, \tau; \mathbf{r}', \tau') - \sum_{\sigma''} \Delta^*_{\sigma''\sigma}(\mathbf{r}) \mathcal{G}_{\sigma''\sigma'}(\mathbf{r}, \tau; \mathbf{r}', \tau') = 0, \tag{10.19}$$

$$\left(-\frac{\partial}{\partial\tau} - (\hat{H}_0 - \mu)\right) \mathcal{F}_{\sigma\sigma'}(\mathbf{r}, \tau; \mathbf{r}', \tau') - \sum_{\sigma''} \Delta_{\sigma\sigma''}(\mathbf{r}) \mathcal{G}_{\sigma'\sigma''}(\mathbf{r}', \tau'; \mathbf{r}, \tau) = 0, \tag{10.20}$$

where

$$\Delta^*_{\sigma'\sigma}(\mathbf{r}) = \lambda \mathcal{F}^{+}_{\sigma\sigma'}(\mathbf{r}, \tau + \eta; \mathbf{r}, \tau). \tag{10.21}$$

These equations are known as Gorkov's equations. Note that Eq. (10.19) contains the complex conjugate of the Hamiltonian $\hat{H}_0$.

It is the presence of the field $\Delta(\mathbf{r})$ that makes the Gorkov equations different from the equations for the Green function in a normal metal. The field Δ is related to the energy gap for quasiparticle excitations in a superconductor (see below). It also serves as an "order parameter" that distinguishes the superconducting state from the normal state. In that sense, it plays the same role as the magnetization in the normal-metal–ferromagnet transition.

Solving these equations by means of a Fourier transform, we find

$$\begin{aligned} \mathcal{G}_{\mathbf{k}\sigma,\mathbf{k}'\sigma'}(i\omega_n) &= -\frac{(i\omega_n + (\varepsilon_{\mathbf{k}} - \mu))\delta_{\mathbf{k}\mathbf{k}'}\delta_{\sigma\sigma'}}{\omega_n^2 + (\varepsilon_{\mathbf{k}} - \mu)^2 + |\Delta_{\uparrow\downarrow}|^2} \\ \mathcal{F}^{+}_{\mathbf{k}\sigma,\mathbf{k}'\sigma'}(i\omega_n) &= \frac{\Delta^*_{\sigma'\sigma}\delta_{\mathbf{k}\mathbf{k}'}}{\omega_n^2 + (\varepsilon_{\mathbf{k}} - \mu)^2 + |\Delta_{\uparrow\downarrow}|^2}. \end{aligned} \tag{10.22}$$

[3]Strictly speaking, one would need to take the finite range of the attractive interaction into account. In accordance with the momentum cut off at $|\varepsilon_{\mathbf{k}} - \mu| \geq \hbar\omega_{\mathrm{D}}$, the interaction (10.2) has a range of order v_F/ω_D. However, as we'll see below, the anomalous Green function $\mathcal{F}(\mathbf{r}, \mathbf{r}')$ is smooth on the scale v_F/ω_D, its spatial variations occurring on the much larger scale v_F/T_c only. This implies that the approximation made in setting both coordinates equal in the argument of $\mathcal{F}$ is justified.

Self-consistency is achieved upon substitution of the solution for $\mathcal{F}$ into the definition of Δ,

$$1 = \lambda \frac{T}{V} \sum_n \sum_{\mathbf{k}} \frac{1}{\omega_n^2 + (\varepsilon_{\mathbf{k}} - \mu)^2 + |\Delta_{\uparrow\downarrow}|^2}. \tag{10.23}$$

Performing the summation over Matsubara frequencies, replacing the summation over momenta $\mathbf{k}$ by an integration over energies $\varepsilon_{\mathbf{k}}$ and remembering that only momenta with $|\varepsilon_{\mathbf{k}} - \mu| < \hbar\omega_{\rm D}$ play a role, we find the self-consistency condition

$$1 = \lambda\nu \int_0^{\hbar\omega_D} d\xi \frac{\tanh[\sqrt{\xi^2 + |\Delta_{\uparrow\downarrow}|^2}/2T]}{\sqrt{\xi^2 + |\Delta_{\uparrow\downarrow}|^2}}. \tag{10.24}$$

This is the same equation as the "gap equation" from standard BCS theory.

The highest temperature with a nontrivial solution of the self-consistency equation is the point where the normal-metal–superconductor phase transition occurs. Since $\Delta_{\uparrow\downarrow} = 0$ at $T = T_c$, we find that the critical temperature satisfies the equation

$$1 = \lambda\nu \int_0^{\hbar\omega_D} d\xi \frac{\tanh(\xi/2T_c)}{\xi}. \tag{10.25}$$

This is precisely the same equation as we found for the divergence of the correlator R in the previous section, see Eq. (10.12) above. Hence

$$T_c = 1.14\hbar\omega_{\rm D} e^{-1/\lambda\nu}. \tag{10.26}$$

Quasiparticle excitations of the superconductor correspond to poles of the retarded Green functions G and F. Analytical continuation of Eq. (10.22) gives

$$\begin{aligned} G^{\rm R}_{\mathbf{k}\sigma,\mathbf{k}'\sigma'}(\omega) &= -\frac{(\omega + \varepsilon_{\mathbf{k}} - \mu)\delta_{\mathbf{k}\mathbf{k}'}\delta_{\sigma\sigma'}}{(\varepsilon_{\mathbf{k}} - \mu)^2 + |\Delta|^2 - (\omega + i\eta)^2} \\ F^{+{\rm R}}_{\mathbf{k}\sigma,\mathbf{k}'\sigma'}(\omega) &= \frac{\Delta^*_{\sigma'\sigma}\delta_{\mathbf{k}\mathbf{k}'}}{(\varepsilon_{\mathbf{k}} - \mu)^2 + |\Delta|^2 - (\omega + i\eta)^2}. \end{aligned} \tag{10.27}$$

We thus conclude that the quasiparticle energies are

$$\xi_{\mathbf{k}} = \pm\sqrt{(\varepsilon_{\mathbf{k}} - \mu)^2 + |\Delta|^2}. \tag{10.28}$$

From here we conclude that the excitation spectrum has a gap of size $|\Delta|$.

We close this section with a few remarks on the role of a vector potential $\mathbf{A}(\mathbf{r})$ and gauge invariance. A vector potential can be included in the Hamiltonian $\hat{H}_0$ by the replacement

$$\partial_{\mathbf{r}} \to \partial_{\mathbf{r}} - \frac{ie}{\hbar c} A. \tag{10.29}$$

In the complex conjugate Hamiltonian $\hat{H}_0^*$ this corresponds to the replacement $\partial_{\mathbf{r}} \to \partial_{\mathbf{r}} + ie\mathbf{A}/\hbar c$. Gauge invariance requires that the theory is invariant under transformations

$$\mathbf{A} \to \mathbf{A} + \partial_{\mathbf{r}}\chi, \tag{10.30}$$

where χ is an arbitrary function of the position $\mathbf{r}$. Green functions are not gauge-invariant objects. Under the gauge transformation (10.30), the Green functions transform as

$$\begin{aligned} \mathcal{G}(\mathbf{r},\mathbf{r}') &\to \mathcal{G}(\mathbf{r},\mathbf{r}')e^{ie(\chi(\mathbf{r})-\chi(\mathbf{r}'))/\hbar c}, \\ \mathcal{F}(\mathbf{r},\mathbf{r}') &\to \mathcal{F}(\mathbf{r},\mathbf{r}')e^{ie(\chi(\mathbf{r})+\chi(\mathbf{r}'))/\hbar c}, \\ \mathcal{F}^+(\mathbf{r},\mathbf{r}') &\to \mathcal{F}^+(\mathbf{r},\mathbf{r}')e^{-ie(\chi(\mathbf{r})+\chi(\mathbf{r}'))/\hbar c}. \end{aligned} \tag{10.31}$$

In particular, this implies that the field $\Delta(\mathbf{r})$ transforms as

$$\Delta(\mathbf{r}) \to \Delta(\mathbf{r})e^{2ie\chi(\mathbf{r})/\hbar c}. \tag{10.32}$$

The Gorkov equations serve as the basis for further investigations of the superconducting state. Results obtained from the Gorkov equations agree with those obtained from the mean-field BCS theory. For reviews, we refer to the book by Tinkham.[4] Here we forego a discussion of thermodynamic properties and the Josephson effect, and limit ourselves to a discussion of the response of superconductors to electromagnetic radiation.

10.3 A superconductor in a weak electromagnetic field

In this section, we calculate the current density in a superconductor in response to an external vector potential $\mathbf{A}$.

Starting point of the calculation is the Kubo formula. Repeating results of Sec. 5.6, we have

$$j_{e,\mathbf{q}\alpha}(\omega) = -\sum_\beta \Pi^{\mathrm{R}}_{\alpha\beta}(\mathbf{q},\omega)A_{\beta,\mathbf{q}}(\omega) - \frac{e\rho_e}{m}A_{\alpha,\mathbf{q}}(\omega), \tag{10.33}$$

where Π^{R} is the retarded current density autocorrelation function,

$$\Pi_{\alpha\beta}(\mathbf{q},\tau) = -\frac{1}{V}\langle T_\tau j_{e,\mathbf{q}\alpha}(\tau)j_{e,-\mathbf{q}\beta}(0)\rangle, \tag{10.34}$$

[4]See *Introduction to Superconductivity*, M. Tinkham (Mc Graw Hill College Div., 1995). Other useful references are *Superconductivity of Metals and Alloys*, P.G. de Gennes (Perseus, 1999) and *Methods of Quantum Field Theory in Statistical Physics*, A.A. Abrikosov, L.P. Gorkov, and I.E. Dzyaloshinski (Dover 1977).

and

$$\mathbf{j}_{e,\mathbf{q}} = \frac{e}{2m}\sum_{\mathbf{k}\sigma}(2\mathbf{k}+\mathbf{q})\hat{\psi}^{\dagger}_{\mathbf{k},\sigma}\hat{\psi}_{\mathbf{k}+\mathbf{q},\sigma}. \tag{10.35}$$

Equation (10.33) describes the linear response of the current density to a vector potential $\mathbf{A}$. We used this relation in Sec. 5.6 to find the conductivity of a disordered normal metal, the coefficient of proportionality between the current density and the electric field $\mathbf{E}(\omega) = i\omega\mathbf{A}(\omega)$. In the normal metal, the choice of the gauge for the vector potential $\mathbf{A}$ was not relevant. This is different for the case of a superconductor. The reason is that the vector potential $\mathbf{A}$ enters in the equation for the single-particle Green functions $\mathcal{G}$ and $\mathcal{F}$, and, hence, affects the value of the "order parameter" Δ. To linear order in $\mathbf{A}$, Δ can only depend on $\partial_{\mathbf{r}}\cdot\mathbf{A}$. Hence, if we choose the gauge such that $\partial_{\mathbf{r}}\cdot\mathbf{A} = 0$, Δ is unchanged to linear order in the vector potential. This choice of the gauge is known as the "London gauge".

Let us now calculate the current density autocorrelation function for the case of a clean superconductor. Using the Matsubara frequency language, we find

$$\begin{aligned}\Pi_{\alpha\beta}(\mathbf{q}, i\Omega_n) &= \frac{e^2T}{2m^2V}\sum_{\mathbf{k},m}(2k_\alpha+q_\alpha)(2k_\beta+q_\beta) \\ &\quad\times\left[\mathcal{G}_{\mathbf{k}+\mathbf{q},\mathbf{k}+\mathbf{q}}(i\omega_m+i\Omega_n)\mathcal{G}_{\mathbf{k};\mathbf{k}}(i\omega_m)+\mathcal{F}_{\mathbf{k}+\mathbf{q},\mathbf{k}+\mathbf{q}}(i\omega_m+i\Omega_n)\mathcal{F}^{+}_{\mathbf{k},\mathbf{k}}(i\omega_m)\right].\end{aligned} \tag{10.36}$$

Changing variables to $\mathbf{k}_\pm = \mathbf{k}\pm(\mathbf{q}/2)$ and $\omega_{m\pm} = \omega_m \pm (\Omega_n/2)$, we rewrite this as

$$\begin{aligned}\Pi_{\alpha\beta}(\mathbf{q}, i\Omega_n) &= \frac{2e^2T}{m^2V}\sum_{\mathbf{k},m}k_\alpha k_\beta\left[\mathcal{G}_{\mathbf{k}_+,\mathbf{k}_+}(i\omega_{m+})\mathcal{G}_{\mathbf{k}_-,\mathbf{k}_-}(i\omega_{m-})+\mathcal{F}_{\mathbf{k}_+,\mathbf{k}_+}(i\omega_{m+})\mathcal{F}^{+}_{\mathbf{k}_-,\mathbf{k}_-}(i\omega_{m-})\right] \\ &= \frac{2e^2T}{m^2V}\sum_{\mathbf{k},m}k_\alpha k_\beta\frac{(i\omega_{m+}+\varepsilon_{\mathbf{k}_+}-\mu)(i\omega_{m-}+\varepsilon_{\mathbf{k}_-}-\mu)+|\Delta|^2}{(\omega^2_{m+}+(\varepsilon_{\mathbf{k}_+}-\mu)^2+|\Delta|^2)(\omega^2_{m-}+(\varepsilon_{\mathbf{k}_-}-\mu)^2+|\Delta|^2)},\end{aligned}$$

where we substituted the solution (10.22) for the Green functions $\mathcal{G}$ and $\mathcal{F}$. Next, we replace the summation over $\mathbf{k}$ by an integration over $\xi = \varepsilon_{\mathbf{k}} - \mu$ and over the angle θ between $\mathbf{q}$ and $\mathbf{k}$.

Next we introduce polar coordinates for the vector $\mathbf{k}$. We choose the direction of $\mathbf{q}$ as the polar axis. The average over the azimuthal angle ϕ can be performed directly. Noting that $\mathbf{q}$ and $\mathbf{A}$ are orthogonal in the London gauge, upon performing the average over ϕ we find that Π is diagonal, and proportional to $(1/2)\sin^2\theta$, where θ is the angle between $\mathbf{q}$ and $\mathbf{k}$. Further, since the main contribution comes from momenta close to the Fermi momentum, we set the magnitude of the factors k_α and k_β equal to k_F. Finally, using the equality $\nu k_F^2/m = 3n/2$, where n is the electron density and ν the normal-metal density of states at

the Fermi level (per spin direction and per unit volume), and replacing the summation over $\mathbf{k}$ by an integration over $\xi = \varepsilon_{\mathbf{k}} - \mu$ and an integration over θ, we find

$$\Pi_{\alpha\beta}(\mathbf{q}, i\Omega_n) = \frac{3Te^2n}{4m}\delta_{\alpha\beta}\sum_m \int d\xi \int_0^\pi d\theta \sin^3\theta \frac{(i\omega_{m+}+\xi_+)(i\omega_{m-}+\xi_-)+|\Delta|^2}{(\omega_{m+}^2+\xi_+^2+|\Delta|^2)(\omega_{m-}^2+\xi_-^2+|\Delta|^2)},$$

where $\xi_\pm = \xi \pm (v_F q/2)\cos\theta$.

Because of the approximations involved, the summation over Matsubara frequencies should be performed before the integration over ξ. Performing the integration over ξ first gives a different answer. The answer depends on the order of the integrations because the integral (10.37) is formally divergent. Our formulas for the ξ-dependence of the single-electron Green functions are valid close to the Fermi level only. After the summation over the Matsubara frequencies, the ξ integration is, in fact, convergent, the main contribution coming from momenta near the Fermi level.

For the case of the superconductor, there is a trick that allows us to do the ξ integration first, nevertheless. The trick is to look at the difference between current density correlation functions for the normal metal and for the superconductor. For this difference, the integrations and summations over ξ and ω_m are convergent, so that the order of integrations is no longer important. Hence, if we calculate the difference between current-current correlation functions for the normal metal and superconducting states, we can perform the ξ integration before the summation over Matsubara frequencies. The current density autocorrelation function for the normal metal is

$$\begin{aligned}\Pi^{\mathrm{N}}_{\alpha\beta}(\mathbf{q}, i\Omega_n) &= \frac{3Te^2n}{4m}\delta_{\alpha\beta}\sum_m \int d\xi \int_0^\pi d\theta \sin^3\theta \frac{1}{(i\omega_{m+}-\xi_+)(i\omega_{m-}-\xi_-)} \\ &= -\frac{e\rho_e}{m}, \end{aligned} \tag{10.37}$$

see Ex. 5.6. Integrating with respect to ξ we then obtain

$$\begin{aligned}\Pi_{\alpha\beta}(\mathbf{q}, i\Omega_n) = &-\frac{e\rho_e}{m} + \frac{3\pi Te\rho_e}{4m}\delta_{\alpha\beta}\sum_m \int_0^\pi d\theta \sin^3\theta \\ &\times \left[\frac{(i\omega_{m+}+i\sqrt{\omega_{m+}^2+|\Delta|^2})(i\omega_{m-}-qv_F\cos\theta+i\sqrt{\omega_{m+}^2+|\Delta|^2})+|\Delta|^2}{(\omega_{m-}^2+|\Delta|^2+(qv_F\cos\theta-i\sqrt{\omega_{m+}^2+|\Delta|^2})^2)\sqrt{\omega_{m+}^2+|\Delta|^2}}\right. \\ &\left. + \frac{(i\omega_{m-}+i\sqrt{\omega_{m-}^2+|\Delta|^2})(i\omega_{m+}-qv_F\cos\theta+i\sqrt{\omega_{m-}^2+|\Delta|^2})+|\Delta|^2}{(\omega_{m+}^2+|\Delta|^2+(qv_F\cos\theta-i\sqrt{\omega_{m-}^2+|\Delta|^2})^2)\sqrt{\omega_{m-}^2+|\Delta|^2}}\right]. \end{aligned} \tag{10.38}$$

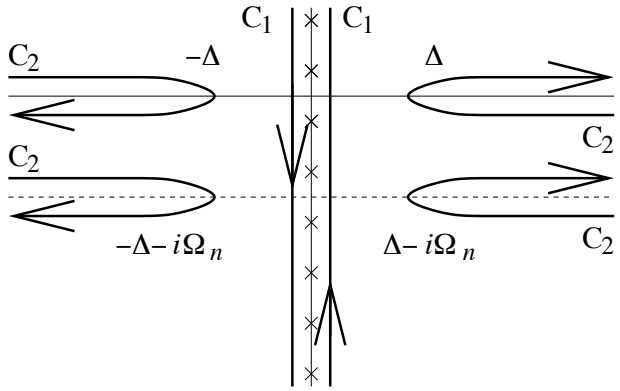

Figure 10.2: Integration contour for the calculation of Eq. (10.40).

Next, we perform the summation over the Matsubara frequency ω_m. We undo the shift of variables for the Matsubara frequencies, i.e., we replace $\omega_{m+} \to \omega_m + \Omega_n$ and $\omega_{m-} \to \omega_m$. We then represent the summation over Matsubara frequencies as an integral in the complex plane and deform the integration contour as shown in Fig. 10.2. The integrand has a square root branch cut. In identifying the correct sign of the square root, one needs the relations

$$\sqrt{|\Delta|^2 - (\omega \pm i\eta)^2} = \begin{cases} \sqrt{|\Delta|^2 - \omega^2} & \text{if } |\omega| < |\Delta|, \\ \mp i \,\mathrm{sign}(\omega) \sqrt{\omega^2 - |\Delta|^2} & \text{if } |\omega| \geq |\Delta|. \end{cases} \tag{10.39}$$

After the integration contours have been deformed as in Fig. 10.2, we can perform the analytical continuation $i\Omega_n \to \omega + i\eta$.

Obtaining the final equations for $\Pi_{\alpha\beta}(\mathbf{q}, \omega)$, which contain one integration over a real energy variable and one integration over the angle θ is straightforward, but tedious. Below, we'll restrict ourselves to static response $\omega \to 0$. In this case, the integration above the lower branch cut cancels the integration below the upper branch cut in Fig. 10.2. What remains is the integration above the upper branch cut and the integration below the lower branch cut,

$$\begin{aligned} \Pi^{\mathrm{R}}_{\alpha\beta}(\mathbf{q}, 0) &= -\frac{e\rho_e}{m} + \frac{3\pi e\rho_e}{8\pi m}\delta_{\alpha\beta} \int_0^\pi d\theta \sin^3\theta \int_\Delta^\infty d\zeta \tanh(\zeta/2T) \\ &\quad \times \sum_\pm \frac{|\Delta|^2}{\sqrt{\zeta^2 - |\Delta|^2}(|\Delta|^2 - (\zeta \pm i\eta)^2 + (v_F^2 q^2/4)\cos^2\theta)}. \end{aligned} \tag{10.40}$$

The easiest way to evaluate this integral is to rewrite it as a sum over Matsubara frequencies,

$$\Pi^{\mathrm{R}}_{\alpha\beta}(\mathbf{q}, 0) = -\frac{e\rho_e}{m}\delta_{\alpha\beta} + \frac{3\pi e\rho_e T}{4m}\delta_{\alpha\beta} \sum_m \int_0^\pi d\theta \sin^3\theta$$

$$\times \frac{|\Delta|^2}{(\omega_m^2 + |\Delta|^2 + (v_F^2 q^2/4)\cos^2\theta)\sqrt{\omega_m^2 + |\Delta|^2}}. \tag{10.41}$$

Evaluation of this expression is further simplified in the limits $qv_F \ll \max(|\Delta|, T)$ and $qv_F \gg \max(|\Delta|, T)$.

If $qv_F \ll \max(|\Delta|, T)$, we can neglect the q-dependence of the summand and find

$$\Pi^{\rm R}_{\alpha\beta}(\mathbf{q}, 0) = -\frac{e\rho_e}{m}\delta_{\alpha\beta}\left(1 - \frac{n_s(T)}{n}\right), \tag{10.42}$$

where n_s is the so-called "superconducting density",

$$n_s = \frac{n\pi T|\Delta|^2}{2}\sum_m \frac{1}{(\omega_m^2 + |\Delta|^2)^{3/2}}. \tag{10.43}$$

For zero temperature the superconducting density is equal to the electron density n. The superconducting density approaches zero as T approaches T_c.

If $qv_F \gg \max(|\Delta|, T)$, the main contribution to the integral over the angle θ comes from angles close to $\theta = \pi/2$. For those angles we may set $\sin\theta = 1$. Replacing the θ-integration by an integration over $\cos\theta$ and extending the integration interval to the entire real axis, we find

$$\begin{aligned}\Pi^{\rm R}_{\alpha\beta}(\mathbf{q}, 0) &= -\frac{e\rho_e}{m}\delta_{\alpha\beta} + \frac{3\pi^2 e\rho_e T}{2mqv_F}\delta_{\alpha\beta}\sum_m \frac{|\Delta|^2}{\omega_m^2 + |\Delta|^2} \\ &= -\frac{e\rho_e}{m}\delta_{\alpha\beta} + \frac{3\pi^2 e\rho_e |\Delta|}{4mqv_F}\delta_{\alpha\beta}\tanh\frac{|\Delta|}{2T}.\end{aligned} \tag{10.44}$$

Unlike in the case of a normal metal, we find that for a superconductor the current density $\mathbf{j}(\mathbf{q}, \omega)$ is proportional to the vector potential $\mathbf{A}$ itself, and not to its time-derivative. This dependence is the cause of the Meissner effect, the phenomenon that no magnetic field can exist in a superconductor, except for a thin layer of thickness δ close to the superconductor surface. For a superconductor for which $v_F/\delta \ll \max(T, \Delta)$, the Meissner effect can be described with the help of Eq. (10.42) above,

$$\mathbf{j} = -\frac{n_s e^2}{m}\mathbf{A}. \tag{10.45}$$

Combining Eq. (10.45) with the Maxwell equation $\partial_{\mathbf{r}}^2\mathbf{A} = -\mathbf{j}$ for the London gauge $\partial_{\mathbf{r}}\cdot\mathbf{A} = 0$, we find $\delta = \sqrt{m/n_s e^2}$. Equation (10.45) is known as the London equation, and δ is known as the London penetration depth. A superconductor for which $\delta \gg v_F/\max(T, \Delta)$ is said to be

"of London type". For a superconductor for which $\delta \ll v_F/\max(T,\Delta)$, Eq. (10.44) has to be used instead of Eq. (10.42). In this case, the mathematical solution is more complicated, but the qualitative conclusion, no magnetic field inside the superconductor, except for a surface layer of thickness δ, remains true. Superconductors for which $\delta \ll v_F/\max(T,\Delta)$ are said to be "of Pippard type". Equation (10.44) is known as the Pippard equation.

Most pure superconductors at $T \ll T_c$ are of Pippard type. Close to T_c, δ increases, and a crossover to the London type of behavior is seen.

These calculations can be repeated for the case of a disordered superconductor with elastic mean free time τ. The calculation proceeds along the lines of Sec. 5.6 and has the following results: First, the addition of impurities does not affect the magnitude of the superconducting order parameter Δ. Second, the effect of impurities is small if $qv_F\tau \gg 1$, whereas, in the opposite limit, $qv_F\tau \ll 1$, one recovers the London equation (10.45), with a reduced superconducting density

$$n_s = \frac{n\pi T|\Delta|^2}{2} \sum_m \frac{1}{(\omega_m^2 + |\Delta|^2)(\sqrt{\omega_m^2 + |\Delta|^2} + 1/2\tau)}. \tag{10.46}$$

As a result of the reduced superconducting density, the London penetration depth δ is strongly enhanced. As a result, for sufficiently strong disorder, disordered superconductors are always in the London limit.

10.4 Quasiclassical theory

The Green functions for a superconductor satisfy the Gorkov equation (10.19). Apart from the fact that they involve three different Green functions, $\mathcal{G}$, $\mathcal{F}$, and $\mathcal{F}^+$, and apart from the self-consistency condition (10.21), the Gorkov equations are nothing but the defining equation for the single-particle Green function of non-interacting particles. For non-interacting particles, we saw that a full quantum mechanical treatment was not necessary in most cases. (The exception is if one is interested in quantum interference effects, such as the weak localization correction to the conductivity.) Instead of a full quantum solution, most problems are amendable to a semiclassical treatment. For normal metals, the resulting equation is the Boltzmann equation. A semiclassical theory is particularly useful if a system is not homogeneous, as is the case, *e.g.*, in the presence of weak electromagnetic fields or near the interface of a normal metal and a superconductor. We now discuss a semiclassical treatment of the Gorkov equations.

As before, we consider the single-particle Green functions as operators on the Hilbert space. The operator action is then nothing but the convolution. In order to be able to deal with non-equilibrium situations, we use the real time formalism. We will be considering

the effect of spatial dependences of the potentials, but we will not consider time-dependent potentials or fields.

In order to simplify our notation, we combine the standard and the anomalous Green functions into a 2×2 matrix,

$$\hat{G}(\mathbf{r},t;\mathbf{r}',t') = \begin{pmatrix} -i\langle T_{\rm c}\hat{\psi}_\uparrow(\mathbf{r},t)\hat{\psi}_\uparrow^\dagger(\mathbf{r}',t')\rangle & -i\langle T_{\rm c}\hat{\psi}_\uparrow(\mathbf{r},t)\hat{\psi}_\downarrow(\mathbf{r}',t')\rangle \\ i\langle T_{\rm c}\hat{\psi}_\downarrow^\dagger(\mathbf{r},t)\hat{\psi}_\uparrow^\dagger(\mathbf{r}',t')\rangle & i\langle T_{\rm c}\hat{\psi}_\downarrow^\dagger(\mathbf{r},t)\hat{\psi}_\downarrow(\mathbf{r}',t')\rangle \end{pmatrix}. \tag{10.47}$$

The matrix notion of Eq. (10.47) was first proposed by Nambu. Using Nambu's notation, and using the operator notation for the Green function, the Gorkov equations read

$$\left(i\hbar\hat{\tau}_3\partial_t - \hat{\mathcal{H}}_0 + \hat{\Delta}\right)\hat{G} = \delta(\mathbf{r}-\mathbf{r}')\delta_{\rm c}(t-t') \tag{10.48}$$

where $\hat{\tau}_3$ is the Pauli matrix with respect to the Nambu grading of Eq. (10.47), $\hat{\mathcal{H}}_0$ is the Hamiltonian without superconducting order parameter,

$$\mathcal{H}_0(\mathbf{r},t;\mathbf{r}',t') \;=\; \delta(\mathbf{r}-\mathbf{r}')\delta(t-t')\left[-\frac{\hbar^2}{2m}\left(\partial_{\mathbf{r}} - \frac{ie}{\hbar c}\hat{\tau}_3\mathbf{A}(\mathbf{r})\right)^2 + e\phi(\mathbf{r}) - \mu\right], \tag{10.49}$$

$\hat{\Delta}$ is the matrix notation for the superconducting order parameter $\Delta(\mathbf{r}) = \lambda\langle\hat{\psi}_\uparrow(\mathbf{r},t)\hat{\psi}_\downarrow(\mathbf{r},t)\rangle$,

$$\hat{\Delta}(\mathbf{r},t;\mathbf{r}',t') = \delta(\mathbf{r}-\mathbf{r}')\delta(t-t')\begin{pmatrix} 0 & \Delta(\mathbf{r}) \\ -\Delta^*(\mathbf{r}) & 0 \end{pmatrix}, \tag{10.50}$$

and the delta function $\delta_{\rm c}(t-t')$ is defined with respect to the contour points t and t', not with respect to times.[5]

If we consider a superconductor with impurities with a short-range potential, the ensemble average over the impurities may be performed. This gives an additional self-energy term that must be included in the in the Gorkov equation. With inclusion of the self energy, the Gorkov equations (10.48) read

$$\left(i\hbar\hat{\tau}_3\partial_t - \hat{\mathcal{H}}_0 - \hat{\Sigma} + \hat{\Delta}\right)\hat{G} = \delta(\mathbf{r}-\mathbf{r}')\delta_{\rm c}(t-t'). \tag{10.51}$$

Following the procedure we used previously for normal metals, we introduce the matrix notation for the Keldysh Green functions, *cf.* Eq. (2.61). Together with the Nambu matrix

[5] If a notation in terms of times is used, $\delta_{\rm c}(t-t') = \delta(t-t')$ if t and t' are both on the upper branch of the Keldysh contour, $\delta_{\rm c}(t-t') = -\delta(t-t')$ if t and t' are both on the lower branch of the Keldysh contour, and $\delta_{\rm c}(t-t') = 0$ otherwise.

notation, this means that the Green function is now represented by a 4×4 matrix. Rewriting the Gorkov equations in this way, one finds

$$\left(i\hbar\hat{\tau}_3\partial_t - \hat{\mathcal{H}}_0 - \hat{\Sigma} + \hat{\Delta}\right)\hat{G} = \mathcal{I}, \tag{10.52}$$

where $\mathcal{I}$ is the identity operator. In Eq. (10.52), the matrices $\hat{\tau}_3$ and $\hat{\Delta}$ are 4×4 matrices in the combined Keldysh/Nambu grading. They are obtained from the corresponding matrices with the Nambu grading only by taking the tensor product with the 2×2 unit matrix in the Keldysh grading.

The Gorkov equation may also be written as

$$\hat{G}\left(i\hbar\hat{\tau}_3\partial_t - \hat{\mathcal{H}}_0 - \hat{\Sigma} + \hat{\Delta}\right) = \hat{\mathcal{I}}. \tag{10.53}$$

Taking the difference of Eqs. (10.52) and (10.53), one finds

$$\left[i\hbar\partial_t\hat{\tau}_3 - \hat{\mathcal{H}}_0 - \hat{\Sigma} + \hat{\Delta}, \hat{G}\right]_- = 0. \tag{10.54}$$

This is the equation we'll study in more detail below.

In order to arrive at a quasiclassical description, we perform a Fourier transform with respect to the coordinate difference $\mathbf{r}-\mathbf{r}'$. We also perform a Fourier transform to the time difference $t-t'$. Since the Green functions and the Hamiltonian do not depend on time, the Fourier transform to time can be taken exactly. The Fourier transform to the coordinate difference is treated in the gradient approximation. One then finds that $\hat{G}(\mathbf{k},\mathbf{R};\omega)$ satisfies the differential equation

$$\left[\hbar\omega\hat{\tau}_3 + i\hbar\mathbf{v}\cdot\hat{\partial}_{\mathbf{R}} + \hat{\Delta} - \hat{\Sigma}, \hat{G}\right]_- - i\left[\partial_{\mathbf{R}}(\hat{\Sigma}+\hat{\Delta}+e\phi), \partial_{\mathbf{k}}\hat{G}\right]_+ + i\left[\partial_{\mathbf{k}}\hat{\Sigma}, \partial_{\mathbf{R}}\hat{G}\right]_+ = 0. \tag{10.55}$$

where $\mathbf{v} = (\hbar/m)(\mathbf{k} - \hat{\tau}_3 e\mathbf{A}/\hbar c)$ is the electron velocity and

$$\hat{\partial}_{\mathbf{R}} = \partial_{\mathbf{R}} - \hat{\tau}_3(ie/\hbar c)\mathbf{A}(\mathbf{R}) \tag{10.56}$$

the covariant derivative. In writing down Eq. (10.55) we neglected the effect of a magnetic field on the motion of the electrons.

If impurities are modeled by the Gaussian white noise potential and impurity scattering is treated in the lowest order Born approximation, the self-energy $\hat{\Sigma}$ reads

$$\hat{\Sigma} = \frac{1}{2\pi\tau}\int d\xi_{\mathbf{k}}\hat{G}(\mathbf{k},\mathbf{R},\omega), \tag{10.57}$$

cf. Eq. (5.34).

We now define the quasiclassical Green function by parameterizing the wavevector $\mathbf{k}$ through the energy ξ and the direction $\mathbf{n}$, and integrating over ξ,

$$g(\mathbf{R},\mathbf{n},\omega) = \frac{i}{\pi}\int d\xi G(\mathbf{R},\mathbf{k},\omega). \tag{10.58}$$

Neglecting the weak ξ dependence of the self energy, as well as the direction of G on $\mathbf{n}$ if multiplied with a spatial derivative, we arrive at an equation for the quasiclassical Green function only,

$$\left[i\hbar v_F \mathbf{n}\cdot\hat{\partial}_{\mathbf{R}} + \hbar\omega\hat{\tau}_3 - \hat{\Delta} - \hat{\sigma}, \hat{g}\right]_- = 0. \tag{10.59}$$

Equation (10.59) is known as the Eilenberger equation. The quasiclassical $\hat{g}$ has a matrix structure in Nambu space,

$$\hat{g} = \begin{pmatrix} g & f \\ f^+ & -g \end{pmatrix}. \tag{10.60}$$

You can verify this either from the definition of the quasiclassical Green function itself, or by noting that the Eilenberger equation contains commutators only, so that one can search for solutions that are linear combinations of the three Pauli matrices $\hat{\tau}_1$, $\hat{\tau}_2$, and $\hat{\tau}_3$. Also, f^+ is the time reversed of f, which need not be the complex conjugate of f. The self-energy now reads

$$\hat{\sigma} = -\frac{i}{2\tau}\langle\hat{g}\rangle_{\mathbf{n}}, \tag{10.61}$$

where the brackets $\langle\ldots\rangle_{\mathbf{n}}$ indicate an average over all directions $\mathbf{n}$.

Note that the Eilenberger equation is homogeneous in $\hat{g}$, so that it does not fix the magnitude of the quasiclassical Green function. One can fix the magnitude of g as follows: Because of the special matrix structure of $\hat{g}$, cf. Eq. (10.60), the square $\hat{g}\hat{g}$ is proportional to the unit matrix. Upon substition into Eq. (10.59) one finds that the proportionality constant is uniform throughout space. Both deep inside a normal metal and deep inside a superconductor the solution for the quasiclassical Green function is known: it obeys

$$\hat{g}\hat{g} = \hat{1}, \tag{10.62}$$

so that the proportionality constant must be unity throughout space.

It is instructive to write down the solutions for the quasiclassical Green functions in equilibrium. In that case, it is sufficient to calculate the retarded Green function, which obeys the equations

$$[\hbar\omega\hat{\tau}_3 + \hat{\Delta}, \hat{g}^{\mathrm{R}}]_- = 0, \quad \hat{g}^{\mathrm{R}}\hat{g}^{\mathrm{R}} = 1. \tag{10.63}$$

Together with the condition that $\hat{g}^{\rm R}$ has the matrix structure (10.60), one then finds

$$\hat{g}^{\rm R} = \frac{1}{\sqrt{\omega^2 - |\Delta|^2}} \begin{pmatrix} \hbar\omega & \Delta \\ -\Delta^* & -\hbar\omega \end{pmatrix}. \tag{10.64}$$

For $\hbar\omega < |\Delta|$ one determines the phase of the square roots by setting $\omega \to \omega + i\eta$, where η is a positive infinitesimal. The advanced Green function then reads $\hat{g}^{\rm A} = -\tau^3 \hat{g}^{\rm R\dagger} \tau^3$, where the superscript $\dagger$ means hermitian conjugation. In a normal metal ($\Delta = 0$), the solutions for the quasiclassical Green functions are $\hat{g}^{\rm R} = \hat{\tau}_3$, $\hat{g}^{\rm A} = -\hat{\tau}_3$, in agreement with Ex. 3.4.

If scattering from impurities is very strong, the electron motion is diffusive, not ballistic, and the equations for the quasiclassical Green functions can be further simplified. As we'll see below, "strong" means that the scattering rate $\hbar/\tau$ is large in comparison to both T and Δ. The role of impurity scattering is to randomize the direction of the electron's velocity. Hence, one expects that a description in terms of a quasiclassical Green function that is averaged over all directions of the electron's velocity is possible. In order to arrive at such a description, we first use an intermediate formulation in which we keep information on the current density: we take $\hat{g}(\mathbf{n})$ to be of the form

$$\hat{g}(\mathbf{n}) = \hat{g}_0 + \mathbf{n} \cdot \hat{\mathbf{g}}_1. \tag{10.65}$$

Similarly, the self energy is written

$$\hat{\sigma}(\mathbf{n}) = \hat{\sigma}_0 + \mathbf{n} \cdot \hat{\boldsymbol{\sigma}}_1. \tag{10.66}$$

For a white noise potential, one then finds from Eq. (10.61) that

$$\hat{\sigma}_0 = -\frac{i}{2\tau}\hat{g}_0, \quad \hat{\boldsymbol{\sigma}}_1 = 0. \tag{10.67}$$

For strong impurity scattering, one expects that $\hat{\mathbf{g}}_1$ is small in comparison to $\hat{\mathbf{g}}_0$. Hence, we expand the Eilenberger equation and the normalization condition up to terms of first order in $\hat{\mathbf{g}}_1$. The normalization condition for the quasiclassical Green function thus reads

$$\hat{g}_0 \hat{g}_0 = 1, \quad [\hat{g}_0, \hat{\mathbf{g}}_1]_+ = 0. \tag{10.68}$$

An equation for the $\mathbf{n}$-averaged Green functions $\hat{g}_0$ and $\hat{\mathbf{g}}_1$ is obtained upon substitution of the angular dependencies (10.65) and (10.66) into the Eilenberger equation (10.59). One then finds

$$\begin{aligned} 0 &= \left[\hbar\omega\hat{\tau}_3 - \hat{\Delta}, \hat{g}_0 + \mathbf{n}\cdot\hat{\mathbf{g}}_1\right]_- + \left[iv_F \mathbf{n}\cdot\hat{\partial}_{\mathbf{R}}, \hat{g}_0 + \mathbf{n}\cdot\hat{\mathbf{g}}_1\right]_- - \left[\hat{\sigma}_0, \hat{g}_0 + \mathbf{n}\cdot\hat{\mathbf{g}}_1\right]_- \\ &\approx \left[\hbar\omega\hat{\tau}_3 - \hat{\Delta}, \hat{g}_0\right]_- + \left[iv_F \mathbf{n}\cdot\hat{\partial}_{\mathbf{R}}, \hat{g}_0 + \mathbf{n}\cdot\hat{\mathbf{g}}_1\right]_- - \frac{i}{2\tau}\left[\hat{g}_0, \mathbf{n}\cdot\hat{\mathbf{g}}_1\right]_- . \end{aligned} \tag{10.69}$$

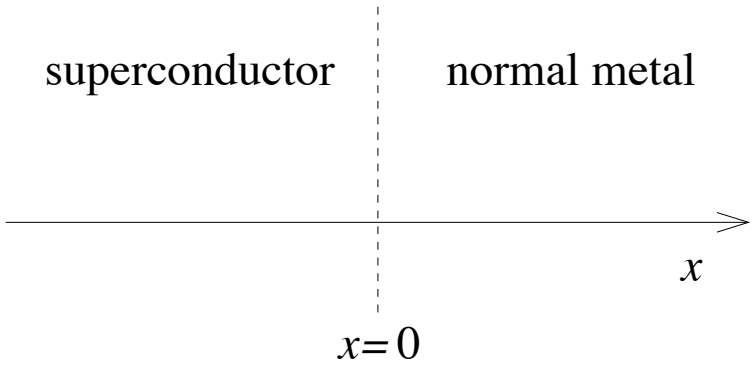

Figure 10.3: Schematic drawing of the interface of a normal-metal and a superconductor. The Usadel equation is used to calculate the density of states in the normal metal.

Since the scattering rate $\hbar/\tau$ is large in comparison to $\hbar\omega$ and Δ, we have neglect the term proportional to $\hat{\mathbf{g}}_1$ in the first commutator in comparison to the commutator of $\hat{g}_0$ and $\hat{\mathbf{g}}_1$. Separate equations for $\hat{g}_0$ and $\hat{\mathbf{g}}_1$ are found upon averaging Eq. (10.69) over $\mathbf{n}$ and upon multiplication of Eq. (10.69) by $\mathbf{n}$, followed by averaging over $\mathbf{n}$,

$$\left[\hbar\omega\hat{\tau}_3 - \hat{\Delta}, \hat{g}_0\right]_- + i\frac{v_F}{3}\left[\hat{\partial}_{\mathbf{R}}, \hat{\mathbf{g}}_1\right]_- = 0, \quad \left[v_F\hat{\partial}_{\mathbf{R}}, \hat{g}_0\right]_- + \frac{1}{2\tau}\left[\hat{g}_0, \hat{\mathbf{g}}_1\right]_- = 0. \tag{10.70}$$

Using the normalization condition for the quasiclassical Green function, the explicit solution for $\hat{\mathbf{g}}_1$ can be found from the second equation,

$$\hat{\mathbf{g}}_1 = -\tau v_F \hat{g}_0 \left[\hat{\partial}_{\mathbf{R}}, \hat{g}_0\right]_- . \tag{10.71}$$

Upon substitution of this equation into the first equation (10.70), one finds

$$\left[\hbar\omega\hat{\tau}_3 - \hat{\Delta}, \hat{g}_0\right]_- - iD\left[\hat{\partial}_{\mathbf{R}}, \hat{g}_0\left[\hat{\partial}_{\mathbf{R}}, \hat{g}_0\right]_-\right]_- = 0, \tag{10.72}$$

where $D = (1/3)v_F\tau^2$ is the diffusion constant. Equation (10.72) is known as the Usadel equation.

As an application of the quasiclassical formalism, we now calculate the density of states in a diffusive normal metal wire that is attached to a superconductor, see Fig. 10.3. This is a calculation that is described in detail in, *e.g.,* W. Belzig, C. Bruder, and G. Schön, Phys. Rev. B **54**, 9443 (1996). The density of states is an equilibrium property, so that it is sufficient to calculate the retarded Green function alone. Taking the retarded component

of the Usadel equation (10.72), one finds

$$\left[\hbar\omega\hat{\tau}_3 - \hat{\Delta}, \hat{g}_0^{\rm R}\right]_- - iD\left[\hat{\partial}_{\mathbf{R}}, \hat{g}_0^{\rm R}\left[\hat{\partial}_{\mathbf{R}}, \hat{g}_0^{\rm R}\right]_-\right]_- = 0. \tag{10.73}$$

In matrix notation, the commutator $[\hat{\partial}_{\mathbf{R}}, \hat{g}]_-$ reads

$$[\hat{\partial}_{\mathbf{R}}, \hat{g}]_- = \begin{pmatrix} \partial_{\mathbf{R}} g & (\partial_{\mathbf{R}} - (2ie/\hbar c)\mathbf{A})f \\ (\partial_{\mathbf{R}} + (2ie/\hbar c)\mathbf{A})f^+ & -\partial_{\mathbf{R}} g \end{pmatrix}. \tag{10.74}$$

Applying this relation twice, one finds that Eq. (10.73) gives the following equation for the anomalous Green function

$$2\hbar\omega f^{\rm R} + \Delta g^{\rm R} - iDg^{\rm R}(\partial_{\mathbf{R}} - (2ie/\hbar c)\mathbf{A})^2 f^{\rm R} + iDf^{\rm R}\partial_{\mathbf{R}}^2 g^{\rm R} = 0. \tag{10.75}$$

We specialize to the case that there is no magnetic field, $\mathbf{A} = 0$, in which one may set $f = f^+$. Then Eq. (10.75), together with the normalization condition $(g^{\rm R})^2 + (f^{\rm R})^2 = 1$ is sufficient to determine the quasiclassical Green functions. We take the order parameter Δ to be purely imaginary, and $i\Delta$ instead of Δ, and parameterize the quasiclassical Green function as

$$\hat{g} = \begin{pmatrix} \cos\Theta & \sin\Theta \\ \sin\Theta & -\cos\Theta \end{pmatrix}. \tag{10.76}$$

We consider the case that the region $x < 0$ is a superconductor and that the region $x > 0$ is a normal metal. We do not calculate the superconductor order parameter $\Delta(\mathbf{r})$ self-consistently. Instead, we set $\Delta(\mathbf{r}) = \Delta$, independent of $\mathbf{r}$, for $x < 0$, and $\Delta(\mathbf{r}) = 0$ for $x > 0$. Not enforcing self-consistency will result in a small quantitative error, but it will not affect our qualitative conclusions. For simplicity, we assume that the superconductor and the normal metal have the same densities of states and the same diffusion coefficients. In that case, Θ is continuous at the interface between the normal metal and the superconductor. Rewriting Eq. (10.75) in terms of the angle Θ and solving it with the boudnary conditions that Θ is continuous at the normal-metal–superconductor interface, that $\cos(\Theta) \to 1$ deep inside the normal metal, and that $\cos(\Theta) \to \hbar\omega/(\omega^2 - \Delta^2)^{1/2}$ deep inside the superconductor, one finds

$$\Theta(x,\omega) = \begin{cases} 4\arctan\left[e^{-x\sqrt{-2i\omega/D}}\tan\frac{\theta_0}{4}\right] & \text{if } x > 0, \\ \theta_{\rm S} + 4\arctan\left[e^{-x\sqrt{2(\Delta^2-\omega^2)^{1/2}/D}}\tan\frac{\theta_0-\theta_{\rm S}}{4}\right] & \text{if } x < 0, \end{cases} \tag{10.77}$$

where the angles $\theta_{\rm S}$ and θ_0 are defined as

$$\theta_{\rm S} = \arctan\frac{i\Delta}{\hbar\omega}, \quad \sin(\theta_0 - \theta_{\rm S}) = \frac{\sqrt{-i\hbar\omega}}{(\Delta^2 - \omega^2)^{1/4}}\sin\frac{\theta_0}{2}. \tag{10.78}$$

From this solution one can calculate the spectral density in the normal metal. Simple expressions are obtained in the limit $|\omega| \ll \Delta$, for which one finds $\theta_{\rm S} = \theta_0 = \pi/2$, and

$$\Theta(x,\omega) \approx 4\tan(\pi/8)e^{-x\sqrt{-2i\omega/D}} \quad \text{for } x \gg \sqrt{D/|\omega|}. \tag{10.79}$$

Hence, we find that the density of states ν is reduced below the normal-state value ν_0, even in the normal metal,

$$\begin{aligned} \nu(\omega) &= \nu_0 \mathrm{Re}\, \cos\Theta(x,\omega) \\ &\approx \nu_0 \left[1 - 8\tan^2(\pi/8)e^{-2x\sqrt{|\omega|/D}} \cos(2x\sqrt{|\omega|/D})\right]. \end{aligned} \tag{10.80}$$

This result is valid for $x \gg \sqrt{D/|\omega|}$ only. One can find a more accurate answer valid for all x by using Eq. (10.77) for $\Theta(x,\omega)$.

Of more interest than the actual numbers one gets is the observation that, in the normal metal, Θ is different from zero. This not only means that the density of states is different from the normal-state density of states. It also means the anomalous Green function is nonzero in the normal metal! Clearly, it is the proximity to the superconductor that is responsible for this fact. The transfer of superconducting properties from a superconductor to a nearby normal metal is referred to as the 'superconductor proximity effect'.

The proximity effect in normal metals has been very well studied, both experimentally and theoretically. You can find more information in the quasiclassical Green function approach in, *e.g.,* W. Belzig *et al.*, Superlatt. Microstruct. **25** 1251 (1999) or in V. Chandrasekhar, in *The Physics of Superconductors: Vol. II*, Ed. K. H. Bennemann and J. B. Ketterson (Springer, Berlin, 2004), cond-mat/0312507.

10.5 Exercises

Exercise 10.1: Thermodynamic properties

One can calculate the effect of the superconductivity on the free energy F using the general relation between F and the interaction Hamiltonian $\hat{H}_1$ of Eq. (10.1).

$$F - F_0 = \int_0^\lambda d\lambda' \frac{1}{\lambda'} \langle \hat{H}_1(\lambda') \rangle. \tag{10.81}$$

(a) Keeping contributions that are specific for a superconductor only, show that the superconductivity contribution δF to the free energy reads

$$\delta F = \int_0^\lambda \frac{d\lambda'}{\lambda'^2} |\Delta(\lambda')|^2, \tag{10.82}$$

where $\Delta(\lambda')$ is the superconducting order parameter at interaction strength λ'.

(b) One can rewrite the gap equation (10.24) as

$$1 = \lambda\nu \left[\ln \frac{2\omega_{\rm D}}{|\Delta|} - 2\sum_{n=1}^{\infty} (-1)^{n+1} K_0(n|\Delta|/T) \right]. \tag{10.83}$$

Using this result, together with Eq. (10.82), show that

$$\delta F = -\nu \left[\frac{|\Delta|^2}{2} - 2\sum_{n=1}^{\infty} (-1)^{n+1} \frac{T^2}{n^2} \int_0^{n|\Delta|/T} K_1(x) x^2 dx \right], \tag{10.84}$$

where K_1 is a Bessel function.

(c) Show that, at temperatures $T \ll T_c$, the heat capacity of a superconductor is

$$C = 2\nu \sqrt{\frac{2\pi\Delta_0^5}{T^3}} e^{-\Delta_0/T}, \tag{10.85}$$

where Δ_0 is the magnitude of the order parameter at zero temperature.

Chapter 11

Electrons in one dimension

11.1 Why is one dimension different?

With the exception of a short discussion in chapter 6 we have studied electrons in three dimensions. We encountered two possible excitations of an electron liquid in three dimensions: particle-hole pairs and plasma modes. These excitations appeared as the support of the imaginary part of the polarizability and susceptibility at finite frequency ω and finite wavevector $\mathbf{q}$. The plasma modes have a high threshold frequency for excitation, leaving the particle-hole pairs as the main type of excitations at long wavelengths and low frequencies. This observation, together with the observation from Fermi liquid theory that particle-hole pairs are long-lived excitations if their energy is low, is the main justification of the use of the non-interacting electron picture as the starting point for our description of the three-dimensional electron liquid.

In one dimension, the situation is completely different. Here, with "one dimension" we mean a truly one dimensional system, i.e., a quantum wire with a width a so small that only one transverse mode is populated at the Fermi energy. In practice, this means $a \sim \lambda_F$, where λ_F is the Fermi wavelength.[1] In order to see why the one-dimensional electron liquid is so different, we reexamine the polarizability and spin susceptibility in a one-dimensional wire.

Before we look at the polarizability, we need to know the Coulomb interaction in one

[1]This use of the word "one dimensional" is different from that of Chapter 6, where "one dimensional" referred to a system that is much longer than it is wide, but that does not need to be as narrow as λ_F. In order to distinguish the two cases, the latter case is sometimes referred to as "quasi one dimensional".

dimension. For a wire of thickness a in vacuum, the Coulomb interaction is

$$\begin{aligned} V_{\mathbf{q}} &= \frac{e^2}{4\pi\epsilon_0}\int dx \frac{e^{-iqx}}{|x|} \\ &\approx \frac{e^2}{2\pi\epsilon_0}\ln\frac{1}{qa}, \end{aligned} \tag{11.1}$$

which is valid for $qa \ll 1$. We have cut off the integral at $x \sim a$, since for $x \lesssim a$ a three-dimensional form of the Coulomb interaction should be used. If interactions in the one-dimensional wire are screened by a nearby metal at distance b, the interaction $V_{\mathbf{q}}$ saturates at $q \sim 1/b$.

In the random phase approximation, the polarizability reads

$$\chi_e(\mathbf{q},\omega)^{\mathrm{RPA}} = \frac{\chi_e^{0\mathrm{R}}(\mathbf{q},\omega)}{1 - V_{\mathbf{q}}\chi_e^{0\mathrm{R}}(\mathbf{q},\omega)/e^2}, \tag{11.2}$$

where $V_{\mathbf{q}}$ is given by Eq. (11.1) above and

$$\chi_e^{0\mathrm{R}}(\mathbf{q},\omega) = \frac{e^2}{V}\sum_{\mathbf{k}} \frac{\tanh[(\varepsilon_{\mathbf{k}+\mathbf{q}}-\mu)/2T] - \tanh[(\varepsilon_{\mathbf{k}}-\mu)/2T]}{\varepsilon_{\mathbf{k}} - \varepsilon_{\mathbf{k}+\mathbf{q}} + \omega + i\eta} \tag{11.3}$$

is the polarizability of the one-dimensional non-interacting electron gas. In one dimension, the $\mathbf{k}$ summation in Eq. (11.3) is easily done: the momentum $\mathbf{k}$ is represented by a real number k, and one has $\varepsilon_{k+q} = \varepsilon_k + qv_F \operatorname{sign} k$. Then, replacing the summation over k by an integration over ε_k, one has

$$\begin{aligned} \chi_e^{0\mathrm{R}}(\mathbf{q},\omega) &= \frac{e^2\nu}{2}\left(\frac{2qv_F}{\omega + i\eta - qv_F} - \frac{2qv_F}{\omega + i\eta + qv_F}\right) \\ &= \frac{2e^2q^2v_F}{\pi[(\omega+i\eta)^2 - q^2v_F^2]}, \end{aligned} \tag{11.4}$$

where we used the fact that, in one dimension, the density of states ν is related to the Fermi velocity v_F as $\nu = 1/\pi v_F$. Substituting this into Eq. (11.2), one finds

$$\chi_e(\mathbf{q},\omega)^{\mathrm{RPA}} = \frac{2e^2q^2v_F}{\pi(\omega+i\eta)^2 - \pi q^2v_F^2 - (e^2/\pi\epsilon_0)\ln(1/qa)q^2v_F}. \tag{11.5}$$

The one-dimensional electron liquid can dissipate energy only if the imaginary part of $\chi_e(\mathbf{q},\omega)$ is nonzero. Inspection of Eq. (11.5) shows that that is the case for

$$\omega = qv_{\mathrm{c}}, \tag{11.6}$$

where the velocity v_c is

$$v_c = v_F \sqrt{1 + \frac{e^2}{\pi^2 v_F \epsilon_0} \ln \frac{1}{qa}}. \tag{11.7}$$

In the presence of a metal gate at distance b from the wire that screens the Coulomb interaction inside the wire, the momentum q in Eq. (11.7) should be replaced by $1/b$.

The result (11.6) describes the one-dimensional version of plasma oscillations. Unlike in three dimensions, where the plasma frequency remained finite (and large) if the wavevector $q \to 0$, in one dimension $\omega \to 0$ if $q \to 0$. However, the plasmon speed is larger than the Fermi velocity, since the plasmon propagation speed is enhanced by the repulsive Coulomb interactions. Hence, in one dimension, plasmons are relevant perturbations in the low frequency, long wavelength limit.

However, this is not the entire story. The result (11.5) differs in one more aspect from its three dimensional counterpart: There is no particle-hole continuum for excitations, not even a single particle-hole branch! Note that at $\omega = \pm q v_F$ the polarizability of Eq. (11.5) is well behaved and has no imaginary part. Hence, we conclude that the only charged excitations in a one dimensional electron gas are the plasmon collective modes.

The situation is different if the wavevector q is of order k_F, or if the temperature or frequency are of order ε_F. In that case, one cannot approximate the spectrum by a linear dispersion. Without interactions, the polarizability function $\chi_e^{0\mathrm{R}}(q,\omega)$ becomes a truly complex function of q and ω for $qv_F - q^2/2m < \omega < qv_F + q^2/2m$, just like in three dimensions, and, hence, the full polarizability χ_e^{RPA} becomes complex as well for that wavevector and frequency range. The support of $\mathrm{Im}\,\chi_e$ for the entire frequency range is shown in Fig. 11.1.

If we want to investigate spin excitations, we should look at the spin susceptibility. Taking the Hubbard-model result for the transverse susceptibility $\chi_{-+}(\mathbf{q},\omega)$,

$$\chi_{-+}^{\mathrm{R}}(\mathbf{q},\omega) = \frac{\chi_{-+}^{0\mathrm{R}}(\mathbf{q},\omega)}{1 - (2U/\mu_B g)\chi_{-+}^{0\mathrm{R}}(\mathbf{q},\omega)}, \tag{11.8}$$

where

$$\begin{aligned} \chi_{-+}^{0\mathrm{R}}(\mathbf{q},\omega) &= -\frac{\mu_G g}{4V} \sum_{\mathbf{k}} \frac{\tanh[(\varepsilon_{\mathbf{k}+\mathbf{q}} - \mu)/2T] - \tanh[(\varepsilon_{\mathbf{k}} - \mu)/2T]}{\varepsilon_{\mathbf{k}} - \varepsilon_{\mathbf{k}+\mathbf{q}} + \omega + i\eta} \\ &= -\frac{\mu_B g q^2 v_F}{2\pi[(\omega + i\eta)^2 - q^2 v_F^2]} \end{aligned} \tag{11.9}$$

is the transverse susceptibility of the non-interacting electron gas, we find that the imaginary part of $\chi_{-+}(\mathbf{q},\omega)$ is nonzero if and only if

$$\omega = v_s q, \tag{11.10}$$

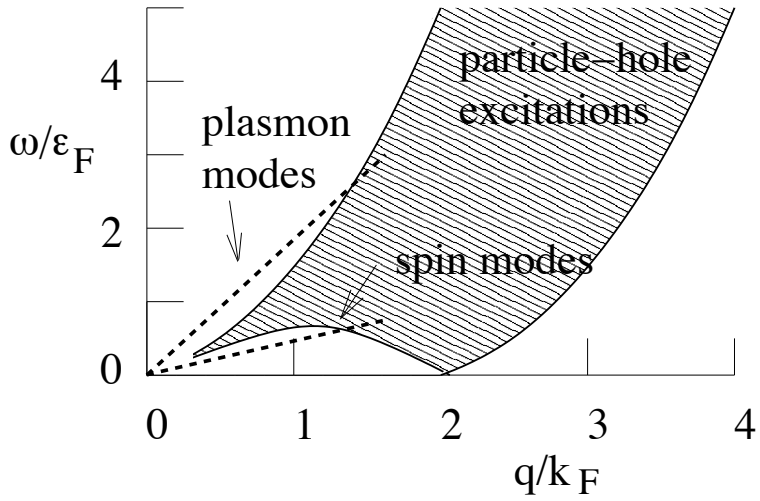

Figure 11.1: Support of the polarizability χ_e and the transverse spin susceptibility χ_{-+} for a one-dimensional interacting electron liquid in the RPA approximation.

where

$$v_{\rm s} = v_F \sqrt{1 - U/\pi v_F}. \tag{11.11}$$

The spin excitations are collective excitations as well, moving at a speed that is below the Fermi velocity. The reason why $v_{\rm s}$ is smaller than v_F is that the propagating of spin excitations is slowed down by the ferromagnetic exchange interaction.[2] At the Stoner instability, $U\nu = 1$, the propagation speed has come to zero, and large-scale ferromagnetic fluctuations become possible. Note that, again, χ_{-+} is purely real at $\omega = v_F q$.

The phenomenon that, in general, $v_{\rm s}$ is different from $v_{\rm c}$ is known as "spin-charge" separation. In a one-dimensional electron liquid, excitations with spin move at a different speed than excitations with charge. In view of what we just discussed, this is not a big surprise. Since, in one dimension, the only possible excitations are collective modes, there is no reason to expect that spin modes and charge modes have the same velocity. You may recall the calculations of the zero sound velocity in a Fermi liquid, where spin and density modes depend on different Fermi-liquid constants and, hence, have different propagation velocities.

Quantitatively, our observations have been based on the random phase approximation. Going beyond the random phase approximation will most certainly change our estimates

[2] In three dimensions, the fact that $v_{\rm s} < v_F$ implies that spin excitations are strongly damped because they can decay into particle-hole pairs (Landau damping). In one dimension, there are no particle-hole excitations, so that spin excitations are long-lived in spite of the fact that their propagation speed is below the Fermi velocity.

for the velocities v_c and v_s of collective charge and spin excitations in the one-dimensional electron system, but not the qualitative conclusion that the collective modes are the only long-wavelength excitations of the one-dimensional electron system. We'll see this in Sec. 11.3, where we start from a microscopic model for electrons in one dimension and show rigorously that all dynamics is collective. Another way to see this is to note the similarity between electrons in one dimension and ions in a lattice. The similarity arises because, in one dimension, electrons cannot pass each other. In that sense, a description in terms of a "solid" would be more appropriate than a description in terms of a "liquid".[3] Indeed, all long-wavelength dynamics of lattice ions is collective; it is only at short wavelengths that the properties of individual ions become important.

We conclude that, for long wavelengths and low frequencies, all excitations of the one-dimensional metal are collective modes; there are no dissipative modes at $|\omega/q| = v_F$, which is the frequency-wavevector relation one expects for particle-hole excitations in a degenerate one-dimensional Fermi gas. This observation makes us wonder whether a better description than a description in terms of particles is possible. Can one make a theory that uses the collective modes as the building blocks, rather than the individual fermions?

Another reason to look for a theory that does not start from a system of non-interacting fermions is that, in one dimension, the quasiparticle lifetime scales inversely proportional to the excitation energy of the quasiparticle. This is different from three dimensions, where the life time is inversely proportional to the square of the excitation energy. In three dimensions, this dependence was the basis for "Fermi Liquid theory", the statement that a picture based on non-interacting electrons is a good starting point. In one dimension, quasiparticle decay is much faster, and Fermi Liquid theory is not valid. What description one uses instead follows from the above considerations, as we'll see in the next sections.

11.2 Effective Hamiltonian

Based on the considerations of the previous section, we now write down an effective Hamiltonian that has the same (collective) excitations as the one-dimensional electron liquid. For simplicity, we consider the case of spinless fermions, so that the only collective excitations are the plasmon modes. Also, we assume that the long-range part of the Coulomb interaction in the wire is screened by a nearby piece of metal, and, hence, take the plasmon velocity v_c

[3] The difference between a "solid" and a "liquid" has to do with the presence of transverse rigidity (shear). In one dimension, there is no transverse direction, so that this formal difference between "solid" and "liquid" disappears. We usually denote the one-dimensional electron system as a "liquid", because of the lack of long-range order. However, as we see from the present discussion, one-dimensional electron systems have characteristics of both solids and liquids.

to be independent of q.

With these observations, we are tempted to write down the following Hamiltonian as an effective Hamiltonian for the one-dimensional electron liquid,

$$H = \sum_q \omega_q (a_q^\dagger a_q + 1/2), \tag{11.12}$$

where the summation over the wavenumber q extends over both positive and negative q, with $\omega_q = v_c|q|$, and where $a_q^\dagger$ and a_q are boson creation and annihilation operators that obey commutation relations,

$$\begin{aligned} \left[a_q, a_{q'}\right]_- &= \left[a_q^\dagger, a_{q'}^\dagger\right]_- = 0 \\ \left[a_q, a_{q'}^\dagger\right]_- &= \delta_{q,q'}. \end{aligned}$$

As we discussed above, the Hamiltonian (11.12) is valid for long wavelengths and low frequencies only. At high wavenumbers $|q| \sim k_F$, particle-hole excitations become important, and our description in terms of collective modes only ceases to be valid.

Although there is nothing wrong with the Hamiltonian (11.12) as an effective Hamiltonian for the spinless one-dimensional electron liquid, we can gain considerably more insight if we replace the creation and annihilation operators $a^\dagger$ and a by "momentum" and "displacement" operators Π and ϕ, where

$$\begin{aligned} \phi_q &= \sqrt{\frac{\hbar}{2K\omega_q}}(a_q + a_{-q}^\dagger), \\ \Pi_q &= \sqrt{\frac{K\hbar\omega_q}{2}}\left(ia_q^\dagger - ia_{-q}\right). \end{aligned} \tag{11.13}$$

We will use the freedom of the arbitrary constant K later in order to give a physical interpretation of the operators Π and ϕ. You verify that these "momentum" and "displacement" operators satisfy the usual commutation rules for canonically conjugate variables,

$$\begin{aligned} [\Pi_q, \Pi_{q'}]_- &= [\phi_q, \phi_{q'}]_- = 0 \\ [\Pi_q, \phi_{q'}]_- &= -i\hbar\delta_{qq'}. \end{aligned} \tag{11.14}$$

In terms of the new variables Π and ϕ we write the Hamiltonian as

$$H = \sum_q \left(\frac{1}{2K}\Pi_q\Pi_{-q} + \frac{1}{2}K\omega_q^2\phi_q\phi_{-q}\right). \tag{11.15}$$

Next, we perform a Fourier transform to real space,

$$\begin{aligned}\Pi(x) &= \sqrt{\frac{1}{L}}\sum_q \Pi_q e^{-iqx},\\ \phi(x) &= \sqrt{\frac{1}{L}}\sum_q \phi_q e^{iqx}.\end{aligned} \tag{11.16}$$

Since the effective Hamiltonian (11.12) is valid for low q only, the summation over q should be restricted to $q \ll k_F$ only. This means that delta functions and divergences appearing in the real-space formulation should be cut off at distances $x \sim 1/k_F$. In the real-space formulation, the effective Hamiltonian becomes

$$H = \int dx \left(\frac{1}{2K}\Pi(x)^2 + \frac{1}{2}Kv_{\rm c}^2(\partial_x\phi(x))^2 \right). \tag{11.17}$$

The commutation relations of the fields $\phi(x)$ and $\Pi(x)$ are

$$\begin{aligned}[\phi(x),\phi(x')]_- &= [\Pi(x),\Pi(x')]_- = 0\\ [\Pi(x),\phi(x')]_- &= -i\hbar\delta(x-x').\end{aligned} \tag{11.18}$$

Let us now calculate time-derivative of $\phi(x)$,

$$\frac{\partial}{\partial t}\phi(x) = \frac{i}{\hbar}[H,\phi(x)]_- = \frac{1}{K}\Pi(x). \tag{11.19}$$

We want the operators Π and ϕ to be related to the electron current density and particle density, respectively. If such an identification is to hold, Eq. (11.19) should represent the continuity equation $\partial_t n = -\partial_x j$. Taking a derivative to x on both sides of the equation, we see that such an identification holds, if we identify the (excess) particle density $n(x)$ with the x-derivative of $\phi(x)$ and the current with $\Pi(x)$. In fact, the following identifications are made,

$$n(x) = \frac{1}{\pi}\partial_x\phi(x), \tag{11.20}$$

$$j(x) = -v_F\Pi(x), \tag{11.21}$$

which implies $K = 1/\pi v_F$. However, different identifications are possible, depending on the microscopic details of the one-dimensional electron liquid.

Combining everything, we see that we have arrived at the effective Hamiltonian

$$H = \frac{\hbar v_F}{2\pi} \int dx \left[\frac{\pi^2}{\hbar^2} \Pi(x)^2 + g^2 \left(\frac{\partial \phi(x)}{\partial x} \right)^2 \right], \tag{11.22}$$

where we introduced the dimensionless parameter

$$g = \frac{v_c}{v_F}. \tag{11.23}$$

You may recognize Eq. (11.22) as the Hamiltonian of an elastic string, where ϕ is the displacement and Π is the momentum density. The Hamiltonian (11.22) is quite different from the Hamiltonian you would write down for non-interacting fermions in one dimension. It reflects the fact that all excitations are collective and, hence, bosonic, rather that quasi-particle like. In order to stress the difference of the collective dynamics of the one-dimensional electron liquid and the quasi-particle dynamics of the Fermi liquid in higher dimensions, the former case is referred to as "Luttinger Liquid".

The Hamiltonian (11.22) is a great starting point if one wants to study the excitation spectrum and thermodynamic quantities of a one-dimensional spinless electron liquid. One example is the calculation of the compressibility κ, which is the derivative of the particle density to the chemical potential $\mu = \partial E/\partial n$, where E is the energy of the electron liquid,

$$\kappa = \frac{\partial n}{\partial \mu} = \left(\frac{\partial^2 E}{\partial n^2} \right)^{-1}. \tag{11.24}$$

According to the effective Hamiltonian (11.22), one has $\kappa = v_F/\pi v_c^2$. Without interactions, when $v_c = v_F$, this simplifies to $\kappa = 1/\pi v_F = \nu$, ν being the density of states. With interactions, κ is decreased by a factor $g^2 = (v_c/v_F)^2$, reflecting the increased energy cost for addition of charge. Similarly, you verify that the specific heat is decreased by a factor $1/g^2$ with respect to the non-interacting electron case.

For some applications it is important to be able to make reference to individual electrons. An example is a tunneling experiment, where electrons tunnel into a one-dimensional electron liquid from a weakly coupled electrode. Since we employ a long-wavelength description, we will not attempt to describe a process in which an electron that is created or annihilated is localized within a wire segment of length comparable to the Fermi wavelength. Instead, we'll want to write down an operator that creates an electron that is delocalized over a piece of wire of length $\lambda \sim \lambda_F$. This spatial "smearing" amounts to a momentum cut off factor $\exp(-|q|\lambda/2)$ in Eq. (11.16) or, equivalently, replacing the fields ϕ and Π by

$$\phi(x) \;\; \rightarrow \;\; \int dx' \frac{2\lambda}{\pi[\lambda^2 + 4(x-x')^2]} \phi(x'),$$

$$\Pi(x) \;\rightarrow\; \int dx' \frac{2\lambda}{\pi[\lambda^2 + 4(x-x')^2]} \Pi(x'). \tag{11.25}$$

On the other hand, since we give up spatial resolution on length scales below λ_F, we can specify the momentum of the electron to within k_F, *i.e.*, we can specify whether the electron moves left (L) or right (R). The creation operator of a right moving electron at position x then becomes[4]

$$\hat{\psi}^\dagger_{\rm R}(x) = \frac{1}{\sqrt{2\pi\lambda}} U^\dagger_{\rm R} e^{-ik_F x + i\phi(x) - i\theta(x)}. \tag{11.26}$$

Similarly, for a left-moving particle one has

$$\hat{\psi}^\dagger_{\rm L}(x) = \frac{1}{\sqrt{2\pi\lambda}} U^\dagger_{\rm L} e^{ik_F x - i\phi(x) - i\theta(x)}. \tag{11.27}$$

Here the auxiliary field $\theta(x)$ is defined as

$$\theta(x) = \frac{\pi}{2\hbar} \int dx' \Pi(x') \mathrm{sign}\,(x-x'). \tag{11.28}$$

You verify that θ commutes with itself, whereas the commutator with ϕ is given by

$$[\theta(x), \phi(x')]_- = [\phi(x), \theta(x')]_- = -i\frac{\pi}{2} \mathrm{sign}\,(x-x'). \tag{11.29}$$

In these equations, the fast exponential factor $\exp(\pm ik_F x)$ corresponds to the orbital phase of left and right moving electrons. The operator $U^\dagger$ is known as the "Klein factor". It is a formal operator that increases the total number of left or right moving particles by one. It is necessary, because the operators $\phi(x)$ and $\Pi(x)$ conserve the total number of particles. The operator $\exp[-i\theta(x)]$ produces a shift of the field $\phi(x')$ by $-\pi/2$ at $x' < x$ and by $\pi/2$ at $x' > x$. Hence, the derivative $\partial_x \phi$ is peaked near x, corresponding to an excess particle density at that point, see Fig. 11.2.[5] The operator $e^{i\phi(x)}$ changes sign each time ϕ is increased by π, i.e., each time a particle passes through the point x. This property enforces the fermion anticommutation rules for the $\hat{\psi}$-operators. Furthermore, $e^{\pm i\phi(x)}$ displaces the field $\Pi(x)$ by one, corresponding to a current density $\mp v_F \delta(x)$. Finally, the prefactor $(2\pi\lambda)^{-1/2}$ is chosen in conjunction with the regularization ("smearing") procedure for the fields ϕ and Π. It is chosen such that a calculation of the fermion Green function for non-interacting electrons gives the same result in boson and in fermion language.

[4] In the next section, where we give a more formal derivation of the Hamiltonian (11.22), you can find more details of the formal relationship between the fields $\phi(x)$ and $\Pi(x)$ and the underlying electron creation and annihilation operators $\hat{\psi}^\dagger$ and $\hat{\psi}$.

[5] This statement does not conflict with the fact that the operator ϕ conserves particle number. At the upper and lower ends of the wire there is an "antikink" in ϕ, corresponding to a decrease of the particle number by one (in total). It is the operator $U^\dagger$ that keeps track of the total particle number.

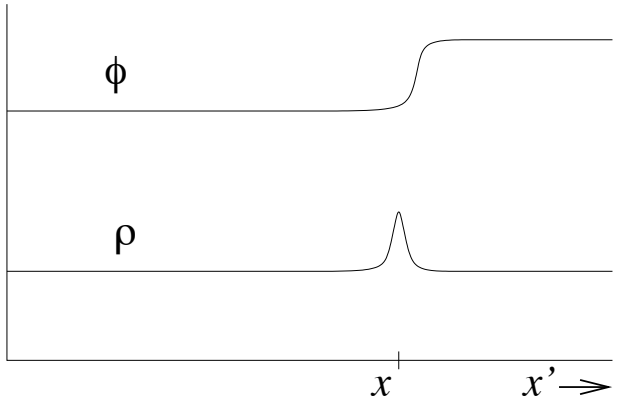

Figure 11.2: Upon creation of an electron at position x, the field ϕ acquires a kink, corresponding to a peak in the excess density ρ.

The information of the boson fields Π and ϕ is contained in their Green functions. The calculation of these Green functions is quite similar to that of the phonon Green functions. For technical reasons, we calculate Green functions for the fields ϕ and θ. In terms of the fields θ and ϕ, the Hamiltonian reads

$$H = \frac{\hbar v_F}{2\pi} \int dx \left[\left(\frac{\partial \theta(x)}{\partial x} \right)^2 + g^2 \left(\frac{\partial \phi(x)}{\partial x} \right)^2 \right]. \tag{11.30}$$

In order to calculate the Green functions of the fields θ and ϕ, we use the equation of motion approach. Hereto we need the imaginary time evolution,

$$\begin{aligned} \frac{\partial}{\partial \tau} \theta(x,\tau) &= -i v_F g^2 \frac{\partial \phi(x,\tau)}{\partial x}, \\ \frac{\partial}{\partial \tau} \phi(x,\tau) &= -i v_F \frac{\partial \theta(x,\tau)}{\partial x}. \end{aligned} \tag{11.31}$$

We define the temperature Green functions

$$\begin{aligned} \mathcal{D}_{\theta\theta}(x,\tau) &= -\langle T_\tau \theta(x,\tau)\theta(0,0)\rangle, \\ \mathcal{D}_{\theta\phi}(x,\tau) &= -\langle T_\tau \theta(x,\tau)\phi(0,0)\rangle, \\ \mathcal{D}_{\phi\phi}(x,\tau) &= -\langle T_\tau \phi(x,\tau)\phi(0,0)\rangle, \\ \mathcal{D}_{\phi\theta}(x,\tau) &= -\langle T_\tau \phi(x,\tau)\theta(0,0)\rangle. \end{aligned} \tag{11.32}$$

Using Eq. (11.31) we find that these Green functions satisfy the equations of motion

$$\frac{\partial}{\partial \tau} \mathcal{D}_{\theta\theta}(x,\tau) = -i v_F g^2 \frac{\partial \mathcal{D}_{\phi\theta}(x,\tau)}{\partial x},$$

$$\begin{aligned}
\frac{\partial}{\partial\tau}\mathcal{D}_{\theta\phi}(x,\tau) &= i\frac{\pi}{2}\delta(\tau)\,\mathrm{sign}\,(x) - iv_F g^2\frac{\partial\mathcal{D}_{\phi\phi}(x,\tau)}{\partial x},\\
\frac{\partial}{\partial\tau}\mathcal{D}_{\phi\theta}(x,\tau) &= i\frac{\pi}{2}\delta(\tau)\,\mathrm{sign}\,(x) - iv_F\frac{\partial\mathcal{D}_{\theta\theta}(x,\tau)}{\partial x},\\
\frac{\partial}{\partial\tau}\mathcal{D}_{\phi\phi}(x,\tau) &= -iv_F\frac{\partial\mathcal{D}_{\theta\phi}(x,\tau)}{\partial x}.
\end{aligned} \tag{11.33}$$

The solution to these equations is easily found by inspection,

$$\begin{aligned}
\mathcal{D}_{\theta\phi}(x,\tau) &= \mathcal{D}_{\phi\theta}(x,\tau)\\
&= \frac{1}{4}\ln\sin[\pi T(\tau+ix/v_{\rm c})\mathrm{sign}\,(\tau)] - \frac{1}{4}\ln\sin[\pi T(\tau-ix/v_{\rm c})\mathrm{sign}\,(\tau)],\\
\frac{v_F}{v_{\rm c}}\mathcal{D}_{\theta\theta}(x,\tau) &= \frac{v_{\rm c}}{v_F}\mathcal{D}_{\phi\phi}(x,\tau)\\
&= \frac{1}{4}\ln\sin[\pi T(\tau+ix/v_{\rm c})\mathrm{sign}\,(\tau)] + \frac{1}{4}\ln\sin[\pi T(\tau-ix/v_{\rm c})\mathrm{sign}\,(\tau)].
\end{aligned} \tag{11.34}$$

Regularization amounts to smearing of the boson fields by a Lorentzian factor $2\lambda/[\pi(\lambda^2 + 4(x-x')^2]$, see Eq. (11.25) above. In the Green functions such a smearing amounts to the substitution $x \to x \pm i\lambda\,\mathrm{sign}\,(\tau)$. This corresponds to the addition of $\lambda\pi T/v_F$ to the argument of the sine function, so that the divergence of the Green functions at $x \to 0$ and $\tau \to 0$ is cut off at distances of order λ and times of order λ/v_F.

As an example, let us now calculate a fermion Green function using the boson language. We consider the temperature Green function for right-moving electrons,

$$\mathcal{G}_{RR}(x,\tau) = -\langle T_\tau\hat{\psi}_R(x,\tau)\hat{\psi}_R^\dagger(0,0)\rangle. \tag{11.35}$$

Using Eq. (11.26), we write this as

$$\mathcal{G}_{RR}(x,\tau) = -\frac{e^{ik_F x}}{2\pi\lambda}\langle T_\tau U_R(\tau)U_R^\dagger(0)\rangle\left\langle T_\tau e^{-i\phi(x,\tau)+i\theta(x,\tau)+i\phi_R(0,0)-i\theta(0,0)}\right\rangle. \tag{11.36}$$

Since the total Green function needs to be antiperiodic in τ, whereas the boson part of the Green function is manifestly periodic in τ, we require that the time-ordering for the Klein factors U_R and $U_R^\dagger$ is that of fermions. Since the operators U_R and $U_R^\dagger$ are simply ladder operators, we have

$$\langle T_\tau U_R(\tau)U_R^\dagger(0)\rangle = \mathrm{sign}\,(\tau). \tag{11.37}$$

Calculating the boson part of the Green function is easier than it seems at first sight. Since the Hamiltonian of the boson fields is quadratic, we can use the cumulant expansion,

which, for $\langle\phi(x,\tau)\rangle = \langle\theta(x,\tau)\rangle = 0$, reads

$$\begin{aligned}\left\langle T_\tau e^{-i\phi(x,\tau)+i\theta(x,\tau)+i\phi(0,0)-i\theta(0,0)}\right\rangle &= e^{\frac{1}{2}\langle(i\phi(0,0)-i\theta(0,0)-i\phi(x,\tau)+i\theta(x,\tau))^2\rangle} \\ &= e^{\mathcal{D}_{\phi\phi}(0,0)-\mathcal{D}_{\phi\theta}(0,0)-\mathcal{D}_{\theta\phi}(0,0)+\mathcal{D}_{\theta\theta}(0,0)} \\ &\quad\times e^{-\mathcal{D}_{\phi\phi}(x,\tau)+\mathcal{D}_{\phi\theta}(x,\tau)+\mathcal{D}_{\theta\phi}(x,\tau)-\mathcal{D}_{\theta\theta}(x,\tau)}. \quad (11.38)\end{aligned}$$

Without regularization, the equal-time and equal-position Green functions $\mathcal{D}_{\phi\phi}(0,0)+\mathcal{D}_{\theta\theta}(0,0)$ are divergent (and negative). With regularization, this divergence is cut off at distances $\sim\lambda$ (see above). Substituting Eq. (11.34) and putting everything together, we find

$$\begin{aligned}\mathcal{G}_{RR}(x,\tau) &= -\frac{1}{(2\pi\lambda)^{1-\nu}}\mathrm{sign}\,(\tau)\left(\frac{T/2v_\mathrm{c}}{\sin[\pi T(\tau+ix/v_\mathrm{c})\mathrm{sign}\,(\tau)]}\right)^{\nu/2-1/2} \\ &\quad\times\left(\frac{T/2v_\mathrm{c}}{\sin[\pi T(\tau-ix/v_\mathrm{c})\mathrm{sign}\,(\tau)]}\right)^{\nu/2+1/2}, \quad (11.39)\end{aligned}$$

where we abbreviated

$$\nu = \frac{1}{2}\left(g+\frac{1}{g}\right) = \frac{1}{2}\left(\frac{v_\mathrm{c}}{v_F}+\frac{v_F}{v_\mathrm{c}}\right). \quad (11.40)$$

It is instructive to compare this result to the electron Green function calculated in the fermion language,

$$\mathcal{G}_{RR}(x,\tau) = -\frac{T/2v_F}{\sin[\pi T(\tau-ix/v_F)]}. \quad (11.41)$$

Taking the result obtained in the boson language, and setting $g=1$, we recover the fermion Green function. This argument, a posteriori, fixes the cut-off dependent prefactor $(2\pi\lambda)^{-1/2}$ in the relations (11.26) and (11.27) between the fermion creation/annihilation operators and the boson fields ϕ and Π.

There is an important difference between the single-electron Green function for $g=1$ and for $g\neq 1$. In the absence of interactions, the single-electron Green function has a simple pole at $-i\tau = x/v_F$. With interactions, the location of the singularity shifts, and the singularity acquires a different analytical structure. This may be brought to light by a calculation of the retarded Green function, *i.e.*, by performing a Fourier transform to Matsubara frequencies followed by analytical continuation $i\omega_n \to \omega+i\eta$. For simplicity we look at the equal-position Green function,

$$\mathcal{G}_{RR}(0,i\omega_n) = \int_0^{1/T}\mathcal{G}_{RR}(0,\tau)e^{i\omega_n\tau}, \quad (11.42)$$

which is related to the spectral density A_{RR} for right-moving electrons. We deform the τ-

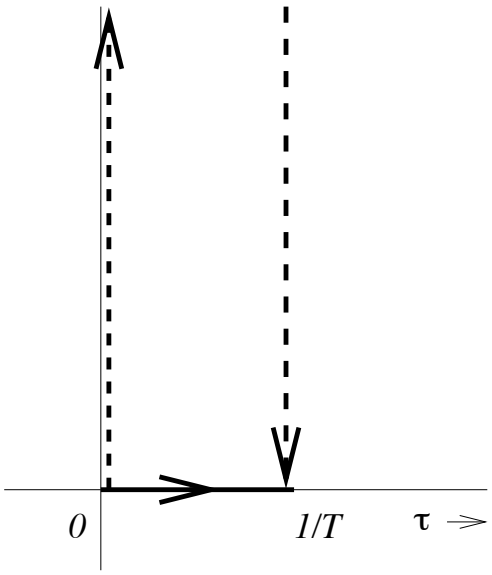

Figure 11.3: Integration contour for the calculation of the density of states in a Luttinger liquid.

integration as shown in Fig. 11.3, avoiding the branch cuts for $\mathrm{Re}\,\tau = 0$ and $\mathrm{Re}\,\tau = 1/T$. After the deformation of the contours, the integral reads

$$\begin{aligned} \mathcal{G}_{RR}(0, i\omega_n) &= -\frac{2i}{(2\pi\lambda)^{1-\nu}} \int_0^\infty dt e^{-\omega_n t} \mathrm{Re} \left(\frac{T/2v_F}{\sin[\pi T(it + \lambda/v_F)]} \right)^\nu \\ &= -\frac{2i}{(2\pi\lambda)^{1-\nu}} \int_0^\infty dt e^{-\omega_n t} \mathrm{Re}\, e^{-i\pi\nu/2} \left(\frac{T/2v_F}{\sinh[\pi T(t - i\lambda/v_F)]} \right)^\nu . \end{aligned} \quad (11.43)$$

Now we can take the analytical continuation $i\omega_n \to \omega + i\eta$ and calculate the retarded Green function,

$$G^{\mathrm{R}}_{RR}(0, \omega) = -\frac{2i}{(2\pi\lambda)^{1-\nu}} \int_0^\infty dt e^{i\omega t} \mathrm{Re}\, e^{-i\pi\nu/2} \left(\frac{T/2v_F}{\sinh[\pi T(t - i\lambda/v_F)]} \right)^\nu . \quad (11.44)$$

Evaluation of the remaining integral depends on whether the energy ω is small or large in comparison to T. If $\omega \ll T$, we find

$$G^{\mathrm{R}}_{RR}(0, \omega) \approx -\frac{2i}{2\pi v_F} \left(\frac{\pi T\lambda}{v_F} \right)^{\nu-1} . \quad (11.45)$$

(The numerical prefactor is valid for ν close to unity.) You verify that one obtains $G^{\rm R}_{RR}(0,\omega) = -i/2v_F$ for the non-interacting case $\nu = 1$, which implies $A_{RR} = 1/v_F$, the result that we expected for the spectral density of right-moving electrons. If, on the other hand, $T \ll \omega$, one finds a result similar to Eq. (11.45) with πT replaced by ω.

We conclude that for an interacting one-dimensional electron liquid the density of states at the Fermi level has a power-law singularity, and vanishes proportional to $\max(\omega, T)^{\nu-1}$. This behavior is quite different from the case of a Fermi liquid, where the density of states is non-singular at the Fermi level. Also note that the cut-off length λ enters into the expression for the density of states if $\nu \neq 1$. For a quantitative estimate, one should replace λ by λ_F.

11.3 Luttinger's model

11.3.1 Formulation of the model

Although the discussion of the previous section provided the physical motivation of the effective Hamiltonian (11.22), it might leave some uneasiness with those of you who want a "constructive" description of a field theory of interacting electrons in one dimension. Therefore, we now return to a description of a one-dimensional electron liquid in fermion language, and derive the effective Hamiltonian (11.22) using formal manipulations. The discussion of this section follows that of F. D. M. Haldane, J. Phys. C **14**, 2585 (1981), although it is less rigorous at points. Those readers who want a fully rigorous treatment are referred to Haldane's article, or to the tutorial review by J. von Delft and H. Schoeller, Annalen Phys. **7**, 225 (1998).

As a starting point, we use a description of the one-dimensional electron system in which we have linearized the electron spectrum, see Fig. 11.4. We shift momenta by an amount $-k_F$ (k_F) for right (left) moving electrons, so that the Fermi points are shifted to $k = 0$, and denote the creation/annihilation operators for right moving (left moving) electrons with shifted momentum k by $c^\dagger_{k\rm R}$ and $c_{k\rm R}$ ($c^\dagger_{k\rm L}$ and $c_{k\rm L}$), respectively. We then write the kinetic energy as

$$\hat{H}_{\rm kin} = v_F \sum_k (k\ :n_{k\rm R}: - k\ :n_{k\rm L}:), \tag{11.46}$$

where $n_{k\rm R} = c^\dagger_{k\rm R} c_{k\rm R}$ is the density of right-moving electrons and $n_{k\rm L} = c^\dagger_{k\rm L} c_{k\rm L}$ is the density of left-moving electrons. The symbol $: \ldots :$ refers to normal ordering, i.e., to subtraction of the densities in the (non-interacting) ground state. The summations over k should be truncated at $|k| \lesssim k_F$ because the linear dispersion is valid for a window of wavevectors of size $\lesssim k_F$ around $k = 0$ only and because the distinction between left movers and right movers implies that the (translated) wavevector of a right mover cannot be smaller than

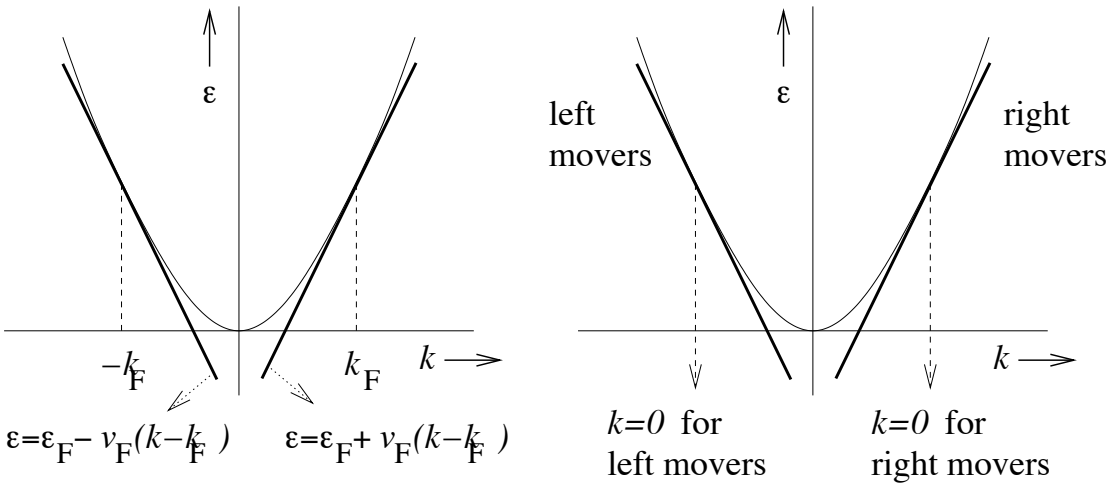

Figure 11.4: Linearized spectrum for electrons in one dimension. In our description, we separate right and left moving electrons and shift momenta such that the Fermi points correspond to $k = 0$.

$-k_F$, whereas the (translated) wavevector of a left mover cannot be larger than k_F, see Fig. 11.4. In terms of the fields

$$\hat{\psi}_{\rm R}(x) = \frac{1}{\sqrt{L}} \sum_k e^{ikx} c_{k{\rm R}}, \quad \hat{\psi}_{\rm L}(x) = \frac{1}{\sqrt{L}} \sum_k e^{ikx} c_{k{\rm L}}, \tag{11.47}$$

the Hamiltonian (11.46) reads[6]

$$\hat{H}_{\rm kin} = v_F \int dx \left[:\hat{\psi}^\dagger_{\rm L}(x)(i\partial_x)\hat{\psi}_{\rm L}(x): - :\hat{\psi}^\dagger_{\rm R}(x)(i\partial_x)\hat{\psi}_{\rm R}(x): \right]. \tag{11.48}$$

11.3.2 Bosonization

We'll now show that $\hat{H}_{\rm kin}$ can be written in terms of the densities $\rho_{q{\rm R}}$ and $\rho_{q{\rm L}}$ of right and left moving electrons,

$$\rho_{q{\rm R}} = \sum_k c^\dagger_{k,{\rm R}} c_{k+q,{\rm R}}, \quad \rho_{q{\rm L}} = \sum_k c^\dagger_{k,{\rm L}} c_{k+q,{\rm L}}. \tag{11.49}$$

[6]The normal ordering in Eq. (11.48) means that $\hat{\psi}^\dagger\hat{\psi}$ has to be replaced by $-\hat{\psi}\hat{\psi}^\dagger$ for states with momentum smaller than k_F. This prescription is not transparent in a real space formulation.

We consider the case $q = 0$ separately; note that we do not need to use normal ordering for $q \neq 0$. The commutation relations of the density operators are

$$\begin{aligned} [\rho_{q,\mathrm{R}}, \rho_{-q',\mathrm{R}}]_- &= \frac{qL}{2\pi}\delta_{qq'}, \\ [\rho_{q,\mathrm{L}}, \rho_{-q',\mathrm{L}}]_- &= -\frac{qL}{2\pi}\delta_{qq'}, \\ [\rho_{q,\mathrm{R}}, \rho_{-q',\mathrm{L}}]_- &= 0. \end{aligned} \tag{11.50}$$

To see how this result is obtained, let us look at the first line of Eq. (11.50) in detail,

$$\begin{aligned} [\rho_{q,\mathrm{R}}, \rho_{-q',\mathrm{R}}]_- &= \sum_{k,k'} \left[c^\dagger_{k,\mathrm{R}} c_{k+q,\mathrm{R}}, c^\dagger_{k',\mathrm{R}} c_{k'-q',\mathrm{R}} \right]_- \\ &= \sum_k \left(c^\dagger_{k,\mathrm{R}} c_{k+q-q',\mathrm{R}} - c^\dagger_{k+q',\mathrm{R}} c_{k+q,\mathrm{R}} \right). \end{aligned} \tag{11.51}$$

If $q \neq q'$, this is zero, as one can see from relabeling the summation index k. Otherwise, if $q = q'$ we find

$$[\rho_{q,\mathrm{R}}, \rho_{-q',\mathrm{R}}]_- = \sum_k \left(n_{k,\mathrm{R}} - n_{k+q,\mathrm{R}} \right). \tag{11.52}$$

The summation on the right hand side of Eq. (11.52) might appear ambiguous. It can be computed unambiguously by normal ordering of the summand. Normal ordering of the operators between brackets gives

$$\begin{aligned} [\rho_{q,\mathrm{R}}, \rho_{-q,\mathrm{R}}]_- &= \frac{qL}{2\pi} - \sum_k :n_{k,\mathrm{R}} - n_{k+q,\mathrm{R}}: \\ &= \frac{qL}{2\pi}. \end{aligned} \tag{11.53}$$

The summation of normal ordered terms gives zero after relabeling of the summation index k. We had to normal order first, since relabeling the summation index is allowed for normal-ordered summands only.

With these commutation relations, the density operators can serve as boson creation and annihilation operators. Operators $\rho_{q\mathrm{R}}$ with $q < 0$ play the role of creation operators, whereas operators $\rho_{q\mathrm{R}}$ with $q > 0$ are annihilation operators. Similarly, for left-moving particles, the creation operators are the $\rho_{q\mathrm{L}}$ with $q > 0$ and annihilation operators are $\rho_{q\mathrm{L}}$ with $q < 0$.[7] When regarded as creation and annihilation operators, the density operators span the entire

[7] Formally, this identification requires that we multiply the density operators by $(L|q|/2\pi)^{-1/2}$.

Hilbert space with fixed numbers $N_{\rm R}$ and $N_{\rm L}$ of left moving and right moving electrons. You can verify this statement by explicit construction of the states, or by comparing the partition functions for the electron liquid in fermion and boson representations, see footnote 8 below. Since the density operators span the entire Hilbert space, the kinetic energy can be represented in terms of the density operators, rather than the fermion operators. In order to achieve this, we look at the time derivative of $\rho_{q,{\rm R}}$ and $\rho_{q,{\rm L}}$, for which we find

$$\begin{aligned}\frac{\partial}{\partial t}\rho_{q,{\rm R}} &= \frac{i}{\hbar}v_F\sum_{k,k'}k\left[c^\dagger_{k,{\rm R}}c_{k,{\rm R}},c^\dagger_{k',{\rm R}}c_{k'+q,{\rm R}}\right]_- \\ &= \frac{i}{\hbar}v_F\sum_{k}k\left(c^\dagger_{k,{\rm R}}c_{k+q,{\rm R}}-c^\dagger_{k-q,{\rm R}}c_{k,{\rm R}}\right) \\ &= \frac{-iqv_F}{\hbar}\rho_{q,{\rm R}}. \end{aligned} \tag{11.54}$$

Similarly, for the left-moving particles we get

$$\frac{\partial}{\partial t}\rho_{q,{\rm L}} = \frac{iqv_F}{\hbar}\rho_{q,{\rm L}}. \tag{11.55}$$

Utilizing the commutation relations of the density operators, we find that we can write the kinetic energy in terms of the boson operators $\rho_{q,{\rm R}}$ and $\rho_{q,{\rm L}}$,

$$\hat{H}_{\rm kin} = \frac{2\pi v_F}{L}\sum_{q>0}\left(\rho_{-q,{\rm R}}\rho_{q,{\rm R}}+\rho_{q,{\rm L}}\rho_{-q,{\rm L}}\right)+\frac{\pi v_F}{L}(N^2_{\rm R}+N^2_{\rm L}), \tag{11.56}$$

where the additive constant reflects the additional cost of adding electrons to the system.[8]

[8] Now we are in a position to prove that the set of states that is spanned by the density operators is complete. Calculating the grand canonical partition function for the fermions, we find

$$Z = \left[\prod_{n=1}^{\infty}(1+w^{2n-1})^2\right]^2,$$

where we abbreviated $w=\exp(-\pi v_F/TL)$ and put the chemical potential precisely between two successive energy levels. The square within the square brackets corresponds to states with different signs of k, i.e., to particle and hole-like excitations, whereas the overall square reflects the identical contributions from left movers and right movers. For the boson basis, we find

$$Z = \prod_{n=1}^{\infty}(1-w^{2n})^{-2}\left(\sum_{m=-\infty}^{\infty}w^{m^2}\right)^2.$$

Here, the first factor is the partition function corresponding to the boson degrees of freedom, whereas the second factor gives the contribution of the total number of particles to the energy. You verify that these two partition functions are, indeed, equal.

Another way to obtain Eq. (11.56) is to note that, by Eq. (11.49), the operator ρ_q creates a multitude of electron-hole pairs, all with the same energy $v_F q$. Hence, the energy of the "boson" created by ρ_q is $v_F q$. Taking into account the normalization factor $(2\pi/qL)^{1/2}$ from the commutation relations (11.50), one arrives at Eq. (11.56).

The interaction Hamiltonian is, in fact, easier to deal with. Since it contains four fermion creation or annihilation operators, it is quadratic in the boson operators $\rho_{q,\mathrm{R}}$ and $\rho_{q,\mathrm{L}}$. Using the observation that the interaction couples to the total density only, one arrives at the Hamiltonian

$$\hat{H}_{\mathrm{int}} = \frac{1}{2L}(V_0 - V_{2k_F}) \sum_{q\neq 0} (\rho_{q,\mathrm{R}} + \rho_{q,\mathrm{L}})(\rho_{-q,\mathrm{R}} + \rho_{-q,\mathrm{L}}). \tag{11.57}$$

The prefactor $(V_0 - V_{2k_F})$ follows from the difference of Hartree and Fock type interactions, assuming that the interaction V_q depends only weakly on q on scales $\ll k_F$. For a point-like interaction, one has $V_{2k_F} = V_0$, and $\hat{H}_{\mathrm{int}}$ vanishes, as is required by the Pauli principle.

The above manipulations, in which the fermion operators in the Hamiltonian are replaced by boson operators, are known as "bosonization".

The total Hamiltonian $H = \hat{H}_{\mathrm{kin}} + \hat{H}_{\mathrm{int}}$ can be rewritten in terms of boson fields $\phi(x)$ and $\Pi(x)$ that depend on the coordinate x only. These fields are related to the particle density and current density as in Eqs. (11.20) and (11.21). In terms of the density operators, the field $\phi(x)$ reads

$$\phi(x) = \pi \int^x dx' :\rho(x):, \tag{11.58}$$

where $\rho(x)$ is the total electron density,

$$\rho(x) = \frac{1}{L} \sum_{q\neq 0} e^{iqx} (\rho_{q,\mathrm{R}} + \rho_{q,\mathrm{L}}) e^{-|q|\lambda/2}, \tag{11.59}$$

whereas the field $\Pi(x)$ is given by

$$\Pi(x) = -\sum_{q\neq 0} e^{iqx} (\rho_{q,\mathrm{R}} - \rho_{q,\mathrm{L})} e^{-|q|\lambda/2}. \tag{11.60}$$

(The exponential high-momentum cutoff is the same as in the previous section.) Using the commutation relations between the density operators $\rho_{q,\mathrm{R}}$ and $\rho_{q,\mathrm{L}}$, you verify that the fields $\phi(x)$ and $\Pi(x)$ obey canonical boson commutation relations, cf. Eq. (11.18). With this change of variables, the Hamiltonian $H = \hat{H}_{\mathrm{kin}} + \hat{H}_{\mathrm{int}}$ acquires the form (11.22), with

$$v_{\mathrm{c}} = v_F \sqrt{1 + \frac{V_0 - V_{2k_F}}{\pi v_F}}. \tag{11.61}$$

Instead of a formulation in terms of the fields $\phi(x)$ and $\Pi(x)$, which refer to total electron density and current density (after normal ordering), one often uses fields $\phi_{\rm R}$ and $\phi_{\rm L}$ that are related to the densities of right and left moving electrons,

$$\rho_{\rm R}(x) = \frac{1}{L}\sum_{q\neq 0} e^{iqx}\rho_{q,{\rm R}}e^{-|q|\lambda/2}, \quad \rho_{\rm L}(x) = \frac{1}{L}\sum_{q\neq 0} e^{iqx}\rho_{q,{\rm L}}e^{-|q|\lambda/2}, \tag{11.62}$$

as

$$\phi_{\rm R}(x) = 2\pi\int^x dx' :\rho_{\rm R}(x'):, \quad \phi_{\rm L}(x) = 2\pi\int^x dx' :\rho_{\rm L}(x'): . \tag{11.63}$$

These fields have commutation rules

$$\begin{aligned} [\phi_{\rm R}(x),\phi_{\rm R}(x')]_- &= i\pi{\rm sign}\,(x-x'), \\ [\phi_{\rm L}(x),\phi_{\rm L}(x')]_- &= -i\pi{\rm sign}\,(x-x'), \\ [\phi_{\rm R}(x),\phi_{\rm L}(x')]_- &= 0. \end{aligned} \tag{11.64}$$

They are related to the original fields $\phi(x)$ and $\Pi(x)$ as

$$\phi_{\rm R}(x) = \phi(x) - \frac{\pi}{2\hbar}\int dx'\Pi(x'){\rm sign}\,(x-x'), \tag{11.65}$$

$$\phi_{\rm L}(x) = \phi(x) + \frac{\pi}{2\hbar}\int dx'\Pi(x'){\rm sign}\,(x-x'). \tag{11.66}$$

In terms of the fields $\phi_{\rm R}(x)$ and $\phi_{\rm L}$, the Hamiltonian reads

$$\begin{aligned} H &= \frac{v_F}{4\pi}\int dx\left[\left(\frac{\partial\phi_{\rm R}}{\partial x}\right)^2 + \left(\frac{\partial\phi_{\rm L}}{\partial x}\right)^2\right] \\ &\quad + \frac{V_0 - V_{2k_F}}{2\pi}\int dx\left(\frac{\partial\phi_{\rm R}}{\partial x} + \frac{\partial\phi_{\rm L}}{\partial x}\right)^2. \end{aligned} \tag{11.67}$$

11.3.3 Fermion creation and annihilation operators

Having formally rewritten the electron Hamiltonian in terms of boson fields $\phi(x)$ and $\Pi(x)$, we still want to be able to express the creation and annihilation operators of a single electron in terms of the boson fields. Before we do this, let us recall the form of the Hilbert space in the boson representation. In the boson representation, any electronic state can be written as density operators $\rho_{q,{\rm R}}$ and $\rho_{q,{\rm L}}$ acting on the ground state with $N_{\rm R}$ right moving electrons

and $N_{\rm L}$ left moving electrons. Hence, every electronic state is represented by occupation numbers $n_{q,{\rm L}}$ with $q>0$ and $n_{q,{\rm R}}$ with $q<0$ for the boson modes, and the numbers $N_{\rm R}$ and $N_{\rm L}$,

$$|\text{state}\rangle = |\{n_q\}, N_{\rm R}, N_{\rm L}\rangle. \tag{11.68}$$

What is the action of a single-fermion creation operator $\hat{\psi}^\dagger_{\rm L}(x)$ or $\hat{\psi}^\dagger_{\rm R}(x)$ in this Hilbert space? First of all, $\hat{\psi}^\dagger_{\rm R}(x)$ ($\hat{\psi}^\dagger_{\rm L}(x)$) increases $N_{\rm R}$ ($N_{\rm L}$) by one. Inside the boson Hilbert space, this is achieved by "ladder operators" $U^\dagger_{\rm R}$ and $U^\dagger_{\rm L}$,

$$\begin{aligned}
U^\dagger_{\rm R}|\{n_q\}, N_{\rm R}, N_{\rm L}\rangle &= |\{n_q\}, N_{\rm R}+1, N_{\rm L}\rangle,\\
U_{\rm R}|\{n_q\}, N_{\rm R}, N_{\rm L}\rangle &= |\{n_q\}, N_{\rm R}-1, N_{\rm L}\rangle,\\
U^\dagger_{\rm L}|\{n_q\}, N_{\rm R}, N_{\rm L}\rangle &= |\{n_q\}, N_{\rm R}, N_{\rm L}+1\rangle,\\
U_{\rm L}|\{n_q\}, N_{\rm R}, N_{\rm L}\rangle &= |\{n_q\}, N_{\rm R}, N_{\rm L}-1\rangle.
\end{aligned} \tag{11.69}$$

In addition to this, the operator $\hat{\psi}^\dagger_{\rm R}(x)$ creates a multitude of electron-hole pairs, so that, in the end, the change in particle and current densities is sharply peaked around x. In order to capture these particle hole pairs in terms of the boson fields, the notation that uses the separate fields $\phi_{\rm R}(x)$ and $\phi_{\rm L}(x)$ for right and left moving electrons is particularly useful. Returning to the qualitative arguments of the previous section — the addition of an electron corresponds to a "kink" in the fields $\phi_{\rm R}(x)$ and $\phi_{\rm L}(x)$ —, we now make an educated guess for $\hat{\psi}^\dagger_{\rm R}(x)$ and $\hat{\psi}^\dagger_{\rm L}(x)$,

$$\hat{\psi}^\dagger_{\rm R}(x) = \frac{1}{\sqrt{2\pi\lambda}} U^\dagger_{\rm R} e^{-i\phi_{\rm R}(x)}, \quad \hat{\psi}^\dagger_{\rm L}(x) = \frac{1}{\sqrt{2\pi\lambda}} U^\dagger_{\rm L} e^{i\phi_{\rm L}(x)}, \tag{11.70}$$

where the cut-off dependent prefactor $(2\pi\lambda)^{-1/2}$ has already been inserted. We verify that this gives, indeed, the correct commutator with the density fields $\rho_{\rm R}(x)$ and $\rho_{\rm L}(x)$,

$$\begin{aligned}
\left[\hat{\psi}^\dagger_{\rm R}(x), \rho_{\rm R}(x')\right]_- &= \frac{1}{2\pi\sqrt{2\pi\lambda}} U^\dagger_{\rm R}\left[e^{-i\phi_{\rm R}(x)}, \frac{\partial}{\partial x'}\phi_{\rm R}(x')\right]_-\\
&= \frac{1}{2\sqrt{2\pi\lambda}} U^\dagger_{\rm R} e^{-i\phi_{\rm R}(x)} \frac{\partial}{\partial x'}\text{sign}\,(x-x')\\
&= -\hat{\psi}^\dagger_{\rm R}(x)\delta(x-x'),\\
\left[\hat{\psi}^\dagger_{\rm L}(x), \rho_{\rm L}(x')\right]_- &= -\hat{\psi}^\dagger_{\rm L}(x)\delta(x-x').
\end{aligned} \tag{11.71}$$

In deriving this result, we used the fact that the commutator $[e^X, Y]_- = e^X[X,Y]_-$ if $[X,Y]_-$ is proportional to the identity operator. Similarly, you verify that the $\hat{\psi}^\dagger_{\rm R}(x)$ and $\hat{\psi}^\dagger_{\rm R}(x')$

anticommute, as well as $\hat{\psi}_{\rm L}^\dagger(x)$ and $\hat{\psi}_{\rm L}^\dagger(x')$. There is a problem, however, with the calculation of the anticommutator of $\hat{\psi}_{\rm R}^\dagger(x)$ and $\hat{\psi}_{\rm R}(x')$, which becomes ambiguous when $x \to x'$. The ambiguity is lifted once the regularizing momentum cut off in Eqs. (11.59) and (11.60) or Eq. (11.62) is taken into account. In coordinate representation, this momentum cut-off amounts to the replacement of the boson fields $\phi_{\rm R}(x)$ and $\phi_{\rm L}(x)$ in the exponents in Eq. (11.70) by the "smeared" fields

$$\begin{aligned} \phi_{\rm R}(x) &\to \int dx' \frac{2\lambda\phi_{\rm R}(x')}{\pi[\lambda^2+4(x-x')^2]}, \\ \phi_{\rm L}(x) &\to \int dx' \frac{2\lambda\phi_{\rm L}(x')}{\pi[\lambda^2+4(x-x')^2]}, \end{aligned} \tag{11.72}$$

where $\lambda \sim \lambda_F$ is the length scale over which the electrons are delocalized. This way, the "kink" in the fields $\phi_R(x)$ and $\phi_L(x)$ that is created by the operators $\hat{\psi}_{\rm R}^\dagger(x)$ and $\hat{\psi}_{\rm L}^\dagger(x)$ is smeared out over a length λ, and, hence, the added electron is delocalized over a segment of length $\sim \lambda$.[9] For the regularized fields, the sign-function in the commutator is smeared over a distance $\sim \lambda$,

$$\begin{aligned} [\phi_{\rm R}(x),\phi_{\rm R}(x')]_- &= 2i\arctan[(x-x')/\lambda], \\ [\phi_{\rm L}(x),\phi_{\rm L}(x')]_- &= -2i\arctan[(x-x')/\lambda]. \end{aligned} \tag{11.73}$$

With this smearing of the boson fields, it can be shown that the ansatz (11.70) provides the correct anticommutation relation for the fermion creation and annihilation operator. For details, see the original paper F. D. M. Haldane, J. Phys. C **14**, 2585 (1981) or the tutorial review J. von Delft and H. Schoeller, Annalen Phys. **7**, 225 (1998). Writing the fields $\phi_{\rm L}(x)$ nd $\phi_{\rm R}(x)$ in terms of the original fields $\phi(x)$ and $\Pi(x)$ and undoing the momentum shift $q \to q \pm k_F$ we performed at the beginning of this section, you recover Eqs. (11.26) and (11.27) of the previous section.

Finally, we have to ensure that operators for left moving and right moving fermions anticommute. There are various ways to achieve this. The simplest method is to postulate that the ladder operators $U_{\rm R}^\dagger$ and $U_{\rm L}^\dagger$ anticommute. An alternative way is to postulate that the commutator between the left-moving and right-moving boson fields $\phi_{\rm L}$ and $\phi_{\rm R}$ is not zero, but $i\pi$ instead. You are referred to the specialized literature for details.

[9] We have chosen a regularization integral in the exponent of Eq. (11.70), instead of a regularization integral before the exponent. The latter choice would amount a superposition of sharply localized electrons, which does not need to be the same as a delocalized electron.

11.4 Electrons with spin

For electrons with spin, one can take the same route as we took in Sec. 11.2, and write down an effective Hamiltonian based on the spin and charge velocities in the one-dimensional electron liquid. Introducing fields $\Pi_{\rm c}$ and $\phi_{\rm c}$ that are related to the particle current density and particle density as

$$\begin{aligned} n_{\rm c}(x) &= n_\uparrow(x) + n_\downarrow(x) = \frac{1}{\pi}\partial_x\phi_{\rm c}(x)\sqrt{2} && (11.74)\\ j_{\rm c}(x) &= j_\uparrow(x) + j_\downarrow(x) = -v_F\Pi_{\rm c}(x)\sqrt{2}, && (11.75)\end{aligned}$$

together with fields $\Pi_{\rm s}$ and $\phi_{\rm s}$ that are related to the spin current density and spin density,

$$\begin{aligned} n_{\rm s}(x) &= n_\uparrow(x) - n_\downarrow(x) = \frac{1}{\pi}\partial_x\phi_{\rm s}(x)\sqrt{2} && (11.76)\\ j_{\rm s}(x) &= j_\uparrow(x) - j_\downarrow(x) = -v_F\Pi_{\rm s}(x)\sqrt{2}, && (11.77)\end{aligned}$$

we can write the Hamiltonian as

$$\begin{aligned} H &= \frac{\hbar v_F}{2\pi}\int dx \left[\frac{\pi^2}{\hbar^2}\left(\Pi_{\rm c}(x)^2 + \Pi_{\rm s}(x)^2\right)\right.\\ &\quad \left. + g_{\rm c}^2(\partial_x\phi_{\rm c}(x))^2 + g_{\rm s}^2(\partial_x\phi_{\rm s}(x))^2\right], \qquad (11.78)\end{aligned}$$

where $g_{\rm c} = v_{\rm c}/v_F$ and $g_{\rm s} = v_{\rm s}/v_F$. The boson fields $\Pi_{\rm c,s}$ and $\phi_{\rm c,s}$ are normalized such that they satisfy canonical commutation relations,

$$\begin{aligned} &[\phi_{\rm c,s}(x), \phi_{\rm c,s}(x')]_- = [\Pi_{\rm c,s}(x), \Pi_{\rm c,s}(x')]_- = 0\\ &[\Pi_{\rm c}(x), \phi_{\rm c}(x')]_- = [\Pi_{\rm s}(x), \phi_{\rm s}(x')]_- = -i\hbar\delta(x-x'), \qquad (11.79)\\ &[\Pi_{\rm c}(x), \phi_{\rm s}(x')]_- = [\Pi_{\rm s}(x), \phi_{\rm c}(x')]_- = 0.\end{aligned}$$

The form of the fermion operators is found in the same way as for the spinless case,

$$\begin{aligned} \hat{\psi}^\dagger_{R\sigma}(x) &= \frac{1}{\sqrt{2\pi\lambda}}U^\dagger_{R\sigma}e^{-ik_Fx - i\phi_{R\sigma}(x)},\\ \hat{\psi}^\dagger_{L\sigma}(x) &= \frac{1}{\sqrt{2\pi\lambda}}U^\dagger_{L\sigma}e^{ik_Fx + i\phi_{L\sigma}(x)}, \qquad (11.80)\end{aligned}$$

where $\sigma = \uparrow, \downarrow$ and where the fields $\phi_{L\sigma}$ and $\phi_{R\sigma}$ are defined as

$$\phi_{R\sigma}(x) = \frac{1}{\sqrt{2}}\Big(\phi_{\rm c}(x) + \sigma\phi_{\rm s}(x)$$

$$
\begin{aligned}
& - \frac{\pi}{2\hbar} \int dx' [\Pi_{\rm c}(x') + \sigma \Pi_{\rm s}(x')] {\rm sign}\,(x - x') \Big) \,, \\
\phi_{L\sigma}(x) \;\; = \;\; & \frac{1}{\sqrt{2}} \Big(\phi_{\rm c}(x) + \sigma \phi_{\rm s}(x) \\
& + \frac{\pi}{2\hbar} \int dx' [\Pi_{\rm c}(x') + \sigma \Pi_{\rm s}(x')] {\rm sign}\,(x - x') \Big) \,.
\end{aligned}
\tag{11.81}
$$

Alternatively, one can find a description starting from a microscopic picture, as in the previous section. In this case, bosonization of the kinetic energy is done as before. For this, we refer to the references cited above for more details.

One important aspect of the one-dimensional electron liquid with spin, is that spin excitations and charge excitations travel at different speeds, see our discussion in Sec. 11.1. We again emphasize that this phenomenon, which is known as "spin-charge separation", also exists for collective modes in higher dimensions. The difference between the higher-dimensional case and the one-dimensional case is that in higher dimensions there are quasiparticle excitations that carry both spin and charge, in addition to the spin-charge separated collective excitations. These quasiparticles dominate the low-energy physics of higher dimensional electron liquids, so that, in the end, spin and charge always travel together. In one dimension, there are no quasiparticle excitations, and the spin-charge separated collective modes dominate the low energy physics.

To illustrate the phenomenon of spin-charge separation, let us create a right-moving electron with spin up at position $x = 0$ at time $t = 0$. As we discussed above, creating an electron corresponds to making a kink of size π in the field $\phi_{R\uparrow}$ around $x = 0$. The time-dependence of the charge density and the spin density then follows from decomposing $\phi_{R\uparrow}$ in terms of the spin and charge fields, and solving for their time-evolution using the Hamiltonian (11.78). A kink in $\phi_{R\uparrow}$ corresponds to kinks in both $\phi_{\rm c}$ and $\phi_{\rm s}$, but these two kinks travel at different velocities. Hence, although initially charge and spin were located at the same point, they are separated after a finite time. Only for a non-interacting electron gas, for which $v_{\rm c} = v_{\rm s} = v_F$, spin and charge are not separated.

11.5 Does a one-dimensional electron liquid exist?

Now that we have seen that electrons in one dimension behave quite differently from electrons in three dimensions, it is natural to ask whether all of this was an academic exercise, or whether one-dimensional electron systems exist in nature. Fortunately, the answer is positive.

One example of a one-dimensional electron liquid is realized in extremely thin and clean wires formed in the two-dimensional electron gas that exists at the interface in a GaAs/GaAlAs heterostructure. This is the example that comes closest to the physics we have discussed in this chapter. Spin-charge separation in these thin wires has been observed directly, in the form of interference between charge and spin excitations in a wire of finite length. You can find more about the experiment and the theory in Y. Tserkovnyak, B. I. Halperin, O. M. Auslaender, and A. Yacoby, cond-mat/0302274 and references therein.

Another example is that of a carbon nanotube. Nanotubes are very good candidates to observe Luttinger Liquid behavior, since they are thin and clean by virtue of their chemistry. (The wires, on the other hand, have to be carefully engineered.) However, carbon nanotubes have two propagating modes at the Fermi level (per spin direction), which slightly modifies some of the properties. The anomalous density of states has been observed in carbon nanotubes, see, *e.g.*, M. Bockrath *et al.*, Nature **397**, 598 (1999).

The third example is that of edge states in the quantum Hall effect. The main difference between edge states and the one-dimensional electron liquid we considered here is that edge states are "chiral": all electrons move in one direction. For more details, you are referred to the original papers by Wen [Phys. Rev. B **41**, 12838 (1990); **43**, 11025 (1991)].

In addition to the question of real existence, one-dimensional electron systems have been used as a model for quite a variety of problems in condensed matter physics. One example is the Kondo problem with a point-like magnetic impurity, where it can be argued that the impurity interacts only with s-wave states in the metal, which, in turn, can be modeled as a one-dimensional electron gas. Another example is that of a Coulomb blockaded quantum dot, where the electron gas in the point contacts between the dot and the bulk electrodes is modeled as a one-dimensional electron gas. In these applications, most of the electron liquid is non-interacting, the role of the impurity or of the quantum dot being to introduce a "localized interaction" in the Luttinger Liquid.